Studying strongly correlated systems with tensor network state methods and quantum information theory

PhD thesis by

Mihály Máté

with the supervision of

Örs Legeza, DSc, scientific advisor
Szilárd Szalay, PhD, research fellow

Institute for Solid-state Physics and Optics

Wigner Research Centre for Physics

presented to the

Material Science and Solid-state Physics program
directed by Dr. István Groma

Doctoral School of Physics
directed by Dr. Gergely Palla

Eötvös Loránd University

2024

DOI: 10.15476/ELTE.2024.024

Contents

Acknowledgements

I would like to express my sincere gratitude to my advisers. It is a pleasure to thank *Örs Legeza*, for his supervising and guidance helped me in all the time of research. I would like to extend my gratitude to *Szilárd Szalay* for steering me in the right direction with his passion for research. This work would not have been possible without the flexible and frequent discussions with them held in lighthearted atmosphere.

Useful discussions on various topics with the members of the *Strongly correlated systems research group* are gratefully acknowledged.

My sincere thanks also go to some of my teachers as well, *Ádám Besenyei*, *Gyula Dávid*, *Milán Mosonyi* and *Jenő Sólyom*, the lectures and books of whom were guides of great value during my studies.

I would like to thank friends of mine, especially *Anna*, for all the nice times we have had and their continuous encouragement throughout my studies.

Last but not least, I am grateful to *my parents* for their everlasting patience, support and love.

Statements

1. I investigated the *coupled cluster method tailored by density matrix renormalization group algorithm (DMRG-TCC)* theoretically and exemplified numerically by the nitrogen dimer for different geometries. I performed a systematic study on the error of the method, in particular when the system becomes strongly correlated. I showed the strong dependence of the DMRG-TCC solution on the basis splitting. I showed the robustness of the entropic quantities, which are the guides in determining the optimal basis splitting, with respect to the DMRG accuracy. In order to minimize the energy error and carry out large-scale DMRG-TCCSD calculations, I developed a rigorous routine procedure to determine the optimal basis splitting.

   The publication belonging to this thesis statement is [**Fau19b**], which is [1] in the list on page v.

2. I studied the *orbital optimization based on entanglement minimization* within the framework of the two-site DMRG and exemplified numerically by the nitrogen dimer for different geometries. My analysis, based on the tomography of the state, occupation numbers and entropic quantities, showed that the developed joint optimization procedure has the potential to compress the multireference character of the wave function. The orbital optimization provides significantly more optimal orbitals for tensor network state methods.

   The publication belonging to this thesis statement is [**Mát23**], which is [2] in the list on page v.

3. I investigated the *Hubbard wheel* lattice model of *hard-core bosons* theoretically and numerically. The tuning of just a single control parameter allows a crossover from one- to "infinite"-dimensionality, which also drives a transition from quasi-condensation to complete Bose–Einstein condensation. I showed that the mutual information possesses the qualitatively similar dependence on the control parameter as the number of the condensed bosons. I showed the existence of an excitation gap, which is usually highly demanding, and also proposed a possible experimental realization.

   The publication belonging to this thesis statement is [**Mát21**], which is [3] in the list on page v.

Publications belonging to thesis statements

[1] F. M. Faulstich, **M. Máté**, A. Laestadius, M. A. Csirik, L. Veis, A. Antalík, J. Brabec, R. Schneider, J. Pittner, S. Kvaal, Ö. Legeza. Numerical and theoretical aspects of the DMRG-TCC method exemplified by the nitrogen dimer. *Journal of Chemical Theory and Computation*, **15 (4)**, 2206, 2019. doi:10.1021/acs.jctc.8b00960

Cited as [**Fau19b**].

[2] **M. Máté**, K. Petrov, Sz. Szalay, Ö. Legeza. Compressing multireference character of wave functions via fermionic mode optimization. *Journal of Mathematical Chemistry*, **61 (2)**, 362, 2023. ISSN 1572-8897. doi:10.1007/s10910-022-01379-y

Cited as [**Mát23**].

[3] **M. Máté**, Ö. Legeza, R. Schilling, M. Yousif, C. Schilling. How creating one additional well can generate Bose–Einstein condensation. *Communications Physics*, **4 (1)**, 29, 2021. doi:10.1038/s42005-021-00533-3

Cited as [**Mát21**].

Further publications

The publications are listed in chronological order.

1. **M. Máté**, G. Barcza, Sz. Szalay, Ö. Legeza. Molekulákba kódolt kvantuminformáció: átmenetifém-klaszterek elektronszerkezete. *Magyar Kémiai Folyóirat*, **125 (3)**, 111, 2019. doi:10.24100/MKF.2019.03.111
2. J. Brandejs, J. Višňák, L. Veis, **M. Máté**, Ö. Legeza, J. Pittner. Toward DMRG-tailored coupled cluster method in the 4c-relativistic domain. *The Journal of Chemical Physics*, **152 (17)**, 174107, 2020. doi:10.1063/1.5144974
3. Sz. Szalay, Z. Zimborás, **M. Máté**, G. Barcza, C. Schilling, Ö. Legeza. Fermionic systems for quantum information people. *Journal of Physics A: Mathematical and Theoretical*, **54 (39)**, 393001, 2021. doi:10.1088/1751-8121/ac0646
4. A. Leszczyk, **M. Máté**, Ö. Legeza, K. Boguslawski. Assessing the accuracy of tailored coupled cluster methods corrected by electronic wave functions of polynomial cost. *Journal of Chemical Theory and Computation*, **18 (1)**, 96, 2022. doi:10.1021/acs.jctc.1c00284

1. CHAPTER

Introduction

Elementary particles in physics are indistinguishable in principle, and they have either *fermionic* or *bosonic* nature. They arrange to different structures according to the environment. In this work special problems are studied in the field of the quantum chemistry and ultracold physics. Although their characteristic energies are of different orders of magnitude, moreover, in the former case we deal with interacting electrons in the external potential of the nuclei, and in the latter case we study interacting trapped bosons, they still require similar treatment because of the emerging strong correlations in the systems.

Composite systems, for example, systems of identical particles, are described by tensor product structure. The dimension of the composite system scales *exponentially* with the number of parts, therefore, there is a need for lossy compression. The *tensor network state (TNS)* methods [**Hac12**, **Cir21**] are based on the subsequent optimization of the tensor factors corresponding to the local factor spaces. There are three main approaches of simulating physical systems by tensor networks: tree tensor network state (TTNS) [**Shi06**, **Mur10**], tensor networks with loops [**Ver04**, **Pip10**], especially projected entangled pair states [**Nis01**, **Ver06b**, **Ver08**, **Sch07**, **Mur07**, **Bau11**]), and the multiscale entanglement renormalization ansatz [**Vid07**, **Eve09**]. Although the *density matrix renormalization group (DMRG)* method [**Whi92**, **Whi93**] was developed to simulate low dimensional strongly correlated systems appearing in the field of solid-state physics, it also shows its potential in strongly correlated many-body problems. This algorithm inherently provides the *matrix product state (MPS)* representation of the wave function [**Ö95**, **Rom97**, **Sch11**], which is a simple case of the TNSs. Also, MPS is a tree tensor network state, so, by the Schmidt decomposition (or, in a numerical point of view, singular value decomposition), we have access to the entanglement in the system for the given bipartition. In the past two decades TNS methods have become vital alternative approaches to treat strongly correlated, that is, multireference problems in quantum chemistry [**Whi99**, **Leg08**, **Cha08**, **Yan09**, **Mar10**, **Wou14**, **Leg14**, **Sza15**, **Cha16**, **Bai20**, **Che22**]. Here we investigate systems in quantum chemistry and ultracold physics that are treated by DMRG or methods that are supported by DMRG.

In quantum chemistry, from the exact solution of the hydrogen atom [**Sch26**], one may infer to the properties of the hydrogen-like atoms and ions, since they can be approximated by a simple system, that is, the problem of the valence electron and the positive core. From the analytic solution of the hydrogen molecule ion, H_2^+, that is, the problem of two fixed protons and a single electron [**Bur27**], the notion of the covalent bond can be grasped [**Lew16**, **Hei27**]. The two analytic solutions give us deeper insight into the characteristics of molecular systems,

however, the many-body problem of the interacting electrons are intractable both analytically and numerically. Both in theoretical and experimental chemistry, it is of central importance to explore the shape of the potential energy surface, since this shows the fundamental properties of a molecule, such as the equilibrium geometry and the corresponding energy, spectroscopic constants and dissociation energy. For this, numerous approximation techniques have been developed [**Hel00**] to find the ground-state energy of the electronic system within chemical accuracy for a fixed nucleus configuration, that is, in the *Born–Oppenheimer approximation*. For a given orbital set, the problem is to solve the eigenvalue problem of the Hamiltonian in the *full configuration interaction* (FCI) space, which dimension scales exponentially with the number of orbitals. To tackle this, iterative algorithms were developed to find the lowest eigenvalues [**Bai00**], however, these *exact diagonalization* approaches only tractable for small molecules even in the restriction on symmetry subspaces. Nevertheless, they can serve as a reference for benchmarking other numerical methods. On the contrary, one of the simplest approximate solution can be obtained by the *Hartree–Fock method*, which gives the best Slater determinant approximation, or one can say that it is an *orbital optimization* with respect to the energy expectation value with Slater determinants. Or from another point of view, the Hartree–Fock method replaces the Coulomb repulsion of electrons by an effective one-body term, therefore it is a member of a broader family, the *mean-field* methods. To go beyond the independent particle picture, but still addressing the curse of dimensionality, kind of standard computational approaches are the *coupled cluster* (CC) methods, especially the *CC up to single and double excitations with perturbative triples* [**Rag89**, **Bar90**, **Bar07**]. These are based on the choice of a reference determinant, which is the Hartree–Fock solution in most of the cases, therefore there is a bias in the method [**Hel00**]. Also there are situations, for example, strongly open-shell systems, where the choice of the reference determinant becomes ambiguous. Moreover, in these cases it is often observed that the CC energy goes below the exact FCI energy, which is the major drawback of the CC approach, namely being *non-variational* [**Kow00**]. In these cases the TTNS methods are powerful alternatives, however, the computational demands are governed by the *bond dimensions*, which are the sizes of the tensors in the approximate wave function representation. However, the TTNS methods are *variational*, and the number of the *variational parameters*, which are the (entries of the) tensors, can be controlled efficiently. Other broad fields, not considered in this work, are the density functional theory based methods [**DSS09**] and the quantum Monte Carlo methods [**Boo09**, **Poz13**, **Vei18**]. The former circumvents the curse of dimensionality, it can be applied moderately correlated system, but the form of the functional used is rather based on numerical experience. The latter is based on sampling, it can treat strongly correlated systems, however, suffers from the sign problem. In general, it can be said that there is no universal method applicable to quantum chemistry systems being superior both in numerical cost and accuracy. Moreover, it is often observed that the correlation in the system changes when going along a path in the potential energy surface. For example, describing the bond breaking of a molecule requires careful treatment, since the system is dominated by dynamical correlation at equilibrium geometry and static correlation close to dissociation. The coupled cluster method performs well in the first case but fails in the latter [**Kow00**, **Lya12**]. From this, two remarks

can be drawn that we elaborate. First, hybrid numerical approaches may be developed to capture both dynamic and static correlation in the system. Second, since the correlation in the system is basis dependent, the optimization of the underlying basis may yield a favourable problem setting for the numerical treatment. The corresponding methods, investigated and discussed in this work, are the *CC tailored by DMRG* (DMRG-TCC) and the *mode transformation and -optimization*, respectively.

Concerning ultracold gases, the Bose–Einstein condensation (BEC) is one of the most striking quantum phenomena in nature [**Gri95**, **Pet02**, **Leg06**, **Pit16**]. While its theoretical prediction dates back almost one hundred years ago, it has more recently seen a revival of interest due to its realization in trapped gases [**And95**, **Bra95**, **Dav95**]. The accurate study of BEC by theoretical and computational approaches, particularly for systems with strong quantum correlations is rather challenging. This has been the reason why most studies of BEC so far were concerned with weakly interacting bosons (corresponding to the experimental situation for ultracold gases) or even ideal Bose gases, eventually allowing for feasible mean-field approaches. Prime examples are the Bogoliubov theory [**Bog47**] for uniform systems, Gross–Pitaevskii theory [**Gro61**, **Gro63**, **Pit61**] for general inhomogeneous systems, and perturbation theoretical approaches [**Lee57b**, **Lee57a**, **Bru57a**, **Bru57b**, **Bel58**, **Hug59**, **Lie63b**]. Although these widely used approaches have led to a deeper understanding of BEC, their range of validity is limited. To go beyond that limitation, various methods were developed [**Dal99**, **And04**, **Caz11**, **Lod20**]. The occurrence of the BEC also depends on the temperature and on the possible inhomogeneities or disorders, for example, due to the presence of an external field [**Sac11**]. In this work, however, we restrict our discussion to the interaction strength and the spatial dimensionality affecting the presence of the BEC, which leads us the *Hubbard wheel of hard-core bosons*.

The structure of the thesis is the following. In chapter 2, we recall the description of quantum systems, the tensor network methods (particularly the two-site DMRG) and the formalism of identical particles. In section 3, the recently developed DMRG-TCC method is analysed theoretically and numerically. In chapter 4, orbital optimization based on entanglement minimization is detailed and demonstrated. In chapter 5, the Hubbard wheel of hard-core bosons is studied. Finally, in chapter 6, we conclude with an outlook. Some further background is given in the appendices. Some technical details of the DMRG are presented in appendices A and B, regarding order optimization and initialization, respectively. In appendix C, the conventional single-reference approaches in computational chemistry are recalled, particularly the CC method.

2. CHAPTER

Description of many-body quantum systems

In this chapter, first, in section 2.1, we recall the basic notions for describing quantum systems. One of the most distinctive features of quantum nature is revealed in composite systems, where a special type of correlation occurs, called *entanglement*. In the classification of quantum states (see section 2.2), and the quantification of correlation and entanglement (see section 2.3), the Schmidt decomposition naturally appears, which is a simultaneous unitary basis transformation resulting diagonal coefficient tensor. This, however, works only for bipartition, and cannot be generalized for more than two parts. Moreover, since the dimension of the composite system scales exponentially with the number of parts, there is a need for lossy compression. These two facts together lead us to the field of *tensor decomposition* and *tensor network methods*, detailed in sections 2.4-2.5. The density matrix renormalization group (DMRG) method approximates the state vector of the system in a special tensor network form, the matrix product state (MPS) form (see sections 2.6-2.7). After the description of quantum states built up from general elementary subsystems (for example, spins, modes, (spatial) orbitals), we turn to the formalism of identical particles (bosons and fermions) in sections 2.8-2.9. In the *first quantization* (or particle picture), we have particles, which are indistinguishable and can occupy some modes, in the *second quantization* (or mode picture), we have modes, which are distinguishable and can be occupied by some particles. Unitary basis transformation and operators (especially the Hamilton operator, by which the physical models are formulated), are discussed in the two pictures in sections 2.10-2.13.

2.1. Description of quantum systems

Quantum mechanics gives a statistical description of a system in terms of linear operators represented on Hilbert spaces [**Neu32**, **Nie00**, **Ben06**, **Pet08**]. In this thesis we consider discrete, finite quantum systems, which are represented on finite dimensional complex Hilbert spaces $\mathcal{H}$, and we omit the trivial cases, so $1 < \dim(\mathcal{H}) < \infty$. Observables (physical quantities treated by quantum mechanics) are represented by self-adjoint operators $O \in \mathrm{Lin}_{\mathrm{SA}}(\mathcal{H})$, and states are linear functionals giving the expectation values $\langle O \rangle$ of the observables O. The quantum *states* can be given by *density operators*, which are positive semidefinite, normalized operators, the space of which is

$$\mathcal{D}(\mathcal{H}) := \Big\{ \varrho \in \mathrm{Lin}(\mathcal{H}) \;\Big|\; \varrho = \varrho^\dagger \geq 0, \mathrm{Tr}(\varrho) = 1 \Big\}. \tag{2.1}$$

Then $\langle O \rangle = \mathrm{Tr}(\varrho O)$ for $\varrho \in \mathcal{D}(\mathcal{H})$. The state space $\mathcal{D}(\mathcal{H})$ is a convex set, that is, the convex combination (statistical mixture) $\sum_i p_i \varrho_i$ of states ϱ_i with weights $p_i \geq 0$, $\sum_i p_i = 1$, is also a

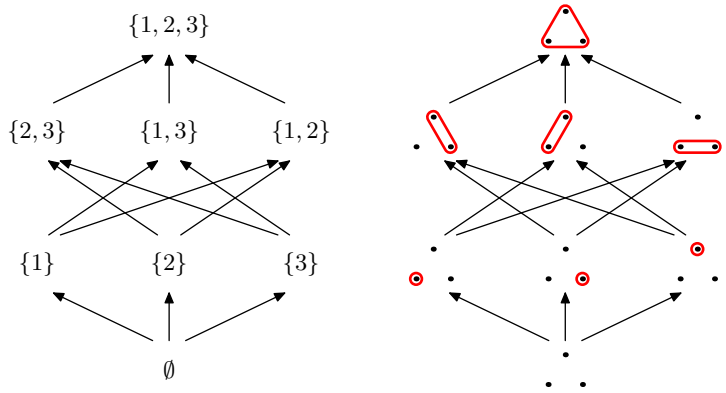

FIGURE 2.1. The subsystem labels of the tripartite system $L = \{1, 2, 3\}$. The lattice of power set $2^{\{1,2,3\}}$ (left) and its graphical illustration (right). The arrows denote the relation between the labels, the set inclusion.

state. The extremal points of the state space are the *pure states*, which turn out to be rank-one projections, the space of which is

$$\mathcal{P}(\mathcal{H}) := \operatorname{Extr} \mathcal{D}(\mathcal{H}) = \Big\{ |\psi\rangle\langle\psi| \;\Big|\; |\psi\rangle \in \mathcal{H}, \operatorname{Tr}\big(|\psi\rangle\langle\psi|\big) = \||\psi\rangle\|^2 = 1 \Big\}. \tag{2.2}$$

Then $\langle O \rangle = \operatorname{Tr}(\pi O) = \langle \psi | O \psi \rangle$ for $\pi \in \mathcal{P}(\mathcal{H})$. The normalized vector $|\psi\rangle \in \mathcal{H}$, by which the pure state is given, is called *state vector*. We also have that the state space is the convex hull of the rank-one projections,

$$\mathcal{D}(\mathcal{H}) = \operatorname{Conv} \mathcal{P}(\mathcal{H}) = \Big\{ \sum_i p_i \pi_i \;\Big|\; \pi_i \in \mathcal{P}(\mathcal{H}), p_i \geq 0, \sum_i p_i = 1 \Big\}. \tag{2.3}$$

Then

$$\langle O \rangle = \operatorname{Tr}(\varrho O) = \sum_i p_i \operatorname{Tr}(\pi_i O) = \sum_i p_i \langle \psi_i | O | \psi_i \rangle \tag{2.4}$$

for $\varrho = \sum_i p_i \pi_i \in \mathcal{D}(\mathcal{H})$. Note that the convex decomposition of a density operator in (2.3) is highly non-unique, contrary to the classical case [**Sch36**, **Gis89**, **Hug93**, **Ben06**].

We deal with *composite*, or *multipartite* systems, where the observables of disjoint subsystems can be measured simultaneously. These quantities are represented by operators of subalgebras commuting with one another, leading to a tensor product structure in the Hilbert space and its operator algebra. For composite systems let the labels of the *elementary subsystems* be denoted by $i \in L$, with $|L| < \infty$ and the associated Hilbert spaces by $\mathcal{H}_i$. A *subsystem* (not elementary in general) is labelled by $X \subseteq L$, so we have the Hilbert space $\mathcal{H}_X = \bigotimes_{i \in X} \mathcal{H}_i$, and similarly to (2.2) and (2.1), the set of pure states $\mathcal{P}_X := \mathcal{P}(\mathcal{H}_X)$, and the set of mixed states $\mathcal{D}_X := \mathcal{D}(\mathcal{H}_X)$ are understood. For simplicity, the labels of the whole system is omitted, $\mathcal{P}_L =: \mathcal{P}$ and $\mathcal{D}_L =: \mathcal{D}$. Every subsystem label X is an element of 2^L, the power set of L, which is a basic example for a lattice structure [**Bir73**, **Dav02**] with respect to set inclusion, intersection and union. For illustration, see figure 2.1.

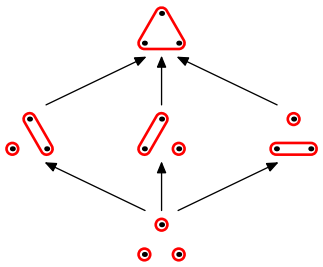

FIGURE 2.2. The partition labels of the tripartite system $L = \{1, 2, 3\}$. Graphical illustration of the lattice structure of the partitions of a tripartite system $\Pi_{\{1,2,3\}}$. The arrows denote the partial order of the lattice, the refinement.

Let us have the nested subsystems $Y \subseteq X \subseteq L$. The observables O_Y of subsystem Y among the observables of subsystem X are given by the *operator extension*

$$\begin{aligned} \iota_{Y,X} : \quad \mathrm{Lin}(\mathcal{H}_Y) \quad &\longrightarrow \quad \mathrm{Lin}(\mathcal{H}_X), \\ O_Y \quad &\longmapsto \quad O_Y \otimes \mathrm{I}_{X \setminus Y}. \end{aligned} \tag{2.5}$$

If the state of subsystem X is given by $\varrho_X \in \mathcal{D}_X$, then the *reduced state* $\varrho_Y := r_{X,Y}(\varrho_X) \in \mathcal{D}_Y$ of subsystem Y is the state that gives back the expectation values of observables of subsystem Y, that is, $\mathrm{Tr}\big(r_{X,Y}(\varrho_X) O_Y\big) = \mathrm{Tr}\big(\varrho_X \iota_{Y,X}(O_Y)\big)$ for all O_Y. This means that the operation of the state reduction $r_{X,Y}$ is just the adjoint map (with respect to the Hilbert–Schmidt inner product) of the operator extension $\iota_{Y,X}$. It turns out that this holds if and only if the state reduction is done by the *partial trace* operation

$$\begin{aligned} r_{X,Y} : \quad \mathcal{D}_X \quad &\longrightarrow \quad \mathcal{D}_Y, \\ \varrho_X \quad &\longmapsto \quad \mathrm{Tr}_{X \setminus Y}(\varrho_X), \end{aligned} \tag{2.6}$$

where $\mathrm{Tr}_{X \setminus Y}$ is linear, and given as $\mathrm{Tr}_{X \setminus Y}(A_Y \otimes B_{X \setminus Y}) = A_Y \, \mathrm{Tr}(B_{X \setminus Y})$ for elementary tensors $A_Y \otimes B_{X \setminus Y}$ [**Nie00**, **Pet08**].

2.2. Correlation and entanglement of quantum systems

A *partition* of the system is a set $\xi = \{X_1, X_2, \ldots, X_{|\xi|}\}$ (with the shorthand notation $\xi = X_1|X_2|\ldots|X_{|\xi|}$) having *parts* $X \subseteq L$ that are non-empty, $X \in 2^L \setminus \{\emptyset\}$, disjoint, $X \cap X' = \emptyset$ if $X \neq X'$, cover the whole system, $\bigcup_{X \in \xi} X = L$. The set of all possible partitions of the system is Π_L. For two partitions $\xi, \upsilon \in \Pi_L$, one can say that υ is the *refinement* of ξ (or "υ is finer than or equal to ξ" or "ξ is coarser than or equal to υ"), if the parts of ξ can be obtained by joining some parts of υ. This is given by the relation

$$\upsilon \preceq \xi \quad \overset{\text{def}}{\iff} \quad \forall Y \in \upsilon, \exists X \in \xi : Y \subseteq X, \tag{2.7}$$

which turns out to be a partial order, moreover, for all pairs of partitions there exist greatest lower bound and least upper bound with respect to $\preceq$, so the poset (partially ordered set) Π_L is a lattice [**Bir73**, **Dav02**]. We have the finest and coarsest partitions, $\bot = \big\{\{i\}, i \in L\big\}$ and $\top = \big\{L\big\}$, respectively. For illustration, see figure 2.2.

With respect to a partition $\xi \in \Pi_L$, let us introduce the *correlation of observables* O_X for $X \in \xi$, defined as

$$C_\xi(\varrho; \{O_X\}_{X\in\xi}) = \Big\langle \bigotimes_{X\in\xi} O_X \Big\rangle - \prod_{X\in\xi} \Big\langle O_X \Big\rangle = \mathrm{Tr}\Big((\varrho - \bigotimes_{X\in\xi} \varrho_X) \bigotimes_{X\in\xi} O_X \Big). \tag{2.8}$$

In mathematical statistics this is called covariance, and the normalized covariance is the correlation. In physics we omit that normalization, which would make the quantity highly nonlinear also in the observables. The state itself is called uncorrelated with respect to a partition $\xi \in \Pi_L$ if the correlation (2.8) vanishes for all $\{O_X\}_{X\in\xi}$ set of observables. The space of ξ-*uncorrelated states* is

$$\mathcal{D}_{\xi\text{-unc}} := \Big\{ \bigotimes_{X\in\xi} \varrho_X \;\Big|\; \varrho_X \in \mathcal{D}_X, \forall X \in \xi \Big\}. \tag{2.9}$$

The rest of the state space contains the ξ-*correlated* states, $\mathcal{D} \setminus \mathcal{D}_{\xi\text{-unc}}$, these cannot be prepared without communication (interaction). With respect to a partition $\xi \in \Pi_L$, the ξ-*separable states* arise when only classical communication is allowed among ξ-uncorrelated subsystems [**Wer89**], the space of which is

$$\mathcal{D}_{\xi\text{-sep}} := \mathrm{Conv}\, \mathcal{D}_{\xi\text{-unc}}. \tag{2.10}$$

The rest of the state space contains the ξ-*entangled* states, $\mathcal{D} \setminus \mathcal{D}_{\xi\text{-sep}}$, these cannot be prepared by classical communication (classical interaction), genuine quantum interaction is needed for that. This is the "*local operation and classical communication*" (*LOCC*) paradigm, also called distant laboratory paradigm [**Wer89**], grabbing an important non-classical feature of quantum correlations. In the special case of pure states, correlation and entanglement in the whole system coincide, $\mathcal{P} \cap \mathcal{D}_{\xi\text{-unc}} = \mathcal{P} \cap \mathcal{D}_{\xi\text{-sep}}$, that is,

$$\mathcal{P}_{\xi\text{-sep}} \equiv \mathcal{P}_{\xi\text{-unc}} = \Big\{ \bigotimes_{X\in\xi} \pi_X \;\Big|\; \pi_X \in \mathcal{P}_X, \forall X \in \xi \Big\}, \tag{2.11}$$

and the other pure states are ξ-*correlated*, or equivalently ξ-*entangled*, $\mathcal{P} \setminus \mathcal{P}_{\xi\text{-unc}} \equiv \mathcal{P} \setminus \mathcal{P}_{\xi\text{-sep}}$ [**Dür99**, **Dür00**, **Ací00**, **See08**, **Szal12**, **Szal13**]. Correlation in pure states is a non-classical feature of quantum theory. Note that by construction $\mathrm{Extr}\, \mathcal{D}_{\xi\text{-sep}} = \mathcal{P}_{\xi\text{-sep}}$. Note that the correlation and entanglement do not coincide inside the subsystems, even if the whole system is described by a pure state, since the state describing the subsystem is mixed in general, see (2.19) later.

If a state is uncorrelated with respect to a partition, then it is uncorrelated with respect to every coarser partition, that is,

$$\upsilon \preceq \xi \quad \Longleftrightarrow \quad \mathcal{D}_{\upsilon\text{-unc}} \subseteq \mathcal{D}_{\xi\text{-unc}}. \tag{2.12a}$$

Because of (2.10), similar expression follows for ξ-separable states [**Szal15**, **Szal17**],

$$\upsilon \preceq \xi \quad \Longleftrightarrow \quad \mathcal{D}_{\upsilon\text{-sep}} \subseteq \mathcal{D}_{\xi\text{-sep}}. \tag{2.12b}$$

That is, the inclusion hierarchy of state sets $\mathcal{D}_{\xi\text{-unc}}$ and $\mathcal{D}_{\xi\text{-sep}}$ is described by the poset Π_L.

To sum up, we have the structure of the state spaces

$$\begin{array}{ccccccccc}
\operatorname{Extr}\mathcal{D} & = & \mathcal{P} & \subset & \mathcal{D} & = & \operatorname{Conv}\mathcal{P} \\
\cup & & \circlearrowleft \quad \circlearrowright & & \circlearrowleft \quad \circlearrowright & & \cup \\
\operatorname{Extr}\mathcal{D}_{\xi\text{-unc}} & = & \mathcal{P}_{\xi\text{-unc}} \equiv \mathcal{P}_{\xi\text{-sep}} & \subset & \mathcal{D}_{\xi\text{-unc}} \subset \mathcal{D}_{\xi\text{-sep}} & = & \operatorname{Conv}\mathcal{P}_{\xi\text{-sep}} \\
\mathrel{|}\cup & & \mathrel{|}\cup \quad \mathrel{|}\cup & & \mathrel{|}\cup \quad \mathrel{|}\cup & & \mathrel{|}\cup \\
\operatorname{Extr}\mathcal{D}_{\upsilon\text{-unc}} & = & \mathcal{P}_{\upsilon\text{-unc}} \equiv \mathcal{P}_{\upsilon\text{-sep}} & \subset & \mathcal{D}_{\upsilon\text{-unc}} \subset \mathcal{D}_{\upsilon\text{-sep}} & = & \operatorname{Conv}\mathcal{P}_{\upsilon\text{-sep}},
\end{array} \tag{2.13}$$

for $\upsilon \preceq \xi$. Note that for the trivial (coarsest) partition $\top = \{L\}$, we have $\mathcal{D}_{\top\text{-unc}} = \mathcal{D}_{\top\text{-sep}} = \mathcal{D}$ and $\mathcal{P}_{\top\text{-unc}} = \mathcal{P}_{\top\text{-sep}} = \mathcal{P}$.

Let us write out the special features of the pure states $|\psi\rangle\langle\psi| \in \mathcal{P}(\mathcal{H}_X \otimes \mathcal{H}_{\bar{X}})$ with respect to bipartitions $\xi = X|\bar{X}$, where $\bar{X} = L \setminus X$. Without the loss of generality, let $D_X = \dim(\mathcal{H}_X) \leq \dim(\mathcal{H}_{\bar{X}}) = D_{\bar{X}}$, and consider the spectral decomposition of the reduced state,

$$\varrho_X = \sum_{\alpha=1}^{D_X} \omega_\alpha |\chi'_{X,\alpha}\rangle\langle\chi'_{X,\alpha}| \in \mathcal{D}_X, \tag{2.14}$$

where the eigenvalues are ordered decreasingly, $\omega_1 \geq \ldots \geq \omega_{D_X} \geq 0$. The number of non-zero eigenvalues are the rank of the state, $\operatorname{rk}(\varrho_X)$. The state vector can be written with this $\{|\chi'_{X,\alpha}\rangle\}_{\alpha=1}^{D_X} \subset \mathcal{H}_X$ orthonormal basis and an arbitrary $\{|\chi_{\bar{X},\alpha}\rangle\}_{\alpha=1}^{D_{\bar{X}}} \subset \mathcal{H}_{\bar{X}}$ orthonormal basis as

$$|\psi\rangle = \sum_{\alpha=1}^{D_X} \sum_{\beta=1}^{D_{\bar{X}}} c_{\alpha,\beta} |\chi'_{X,\alpha}\rangle \otimes |\chi_{\bar{X},\beta}\rangle = \sum_{\alpha=1}^{D_X} |\chi'_{X,\alpha}\rangle \otimes |\psi_{\bar{X},\alpha}\rangle, \tag{2.15}$$

where $|\psi_{\bar{X},\alpha}\rangle := \sum_{\beta=1}^{D_{\bar{X}}} c_{\alpha,\beta} |\chi_{\bar{X},\beta}\rangle$. (We note that in the whole work, the term *basis* is used for a linearly independent complete set of vectors. In the quantum-chemistry community the similar word is used for an orbital set, hence we use *orbital set* in those cases.) Applying the partial trace (2.6) to the bipartite pure state given by the state vector (2.15), and comparing with (2.14) yields

$$0 = \varrho_X - \operatorname{Tr}_{\bar{X}}(|\psi\rangle\langle\psi|) = \sum_{\alpha,\alpha'=1}^{D_X} \Big(\omega_\alpha \delta_{\alpha,\alpha'} - \langle\psi_{\bar{X},\alpha'}|\psi_{\bar{X},\alpha}\rangle\Big) |\chi'_{X,\alpha}\rangle\langle\chi'_{X,\alpha'}|. \tag{2.16}$$

Since the dyads in (2.16) are linearly independent (form a basis in $\operatorname{Lin}(\mathcal{H}_X)$), the expression in the parentheses must vanish for all $\alpha, \alpha' = 1, \ldots, D_X$. This leads to that the vectors $|\chi'_{\bar{X},\alpha}\rangle := \frac{1}{\sqrt{\omega_\alpha}} |\psi_{\bar{X},\alpha}\rangle$ for all the non-zero ω_α eigenvalues, $\alpha = 1, \ldots, \operatorname{rk}(\varrho_X)$, form an orthonormal set, and we have

$$|\psi\rangle = \sum_{\alpha=1}^{\operatorname{rk}(\varrho_X)} \sqrt{\omega_\alpha} |\chi'_{X,\alpha}\rangle \otimes |\chi'_{\bar{X},\alpha}\rangle, \tag{2.17a}$$

$$\varrho_X = \sum_{\alpha=1}^{\operatorname{rk}(\varrho_X)} \omega_\alpha |\chi'_{X,\alpha}\rangle\langle\chi'_{X,\alpha}|, \qquad \varrho_{\bar{X}} = \sum_{\alpha=1}^{\operatorname{rk}(\varrho_X)} \omega_\alpha |\chi'_{\bar{X},\alpha}\rangle\langle\chi'_{\bar{X},\alpha}|. \tag{2.17b}$$

The *Schmidt rank* of $|\psi\rangle \in \mathcal{H}$ with respect to the bipartition $X|\bar{X}$ is the number of the terms in the above sums, which equals the rank of the reduced states, $\operatorname{rk}(|\psi\rangle) := \operatorname{rk}(\varrho_X) = \operatorname{rk}(\varrho_{\bar{X}})$.

The D_X orthonormal vectors $\{|\chi'_{X,\alpha}\rangle\}_{\alpha=1}^{D_X}$ in $\mathcal{H}_X$ were fixed by the spectral decomposition of ϱ_X (non-uniquely, if there are degenerate eigenvalues), but only $\mathrm{rk}(\varrho_X)$ orthonormal vector is fixed so far in $\mathcal{H}_{\bar{X}}$, however, the remaining $D_{\bar{X}} - \mathrm{rk}(\varrho_X)$ vectors can be chosen to be orthonormal on $\mathcal{H}_{\bar{X}}$, resulting an orthonormal basis $\{|\chi'_{\bar{X},\alpha}\rangle\}_{\alpha=1}^{D_{\bar{X}}}$ on $\mathcal{H}_{\bar{X}}$. By the use of these two bases we can also write

$$|\psi\rangle = \sum_{\alpha=1}^{D_X} \sqrt{\omega_\alpha} |\chi'_{X,\alpha}\rangle \otimes |\chi'_{\bar{X},\alpha}\rangle, \tag{2.18a}$$

$$\varrho_X = \sum_{\alpha=1}^{D_X} \omega_\alpha |\chi'_{X,\alpha}\rangle\langle\chi'_{X,\alpha}|, \qquad \varrho_{\bar{X}} = \sum_{\alpha=1}^{D_{\bar{X}}} \omega_\alpha |\chi'_{\bar{X},\alpha}\rangle\langle\chi'_{\bar{X},\alpha}|, \tag{2.18b}$$

where $\omega_\alpha = 0$ for $D_X < \alpha \leq D_{\bar{X}}$. The two bases are called *Schmidt bases* (which are also the eigenvectors of the reduced states), the coefficients $\sqrt{\omega_\alpha}$ *Schmidt coefficients* (which are also the square roots of the eigenvalues of the reduced states), the procedure *Schmidt decomposition* and the form (2.17) *Schmidt canonical form* [**Sch07**, **Sch36**]. Note that the sum of the square of the Schmidt coefficients is one, being the norm square of the state vector, $\|\psi\|^2 = \mathrm{Tr}(\varrho_X) = \mathrm{Tr}(\varrho_{\bar{X}}) = \sum_\alpha \omega_\alpha = 1$. It is also easy to see that the $X|\bar{X}$-separable pure states (2.11) are given by state vectors of Schmidt rank one, or equivalently having pure marginals, $\mathrm{rk}(|\psi\rangle) = \mathrm{rk}(\varrho_X) = \mathrm{rk}(\varrho_{\bar{X}}) = 1$, that is,

$$|\psi\rangle\langle\psi| \in \mathcal{P}_{X|\bar{X}\text{-sep}} \quad \Longleftrightarrow \quad \mathrm{Tr}_{\bar{X}}(|\psi\rangle\langle\psi|) \in \mathcal{P}_X \quad \Longleftrightarrow \quad \mathrm{Tr}_X(|\psi\rangle\langle\psi|) \in \mathcal{P}_{\bar{X}}. \tag{2.19}$$

Note that, with respect to partition of more than two parts, there is no (2.17)-like decomposition with orthogonal vectors in the subsystems. This leads to the field of *tensor decomposition*, the main concern of this work. Before turning to this, we recall the quantification of correlation and entanglement, which also plays an important role in approaches based on tensor decompositions.

2.3. Measures of correlation and entanglement

Having introduced the notions of uncorrelated (2.9) and separable states (2.10), and correlation of observables (2.8), our aim is to quantify the correlation and the entanglement of the states themselves. We use some important functions over the state space $\mathcal{D}$. The *von Neumann entropy* of a state $\varrho \in \mathcal{D}$,

$$S(\varrho) = -\mathrm{Tr}(\varrho \ln(\varrho)), \tag{2.20}$$

quantifies the *information content* of the state by means of encoding (convertibility) task. It shows important properties, it is non-negative, continuous, concave (that is, $S(\sum_i p_i \varrho_i) \geq \sum_i p_i S(\varrho_i)$ for all decompositions), additive for uncorrelated states, faithful (zero if and only if the state is pure), non-decreasing in bistochastic quantum channels and recursive [**Neu27**, **Ohy93**, **Sch95**, **Wil13**]. The recursive property means that $S(\sum_i p_i \varrho_i) = \sum_i p_i S(\varrho_i) + S(\boldsymbol{p})$ for decompositions of states with mutually orthogonal support, where $S(\boldsymbol{p})$ is the Shannon entropy of the weights. The main point is that the recursive property together with some further natural ones uniquely determines the von Neumann entropy in an axiomatic treatment

[**Sha49**, **Khi57**, **Ohy93**]. The *Rényi entropies*

$$S_\alpha^{\mathrm{R}}(\varrho_{X'}) = \frac{1}{1-\alpha}\ln\bigl(\mathrm{Tr}(\varrho_{X'}^\alpha)\bigr) \tag{2.21}$$

with parameter $\alpha \geq 0$ show slightly less nice properties than the von Neumann entropy. They are non-negative, continuous, concave if $0 < \alpha \leq 1$, additive for uncorrelated states, faithful (zero if and only if the state is pure) and non-decreasing in bistochastic quantum channels, however, not recursive [**Rén61**, **Ohy93**]. In the $\alpha = 0$ case it is the *Hartley entropy* and $\alpha \to 1$ the von Neumann entropy. The *Umegaki relative entropy* of the states $\varrho, \sigma \in \mathcal{D}$,

$$D(\varrho||\sigma) = \mathrm{Tr}\bigl(\varrho(\ln(\varrho) - \ln(\sigma))\bigr), \tag{2.22}$$

quantifies the *distinguishability* of the states as being the exponent of the error probability in hypothesis testing tasks. It has important properties, it is non-negative, continuous, jointly convex, additive for uncorrelated states, zero if and only if $\varrho = \sigma$ and non-increasing in all quantum channels [**Ume62**, **Hia91**, **Ohy93**, **Wil13**].

The correlation of observables was defined previously (2.8), however, our aim is to give to how much extent the state ϱ itself is correlated with respect to a partition. The correlation of a state $\varrho \in \mathcal{D}$ with respect to a partition ξ can be quantified by its distinguishability from the ξ-uncorrelated states (2.9) using the relative entropy (2.22). This is called the *relative entropy of ξ-correlation*, which turns out to be the same as the *ξ-mutual information* [**Her04**, **Pet08**, **Mod10**, **Szal15**, **Szal17**],

$$I_\xi(\varrho) := \min_{\sigma\in\mathcal{D}_{\xi\text{-unc}}} D(\varrho||\sigma) = \sum_{X\in\xi} S(\varrho_X) - S(\varrho), \tag{2.23a}$$

where $\varrho_X = \mathrm{Tr}_{\bar{X}}(\varrho)$. This is because the minimal value is attained when $\sigma = \bigotimes_{X\in\xi}\varrho_X$ [**Mod10**]. The relative entropy of ξ-correlation is a proper correlation measure, since it is *faithful*, that is, it vanishes if and only if the state is ξ-uncorrelated, and *non-increasing* with respect to local operations (LO). The entanglement of a state $\varrho \in \mathcal{D}$ with respect to a partition ξ can also be quantified by its distinguishability from the ξ-separable states (2.10) using the relative entropy (2.22). This is called the *relative entropy of ξ-entanglement* [**Ved98**, **Mod10**],

$$E_\xi(\varrho) := \min_{\sigma\in\mathcal{D}_{\xi\text{-sep}}} D(\varrho||\sigma). \tag{2.23b}$$

Similarly to other motivated entanglement measures [**Hor01**, **Hor09**], this cannot be expressed with a (2.23a)-like, closed formula. The relative entropy of ξ-entanglement is a proper entanglement measure, since it is *faithful*, that is, it vanishes if and only if the state is ξ-separable, and *non-increasing* with respect to local operations and classical communication (LOCC). The quantities defined above by the relative entropy obeys the inequality $E_\xi \leq I_\xi$ by construction, which is the manifestation of that entanglement is a "part" of the "whole" correlation, the "part" which cannot be addressed classically, by means of LOCC [**Mod10**].

A simple consequence of the isomorphisms (2.12) is the *multipartite monotonicity* of the relative entropy of ξ-correlation and ξ-entanglement [**Szal15**, **Szal17**],

$$\upsilon \preceq \xi \quad \Longleftrightarrow \quad I_\upsilon \geq I_\xi, \tag{2.24a}$$

$$\upsilon \preceq \xi \quad \Longleftrightarrow \quad E_\upsilon \geq E_\xi. \tag{2.24b}$$

That is, for finer partitions the states are more correlated and entangled, so the sets of these functions describing correlation and entanglement inherit the structure of the poset Π_L. The smallest functions correspond to the top element $\xi = \top$, which vanish for all $\varrho \in \mathcal{D}$ states, $I_\top(\varrho) = 0$, $E_\top(\varrho) = 0$. The largest functions correspond to the bottom element $\xi = \bot$, these are also called *total correlation* and *total entanglement*. The total correlation can be expressed with the entropies (2.23a),

$$I_{\mathrm{tot}}(\varrho) := I_\bot(\varrho) = \sum_{i \in L} S(\varrho_i) - S(\varrho), \tag{2.25}$$

where $\varrho_i = \mathrm{Tr}_{\overline{\{i\}}}(\varrho)$. For pure states this reduces to the sum of the entropies of the elementary subsystems.

Let us write out the special features of a pure state of the bipartite case, $|\psi\rangle\langle\psi| \in \mathcal{P}(\mathcal{H}_X \otimes \mathcal{H}_{\bar{X}})$. Due to the Schmidt decomposition (2.17), the (non-zero part of the) spectra of the marginals of pure states are equal, counting multiplicities, so

$$S\big(\mathrm{Tr}_{\bar{X}}(|\psi\rangle\langle\psi|)\big) = S\big(\mathrm{Tr}_X(|\psi\rangle\langle\psi|)\big) = -\sum_{\alpha=1}^{\mathrm{rk}(\varrho_X)} \omega_\alpha \ln \omega_\alpha, \tag{2.26}$$

which is the *Shannon entropy* of the square of the Schmidt coefficients. Therefore the $X|\bar{X}$-mutual information (2.23a) is

$$I_{X|\bar{X}}(|\psi\rangle\langle\psi|) = 2S\big(\mathrm{Tr}_{\bar{X}}(|\psi\rangle\langle\psi|)\big) = 2S\big(\mathrm{Tr}_X(|\psi\rangle\langle\psi|)\big). \tag{2.27a}$$

The $X|\bar{X}$-entanglement (2.23b) can also be calculated in this case, which is a far more difficult task [**Ved98**],

$$E_{X|\bar{X}}(|\psi\rangle\langle\psi|) = S\big(\mathrm{Tr}_{\bar{X}}(|\psi\rangle\langle\psi|)\big) = S\big(\mathrm{Tr}_X(|\psi\rangle\langle\psi|)\big). \tag{2.27b}$$

This is just the usual *entanglement entropy* for pure states of bipartite systems, quantifying the entanglement of the state by means of LOCC convertibility task [**Ben96a**, **Ben96b**].

2.4. Tensor decompositions

An arbitrary state vector of the composite system of $n = |L|$ elementary subsystems can be written with respect to tensor product basis formed by local orthonormal bases $\{|\chi_{i,\alpha}\rangle\}_{\alpha=1}^{D_i}$ as

$$|\psi\rangle = \sum_{\alpha_1,\ldots,\alpha_n=1}^{D_1,\ldots,D_n} \psi_{\alpha_1,\ldots,\alpha_n} |\chi_{1,\alpha_1}\rangle \otimes \ldots \otimes |\chi_{n,\alpha_n}\rangle \in \bigotimes_{i=1}^{n} \mathcal{H}_i = \mathcal{H}_L. \tag{2.28}$$

The number of the entries of the coefficient tensor $\boldsymbol{\psi} \in \mathbb{C}^{D_1} \otimes \ldots \otimes \mathbb{C}^{D_n}$ scales exponentially with the n number of elementary subsystems, thus the numerical treatment is unfeasible even for not too large systems. To handle this, we consider methods of *tensor decompositions*. The idea of tensor decompositions is the separation of variables, that is, write a multi-variable function as a sum of product of single-variable functions. Note that, although normalization is not really

an important point here, we consider only state vectors, that is, normalized vectors, $\|\psi\| = 1$, for convenience. For the easier understanding, tensor diagrams are used consisting of boxes and lines. The boxes represent the tensors, lines represent the indices, and the connected lines are the summation indices. In the sequel we consider the decompositions of the coefficient tensor $\boldsymbol{\psi}$, and also illustrate in figure 2.3.

In section 2.2 we have already seen the most basic tensor decomposition method, the Schmidt decomposition (2.18), discussed from the point of view of bipartite quantum state vectors and their entanglement. Now we give a more general discussion from the point of view of basis transformations, which is in general called *singular value decomposition (SVD)* being applicable to arbitrary tensors. For example, in case of $\mathcal{H}_X \otimes \mathcal{H}_{X'}^*$ this is operator SVD, while in case of $\mathcal{H}_X \otimes \mathcal{H}_{\bar{X}}$ this is vector SVD, which is the Schmidt decomposition.

Let us have two finite dimensional Hilbert spaces $\mathcal{H}_X$ and $\mathcal{H}_{X'}$, for which, without the loss of generality, $D_X = \dim(\mathcal{H}_X) \leq \dim(\mathcal{H}_{X'}) = D_{X'}$. For any operator $A \in \mathrm{Lin}(\mathcal{H}_{X'}, \mathcal{H}_X) \cong \mathcal{H}_X \otimes \mathcal{H}_{X'}^*$ there exist non-negative numbers $\sqrt{\omega_\alpha}$, called *singular values*, and orthonormal bases $\{|\chi'_{X,\alpha}\rangle\}_{\alpha=1}^{D_X} \subset \mathcal{H}_X$ and $\{|\chi'_{X',\alpha}\rangle\}_{\alpha=1}^{D_{X'}} \subset \mathcal{H}_{X'}$ such that

$$A = \sum_{\alpha=1}^{D_X} \sqrt{\omega_\alpha} |\chi'_{X,\alpha}\rangle\langle\chi'_{X',\alpha}|, \tag{2.29a}$$

which is the *singular value decomposition* of operator A. This fundamental result in linear algebra, which provides a canonical form [**Ree80**], follows from that all compact operators have polar decomposition, resulting a unitary and a positive semidefinite (that is, normal) operator, and all normal operators have spectral decomposition. We can formulate this equivalently with matrices. Let us write $A = \sum_{\alpha,\beta=1}^{D_X,D_{X'}} A_{\alpha,\beta} |\chi_{X,\alpha}\rangle\langle\chi_{X',\beta}|$ with arbitrary orthonormal bases $\{|\chi_{X,\alpha}\rangle\}_{\alpha=1}^{D_X} \subset \mathcal{H}_X$ and $\{|\chi_{X',\alpha}\rangle\}_{\alpha=1}^{D_{X'}} \subset \mathcal{H}_{X'}$. Then there exist a diagonal matrix $\boldsymbol{S}$ having non-negative entries, and unitary matrices $\boldsymbol{U} \in \mathrm{U}(D_X)$ and $\boldsymbol{V} \in \mathrm{U}(D_{X'})$, such that $\boldsymbol{A} = \boldsymbol{U}\boldsymbol{S}\boldsymbol{V}^\dagger$, that is,

$$A = \sum_{\alpha,\beta=1}^{D_X,D_{X'}} \sum_{\gamma=1}^{D_X} U_{\alpha,\gamma} S_{\gamma,\gamma} V^*_{\beta,\gamma} |\chi_{X,\alpha}\rangle\langle\chi_{X',\beta}|. \tag{2.29b}$$

The connection between the two formulations is that the diagonal matrix contains the singular values, $S_{\alpha,\beta} = \delta_{\alpha,\beta}\sqrt{\omega_\alpha}$, and the basis transformations are performed by unitaries $U = \sum_{\alpha=1}^{D_X} |\chi'_{X,\alpha}\rangle\langle\chi_{X,\alpha}|$ and $V = \sum_{\alpha=1}^{D_{X'}} |\chi'_{X',\alpha}\rangle\langle\chi_{X',\alpha}|$, which have matrix entries $U_{\alpha,\beta} = \langle\chi_{X,\alpha}|\chi'_{X,\beta}\rangle$ and $V_{\alpha,\beta} = \langle\chi_{X',\alpha}|\chi'_{X',\beta}\rangle$ (in both bases). This decomposition is essentially unique, that is, up to reordering and unitary transformation on subspaces corresponding to the same singular value (phases in case of non-degenerate singular values). The Frobenius norm, which is induced by the Hilbert–Schmidt inner product, is the Euclidean norm of the singular values, that is, $\|A\|_{\mathrm{F}}^2 := \mathrm{Tr}(A^\dagger A) = \sum_\alpha \omega_\alpha$.

As we saw in section 2.2, the *Schmidt decomposition* (2.18) states that for any bipartite state vector $|\psi\rangle \in \mathcal{H}_X \otimes \mathcal{H}_{\bar{X}}$ there exist non-negative numbers, $\sqrt{\omega_\beta}$, called *Schmidt coefficients*, and

orthonormal bases $\{|\chi'_{X,\beta}\rangle\}_{\beta=1}^{D_X} \subset \mathcal{H}_X$ and $\{|\chi'_{\bar{X},\bar{\beta}}\rangle\}_{\bar{\beta}=1}^{D_{\bar{X}}} \subset \mathcal{H}_{\bar{X}}$, such that

$$|\psi\rangle = \sum_{\beta=1}^{D_X} \sqrt{\omega_\beta} |\chi'_{X,\beta}\rangle \otimes |\chi'_{\bar{X},\beta}\rangle. \tag{2.30a}$$

We can formulate this equivalently with matrices. The Schmidt decomposition (2.18) states that if we write $|\psi\rangle = \sum_{\alpha,\bar{\alpha}=1}^{D_X,D_{\bar{X}}} \psi_{\alpha,\bar{\alpha}} |\chi_{X,\alpha}\rangle \otimes |\chi_{\bar{X},\bar{\alpha}}\rangle$ with arbitrary orthonormal bases $\{|\chi_{X,\alpha}\rangle\}_{\alpha=1}^{D_X} \subset \mathcal{H}_X$ and $\{|\chi_{\bar{X},\bar{\alpha}}\rangle\}_{\bar{\alpha}=1}^{D_{\bar{X}}} \subset \mathcal{H}_{\bar{X}}$, then, there exist a "diagonal" vector $\boldsymbol{S}$ having non-negative entries, and unitary matrices $\boldsymbol{U} \in \mathrm{U}(D_X)$ and $\boldsymbol{V} \in \mathrm{U}(D_{\bar{X}})$, such that the column vector is $\boldsymbol{\psi} = (\boldsymbol{U} \otimes \boldsymbol{V})\boldsymbol{S}$ (or $\boldsymbol{\psi} = \boldsymbol{U}\boldsymbol{S}\boldsymbol{V}^{\mathrm{t}}$ if we consider $\boldsymbol{S}$ as a matrix), that is,

$$|\psi\rangle = \sum_{\alpha,\bar{\alpha}=1}^{D_X,D_{\bar{X}}} \sum_{\beta=1}^{D_X} U_{\alpha,\beta} S_{\beta,\beta} V_{\bar{\alpha},\beta} |\chi_{X,\alpha}\rangle \otimes |\chi_{\bar{X},\bar{\alpha}}\rangle. \tag{2.30b}$$

The connection between the two formulations is that the vector $\boldsymbol{S}$ contains the Schmidt coefficients, $S_{\alpha,\bar{\alpha}} = \delta_{\alpha,\bar{\alpha}} \sqrt{\omega_\alpha}$, and the basis transformations are performed by unitaries $U = \sum_{\alpha=1}^{D_X} |\chi'_{X,\alpha}\rangle\langle\chi_{X,\alpha}|$ and $V = \sum_{\bar{\alpha}=1}^{D_{\bar{X}}} |\chi'_{\bar{X},\bar{\alpha}}\rangle\langle\chi_{\bar{X},\bar{\alpha}}|$, which have matrix entries $U_{\alpha,\bar{\alpha}} = \langle\chi_{X,\alpha}|\chi'_{X,\bar{\alpha}}\rangle$ and $V_{\alpha,\bar{\alpha}} = \langle\chi_{\bar{X},\alpha}|\chi'_{\bar{X},\bar{\alpha}}\rangle$ (in both bases). The norm is the Euclidean norm of the singular values, that is, $\|\psi\|^2 = \langle\psi|\psi\rangle = \sum_\alpha \omega_\alpha$. The Schmidt decomposition is illustrated in figure 2.3 (b).

We note that the SVD of the operator A is sometimes given as a triple (U, S, V) in the literature, where the entries are the array of orthonormal vectors $|\chi'_{X,\alpha}\rangle \in \mathcal{H}_X$, the array of singular values $\sqrt{\omega_\alpha}$ and the array of orthonormal vectors $|\chi'_{X',\alpha}\rangle \in \mathcal{H}_{X'}$, respectively, such that (2.29a) is fulfilled. When we turn to numerics, instead of abstract tensors, we want to deal with arrays, which can be manipulated, decomposed or approximated, therefore we fix a basis. So we say, equivalently, that we have the SVD of A with respect to orthonormal bases $\{|\chi_{X,\alpha}\rangle\}_{\alpha=1}^{D_X}$ and $\{|\chi_{X',\alpha}\rangle\}_{\alpha=1}^{D_{X'}}$, such that (2.29b) is fulfilled. Similary, we say that we have the Schmidt decomposition of $|\psi\rangle$ with respect to orthonormal bases $\{|\chi_{X,\alpha}\rangle\}_{\alpha=1}^{D_X}$ and $\{|\chi_{\bar{X},\bar{\alpha}}\rangle\}_{\bar{\alpha}=1}^{D_{\bar{X}}}$, such that (2.30b) is fulfilled. From the numerical analysis point of view, the Schmidt decomposition (2.18) can be considered as a direct consequence of the singular value decomposition of the coefficient tensor $\psi_{\alpha,\bar{\alpha}}$. With this simultaneous basis transformation, having numerical cost scaling $\mathcal{O}(D_X^2 D_{\bar{X}})$, the coefficient tensor becomes diagonal, yielding reduction of entries to D_X, assuming $D_X < D_{\bar{X}}$ [**Hac12**]. The main features of the Schmidt decomposition (or the SVD) are that, on the one hand, there is only *one summation*, on the other hand, the transformation to the new bases is *unitary*, that is, orthonormalization is preserved. For more than two tensor factors, these cannot be fulfilled simultanously. Keeping the orthogonality we end up with the *Tucker decomposition*, while keeping the single summation we end up with the *canonical decomposition*.

The tensor product space $\mathcal{H}_1 \otimes \ldots \otimes \mathcal{H}_n$ is spanned by the tensor products of n (not necessarily basis) vectors $|\chi'_i\rangle \in \mathcal{H}_i$, called *elementary tensors* $|\chi'_1\rangle \otimes \ldots \otimes |\chi'_n\rangle$. Then one can write the highly non-unique *canonical decomposition* or m-term representation [**Hac12**] of the state vector (2.28),

$$|\psi\rangle = \sum_{\beta=1}^{m} |\chi'_{1,\beta}\rangle \otimes \ldots \otimes |\chi'_{n,\beta}\rangle. \tag{2.31a}$$

We can formulate this equivalently with matrices. If we have (2.28), we can separate the variables of the coefficient tensor as $\psi_{\alpha_1,\ldots,\alpha_n} = \sum_{\beta=1}^{m} c^{(1)}_{\alpha_1,\beta} \cdot \ldots \cdot c^{(n)}_{\alpha_n,\beta}$, then

$$|\psi\rangle = \sum_{\alpha_1,\ldots,\alpha_n=1}^{D_1,\ldots,D_n} \sum_{\beta=1}^{m} c^{(1)}_{\alpha_1,\beta} \ldots c^{(n)}_{\alpha_n,\beta} |\chi_{1,\alpha_1}\rangle \otimes \ldots \otimes |\chi_{n,\alpha_n}\rangle. \tag{2.31b}$$

(Here we moved the subsystem indices to superscript for brevity.) The connection between the two formulations is that the basis transformations are performed by linear transformation $c^{(i)} = \sum_{\alpha=1}^{m} |\chi'_{i,\alpha}\rangle\langle\chi_{i,\alpha}|$, which have matrix entries $c^{(i)}_{\alpha,\beta} = \langle\chi_{i,\alpha}|\chi'_{i,\beta}\rangle$ (in the not-primed basis). This is, however, not a unitary transformation, so $|\chi'_{i,\alpha}\rangle$ vectors are neither orthogonal nor normalized in general. Finding this factorization with lowest rank m is NP-hard [**Hil13**], and also finding the best $m = 1$ approximation ($n > 2$) is NP-hard. Moreover, this decomposition results a form that suffers from the border rank problem [**Hac12**], that is, sequence of vectors with fixed rank m can converge to one with higher m for $n > 2$. The canonical decomposition is illustrated in figure 2.3 (c), where the single summation index is highlighted on the horizontal legs.

Let us have the state vector (2.28) but now written with respect to another orthonormal tensor product basis indicated by prime. We say that the *Tucker decomposition* with *core tensor* $\tilde{\psi}$ is

$$|\psi\rangle = \sum_{\beta_1,\ldots,\beta_n=1}^{m_1,\ldots,m_n} \tilde{\psi}_{\beta_1,\ldots,\beta_n} |\chi'_{1,\beta_1}\rangle \otimes \ldots \otimes |\chi'_{n,\beta_n}\rangle, \tag{2.32a}$$

where $m_i \leq D_i$ for $i \in [n]$. We can formulate this equivalently with matrices. Consider the Schmidt decompositions with respect to each tensor factor versus the rest, that is, for bipartitions $\{i\}|\overline{\{i\}}$ for all $i \in [n]$ with basis $\{|\chi_{1,\alpha_1}\rangle \otimes \ldots \otimes |\chi_{n,\alpha_n}\rangle\}$. By the obtained unitaries $\boldsymbol{U}^{(i)} \in \mathrm{U}(D_i)$ we have $\boldsymbol{\psi} = (\boldsymbol{U}^{(1)} \otimes \ldots \otimes \boldsymbol{U}^{(n)})\tilde{\boldsymbol{\psi}}$, that is,

$$|\psi\rangle = \sum_{\alpha_1,\ldots,\alpha_n=1}^{D_1,\ldots,D_n} \sum_{\beta_1,\ldots,\beta_n=1}^{m_1,\ldots,m_n} \tilde{\psi}_{\beta_1,\ldots,\beta_n} U^{(1)}_{\alpha_1,\beta_1} \ldots U^{(n)}_{\alpha_n,\beta_n} |\chi_{1,\alpha_1}\rangle \otimes \ldots \otimes |\chi_{n,\alpha_n}\rangle. \tag{2.32b}$$

The connection between the two formulations is that the basis transformations are performed by partial isometries $U^{(i)} = \sum_{\alpha=1}^{m_i} |\chi'_{i,\alpha}\rangle\langle\chi_{i,\alpha}|$, which have matrix entries $U^{(i)}_{\alpha,\beta} = \langle\chi_{i,\alpha}|\chi'_{i,\beta}\rangle$. If the local rank $m_i = D_i$, the operator $U^{(i)}$ is unitary. If the local ranks m_i are less than the local dimensions D_i, this decomposition yields the reduction of entries of $\tilde{\psi}$ compared to the original tensor ψ. However, the core tensor $\tilde{\psi}$ has still exponentially many entries in terms of the number of subsystems, even by truncation to m Schmidt coefficients, scaling as $\mathcal{O}(m^n)$. Moreover, one can easily overshoot with a truncation $m < D_i$ since in applications for physical systems the dimensions of the elementary subsystems are $D_i = \mathcal{O}(1)$. In numerics this decomposition is usually called *higher order SVD*, and illustrated in figure 2.3 (d).

As we begin section 2.1, we have elementary subsystems $i \in \{1, \ldots, n\}$ and the associated Hilbert spaces $\mathcal{H}_1, \ldots, \mathcal{H}_n$, on which observables (that is, physical quantities, for example, projection of angular momentum or the occupation number of orbitals) are represented by self-adjoint operators. When we turn to numerics, we consider some fixed bases (for example, the eigenbases of some distinguished observables) $\{|\chi_{i,\alpha_i}\rangle\}_{\alpha_i=1}^{D_i}$ in $\mathcal{H}_i$ for all $i \in [n]$. That is, the coefficient

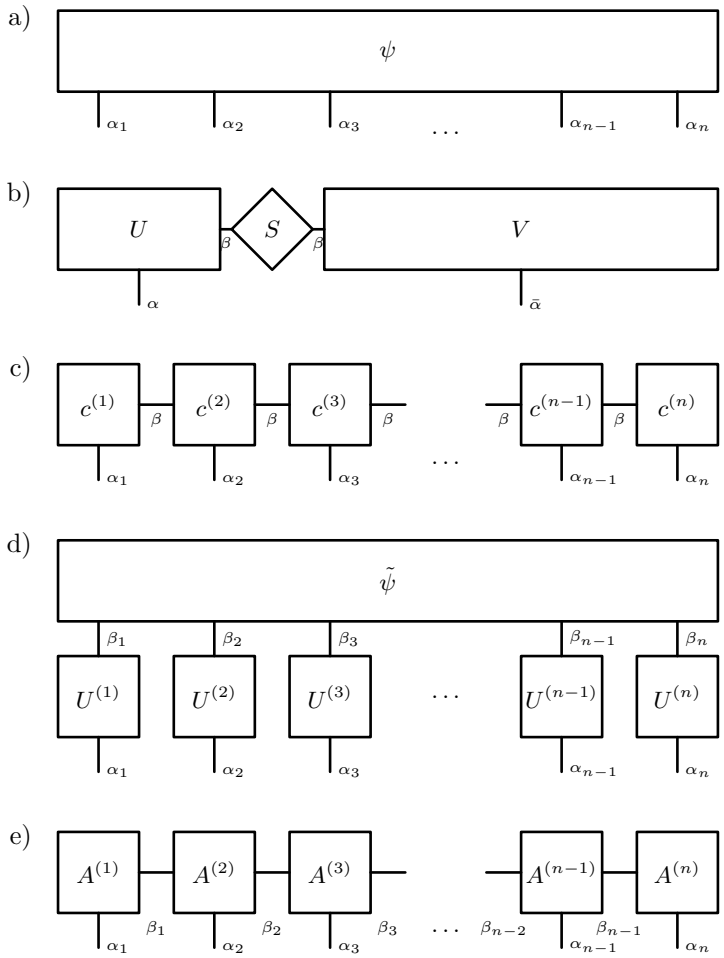

FIGURE 2.3. Graphical illustration of the coefficient tensor (a), its singular value decomposition (b), its canonical decomposition (c), its Tucker decomposition (d) and its matrix product (tensor train) decomposition (e).

tensor $\psi_{\alpha_1,\ldots,\alpha_n}$ in (2.28) determines the state vector $|\psi\rangle$, so the α_i indices are called *physical indices*. While, for example in the (2.32b), indices β_i appear in the given decomposition, that is, performing the summation over them recovers the coefficient tensor $\psi_{\alpha_1,\ldots,\alpha_n}$. On the Hilbert spaces associated to the indices β_i, we do not represent observables hence they are called *virtual indices*. We do not even introduce those Hilbert spaces here, although, from the entanglement point of view, the Schmidt decomposition in section 2.2 shows how to do that. In the graphical illustration, see figure 2.3, they are called *physical* and *virtual legs*, respectively.

2.5. Matrix product states

Another way to factorize the coefficient tensor, which is of central importance in this work, is the *matrix product state (MPS)* or *tensor train decomposition*. To see the construction of the

MPS let us have the state vector (2.28) but now written with respect to another orthonormal tensor product basis. We say that the *left block decimation* of the first i subsystem is [**Sch11**]

$$|\psi\rangle = \sum_{\beta_i,\alpha_{i+1},\dots\alpha_n=1} C^{(i+1)}_{\beta_i,(\alpha_{i+1},\dots\alpha_n)} |\tilde{\chi}_{[i],\beta_i}\rangle \otimes |\chi_{i+1,\alpha_{i+1}}\rangle \otimes \dots \otimes |\chi_{n,\alpha_n}\rangle, \tag{2.33a}$$

where, besides the orthonormal bases of the $i+1,\dots,n$ elementary subsystems, we have the orthonormal basis $|\tilde{\chi}_{[i],\beta_i}\rangle \in \tilde{\mathcal{H}}_{[i]} = \mathcal{H}_{[i]} = \mathcal{H}_1 \otimes \dots \otimes \mathcal{H}_i$, which groups together the elementary subsystems $1,\dots,i$. The ranges of the indices of the elementary subsystems are $\alpha_i \in [D_i]$ and that of the composite system is $\beta_i \in [D_{[i]}]$, where $D_{[i]} = D_1 \cdot \dots \cdot D_i$. (Here tilde is used for the transformed vectors because these will be truncated later.) We can formulate this equivalently with matrices. We have the *tensor train decomposition* from the first to the i-th site,

$$|\psi\rangle = \sum_{\substack{\alpha_1,\alpha_2,\dots,\alpha_n \\ \beta_1,\beta_2,\dots,\beta_i}} U^{(1)}_{(\alpha_1),\beta_1} U^{(2)}_{(\beta_1,\alpha_2),\beta_2} \dots U^{(i)}_{(\beta_{i-1},\alpha_i),\beta_i} C^{(i+1)}_{\beta_i,(\alpha_{i+1},\dots\alpha_n)} |\chi_{1,\alpha_1}\rangle \otimes |\chi_{2,\alpha_2}\rangle \otimes \dots \otimes |\chi_{n,\alpha_n}\rangle. \tag{2.33b}$$

The connection between the two formulations can be shown with *successive Schmidt decompositions* from the first to the i-th site. So let us consider (2.28) and the Schmidt decomposition with respect to bipartition $\{1\}|\{2,3,\dots,n\}$ and basis $\{|\chi_{1,\alpha_1}\rangle \otimes \dots \otimes |\chi_{n,\alpha_n}\rangle\}$. That is, the decomposition of the reshaped $\psi_{\alpha_1,\alpha_2,\alpha_3,\dots,\alpha_n} = C^{(1)}_{(\alpha_1),(\alpha_2,\alpha_3,\dots,\alpha_n)}$ matrix is

$$C^{(1)}_{(\alpha_1),(\alpha_2,\alpha_3,\dots,\alpha_n)} = \sum_{\beta_1} U^{(1)}_{(\alpha_1),\beta_1} S^{(1)}_{\beta_1,\beta_1} V'_{(\alpha_2,\alpha_3,\dots,\alpha_n),\beta_1} \equiv \sum_{\beta_1} (A^{(1)}_{\alpha_1})_{\beta_1} C^{(2)}_{(\beta_1,\alpha_2),(\alpha_3,\dots,\alpha_n)}. \tag{2.34a}$$

In the second equation we merge the Schmidt coefficients $S^{(1)}_{\beta_1,\beta'_1} = \delta_{\beta_1,\beta'_1}\sqrt{\omega^{(1)}_{\beta_1}}$ into $\boldsymbol{V}'$ to get $C^{(2)}$ and $\boldsymbol{U}^{(1)}$ should be considered as the collection of vectors $\boldsymbol{A}^{(1)}_{\alpha_1}$. In the next step, Schmidt decomposition is performed with respect to bipartition $\{1,2\}|\{3,4,\dots,n\}$ and basis $\{U^{(1)}|\chi_{1,\alpha_1}\rangle \otimes \dots \otimes |\chi_{n,\alpha_n}\rangle\}$,

$$C^{(2)}_{(\beta_1,\alpha_2),(\alpha_3,\dots,\alpha_n)} = \sum_{\beta_2} U^{(2)}_{(\beta_1,\alpha_2),\beta_2} S^{(2)}_{\beta_2,\beta_2} V''_{(\alpha_3,\dots,\alpha_n),\beta_2} \equiv \sum_{\beta_2} (A^{(2)}_{\alpha_2})_{\beta_1,\beta_2} C^{(3)}_{(\beta_2,\alpha_3),(\alpha_4,\dots,\alpha_n)}, \tag{2.34b}$$

where $\boldsymbol{U}^{(2)}$ is considered as the collection of matrices $\boldsymbol{A}^{(2)}_{\alpha_2}$. Continuing the decomposition until the i-th subsystem, we get (2.33b), and by setting $i = n$ we have $\psi_{\alpha_1,\alpha_2,\dots,\alpha_n} = \boldsymbol{A}^{(1)}_{\alpha_1}\boldsymbol{A}^{(2)}_{\alpha_2}\dots\boldsymbol{A}^{(n)}_{\alpha_n}$. That is, we can write the state vector in a *matrix product state (MPS)* form corresponding to the tensor product space $\bigotimes_{i=1}^n \mathcal{H}_i$ and bases $\{|\chi_{i,\alpha_i}\rangle\}$ as

$$|\psi\rangle = \sum_{\alpha_1,\alpha_2,\dots,\alpha_n} \boldsymbol{A}^{(1)}_{\alpha_1}\boldsymbol{A}^{(2)}_{\alpha_2}\dots\boldsymbol{A}^{(n)}_{\alpha_n} |\chi_{1,\alpha_1}\rangle \otimes |\chi_{2,\alpha_2}\rangle \otimes \dots \otimes |\chi_{n,\alpha_n}\rangle \in \bigotimes_{i=1}^n \mathcal{H}_i, \tag{2.35a}$$

where the *MPS matrices* are $(A^{(i)}_{\alpha_i})_{\beta_{i-1},\beta_i} := U^{(i)}_{(\beta_{i-1},\alpha_i),\beta_i}$. Writing out the matrix multiplications, we have

$$\psi_{\alpha_1,\alpha_2,\dots,\alpha_n} = \sum_{\beta_1,\beta_2,\dots,\beta_{n-1}=1}^{\tilde{D}_{[1]},\tilde{D}_{[2]},\dots,\tilde{D}_{[n-1]}} (A^{(1)}_{\alpha_1})_{\beta_0,\beta_1} (A^{(2)}_{\alpha_2})_{\beta_1,\beta_2} \dots (A^{(n)}_{\alpha_n})_{\beta_{n-1},\beta_n}, \tag{2.35b}$$

so in this decomposition the number of factor tensors are n, and each has one physical index, and two virtual indices, except for the first and n-th which have one (β_0 and β_n are dummy indices). This can be illustrated well with boxes and lines in figure 2.3 (e). Note that although the illustration of the canonical decomposition looks similar, in that case the tensor factors were not coming form a unitary transformation, and there was only a single summation index.

If the state vector is of maximal rank, then the size of MPS matrices grow exponentially, that is, the range of the indices in (2.35b) are $\tilde{D}_{[i]} = \min\{D_{[i]}, D_{\overline{[i]}}\}$. One of the main reasons for using MPS is that the approximation of the exact tensor $\psi_{\alpha_1,\alpha_2,\ldots,\alpha_n}$ can be made easily by the controlling the $\tilde{D}_{[i]}$ numbers. Also, in TNS methods we want to build a procedure in which the approximation is performed iteratively, that is, performing local updates on the factor spaces. In case of MPS, this means sweeping through the tensor network from the left to right and from right to left. To elucidate this let us write the recursion of the basis transformation from the left

$$U^{(i+1)} = \sum_{\alpha_X,\alpha_{i+1}=1}^{\tilde{D}_X,D_{i+1}} |\tilde{\chi}_{X',(\alpha_X,\alpha_{i+1})}\rangle(\langle\tilde{\chi}_{X,\alpha_X}| \otimes \langle\chi_{i+1,\alpha_{i+1}}|). \tag{2.36a}$$

This shows how the composite left block $X = \{1,\ldots,i\}$ and the elementary subsystems $i+1$ are folded into the new left block $X' = X \cup \{i+1\}$. The recursion continues with the relabelling $X' \mapsto X$ and the mapping of the composite index $\alpha_{X'} = (\alpha_X, \alpha_{i+1}) \mapsto \alpha_X$. The same successive Schmidt decompositions can be done as before in (2.34), but performing decimation from the right, which yields the recursion of the basis transformation from the right

$$V^{(i-1)} = \sum_{\alpha_{i-1},\alpha_Z=1}^{D_{i-1},\tilde{D}_Z} |\tilde{\chi}_{Z',(\alpha_{i-1},\alpha_Z)}\rangle(\langle\chi_{i-1,\alpha_{i-1}}| \otimes \langle\tilde{\chi}_{Z,\alpha_Z}|). \tag{2.36b}$$

This shows how the elementary subsystems $i-1$ and the composite right block $Z = \{i,\ldots,n\}$ are folded into the new right block $Z' = \{i-1\} \cup Z$. The recursion continues with the relabelling $Z' \mapsto Z$ and the mapping of the composite index $\alpha_{Z'} = (\alpha_{i-1}, \alpha_Z) \mapsto \alpha_Z$. We obtain a subspace approximation by applying *truncation* on the $\tilde{D}_{X'} \leq \tilde{D}_X D_{i+1} \leq D_{X'}$ number of the new basis vectors of the left block,

$$\mathrm{Span}\big\{|\tilde{\chi}_{X',\alpha_{X'}}\rangle \;\big|\; \alpha_{X'} = 1,\ldots,\tilde{D}_{X'}\big\} =: \tilde{\mathcal{H}}_{X'} \subseteq \tilde{\mathcal{H}}_X \otimes \mathcal{H}_{i+1} \subseteq \mathcal{H}_{X'} = \mathcal{H}_1 \otimes \ldots \otimes \mathcal{H}_{i+1}, \tag{2.37a}$$

and similarly, by applying truncation on the $\tilde{D}_{Z'} \leq D_{i-1}\tilde{D}_Z \leq D_{Z'}$ number of the new basis vectors of the right block,

$$\mathrm{Span}\big\{|\tilde{\chi}_{Z',\alpha_{Z'}}\rangle \;\big|\; \alpha_{Z'} = 1,\ldots,\tilde{D}_{Z'}\big\} =: \tilde{\mathcal{H}}_{Z'} \subseteq \mathcal{H}_{i-1} \otimes \tilde{\mathcal{H}}_Z \subseteq \mathcal{H}_{Z'} = \mathcal{H}_{i-1} \otimes \ldots \otimes \mathcal{H}_n. \tag{2.37b}$$

This reveals why we call (2.33a) decimation. This subspace approximation method will be further motivated by the density matrix renormalization group method, discussed in the next section. The truncation in the number of basis vectors, that is, restricting the sum in (2.36), yields not unitaries but partial isometries on $\tilde{\mathcal{H}}_X \otimes \mathcal{H}_{i+1}$ and $\mathcal{H}_{i-1} \otimes \tilde{\mathcal{H}}_Z$, respectively. The corresponding MPS matrices are

$$(A^{(i+1)}_{\alpha_{i+1}})_{\alpha_X,\alpha_{X'}} := U^{(i+1)}_{(\alpha_X,\alpha_{i+1}),\alpha_{X'}}, \qquad (A^{(i-1)}_{\alpha_{i-1}})_{\alpha_{Z'},\alpha_Z} := V^{(i-1)*}_{(\alpha_{i-1},\alpha_Z),\alpha_{Z'}}, \tag{2.38}$$

which are of sizes $\tilde{D}_X \times \tilde{D}_{X'}$ and $\tilde{D}_{Z'} \times \tilde{D}_Z$, respectively. This makes the range of virtual indices (horizontal legs in figure 2.3) truncated to the $\tilde{D}_{X'}$ and $\tilde{D}_{Z'}$ numbers, which are called *bond dimensions*. Sweeping from the left (2.36a), the MPS matrices are *left-canonical*, $\sum_\alpha \boldsymbol{A}_\alpha^{(i+1)\dagger}\boldsymbol{A}_\alpha^{(i+1)} = \mathbf{I}_{\tilde{D}_{X'}}$, which is the consequence of the decomposition into unitary matrices. After truncation to partial isometries we do not have the resolution of identity in X, that is, $\sum_\alpha \boldsymbol{A}_\alpha^{(i+1)}\boldsymbol{A}_\alpha^{(i+1)\dagger} \neq \mathbf{I}_{\tilde{D}_X}$. Sweeping from the right (2.36b), the MPS matrices are *right-canonical*, $\sum_\alpha \boldsymbol{A}_\alpha^{(i-1)}\boldsymbol{A}_\alpha^{(i-1)\dagger} = \mathbf{I}_{\tilde{D}_{Z'}}$, which is the consequence of the decomposition into unitary matrices. After truncation to partial isometries we do not have the resolution of identity in Z, that is, $\sum_\alpha \boldsymbol{A}_\alpha^{(i-1)\dagger}\boldsymbol{A}_\alpha^{(i-1)} \neq \mathbf{I}_{\tilde{D}_Z}$. As a consequence, the MPS decomposition in the form of (2.35) is non-unique, moreover, arbitrary invertible $\tilde{D}_X \times \tilde{D}_X$ matrix and its inverse can be inserted between the MPS matrices. As we will see in the DMRG algorithm, the state vector appears in the *mixed-canonical* MPS form, that is, there are left-canonical matrices on the left, right-canonical ones on the right and some remaining tensors between them.

We consider the set of (normalized) state vectors which have MPS form (2.35) corresponding to the tensor product space $\bigotimes_{i=1}^n \mathcal{H}_i$ and bases $\{|\chi_{i,\alpha_i}\rangle\}$ with *fixed bond dimensions* $\tilde{\boldsymbol{D}}$,

$$\mathcal{M}_{\tilde{\boldsymbol{D}}}\Big(\bigotimes_{i=1}^n \mathcal{H}_i\Big) := \Big\{|\psi\rangle \in \bigotimes_{i=1}^n \mathcal{H}_i \;\Big|\; \tilde{\boldsymbol{D}} = (\tilde{D}_{[1]},\dots,\tilde{D}_{[n-1]}), \boldsymbol{A}_\alpha^{(i)} \in \mathbb{C}^{\tilde{D}_{[i-1]}\times\tilde{D}_{[i]}} \text{ in (2.35)}\Big\}. \quad (2.39)$$

In the sequel we consider the tensor product space and the bases to be fixed in (2.39), therefore, for simplicity, the argument of $\mathcal{M}_{\tilde{\boldsymbol{D}}}$ is dropped in (2.39). If we happen to write MPS corresponding to a different bases, and we will do so in chapter 4, we can express it in terms of a unitary basis transformation $U \in \mathrm{U}(\mathcal{H}_L)$, that is, $\mathcal{M}_{\tilde{\boldsymbol{D}}}(U)$. This will be important when applying fermionic mode transformation in chapter 4. Taking the sum of two vectors in $\mathcal{M}_{\tilde{\boldsymbol{D}}}$ will result in general an MPS with bond dimensions $(2\tilde{D}_{[1]}, 2\tilde{D}_{[2]},\dots,2\tilde{D}_{[n-1]})$, therefore $\mathcal{M}_{\tilde{\boldsymbol{D}}}$ is not a vector subspace rather a manifold in $\mathcal{H}_L$ [**Hae14**]. This sum can be compressed back to a vector in $\mathcal{M}_{\tilde{\boldsymbol{D}}}$ by SVD or by a variational method [**Sch11**]. We write $\mathcal{M}_{\tilde{D}_{\max}}$ if the bond dimension on each virtual index is maximized to $\tilde{D}_{\max}$. One can also think of these MPSs that the matrices are of the same size $\tilde{D}_{\max}\times\tilde{D}_{\max}$ but some are padded with zeros since we do not force full rank matrices in the definition (2.39). We note that, contrary to the canonical decomposition, the MPS form does not suffer from the border rank problem [**Hac12**]. For more about the geometry of MPS see [**Hac12**, **Hol12b**, **Hae14**].

Now the question is, which basis vectors should be kept and which thrown, and what error is made by this truncation. For this, assume we had generated the exact left-canonical MPS form of the state vector $|\psi\rangle$, that is, we have access to the Schmidt coefficients and the MPS matrices (2.38) (or equivalently to the unitary (2.36a)), which have bond dimensions $\min\{D_{[i]}, D_{\overline{[i]}}\}$ if the rank is maximal. Then, according to (2.37a), the projection $\mathrm{I}_{\tilde{\mathcal{H}}_{[i]}} = \sum_{\alpha=1}^{\tilde{D}_{[i]}} |\tilde{\chi}_{[i],\alpha}\rangle\langle\tilde{\chi}_{[i],\alpha}|$ maps onto the truncated subspace $\tilde{\mathcal{H}}_{[i]}$, and let us choose the basis vectors in (2.37a) such that they correspond to the $\tilde{D}_{[i]}$ largest Schmidt coefficients. It is easy to see that by the application of the series of projections $P_i = \mathrm{I}_{\tilde{\mathcal{H}}_{[i]}} \otimes \mathrm{I}_{\mathcal{H}_{\overline{[i]}}}$, the truncated vector $P_{n-1}\dots P_2P_1|\psi\rangle$ is a non-normalised MPS (2.39) with bond dimensions $\tilde{\boldsymbol{D}} = (\tilde{D}_{[1]},\dots,\tilde{D}_{[n-1]})$. The emerging error can be bounded

[Ver06a] as

$$\||\psi\rangle - P_{n-1}\dots P_2P_1|\psi\rangle\|^2 \leq \sum_{i=1}^{n-1}\epsilon_i(\tilde{D}_{[i]}), \tag{2.40}$$

where the *truncation error* at the i-th cut is the sum of the discarded squared Schmidt coefficients,

$$\epsilon_i(D) := 1 - \sum_{\alpha=1}^{D}\omega_\alpha^{(i)}. \tag{2.41}$$

Note that we use again the convention of decreasingly ordered Schmidt coefficients. That is, the accumulated truncation error from the *exact* successive Schmidt decompositions gives an upper bound for the error of the state vector. In practice, of course, we have only access to the truncation error (2.41) made on the *current* state vector, which can be used in applications as an error estimator [Leg96, Leg03a].

In practice one can predefine a $\tilde{D}_{\max}$ maximal bond dimension, however, a more sophisticated treatment is to control the bond dimension such that the Schmidt coefficients below the fixed *truncation error threshold* ω_{Tr} are discarded. By this the bond dimensions

$$\tilde{D}_{[i]}(\omega_{\mathrm{Tr}}) = \max\left\{\alpha \;\middle|\; \omega_\alpha^{(i)} \geq \omega_{\mathrm{Tr}}\right\} \tag{2.42}$$

are set dynamically for all i-th cut. If the decay of the Schmidt spectrum is exponential, which is often observed in physical systems, then the truncation error (2.41) is of the same order of magnitude as ω_{Tr} [Ver06a].

The pure state of the system given by the MPS (2.35) is

$$\begin{aligned}|\psi\rangle\langle\psi| = \sum_{\substack{\alpha_1,\alpha_2,\dots,\alpha_n\\ \alpha_1',\alpha_2',\dots,\alpha_n'}} &\boldsymbol{A}^{(1)}_{\alpha_1}\boldsymbol{A}^{(2)}_{\alpha_2}\dots\boldsymbol{A}^{(n)}_{\alpha_n}\boldsymbol{A}^{(n)\dagger}_{\alpha_n'}\dots\boldsymbol{A}^{(2)\dagger}_{\alpha_2'}\boldsymbol{A}^{(1)\dagger}_{\alpha_1'}\times\\ &\times|\chi_{1,\alpha_1}\rangle\langle\chi_{1,\alpha_1'}|\otimes|\chi_{2,\alpha_2}\rangle\langle\chi_{2,\alpha_2'}|\otimes\dots\otimes|\chi_{n,\alpha_n}\rangle\langle\chi_{n,\alpha_n'}|.\end{aligned} \tag{2.43}$$

The reduced density matrix can be obtained by the contraction on the legs on which the partial trace is applied. The expectation value of a product observable $O = O^{(1)}\otimes O^{(2)}\otimes\dots\otimes O^{(n)}$ in the pure state $|\psi\rangle\langle\psi|$ is

$$\begin{aligned}&\langle\psi|O|\psi\rangle =\\ &\sum_{\substack{\alpha_n,\\ \alpha_n'}} O^{(n)}_{n,\alpha_n',\alpha_n}\boldsymbol{A}^{(n)\dagger}_{n,\alpha_n'}\left(\dots\left(\sum_{\substack{\alpha_2,\\ \alpha_2'}} O^{(2)}_{\alpha_2',\alpha_2}\boldsymbol{A}^{(2)\dagger}_{\alpha_2'}\left(\sum_{\substack{\alpha_1,\\ \alpha_1'}} O^{(1)}_{\alpha_1',\alpha_1}\boldsymbol{A}^{(1)\dagger}_{\alpha_1'}\boldsymbol{A}^{(1)}_{\alpha_1}\right)\boldsymbol{A}^{(2)}_{\alpha_2}\right)\dots\right)\boldsymbol{A}^{(n)}_{\alpha_n},\end{aligned} \tag{2.44}$$

where $O^{(i)} \in \mathrm{Lin}(\mathcal{H}_i)$ and its matrix elements are $O^{(i)}_{\alpha_i',\alpha_i} = \langle\chi_{i,\alpha_i'}|O^{(i)}|\chi_{i,\alpha_i}\rangle$. For graphical illustrations see figure 2.4.

If we consider the Hamiltonian $H \in \mathrm{Lin}_{\mathrm{SA}}(\mathcal{H}_L)$ of the system, we can put the MPS approximation into a different, variational perspective, which will be argued in the following sections. The q-th lowest *energy eigenvalue* of H, for $q = 0,\dots,D_L-1$, can be expressed as

$$E_q^{\mathrm{FCI}} = \min\left\{\langle\psi|H|\psi\rangle \;\middle|\; |\psi\rangle\in\mathcal{H}_L, \|\psi\|=1, \langle\psi_{q'}^{\mathrm{FCI}}|\psi\rangle = 0, \forall q' < q\right\}, \tag{2.45}$$

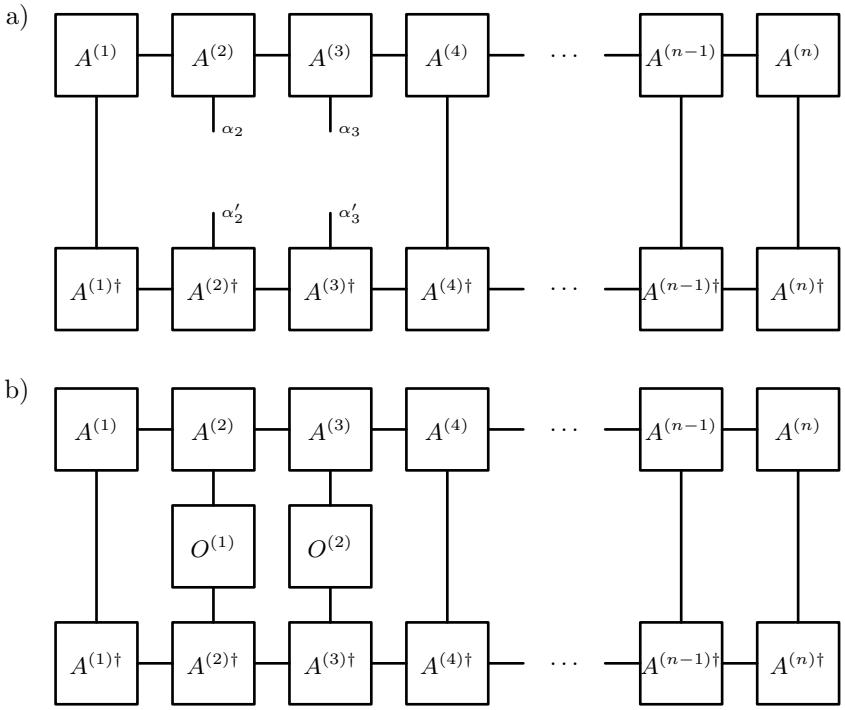

FIGURE 2.4. The calculation of the reduced density matrix $\mathrm{Tr}_{\overline{\{2,3\}}}(|\psi\rangle\langle\psi|)$ (a) and the expectation value of the bilocal operator $O = \mathrm{I}\otimes O^{(2)}\otimes O^{(3)}\otimes \mathrm{I}\otimes\ldots\otimes\mathrm{I}$ (b) is performed by the contraction of the tensor network.

where the vector $|\psi_q^{\mathrm{FCI}}\rangle$ is the corresponding minimizer. The *full configuration interaction (FCI)* notation (motivated by quantum chemistry notions, and discussed in appendix C) refers to the exact treatment of the eigenvalue problem of H in the Hilbert space $\mathcal{H}_L$. Contrary, an approximate solution can be obtained by the MPS approach. The q-th lowest *energy expectation value* of H, for $q = 0,\ldots,D_L-1$, among the MPSs with bond dimensions $\tilde{\boldsymbol{D}}$ can be expressed as

$$E_q^{\tilde{\boldsymbol{D}}} = \min\Big\{\langle\psi|H|\psi\rangle \;\Big|\; |\psi\rangle\in\mathcal{M}_{\tilde{\boldsymbol{D}}}, \langle\psi_{q'}^{\tilde{\boldsymbol{D}}}|\psi\rangle = 0, \forall q' < q\Big\}, \tag{2.46}$$

where the vector $|\psi_q^{\tilde{\boldsymbol{D}}}\rangle$ is the corresponding minimizer. Note that, $\mathcal{M}_{\tilde{\boldsymbol{D}}}$ contains normalized vectors only. Since $\mathcal{M}_{\tilde{\boldsymbol{D}}}$ is a submanifold in $\mathcal{H}_L$, the inequality $E_q^{\mathrm{FCI}} \le E_q^{\tilde{\boldsymbol{D}}}$ holds, and we say that the energy of the system is $E_q^{\tilde{\boldsymbol{D}}}$ within the MPS the approximation with bond dimensions $\tilde{\boldsymbol{D}}$. If the bond dimensions are the maximal, that is, there is no truncation in (2.37), the MPS energy is the exact eigenvalue. One can introduce a partial order between the bond dimension vectors, $\tilde{\boldsymbol{D}} \le \tilde{\boldsymbol{D}}'$ if $\tilde{D}_i \le \tilde{D}'_i$ for all i. With this we have the nested manifolds $\mathcal{M}_{\tilde{\boldsymbol{D}}} \subseteq \mathcal{M}_{\tilde{\boldsymbol{D}}'}$ if $\tilde{\boldsymbol{D}} \le \tilde{\boldsymbol{D}}'$. In (2.46) the MPS matrices can be considered as variational parameters, so the minimisation is in bigger set, therefore, $E_q^{\mathrm{FCI}} \le E_q^{\tilde{\boldsymbol{D}}'} \le E_q^{\tilde{\boldsymbol{D}}}$. The aim is to solve (2.45), in which one meets the curse of dimensionality, so the minimization (2.46) is considered instead. However, it is also unfeasible to do the minimization simultaneously on the all matrices, so iterative minimization is

carried out. This approach has an intimate connection with the density matrix renormalization group algorithm, which is discussed in the next section.

2.6. Density matrix renormalization group algorithm

Let us consider the Hamiltonian of the composite system in a general form

$$H = \sum_k H_{1,k} \otimes \ldots \otimes H_{n,k} \in \mathrm{Lin}_{\mathrm{SA}}(\mathcal{H}_1 \otimes \ldots \otimes \mathcal{H}_n), \tag{2.47}$$

where, as in (2.28), the factor Hilbert spaces $\mathcal{H}_i$ corresponding to elementary subsystems $i \in L = [n]$ are of dimensions D_i. Here the summation over k just indicates an arbitrary decomposition of H into elementary tensors, however, in a clever implementation there are *m*any *p*ossibilities for *o*ptimization, leading to the matrix product operator MPO decomposition of H [**Sch11**]. Our aim is to find approximate solutions of some of the lowest eigenvalues and eigenvectors and quantities calculated from them. The *density matrix renormalization group (DMRG)* algorithm is based on the observation that the relevant quantities in physical systems can be captured by a decimation (truncation) based on the spectrum of the reduced state (2.18).

In the algorithm an iteration step is called the *s-site DMRG step* at the ℓ-th cut, where s is usually one or two. In an s-site DMRG step the following steps are carried out,

(i) diagonalization of the effective Hamiltonian $H_{(\ell)}$,
(ii) truncation of the reduced density matrix $\mathrm{Tr}_{\overline{X'}}(\varrho)$,
(iii) renormalization of the operators $\tilde{H}_{X',k}$ building the effective Hamiltonian of the next step.

A *rightward sweep* is the consecutive iteration steps for $\ell = 1, 2, \ldots, n-s$, and a *leftward sweep* is the consecutive iteration steps for $\ell = n-s-1, n-s-2, \ldots, 2$. The whole DMRG run consists of several consecutive leftward- and rightward sweeps. Now let us detail each step.

In step (i), the Hamiltonian of form (2.47) is approximated by the *effective Hamiltonian* at the ℓ-th cut

$$H_{(\ell)} = \sum_k \tilde{H}_{X,k} \otimes H_{Y,k} \otimes \tilde{H}_{Z,k} \in \mathrm{Lin}_{\mathrm{SA}}(\tilde{\mathcal{H}}_X \otimes \mathcal{H}_Y \otimes \tilde{\mathcal{H}}_Z). \tag{2.48}$$

The subsystem $Y = \{\ell+1, \ldots \ell+s\}$ consists of s elementary subsystems, $\mathcal{H}_Y = \otimes_{i\in Y}\mathcal{H}_i$ of dimension $D_Y = \prod_{i\in Y} D_i$. Here the operators $H_{Y,k} \in \mathrm{Lin}(\mathcal{H}_Y)$ are written without approximation, that is, in their exact form. Contrary, the Hilbert spaces $\tilde{\mathcal{H}}_X$ and $\tilde{\mathcal{H}}_Z$ correspond to the *left block* and *right block*, compress the comprising elementary subsystems $X = \{1, \ldots, \ell\}$ and $Z = \{\ell+s+1, \ldots, n\}$, respectively, which are, we will see in the sequel, subspaces $\tilde{\mathcal{H}}_X \subseteq \mathcal{H}_X$, $\tilde{\mathcal{H}}_Z \subseteq \mathcal{H}_Z$. The dimensions of the left and right blocks are called *block sizes*, $\tilde{D}_X \leq D_X$ and $\tilde{D}_Z \leq D_Z$, respectively, which are controlled and depending on the resources. The operators $\tilde{H}_{X,k} \in \mathrm{Lin}(\tilde{\mathcal{H}}_X)$ and $\tilde{H}_{Z,k} \in \mathrm{Lin}(\tilde{\mathcal{H}}_Z)$ in these spaces are written in an approximate form (hence the tilde above the operators) and constructed in an iterative manner. In figure 2.5 the $s = 2$ setting is depicted. The q-th lowest *energy eigenvalue* of the effective Hamiltonian, for $q = 0, \ldots, \tilde{D}_X D_Y \tilde{D}_Z - 1$, can be expressed as

$$E_q^{(\ell)} = \min\Big\{ \langle\psi|H_{(\ell)}|\psi\rangle \;\Big|\; |\psi\rangle \in \tilde{\mathcal{H}}_X \otimes \mathcal{H}_Y \otimes \tilde{\mathcal{H}}_Z, \|\psi\| = 1, \langle\psi_{q'}^{(\ell)}|\psi\rangle = 0, \forall q' < q \Big\}, \tag{2.49}$$

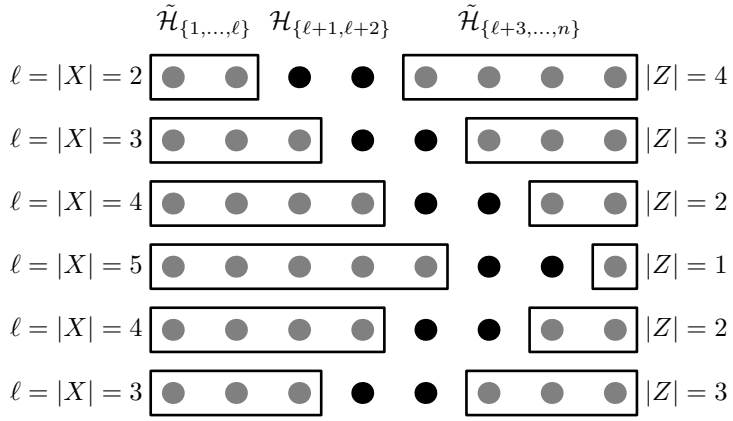

FIGURE 2.5. Subsystems of the two-site DMRG ($s = 2$). Sweeping in the two-site DMRG algorithm

where the vector $|\psi_q^{(\ell)}\rangle$ is the minimizer. Solving the full eigenvalue problem (2.49) of the effective Hamiltonian is unfeasible, and not even necessary in most of the applications. Therefore some of the lowest eigenvalues and the corresponding eigenvectors, which are of the form

$$|\psi_q^{(\ell)}\rangle = \sum_{\alpha_X,\alpha_Y,\alpha_Z=1}^{\tilde{D}_X,D_Y,\tilde{D}_Z} x^{(q)}_{\alpha_X,\alpha_Y,\alpha_Z} |\tilde{\chi}_{X,\alpha_X}\rangle \otimes |\chi_{Y,\alpha_Y}\rangle \otimes |\tilde{\chi}_{Z,\alpha_Z}\rangle, \tag{2.50}$$

are calculated by *iterative diagonalization* algorithms (for example, Lánczos or Davidson algorithm).

In step (ii), the state of the whole system $L = \{X \cup Y \cup Z\}$, which is in $\mathcal{D}(\mathcal{H}_L)$, is approximated by $\varrho \in \mathcal{D}(\tilde{\mathcal{H}}_X \otimes \mathcal{H}_Y \otimes \tilde{\mathcal{H}}_Z)$. In the simplest case, which is the usual practice, the pure state $\varrho = |\psi_0^{(\ell)}\rangle\langle\psi_0^{(\ell)}|$ is considered. One can also form the statistical mixture of excited eigenstates with weights w_q, for example Gibbs(-like) states, $\varrho = \sum_q w_q |\psi_q^{(\ell)}\rangle\langle\psi_q^{(\ell)}|$ [**Sch05**, **Noa05**, **Sza15**]. The reduced state of the extended left-/right block is constructed, and the truncation is performed in its eigenbasis. So in case of the rightward sweep, we obtain the *reduced state* $\varrho_{X'} = \mathrm{Tr}_{\overline{X'}}(\varrho) \in \mathcal{D}(\tilde{\mathcal{H}}_X \otimes \mathcal{H}_{\ell+1})$ of the subsystem $X' = X \cup \{\ell+1\}$ by the partial trace (2.6),

$$\varrho_{X'} = \sum_{\alpha_X,\alpha'_X=1}^{\tilde{D}_X} \sum_{\alpha_{\ell+1},\alpha'_{\ell+1}=1}^{D_{\ell+1}} (\varrho_{X'})_{(\alpha_X,\alpha_{\ell+1}),(\alpha'_X,\alpha'_{\ell+1})} |\tilde{\chi}_{X,\alpha_X} \otimes \chi_{\ell+1,\alpha_{\ell+1}}\rangle\langle\tilde{\chi}_{X,\alpha'_X} \otimes \chi_{\ell+1,\alpha'_{\ell+1}}|, \tag{2.51a}$$

where the coefficients are the entries of the *reduced density matrix* $\boldsymbol{\varrho}_{X'}$ of the *new left block* X' written in the composite Hilbert space $\tilde{\mathcal{H}}_X \otimes \mathcal{H}_{\ell+1}$. This is the point in the algorithm where one sets a limit to the growing dimensions. The reduced state $\varrho_{X'}$ is approximated in the subspace $\tilde{\mathcal{H}}_{X'} \subseteq \tilde{\mathcal{H}}_X \otimes \mathcal{H}_{\ell+1}$ spanned by eigenvectors $|\tilde{\chi}_{X',\alpha_{X'}}\rangle$ corresponding to the $\tilde{D}_{X'} \leq \tilde{D}_X D_{\ell+1}$ highest eigenvalues of $\varrho_{X'}$. Thus the *truncated* reduced state $\tilde{\varrho}_{X'} \in \mathcal{D}(\tilde{\mathcal{H}}_{X'})$ in the eigenbasis is

$$\tilde{\varrho}_{X'} = \sum_{\alpha_{X'}=1}^{\tilde{D}_{X'}} \omega_{\alpha_{X'}} |\tilde{\chi}_{X',\alpha_{X'}}\rangle\langle\tilde{\chi}_{X',\alpha_{X'}}|, \tag{2.51b}$$

where the $\omega_{\alpha_{X'}}$ eigenvalues are re-normalized such that $\mathrm{Tr}(\tilde{\varrho}_{X'}) = 1$. The connection between the two states can be expressed by the partial isometry

$$U^{(\ell+1)} = \sum_{(\alpha_X,\alpha_{\ell+1})=1}^{\tilde{D}_{X'}} |\tilde{\chi}_{X',(\alpha_X,\alpha_{\ell+1})}\rangle\langle\tilde{\chi}_{X,\alpha_X} \otimes \chi_{\ell+1,\alpha_{\ell+1}}|, \tag{2.51c}$$

where the composite index $\alpha_{X'} = (\alpha_X, \alpha_{\ell+1})$ is ordered such that the $\omega_{\alpha_{X'}}$ eigenvalues are ordered non-increasingly. This partial isometry maps from the composite system $\tilde{\mathcal{H}}_X \otimes \mathcal{H}_{\ell+1}$ to its subspace, the Hilbert space of the new left block $\tilde{\mathcal{H}}_{X'}$. The truncation yields $U^{(\ell+1)\dagger}U^{(\ell+1)} \neq \mathrm{I}_{\tilde{\mathcal{H}}_X\otimes\mathcal{H}_{\ell+1}}$. With the projection $U^{(\ell+1)}U^{(\ell+1)\dagger} = \mathrm{I}_{\tilde{\mathcal{H}}_{X'}}$, which is the identity in the new left block, the reduced state of the new left block is $\tilde{\varrho}_{X'} = \mathrm{I}_{\tilde{\mathcal{H}}_{X'}}\varrho_{X'}\mathrm{I}_{\tilde{\mathcal{H}}_{X'}}/\mathrm{Tr}(\mathrm{I}_{\tilde{\mathcal{H}}_{X'}}\varrho_{X'}\mathrm{I}_{\tilde{\mathcal{H}}_{X'}})$. We can formulate this equivalently with matrices. The reduced density matrix of the new left block is $\boldsymbol{\omega} = \boldsymbol{U}^{(\ell+1)\dagger}\boldsymbol{\varrho}_{X'}\boldsymbol{U}^{(\ell+1)}/\mathrm{Tr}(\boldsymbol{U}^{(\ell+1)\dagger}\boldsymbol{\varrho}_{X'}\boldsymbol{U}^{(\ell+1)})$, where the matrix of the partial isometry is rectangular, $\boldsymbol{U}^{(\ell+1)} \in \mathbb{C}^{\tilde{D}_X D_{\ell+1}\times\tilde{D}_{X'}}$, with entries $U^{(\ell+1)}_{(\alpha_X,\alpha_{\ell+1}),\alpha_{X'}} = \langle\tilde{\chi}_{X,\alpha_X} \otimes \chi_{\ell+1,\alpha_{\ell+1}}|\tilde{\chi}_{X',(\alpha_X,\alpha_{\ell+1})}\rangle$, and the $\boldsymbol{\omega}$ is diagonal containing the eigenvalues. Similarly, in case of leftward sweep, we obtain the *reduced state* $\varrho_{Z'} \in \mathcal{H}_{\ell+s} \otimes \tilde{\mathcal{H}}_Z$ of the subsystem $Z' = \{\ell + s\} \cup Z$,

$$\varrho_{Z'} = \sum_{\alpha_{\ell+s},\alpha'_{\ell+s}=1}^{D_{\ell+s}} \sum_{\alpha_Z,\alpha'_Z=1}^{\tilde{D}_Z} (\varrho_{Z'})_{(\alpha_{\ell+s},\alpha_Z),(\alpha'_{\ell+s},\alpha'_Z)}|\chi_{\ell+s,\alpha_{\ell+s}} \otimes \tilde{\chi}_{Z,\alpha_Z}\rangle\langle\chi_{\ell+s,\alpha'_{\ell+s}} \otimes \tilde{\chi}_{Z,\alpha'_Z}|, \tag{2.51d}$$

where the coefficients are the entries of the *reduced density matrix* $\boldsymbol{\varrho}_{Z'}$ of the *new right block* Z' written in the composite Hilbert space. The reduced state $\varrho_{Z'}$ is approximated in the subspace $\tilde{\mathcal{H}}_{Z'} \subseteq \mathcal{H}_{\ell+s}\otimes\tilde{\mathcal{H}}_Z$ spanned by eigenvectors $|\tilde{\chi}_{Z',\alpha_{Z'}}\rangle$ corresponding to the $\tilde{D}_{Z'} \leq D_{\ell+s}\tilde{D}_Z$ highest eigenvalues of $\varrho_{Z'}$. Thus the *truncated* reduced state $\tilde{\varrho}_{Z'} \in \mathcal{D}(\tilde{\mathcal{H}}_{Z'})$ in the eigenbasis is

$$\tilde{\varrho}_{Z'} = \sum_{\alpha_{Z'}=1}^{\tilde{D}_{Z'}} \sigma_{\alpha_{Z'}}|\tilde{\chi}_{Z',\alpha_{Z'}}\rangle\langle\tilde{\chi}_{Z',\alpha_{Z'}}| \tag{2.51e}$$

where the $\sigma_{\alpha_{Z'}}$ eigenvalues are re-normalized such that $\mathrm{Tr}(\tilde{\varrho}_{Z'}) = 1$. The connection between the two states can be expressed by the partial isometry

$$V^{(\ell+s)} = \sum_{(\alpha_{\ell+s},\alpha_Z)=1}^{\tilde{D}_{Z'}} |\tilde{\chi}_{Z',(\alpha_{\ell+s},\alpha_Z)}\rangle\langle\chi_{\ell+s,\alpha_{\ell+s}} \otimes \tilde{\chi}_{Z,\alpha_Z}|, \tag{2.51f}$$

where the composite index $\alpha_{Z'} = (\alpha_{\ell+s}, \alpha_Z)$ is ordered such that the $\sigma_{\alpha_{Z'}}$ eigenvalues are ordered non-increasingly. This partial isometry maps from the composite system $\mathcal{H}_{\ell+s} \otimes \tilde{\mathcal{H}}_Z$ to its subspace, the Hilbert space of the new right block $\tilde{\mathcal{H}}_{Z'}$. The truncation yields $V^{(\ell+s)\dagger}V^{(\ell+s)} \neq \mathrm{I}_{\mathcal{H}_{\ell+s}\otimes\tilde{\mathcal{H}}_Z}$. With the projection $V^{(\ell+s)}V^{(\ell+s)\dagger} = \mathrm{I}_{\tilde{\mathcal{H}}_{Z'}}$, which is the identity in the new right block, the reduced state of the new right block is $\tilde{\varrho}_{Z'} = \mathrm{I}_{\tilde{\mathcal{H}}_{Z'}}\varrho_{Z'}\mathrm{I}_{\tilde{\mathcal{H}}_{Z'}}/\mathrm{Tr}(\mathrm{I}_{\tilde{\mathcal{H}}_{Z'}}\varrho_{Z'}\mathrm{I}_{\tilde{\mathcal{H}}_{Z'}})$. We can formulate this equivalently with matrices. The reduced density matrix of the new right block is $\boldsymbol{\sigma} = \boldsymbol{V}^{(\ell+s)\dagger}\boldsymbol{\varrho}_{Z'}\boldsymbol{V}^{(\ell+s)}/\mathrm{Tr}(\boldsymbol{V}^{(\ell+s)\dagger}\boldsymbol{\varrho}_{Z'}\boldsymbol{V}^{(\ell+s)})$, where the matrix of the partial isometry is rectangular, $\boldsymbol{V}^{(\ell+s)} \in \mathbb{C}^{D_{\ell+s}\tilde{D}_Z\times\tilde{D}_{Z'}}$, with entries $V^{(\ell+s)}_{(\alpha_{\ell+s},\alpha_Z),\alpha_{Z'}} = \langle\chi_{\ell+s,\alpha_{\ell+s}} \otimes \tilde{\chi}_{Z,\alpha_Z}|\tilde{\chi}_{Z',(\alpha_{\ell+s},\alpha_Z)}\rangle$, and the $\boldsymbol{\sigma}$ is diagonal containing the eigenvalues.

In step (iii), operators in the effective Hamiltonian are constructed such that the operators of the new extended left-/right block are expressed in the eigenbasis of the truncated reduced

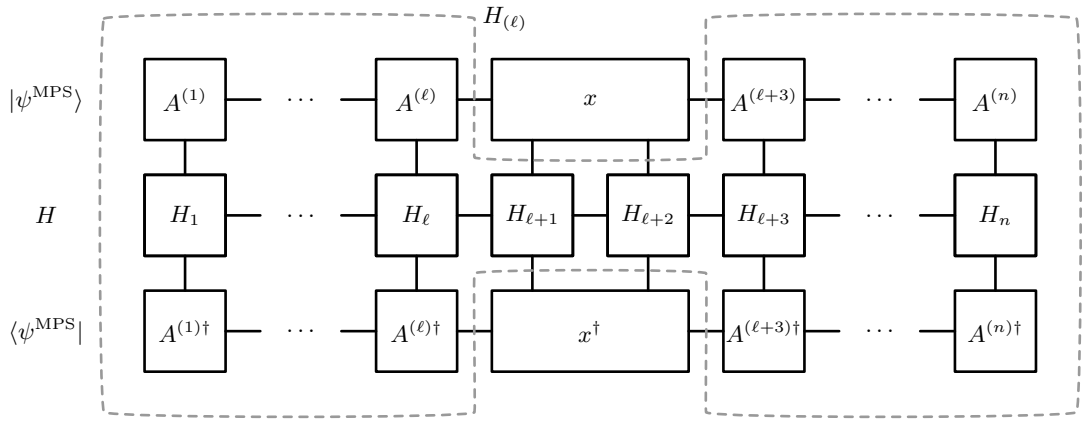

FIGURE 2.6. Graphical representation of the energy expectation value (2.54). The effective Hamiltonian $H_{(\ell)}$ is obtained by the contractions inside the dashed line. The renormalized operators of the left block $\tilde{H}_{X,k}$ and the right block $\tilde{H}_{Z,k}$ can be obtained by the contractions of tensors corresponding to $X = \{1, \dots, \ell\}$ and $Z = \{\ell + 3, \dots, n\}$, respectively. The operators $H_{Y,k}$ of the subsystem $Y = \{\ell + 1, \ell + 2\}$ are written in their exact form.

state. In case of rightward sweep, the operators in (2.48) are transformed, we say *renormalized*, according to the truncation of the reduced state (2.51c),

$$\tilde{H}_{X',k} = U^{(\ell+1)}(\tilde{H}_{X,k} \otimes H_{\{\ell+1\},k})U^{(\ell+1)\dagger} \in \mathrm{Lin}(\tilde{\mathcal{H}}_{X'}). \tag{2.52a}$$

The algorithm steps to the next $\ell \mapsto \ell + 1$ iteration with the relabelling $X' \mapsto X$, as depicted in figure 2.5 for the $s = 2$ site case. The new operators for the right block are loaded (form the disk or memory), which had been renormalized during leftward sweep (2.52b). Similarly, in case of leftward sweep the renormalization is

$$\tilde{H}_{Z',k} = V^{(\ell+s)}(H_{\{\ell+s\},k} \otimes \tilde{H}_{Z,k})V^{(\ell+s)\dagger} \in \mathrm{Lin}(\tilde{\mathcal{H}}_{Z'}). \tag{2.52b}$$

The algorithm steps to the next $\ell \mapsto \ell - 1$ iteration with the relabelling $Z' \mapsto Z$, as depicted in figure 2.5 for the $s = 2$ site case. The new operators for the left block are loaded (form the disk or memory), which had been renormalized during rightward sweep (2.52a).

2.7. DMRG and MPS

The main aspects of DMRG, the concept of matrix product operators and the relation between DMRG and MPS are comprehensively detailed in reference [**Sch11**]. Here we mention just some practical points which are relevant to the present work. To show the connection of the DMRG to the MPS, let us write out the transformation and truncation (renormalization) of the operators of blocks X and Z. From the recursion (2.52a) and (2.52b) we are able to express the

renormalized operators in terms of the exact operators,

$$\tilde{H}_{X,k} = U^{(\ell)\dagger}\Big(\dots\Big(U^{(2)\dagger}\big((U^{(1)\dagger}H_{1,k}U^{(1)})\otimes H_{2,k}\big)U^{(2)}\Big)\dots\otimes H_{\ell,k}\Big)U^{(\ell)}, \tag{2.53a}$$

$$\tilde{H}_{Z,k} = V^{(\ell+s+1)\dagger}\Big(H_{\ell+s+1,k}\otimes\dots\Big(V^{(n-1)\dagger}\big(H_{n-1,k}\otimes(V^{(n)\dagger}H_{n,k}V^{(n)})\big)V^{(n-1)}\Big)\dots\Big)V^{(\ell+s+1)}. \tag{2.53b}$$

Note that, these are not explicit expressions since the $U^{(i)}$ and $V^{(i)}$ isometries are determined from the eigenvalue problem of the effective Hamiltonian, which is built from the renormalized operators of the previous step. With this, the energy expectation value with a state vector (2.50) (omitting the q index) can be expressed as

$$\begin{aligned}\langle\psi^{(\ell)}(\boldsymbol{x})|H_{(\ell)}|\psi^{(\ell)}(\boldsymbol{x})\rangle_{\tilde{\mathcal{H}}_X\otimes\mathcal{H}_Y\otimes\tilde{\mathcal{H}}_Z} &= \sum_k \sum_{\substack{\alpha_X,\alpha_Y,\alpha_Z\\ \alpha'_X,\alpha'_Y,\alpha'_Z}} x_{\alpha'_X,\alpha'_Y,\alpha'_Z}{}^* \tilde{H}_{X,k}^{\alpha'_X,\alpha_X} H_{Y,k}^{\alpha'_Y,\alpha_Y} \tilde{H}_{Z,k}^{\alpha'_Z,\alpha_Z} x_{\alpha_X,\alpha_Y,\alpha_Z} = \\ &= \langle\psi^{\mathrm{MPS}}(\boldsymbol{x})|H|\psi^{\mathrm{MPS}}(\boldsymbol{x})\rangle_{\mathcal{H}_1\otimes\dots\otimes\mathcal{H}_n},\end{aligned} \tag{2.54}$$

where after the second equation the expectation value of the Hamiltonian in form of (2.47) is written with a state vector

$$|\psi^{\mathrm{MPS}}(\boldsymbol{x})\rangle = \sum_{\alpha_1,\dots,\alpha_n} \boldsymbol{A}_{1,\alpha_1}\dots\boldsymbol{A}_{\ell,\alpha_\ell}\boldsymbol{x}_{\alpha_Y}\boldsymbol{A}_{\ell+s+1,\alpha_{\ell+s+1}}\dots\boldsymbol{A}_{n,\alpha_n}|\chi_{1,\alpha_1}\rangle\otimes\dots\otimes|\chi_{n,\alpha_n}\rangle, \tag{2.55}$$

which is expressed with left-canonical MPS matrices on the left, right-canonical MPS matrices on the right and a remaining in-between tensor $\boldsymbol{x}$. These messy formulas can be illustrated well by boxes and lines in figure 2.6 for the $s = 2$ case. The ground-state energy in the DMRG framework (2.49), that is, the lowest eigenvalue of the effective Hamiltonian in step (i), can be expressed now in terms of the optimization of the local tensor $\boldsymbol{x}$

$$\begin{aligned}E_0^{(\ell)} &= \min\Big\{\langle\psi(\boldsymbol{x})|H_{(\ell)}|\psi(\boldsymbol{x})\rangle \;\Big|\; \boldsymbol{x}\in\mathbb{C}^{\tilde{D}_X\times D_Y\times\tilde{D}_Z}, \|\boldsymbol{x}\|=1\Big\}\\ &= \min\Big\{\langle\psi^{\mathrm{MPS}}(\boldsymbol{x})|H|\psi^{\mathrm{MPS}}(\boldsymbol{x})\rangle \;\Big|\; \boldsymbol{x}\in\mathbb{C}^{\tilde{D}_X\times D_Y\times\tilde{D}_Z}, \|\boldsymbol{x}\|=1\Big\}.\end{aligned} \tag{2.56}$$

From the reshaping and decomposition of the minimizer $x_{\alpha_X,\alpha_Y,\alpha_Z}$ of (2.56),

$$x_{(\alpha_X,\alpha_{\ell+1}),\alpha_{\bar{X}'}} = \sum_{\alpha_{X'}=1}^{\tilde{D}_X D_{\ell+1}} U^{(\ell+1)}_{(\alpha_X,\alpha_{\ell+1}),\alpha_{X'}}\sqrt{\omega_{\alpha_{X'}}}V'_{\alpha_{\bar{X}'},\alpha_{X'}}, \tag{2.57a}$$

$$x_{\alpha_{\bar{Z}'},(\alpha_{\ell+s},\alpha_Z),} = \sum_{\alpha_{Z'}=1}^{D_{\ell+s}\tilde{D}_Z} U'_{\alpha_{\bar{Z}'},\alpha_{Z'}}\sqrt{\sigma_{\alpha_{Z'}}}V^{(\ell+s)}_{(\alpha_{\ell+s},\alpha_Z),\alpha_{Z'}}, \tag{2.57b}$$

one can obtain the updated left- and right-canonical MPS matrices according to (2.38). Substituting (2.57a) into the DMRG state form (2.50) and applying partial trace on the pure ground state, one can get the reduced state (2.51b) in its eigenbasis, hence the same symbol $U^{(\ell+1)}$ were used for unitaries (partial isometries) in (2.51c) and (2.57a). Similar applies for $V^{(\ell+s)}$. The truncation here is the same as in (2.51b) and (2.51e) in step (ii), namely, the restriction of the range of indices $\alpha_{X'} = 1,\dots,\tilde{D}_{X'} \le \tilde{D}_X D_{\ell+1}$ and $\alpha_{Z'} = 1,\dots,\tilde{D}_{Z'} \le D_{\ell+s}\tilde{D}_Z$. That is, the

MPS bond dimensions $\tilde{D}_X$ are the block sizes in the traditional DMRG context. In step (iii) the renormalization of operators are carried out for the left and right block, which is the contraction of the tensors corresponding to X' and Z', respectively.

The variational MPS approach is the optimization of the energy expectation value in (2.46) in terms of the MPS matrices (being variational parameters) in a fixed bond dimension manifold $\mathcal{M}_{\tilde{\boldsymbol{D}}}$ [**Sch11**]. The simultaneous optimization of the MPS matrices is still unfeasible, however, the approach is equivalent to the $s = 1$ site DMRG method [**Tak99**, **Whi05**] with predefined fixed block sizes $\tilde{\boldsymbol{D}} = (\tilde{D}_{[1]}, \tilde{D}_{[2]}, \dots, \tilde{D}_{[n-1]})$. This can be seen by setting $Y = \{\ell + 1\}$ in (2.55), so we have $\overline{X'} = Z$ in (2.57), and by the property of the rank of the Schmidt decomposition (2.17), the dimension of the MPS matrices cannot increase during the one-site DMRG iteration. So the optimization is carried out in a submanifold $\mathcal{M}_{\tilde{\boldsymbol{D}}}$.

Contrary, the $s = 2$ site DMRG provides the advantageous property that the bond dimension can increase during the iterations, that is, the decomposition (2.57) for $Y = \{\ell + 1, \ell + 2\}$ is

$$x_{(\alpha_X,\alpha_{\ell+1}),(\alpha_{\ell+2},\alpha_Z)} = \sum_{\alpha_{X'}=1}^{\tilde{D}_X D_{\ell+1}} (A^{(\ell+1)}_{\alpha_{\ell+1}})_{\alpha_X,\alpha_{X'}} \sqrt{\omega_{\alpha_{X'}}} (A^{(\ell+2)}_{\alpha_{\ell+2}})^*_{\alpha_{X'},\alpha_Z}. \tag{2.58}$$

One can control the bond dimensions $\tilde{D}_{X'}$ according to a predefined maximal value (possibly for each ℓ). The more rigorous way to control the error is setting the $\tilde{D}_{X'}$ adaptively, for example, by a prior defined truncation error threshold (2.42) [**Leg03a**, **Hol12a**, **Hol12b**]. In this case the bond dimension strongly depends on the correlation in the system, and in case of general TNS methods, on the network topology [**Leg03b**, **Nak13**, **Mur15**] and on the properties of the component tensors [**Gun18**]. Also, the two-site DMRG framework provides the advantageous property that the action of an arbitrary neighbouring two-site operator, that is, operator acting non-trivially only on subsystem $Y = \{\ell + 1, \ell + 2\}$, can be evaluated easily. By this, time evolution, imaginary time evolution and mode transformation [**Kru16**] can be straightforwardly implemented.

The performance of the DMRG algorithm relies on the efficiency of the diagonalization in step (i) [**Men23**]. When the full diagonalization of a matrix A is not necessary, only some of the lowest (or highest) eigenvalues and eigenvectors are searched for, iterative diagonalization algorithms [**Bai00**] can be applied (for example, by Lánczos [**Lan50**, **Cul02**, **Gol13**] or Davidson [**Dav75**, **Sle96**] algorithm), which needs only the efficient evaluation of the matrix-vector product Ax of an arbitrary vector x. That is, to store A as a full matrix is not even needed. The cost of a two-site DMRG step scales as

$$\mathcal{O}(\tilde{D}^3_{\max} D^3 + \tilde{D}^2_{\max} n^4), \tag{2.59}$$

supposing $D = D_i$ for all $i \in [n]$. The first term is coming from the diagonalization and the second is from the renormalization step.

Numerical efficiency can be significantly increased by the exploitation of symmetries [**McC07**, **Sza15**], that is, by the restriction of the eigenvalue problem into a subspace determined by the symmetry operator that commutes with the Hamiltonian. The examples of the Abelian U(1) symmetry are the total spin projection conservation [**Whi96**], the particle number conservation

[Cha02, Leg03b, Kur09], the point group symmetry [Leg03b, Cha04] and the translational invariance [Xia96, Por06, Ver08, Pip10, Pir11]. Another Abelian symmetry is the Z_2 spin reflection symmetry [Leg97]. Several implementation for the non-Abelian SU(2) symmetry exist [Sie97, McC02, Pit06, Zgi08, Wei12, Sha12, Sin12, Wou12, Kel16] and also for the more general SU(N) case [Tót08, Sin10, Wer20].

In order to improve the convergence properties and perform large-scale DMRG simulations routinely and consistently, some consideration are employed at the initialization stage of the DMRG algorithm [Sza15]. These are the order optimisation (see appendix A), basis optimisation (see chapter 4) and the initialization of the MPS tensors (see appendix B). We note here, that the sophisticated implementation of the initialization procedure, called the configuration interaction based dynamically extended active space method [Bar11, Sza15], opens the way for the *restricted active space (RAS)* methods [Bar22]. It was recently shown that the *DMRG-RAS* yields a powerful extrapolation method for strongly correlated systems [Fri23].

2.8. Identical particles: particle picture

In section 2.2, the composite quantum systems were represented on tensor product Hilbert spaces. In the following, the formalism of identical particles is summarized.

The indistinguishability of identical particles is formulated by the *symmetrization-/antisymmetrization postulate*, which can be taken as an experimental fact. Although, it cannot be derived from the other postulates of quantum mechanics within the non-relativistic framework, but omitting it leads to non-physical (in sense of measurement postulate) state vectors and operators. Based on certain assumptions, theoretical derivation can be given in quantum field theory to show that there are two sufficient ways to construct many-body state vectors of identical particles. By this, particles have either *fermionic* or *bosonic* nature, corresponding to the (totally) symmetric and antisymmetric representation of the permutation group, respectively.

We would like to describe N (fermionic or bosonic) *particles*, so let us begin with N copies of $\mathcal{K}_r$, for $r \in [N]$, of the *one-particle Hilbert space* $\mathcal{K}$. The tensor products of N (not necessarily basis) vectors $|\psi_r\rangle \in \mathcal{K}_r$, called *elementary tensors* $|\psi_1\rangle \otimes \ldots \otimes |\psi_N\rangle$, span the tensor product space $\mathcal{K}^{\otimes N} := \bigotimes_{r\in[N]} \mathcal{K}_r$. The elementary *symmetric* and *antisymmetric vectors* (denoted by $\vee$ and $\wedge$, respectively) are of the form

$$|\psi_1\rangle \overset{\vee}{\wedge} \ldots \overset{\vee}{\wedge} |\psi_N\rangle := \frac{1}{\sqrt{N!}} \sum_{\sigma\in \mathrm{S}_{[N]}} (\pm 1)^{\mathrm{Par}(\sigma)} R_\sigma(|\psi_1\rangle \otimes \ldots \otimes |\psi_N\rangle), \tag{2.60}$$

and span the symmetric and antisymmetric subspaces $\mathcal{K}^{\overset{\vee}{\wedge} N} \subseteq \mathcal{K}^{\otimes N}$, where $\mathrm{S}_{[N]}$ is the set of permutations of the set $[N]$, and $\mathrm{Par}(\sigma) \in \{0, 1\}$ is the parity of the permutation σ, and R_σ is the usual representation of the symmetric group on the tensor product space, $R_\sigma(|\psi_1\rangle \otimes \ldots \otimes |\psi_N\rangle) = |\psi_{\sigma(1)}\rangle \otimes \ldots \otimes |\psi_{\sigma(N)}\rangle$. Note that, for $N = 1$ we have $\mathcal{K}^{\otimes 1} = \mathcal{K}^{\wedge 1} = \mathcal{K}^{\vee 1} = \mathcal{K}$, while for $N = 0$ we define $\mathcal{K}^{\otimes 0} = \mathcal{K}^{\wedge 0} = \mathcal{K}^{\vee 0} \cong \mathbb{C}$. It is straightforward to show that both the symmetric and antisymmetric vectors (2.60) are N-linear, that is, linear in each $|\psi_r\rangle$, and the inner product in the symmetric and antisymmetric subspaces $\mathcal{K}^{\overset{\vee}{\wedge} N}$ are inherited from the tensor product space

$\mathcal{K}^{\otimes N}$,

$$\big(\langle\psi_1| \overset{\vee}{\wedge} \ldots \overset{\vee}{\wedge} \langle\psi_N|\big)\big(|\kappa_1\rangle \overset{\vee'}{\wedge} \ldots \overset{\vee'}{\wedge} |\kappa_N\rangle\big) = \\ = \Big(\frac{1}{N!}\sum_{\sigma\in \mathrm{S}_{[N]}} \big((\pm 1)(\pm' 1)\big)^{\mathrm{Par}(\sigma)}\Big) \det{}_{\pm}\langle\psi_i|\kappa_j\rangle = \delta_{\pm,\pm'} \det{}_{\pm}\langle\psi_i|\kappa_j\rangle \quad (2.61)$$

where $\det_{\pm}\langle\psi_i|\kappa_j\rangle$ denotes the matrix permanent and determinant in the indices i, j, respectively. This shows also the orthogonality of the symmetric and antisymmetric subspaces. Note, however, that they are not othocomplements of each other in general, there are other irreps of $\mathrm{S}_{[N]}$ if $n \geq 2$.

The normalized vectors of $\mathcal{K}$ are called *modes*, let us single out $\{|\varphi_i\rangle\}_{i\in[d]} \subseteq \mathcal{K}$ orthonormal basis describing to d modes. The standard orthonormal basis of $\mathcal{K}^{\otimes N}$ is

$$\big\{|\varphi_{\boldsymbol{i}}\rangle = |\varphi_{i_1}\rangle \otimes \ldots \otimes |\varphi_{i_N}\rangle \;\big|\; \boldsymbol{i} \in I_N^{\otimes}\big\}, \quad (2.62)$$

where the index set

$$I_N^{\otimes}([d]) := [d]^{\times N} = \big\{\boldsymbol{i} = (i_1, \ldots, i_N) \;\big|\; i_r \in [d], r \in [N]\big\} \quad (2.63)$$

has d^N elements, so $\dim(\mathcal{K}^{\otimes N}) = d^N$. It follows from (2.61) by the identity $\det_{\pm}(A \oplus B) = (\det_{\pm}(A))(\det_{\pm}(B))$ that the standard orthonormal bases of $\mathcal{K}^{\overset{\vee}{\wedge} N}$ are

$$\Big\{|\varphi^{\overset{\vee}{\wedge}}_{\boldsymbol{i}}\rangle = \big(\textstyle\prod_{j=1}^{d} \nu_j!\big)^{-1/2} |\varphi_{i_1}\rangle \overset{\vee}{\wedge} \ldots \overset{\vee}{\wedge} |\varphi_{i_N}\rangle \;\Big|\; \boldsymbol{i} \in I_N^{\overset{\vee}{\wedge}}\Big\}, \quad (2.64)$$

where the index sets

$$I_N^{\vee}([d]) := \{\boldsymbol{i} \in I_N^{\otimes} : 1 \leq i_1 \leq \ldots \leq i_N \leq d\} \quad (2.65a)$$

and

$$I_N^{\wedge}([d]) := \{\boldsymbol{i} \in I_N^{\otimes} : 1 \leq i_1 < \ldots < i_N \leq d\} \quad (2.65b)$$

have $\binom{d+N-1}{N}$ and $\binom{d}{N}$ elements, respectively, so $\dim(\mathcal{K}^{\vee N}) = \binom{d+N-1}{N}$ and $\dim(\mathcal{K}^{\wedge N}) = \binom{d}{N}$. The argument of the index sets, that is, the index set of the modes, are omitted if this does not lead to confusion. Here the *occupation number* ν_j of the mode $j = 1, \ldots, d$ is

$$\nu_j = \big|\{r \in [N] \mid i_r = j\}\big|. \quad (2.66)$$

To be able to treat different numbers of particles simultaneously, we have the direct sum

$$\mathcal{F} := \bigoplus_{N\in\mathbb{N}_0} \mathcal{K}^{\overset{\vee}{\wedge} N}, \quad (2.67)$$

called *Fock space*, which is a Hilbert space, with inner product inherited from the $\mathcal{K}^{\overset{\vee}{\wedge} N}$ Hilbert spaces. Transition among subspaces of fixed particle number can be realized by the *creation operator* $a^\dagger(|\kappa\rangle) \in \mathrm{Lin}(\mathcal{F})$ of mode $|\kappa\rangle \in \mathcal{K}$,

$$a^\dagger\big(|\kappa\rangle\big)\big(|\psi_1\rangle \overset{\vee}{\wedge} \ldots \overset{\vee}{\wedge} |\psi_N\rangle\big) = |\kappa\rangle \overset{\vee}{\wedge} |\psi_1\rangle \overset{\vee}{\wedge} \ldots \overset{\vee}{\wedge} |\psi_N\rangle, \quad (2.68a)$$

and its adjoint, the *annihilation operator*,

$$a\big(|\kappa\rangle\big)\big(|\psi_1\rangle \overset{\vee}{\wedge} \ldots \overset{\vee}{\wedge} |\psi_N\rangle\big) = \sum_{r=1}^{N} (\pm)^{r-1} \langle\kappa|\psi_r\rangle |\psi_1\rangle \overset{\vee}{\wedge} \ldots \cancel{|\psi_r\rangle} \ldots \overset{\vee}{\wedge} |\psi_N\rangle. \quad (2.68b)$$

These satisfy the *canonical commutation-/anticommutation relations*

$$\Big[a\big(|\psi\rangle\big), a^\dagger\big(|\kappa\rangle\big)\Big]_\pm = \langle\psi|\kappa\rangle \mathrm{I}, \qquad \Big[a\big(|\psi\rangle\big), a\big(|\kappa\rangle\big)\Big]_\pm = 0. \tag{2.69}$$

Here the commutator/anticommutator of operators A and B is $[A,B]_\pm = AB - (\pm BA)$.

The basis vectors (2.64) can be expressed as

$$|\varphi_{\boldsymbol{i}}^{\curlyvee}\rangle = \big(\textstyle\prod_{j=1}^d \nu_j!\big)^{-1/2} |\varphi_{i_1}\rangle \mathbin{\curlyvee} \ldots \mathbin{\curlyvee} |\varphi_{i_N}\rangle = \big(\textstyle\prod_{j=1}^d \nu_j!\big)^{-1/2} a^\dagger\big(|\varphi_{i_1}\rangle\big) \ldots a^\dagger\big(|\varphi_{i_N}\rangle\big)|\varphi_{\mathrm{vac}}\rangle, \tag{2.70}$$

where $a^\dagger\big(|\varphi_j\rangle\big)$ is the creation operator of the j-th mode, and $|\varphi_{\mathrm{vac}}\rangle := |\varphi_{()}\rangle \in \mathcal{K}^0 \cong \mathbb{C}$ is the zero-particle state vector, referred to as *vacuum state*. The eigenvalue of the *particle number operator* of the j-th mode $a^\dagger\big(|\varphi_j\rangle\big)a\big(|\varphi_j\rangle\big)$ is the occupation number ν_j indeed, which can be expressed by (2.66). The canonical commutation/anticommutation relations with respect to the one-particle basis take the form

$$\Big[a\big(|\varphi_i\rangle\big), a^\dagger\big(|\varphi_j\rangle\big)\Big]_\pm = \delta_{i,j}\mathrm{I}, \qquad \Big[a\big(|\varphi_i\rangle\big), a\big(|\varphi_j\rangle\big)\Big]_\pm = 0. \tag{2.71}$$

2.9. Identical particles: mode picture

In the particle picture, also called *first quantitation*, the elementary subsystems were the indistinguishable particles, which could occupy given modes, although the symmetrization-/antisymmetrization principle made this picture problematic to imagine. In the mode picture, also called *second quantization*, we change our focus, the elementary subsystems are the distinguishable modes, which can be occupied by given number of particles. This is formulated with respect to a fixed mode set $\{|\varphi_i\rangle\}_{i\in[d]} \subseteq \mathcal{K}$, by which we express $|\varphi_{\boldsymbol{i}}^{\curlyvee}\rangle \in \mathcal{F}$ in terms of the occupation numbers ν_i, given by (2.66). To this end, let us have the one-mode occupation Hilbert spaces $\mathcal{N}_i$ for $i \in [d]$, and let $\{|\phi_{i,\nu_i}\rangle\}$ be orthonormal bases in these, where ν_j ranges in $\mathbb{N}_0$ and $\{0,1\}$ for bosons and fermions, respectively. The orthonormal basis vectors $|\phi_{\boldsymbol{\nu}}\rangle = |\phi_{1,\nu_1}\rangle \otimes \ldots \otimes |\phi_{d,\nu_d}\rangle \in \mathcal{N}_1 \otimes \ldots \otimes \mathcal{N}_d =: \mathcal{N}_{[d]}$ represent the occupation number configurations of d modes by the linear isomorphism

$$\begin{aligned} F : \mathcal{F} &\longrightarrow \mathcal{N}_{[d]}, \\ |\varphi_{\boldsymbol{i}}^{\curlyvee}\rangle &\longmapsto |\phi_{\boldsymbol{\nu}}\rangle \equiv |\phi_{\nu(\boldsymbol{i})}\rangle. \end{aligned} \tag{2.72}$$

where the map of the indices in (2.65) is $\nu : \boldsymbol{i} \mapsto \boldsymbol{\nu}$, given by (2.66). If the *occupation number space* $\mathcal{N}_{[d]}$ is not distinguished from the Fock space $\mathcal{F}$, then the occupation number labelling induces a tensor product structure in the Fock space. We make this distinction for clarity. We note that the tensor product structure in $\mathcal{N}_{[d]}$ is not physical in the fermionic case [**Sza21**], however, it is useful in the description in the concrete representation. We also have the *N-particle subspaces*

$$\mathcal{N}_{[d]}^N := F\big(\mathcal{K}^{\curlyvee N}\big) = \mathrm{Span}\big\{|\phi_{\boldsymbol{\nu}}\rangle \;\big|\; \boldsymbol{\nu} \in \nu\big(I_N^{\curlyvee}([d])\big)\big\} \subseteq \mathcal{N}_{[d]} \tag{2.73a}$$

and the corresponding projections $P_{[d]}^N$. Also, we introduce subspaces by imposing occupation number restrictions $N_1, \ldots, N_r$ to disjoint subsets $X_1, \ldots, X_r \subseteq [d]$,

$$\mathcal{N}_{X_1,\ldots,X_r}^{N_1,\ldots,N_r} := \mathrm{Span}\big\{|\phi_{\boldsymbol{\nu}}\rangle \;\big|\; \sum_{i\in X_k} \nu_i = N_k, \forall k = 1,\ldots,r\big\} \subseteq \mathcal{N}_{[d]} \tag{2.73b}$$

and the corresponding projection $P^{N_1,\dots,N_r}_{X_1,\dots,X_r}$. If $X_1|\dots|X_r$ is a partition of $[d]$ and $N_1+\dots+N_r = N$, then $\mathcal{N}^{N_1,\dots,N_r}_{X_1,\dots,X_r} \subseteq \mathcal{N}^N_{[d]}$.

The construction of the N-particle state from the vacuum (2.70) can be done in the second quantized picture as

$$|\phi_{\boldsymbol{\nu}}\rangle = |\phi_{1,\nu_1}\rangle \otimes \dots \otimes |\phi_{d,\nu_d}\rangle = \big(\textstyle\prod_{j=1}^d \nu_j!\big)^{-1/2} \big(a^\dagger_{i_1}\big)^{\nu_1} \dots \big(a^\dagger_{i_N}\big)^{\nu_N} |\phi_{\mathrm{vac}}\rangle, \tag{2.74}$$

where the vacuum state $|\phi_{\mathrm{vac}}\rangle = F(|\varphi_{\mathrm{vac}}\rangle) = |\phi_{(0,\dots,0)}\rangle$, and the *Jordan–Wigner representation* of the creation operator acting on $\mathcal{N}_{[d]}$ is

$$a^\dagger_j := F a^\dagger\big(|\varphi_j\rangle\big) F^{-1} = \begin{cases} \big(\bigotimes_{k<j} \mathrm{I}_k\big) \otimes \big(\sum_{\nu\in\mathbb{N}_0} |\phi_{j,\nu+1}\rangle\langle\phi_{j,\nu}|\big) \otimes \big(\bigotimes_{j<k} \mathrm{I}_k\big), \\ \big(\bigotimes_{k<j} \mathrm{P}_k\big) \otimes |\phi_{j,1}\rangle\langle\phi_{j,0}| \otimes \big(\bigotimes_{j<k} \mathrm{I}_k\big) \end{cases} \tag{2.75}$$

in the bosonic and fermionic cases, respectively, where the fermionic *phase operator* is $\mathrm{P}_k = |\phi_{k,0}\rangle\langle\phi_{k,0}| - |\phi_{k,1}\rangle\langle\phi_{k,1}|$ [Jor28]. The *canonical commutation-/anticommutation relations* in the second quantized picture take the form

$$[a_i, a^\dagger_j]_\pm = \delta_{i,j}\mathrm{I}, \qquad [a_i, a_j]_\pm = 0. \tag{2.76}$$

2.10. Mode transformation

Changing the modes in the first quantized picture is simple, since it does not affect the structure of $\mathcal{F} = \bigoplus_{N\in\mathbb{N}_0} \mathcal{K}^{\curlyvee N}$. However, since the second quantized picture is constructed with respect to fixed modes, the mode transformation in this case needs some more elaboration. Having the modes $\{|\varphi_i\rangle\}_{i=1}^d \subseteq \mathcal{K}$, let $U \in \mathrm{U}(\mathcal{K})$ be a unitary transformation by which $|\tilde\varphi_i\rangle := U|\varphi_i\rangle = \sum_{j=1}^d U_{j,i}|\varphi_j\rangle$ in the one-particle Hilbert space $\mathcal{K}$. By (2.60) the N-particle bosonic/fermionic state vector transforms as

$$(U\otimes\dots\otimes U)|\varphi_{i_1}\rangle \curlyvee \dots \curlyvee |\varphi_{i_N}\rangle = U|\varphi_{i_1}\rangle \curlyvee \dots \curlyvee U|\varphi_{i_N}\rangle = |\tilde\varphi_{i_1}\rangle \curlyvee \dots \curlyvee |\tilde\varphi_{i_N}\rangle \in \mathcal{K}^{\curlyvee N}, \tag{2.77}$$

that is, $\mathcal{K}^{\curlyvee N}$ are invariant subspaces of $U^{\otimes N}$, acting over the whole $\mathcal{K}^{\otimes N}$. The linearity of $a^\dagger\big(|\varphi_j\rangle\big)$ in $|\varphi_j\rangle$ follows from its definition (2.68a) and form the N-linearity of the symmetric and antisymmetric vectors (2.60), so the creation operator corresponding to the transformed state vector reads as

$$a^\dagger\big(|\tilde\varphi_i\rangle\big) = \sum_{j\in[d]} U_{ji} a^\dagger\big(|\varphi_j\rangle\big) \in \mathrm{Lin}(\mathcal{F}), \tag{2.78a}$$

$$\tilde a^\dagger_i = \sum_{j\in[d]} U_{ji} a^\dagger_j \overset{!}{=} g(U) a^\dagger_i g(U)^\dagger \in \mathrm{Lin}(\mathcal{N}_{[d]}), \tag{2.78b}$$

where $g(U) \in \mathrm{U}(\mathcal{N}_{[d]})$ is unitary and it is block-diagonal with respect to the fixed particle number subspaces $\mathcal{N}^N_{[d]}$. The canonical commutation-/anticommutation relations (2.69) and (2.71) are preserved by such a unitary transformation. Substituting the ansatz $g(U)(\theta) = \mathrm{e}^{-\mathrm{i}\theta\sum_{i,j\in[d]} J_{i,j} a^\dagger_i a_j}$, with $\theta\in\mathbb{R}$, $J_{i,j} = {J_{j,i}}^* \in \mathbb{C}$ into (2.78b), taking its derivative in θ and using the canonical commutation-/anticommutation relations (2.76) one can derive

$$g(U) = \mathrm{e}^{\sum_{i,j\in[d]} (\ln U)_{i,j} a^\dagger_i a_j}, \tag{2.79}$$

for both bosons and fermions. The important point is that the restriction of $U^{\otimes N}$ to the fixed particle number subspace, as in (2.77), is a highly non-trivial task, which is achieved by the formula (2.79) in terms of the particle number preserving combination of creation and annihilation operators, acting naturally not only on the fixed particle number subspace, but also on the whole Fock space or occupation number space.

2.11. Many-body observables and states: particle picture

We would like to deal with operators, states and reduced states in the particle picture. We are interested in operators that leave the symmetric and antisymmetric subspaces $\mathcal{K}^{\wedge N}$ invariant. For example, we have seen that the operator $U^{\otimes N}$ in (2.77) is of this kind. Now, we consider *permutation invariant* operators, which are also of this kind, and we would like to express these in terms of creation and annihilation operators. To this end, let us have a permutation invariant operator $O_M \in \mathrm{Lin}_{\mathrm{PI}}(\mathcal{K}^{\otimes M})$, that is, $[R_\sigma, O_M]_+ = 0$ for all $\sigma \in \mathrm{S}_{[M]}$ permutations. For $M \leq N$, for all M-particle subsystems $X \subseteq [N]$, $|X| = M$, let O_X be the copy of O_M. With these, let us have the *permutational invariant particle operator extension*

$$\begin{aligned} \iota_{M,N}: \quad \mathrm{Lin}_{\mathrm{PI}}(\mathcal{K}^{\otimes M}) &\longrightarrow \mathrm{Lin}_{\mathrm{PI}}(\mathcal{K}^{\otimes N}), \\ O_M &\longmapsto \sum_{\substack{X\subseteq[N],\\ |X|=M}} O_X \otimes \mathrm{I}_{[N]\setminus X}. \end{aligned} \tag{2.80}$$

The main point is that this is a "collective" verison of O_M. For example, the one-particle identity operator $\mathrm{I} \in \mathrm{Lin}_{\mathrm{PI}}(\mathcal{K}^{\otimes 1})$ is mapped to $\iota_{1,N}(\mathrm{I}) = N\mathrm{I} \in \mathrm{Lin}_{\mathrm{PI}}(\mathcal{K}^{\otimes N})$, however, the two-particle identity operator $\mathrm{I}\otimes\mathrm{I} \in \mathrm{Lin}_{\mathrm{PI}}(\mathcal{K}^{\otimes 2})$ is mapped to $\iota_{2,N}(\mathrm{I}\otimes\mathrm{I}) = \binom{N}{2}\mathrm{I} \in \mathrm{Lin}_{\mathrm{PI}}(\mathcal{K}^{\otimes N})$. This is the natural practice in many-body physics, although, we will see that the resulting state reduction behaves in a slightly different way than in the usual distinguishable setting (2.6). Because of the same reason, the composition rule of this extension is the slightly unusual $\iota_{M,N}\circ\iota_{K,M} = \binom{N-K}{M-K}\iota_{K,N}$ for $K \leq M \leq N$. We note that one may define a normalized extension $\hat{\iota}_{M,N} := \binom{N}{M}^{-1}\iota_{M,N}$, by which $\hat{\iota}_{M,N}\circ\hat{\iota}_{K,M} = \hat{\iota}_{K,N}$. The extension of the identity by this is the identity, $\hat{\iota}_{1,N}(\mathrm{I}) = \mathrm{I} \in \mathrm{Lin}_{\mathrm{PI}}(\mathcal{K}^{\otimes N})$.

Let us consider $M \leq N$-particle subsystems. The observables O_M of the M-particle subsystem are given by the exension (2.80) among the observables of the N-particle subsystem. If the state of the N-particle subsystem is given by $\gamma_N \in \mathcal{D}(\mathcal{K}^{\wedge N})$, then the *reduced state* $\gamma_M := r_{N,M}(\gamma_N)$ of the M-particle subsystem is the state that gives back the expectation values of observables of the M-particle subsystem, as before, $\mathrm{Tr}\big(r_{N,M}(\gamma_N)O_M\big) = \mathrm{Tr}\big(\gamma_N\iota_{M,N}(O_M)\big)$ for all O_M. This means again that the operation of the state reduction $r_{N,M}$ is just the adjoint map of the operator extension $\iota_{M,N}$. It turns out that this holds if and only if the state reduction is done by the unusually normalized partial trace operation

$$\begin{aligned} r_{N,M}: \quad \mathcal{D}(\mathcal{K}^{\wedge N}) &\longrightarrow \binom{N}{M}\mathcal{D}(\mathcal{K}^{\wedge M}), \\ \gamma_N &\longmapsto \binom{N}{M}\mathrm{Tr}_{[N]\setminus X}(\gamma_N) = \binom{N}{M}\mathrm{Tr}_{N-M}(\gamma_N), \end{aligned} \tag{2.81}$$

where the Tr_{N-M} symbolizes that the partial trace $\mathrm{Tr}_{[N]\setminus X}$ is independent on which spaces $[N]\setminus X$ it is applied, and the $\binom{N}{M}$ factor shows that the M-particle reduced state $\gamma_M = r_{N,M}(\gamma_N)$ is not normalized. For example, the trace of the one-particle reduced state $\gamma_1 = r_{N,1}(\gamma_N)$ is the particle number $\mathrm{Tr}(\gamma_1) = N$. Note, that the normalization (trace) of γ_M is somewhat ambiguous, it is $\binom{N}{M}$ (because the partial trace is trace preserving), which depends on N, the particle number of the subsystem from which the state comes. This is the manifestation of the slightly unusual composition rule of the reduction, $r_{M,K}\circ r_{N,M} = \binom{N-K}{M-K} r_{N,K}$ for $K \leq M \leq N$, coming from that of the extension $\iota_{M,N}$. We note that the normalized reduction $\hat{r}_{N,M} = \binom{N}{M}^{-1} r_{N,M} = \mathrm{Tr}_{N-M}$, being the adjoint of the normalized extension $\hat{\iota}_{M,N}$, is free of these ambiguities, $\hat{r}_{M,K} \circ \hat{r}_{N,M} = \hat{r}_{N,K}$, by which the reduction of a state $\gamma_N \in \mathcal{D}(\mathcal{K}^{\veebar N})$ is a state $\hat{r}_{N,M}(\gamma_N) \in \mathcal{D}(\mathcal{K}^{\veebar M})$.

The introduction of the Fock space was motivated by the need for the treatment of different number of particles together. So we would like to have the form of $O_M \in \mathrm{Lin}_{\mathrm{PI}}(\mathcal{K}^{\otimes M})$ not only in the N-particle collective form as in (2.80), but also that can act on the whole Fock space. This can be achieved by utilizing the creation and annihilation operators as

$$\begin{aligned} \iota_M : \quad \mathrm{Lin}_{\mathrm{PI}}(\mathcal{K}^{\otimes M}) \quad &\longrightarrow \quad \mathrm{Lin}(\mathcal{F}), \\ O_M \quad &\longmapsto \quad \frac{1}{M!} \sum_{\boldsymbol{i},\boldsymbol{j}\in I_M^{\otimes}} \langle \varphi_{\boldsymbol{i}} | O_M | \varphi_{\boldsymbol{j}} \rangle a^\dagger\big(|\varphi_{i_1}\rangle\big) \dots a^\dagger\big(|\varphi_{i_M}\rangle\big) a\big(|\varphi_{j_M}\rangle\big) \dots a\big(|\varphi_{j_1}\rangle\big). \end{aligned} \tag{2.82}$$

With this map we have that all N-particle restriction of (2.80) and (2.82) are the same, that is, $\iota_M(O_M)|_{\mathcal{K}^{\veebar N}} = \iota_{M,N}(O_M)|_{\mathcal{K}^{\veebar N}}$. These operators leave the fixed particle number subspaces $\mathcal{K}^{\veebar N}$ invariant for all N [**Ali01**]. Note that for $N \leq M$, these map to the null vector, which is of course an element of the given subspace, that is, $\mathcal{K}^{\veebar N} \subseteq \ker(\iota_M(O_M))$ for all $N \leq M$. It is easy to check that ι_M preserves positivity. For example, the one-particle identity operator $\mathrm{I} \in \mathrm{Lin}_{\mathrm{PI}}(\mathcal{K}^{\otimes 1})$ is mapped to the particle number operator $\iota_1(\mathrm{I}) = \sum_{i\in[d]} a_i^\dagger a_i$, and the two-particle identity operator $\mathrm{I}\otimes\mathrm{I} \in \mathrm{Lin}_{\mathrm{PI}}(\mathcal{K}^{\otimes 2})$ is mapped to the pair correlation operator $\iota_2(\mathrm{I}\otimes\mathrm{I}) = \frac{1}{2}\sum_{i\in[d]}\sum_{j\in[d],j\neq i} a_i^\dagger a_i (a_j^\dagger a_j - \mathrm{I})$.

The observables O_M of the M-particle subsystem are given by the extension (2.82) among the observables of the full Fock space. Let us consider an N-particle state $\gamma_N \in \mathcal{D}(\mathcal{F})$ among the states of the full Fock space, that is, $\iota_1(\mathrm{I})\gamma_N = \gamma_N \iota_1(\mathrm{I}) = N\gamma_N$. Then the *reduced state* $\gamma_M := r_M(\gamma_N)$ of the M-particle subsystem is the state that gives back the expectation values of observables of the M-particle subsystem, as before, $\mathrm{Tr}\big(r_M(\gamma_N)O_M\big) = \mathrm{Tr}\big(\gamma_N \iota_M(O_M)\big)$ for all O_M. This means again that the operation of the state reduction r_M is just the adjoint map of the operator extension ι_M. It turns out that this holds if and only if the state reduction is done by

$$\begin{aligned} r_M : \quad \mathcal{D}(\mathcal{F}) \quad &\longrightarrow \quad \binom{N}{M} \mathcal{D}(\mathcal{K}^{\veebar M}), \\ \gamma_N \quad &\longmapsto \quad \frac{1}{M!} \sum_{\boldsymbol{i},\boldsymbol{j}\in I_M^{\otimes}} \mathrm{Tr}\Big(\gamma a^\dagger\big(|\varphi_{j_1}\rangle\big) \dots a^\dagger\big(|\varphi_{j_M}\rangle\big) a\big(|\varphi_{i_M}\rangle\big) \dots a\big(|\varphi_{i_1}\rangle\big)\Big) |\varphi_{\boldsymbol{i}}\rangle\langle\varphi_{\boldsymbol{j}}|, \end{aligned} \tag{2.83}$$

For example, the one-electron reduced state of an N-electron state $\gamma_N \in \mathcal{D}(\mathcal{F})$ is

$$r_1(\gamma_N) = \sum_{i,j=1}^{d} \mathrm{Tr}\Big(\gamma_N a^\dagger\big(|\varphi_j\rangle\big) a\big(|\varphi_i\rangle\big)\Big) |\varphi_i\rangle\langle\varphi_j| =: \sum_{i=1}^{d} \lambda_i |\tilde{\varphi}_i\rangle\langle\tilde{\varphi}_i|, \tag{2.84}$$

where the eigenvectors $|\tilde{\varphi}_i\rangle$ are called *natural orbitals* and the eigenvalues λ_i (summing up to N) are the *natural occupations*. For example, if the fermionic state is the pure state of a basis vector (2.64), then the one-body reduced state is the uniform mixture of the one-body states of the component vectors, $r_1(|\varphi_{\boldsymbol{i}}\rangle\langle\varphi_{\boldsymbol{i}}|) = \sum_{i\in\boldsymbol{i}} |\varphi_i\rangle\langle\varphi_i|$, so the natural orbitals are the basis vectors.

2.12. Many-body observables and states: mode picture

We can also consider operators, states and reduced states in the mode picture. Here we deal with finite, $d < \infty$ number of modes only, labelled by $L = [d]$.

In the bosonic case we can obtain the extension (2.5), reduction (2.6) and the reduced state as it was introduced in the distinguishable case in section 2.2, since the modes are distinguishable, and the bosonic mode operators of distinct mode subsets are commuting (2.76). In numerical calculations the number of maximal occupation is restricted, leading to finite dimensional occupation spaces, $\dim(\mathcal{N}_i) = \nu_{\max} < \infty$ for $i \in [d]$. In this case, however, the canonical commutation relation (2.76) cannot be satisfied, and the formula (2.79) of the mode transformation cannot be derived either. So such restricted occupation description is valid only if we operate on physically and numerically relevant subspace of the Hilbert space for which $\nu_i < \nu_{\max}$. In the extremal case, due to the strong one-mode repulsion, the bosons become the so-called hard-core bosons, for which $\nu_{\max} = 1$, leading to a mixed commutation relation. We discuss this in chapter 5.

In the fermionic case, the tensor product structure on the occupation number space $\mathcal{N}_{[d]}$ does not resemble well the mode subset structure. This is because the Jordan–Wigner representation of the creation and annihilation operators (2.75) are non-local with respect to that. This holds of course not only for the Jordan–Wigner representation, the fermionic mode operators cannot be represented locally, since they anticommute (2.76), while the local operators of disjoint mode subsets, given by (2.5), commute. The parity superselection rule restores commutativity (algebraic independence) of disjoint mode subsets, by which the locality of disjoint mode subsets and maps acting on those become meaningful, on which the mere definition of correlation and entanglement rely. Let us have the nested mode subsets $Y \subseteq X \subseteq L = [d]$. It turns out [**Sza21**] that the observables O_Y of mode subset Y among the observables of mode subset X are given by the *fermionic mode operator extension*

$$\begin{aligned} \tilde{\iota}_{Y,X} = \mathrm{Ad}_{U_{Y,\bar{Y}}} \circ \iota_{Y,X} : \mathrm{Lin}(\mathcal{N}_Y) &\longrightarrow \mathrm{Lin}(\mathcal{N}_X), \\ O_Y &\longmapsto U_{Y,\bar{Y}} (O_Y \otimes \mathrm{I}_{\bar{Y}}) U_{Y,\bar{Y}}^\dagger, \end{aligned} \tag{2.85}$$

where the non-local unitary $U_{Y,\bar{Y}}$ is diagonal, given as

$$U_{Y,\bar{Y}} = \sum_{\boldsymbol{\nu}\in\{0,1\}^d} (-1)^{\sum_{i\in\bar{Y}} \nu_i \sum_{j\in X, i<j} \nu_j} |\phi_{\boldsymbol{\nu}}\rangle\langle\phi_{\boldsymbol{\nu}}|. \tag{2.86}$$

If the state of mode subset X is given by $\varrho_X \in \mathcal{D}_X$, $\varrho_Y := \tilde{r}_{X,Y}(\varrho_X) \in \mathcal{D}_Y$ of mode subset Y is the state that gives back the expectation values of observables of mode subset Y, that is,

$\mathrm{Tr}\big(\tilde{r}_{X,Y}(\varrho_X)O_Y\big) = \mathrm{Tr}\big(\varrho_X \tilde{\iota}_{Y,X}(O_Y)\big)$ for all O_Y. This means that the operation of the state reduction $\tilde{r}_{X,Y}$ is just the adjoint map of the operator extension $\tilde{\iota}_{Y,X}$. It turns out that this holds if and only if the fermionic mode state reduction is done by the *fermionic partial trace* operation

$$\begin{aligned} \tilde{r}_{X,Y} = r_{X,Y} \circ \mathrm{Ad}_{U^\dagger_{Y,\bar{Y}}} : \quad \mathrm{Lin}(\mathcal{N}_X) &\longrightarrow \mathrm{Lin}(\mathcal{N}_Y), \\ \varrho_X &\longmapsto \mathrm{Tr}_{X\setminus Y}(U^\dagger_{Y,\bar{Y}} \varrho_X U_{Y,\bar{Y}}), \end{aligned} \tag{2.87}$$

with the unitary above (2.86) and the partial trace (2.6).

The corresponding operator on the occupation number space $\mathcal{N}_{[d]}$ can be obtained by the map the (2.72),

$$F\iota_M(O)F^{-1} = \frac{1}{M!} \sum_{\boldsymbol{i},\boldsymbol{j}\in I_M^\otimes} \langle\varphi_{\boldsymbol{i}}|O_M|\varphi_{\boldsymbol{j}}\rangle a^\dagger_{i_1} \dots a^\dagger_{i_M} a_{j_M} \dots a_{j_1} \in \mathrm{Lin}(\mathcal{N}_{[d]}). \tag{2.88}$$

2.13. The many-body Hamiltonian

Equipped with the formulas of classical Hamiltonian mechanics, it is intuitive to construct the quantum Hamiltonian by replacing the dynamical variables (such as positions, momenta, angular momentum, ...) by their corresponding operators. However, there is no logical way to derive quantum mechanics from classical mechanics, but predictions of quantum mechanics in the high-energy limit must coincide with that of classical physics. For example, the Ehrenfest relation and the Wentzel–Kramers–Brillouin approximation describes the connection between the evolution of the wave packet and the trajectory of the classical point particle.

In most of the cases, we have one-particle terms (corresponding to the kinetic energy and external potential) described by $H_1 \in \mathrm{Lin}_{\mathrm{PI}}(\mathcal{K}^{\otimes 1})$, and two-particle terms (corresponding to the particle-particle interaction) described by $H_2 \in \mathrm{Lin}_{\mathrm{PI}}(\mathcal{K}^{\otimes 2})$, and the number of particles is fixed (open systems are not considered here). By (2.88), the Hamiltonian acting on the occupation number space is

$$\begin{aligned} H &= F(\iota_1(H_1) + \iota_2(H_2))F^{-1} = \\ &= \sum_{i,j=1}^{d} (H_1)_{i,j} a^\dagger_i a_j + \frac{1}{2} \sum_{i_1,i_2,j_1,j_2=1}^{d} (H_2)_{(i_1,i_2),(j_1,j_2)} a^\dagger_{i_1} a^\dagger_{i_2} a_{j_2} a_{j_1}. \end{aligned} \tag{2.89}$$

This Hamiltonian is block diagonal with respect to the particle number subspaces, $\mathcal{N}^N_{[d]} \subset \mathcal{N}_{[d]}$, so the solution of the eigenvalue problem can be searched in these $\binom{d+N-1}{N}$ or $\binom{d}{N}$ dimensional subspaces. In the special case, when there are only one-particle terms, the problem reduces to the diagonalization of the one-particle operator H_1 in the d dimensional one-particle Hilbert space $\mathcal{K}$. By this we have

$$\begin{aligned} F\iota_1(H_1)F^{-1} = F\iota_1\big(\sum_{i,j=1}^{d} (H_1)_{i,j}|\varphi_i\rangle\langle\varphi_j|\big)F^{-1} = \\ = \sum_{i,j=1}^{d} (H_1)_{i,j} a^\dagger_i a_j = \sum_{i,j,k=1}^{d} U_{j,k}\varepsilon_k U^*_{i,k} a^\dagger_i a_j = \sum_{i=1}^{d} \varepsilon_k \tilde{a}^\dagger_k \tilde{a}_k, \end{aligned} \tag{2.90a}$$

where $\tilde{a}_i^\dagger$ are the eigenmodes obtained by mode transformation (2.78b), $\tilde{a}_i^\dagger = \sum_j U_{j,i} a_j^\dagger$. The solution of the one-mode energies (and also the dimension) does not depend on the number of particles, and being independent particles, the total energy of the system is the sum of the one-mode energies,

$$\big(F\iota_1(H_1)F^{-1}\big)|\tilde{\phi}_{\boldsymbol{\nu}}\rangle = \big(\sum_{k=1}^{d} \nu_k \varepsilon_k\big)|\tilde{\phi}_{\boldsymbol{\nu}}\rangle, \tag{2.90b}$$

where $|\tilde{\phi}_{\boldsymbol{\nu}}\rangle = g(U)|\phi_{\boldsymbol{\nu}}\rangle$.

In the presence of two-particle interactions, the solution cannot be obtained so easily. However, as we will see in chapter 4, in numerical treatment it is favourable to perform a mode transformation to get a basis that somehow fits better to the problem. In practice, when turn to numerical simulation including mode transformation, it is favourable not to transform the operators themselves to keep robustness. Rather it is practical to perform mode transformation (2.78b) in terms of the matrix elements of H_1 and H_2 in the Hamiltonian, that is,

$$\begin{aligned} g(U)Hg(U)^\dagger = &\sum_{i,j=1}^{d} \Big(\sum_{i',j'=1}^{d} U_{i,i'} (H_1)_{i'j'} U^*_{j',j} \Big) a_i^\dagger a_j + \\ &\frac{1}{2} \sum_{i_1,i_2,j_1,j_2=1}^{d} \Big(\sum_{i'_1,i'_2,j'_1,j'_2=1}^{d} U_{i_1,i'_1} U_{i_2,i'_2} (H_2)_{(i'_1,i'_2),(j'_1,j'_2)} U^*_{j'_1,j_1} U^*_{j'_2,j_2} \Big) a_{i_1}^\dagger a_{i_2}^\dagger a_{j_2} a_{j_1}. \end{aligned} \tag{2.91}$$

Usually the coefficients $(H_1)_{i,j}$ are the matrix elements of the operators of the kinetic energy and the external potential, and the coefficients $(H_2)_{(i_1,i_2),(j_1,j_2)}$ are the matrix elements of the operator of the particle-particle interaction. However, in many cases the model of the physical system is formulated directly in the second-quantized framework, and there no first-quantized form behind. We have the former case in chapters 3 and 4 (and appendix C), and the latter case in chapter 5.

3. CHAPTER

Analysis of the tailored coupled cluster in multireference systems

In quantum chemistry, a kind of standard computational method is the coupled cluster (CC) up to single and double excitations with perturbative triples, which performs well in many cases of small and medium sized molecules [**Rag89**, **Bar90**, **Bar07**]. Since this method relies on one reference Slater determinant, it may work if the system can be approximated well with one Slater determinant and fail otherwise, hence we say for these two cases that the system is of *single-reference character* and *multireference character*, respectively. Also, we say that the system is *dynamically correlated* and *statically correlated* (or it is *strongly correlated*, with terminology in physics), respectively. Moreover, the CC approach also fails if the energy gap between the highest occupied molecular orbital and the lowest unoccupied molecular orbital (*HOMO-LUMO gap*) becomes small. (See appendix C for a brief summary of the single-reference approaces.) On the other hand, the DMRG is a powerful method in statically correlated systems [**Whi99**], however, the computational demands are governed by the bond dimension.

One of the possibilities to overcome this problem is using externally corrected CC, that is, splitting of the FCI space into active space and an external space (see section 3.1) to resolve the static and dynamical correlation, respectively. Computational advantages can be gained by the CC method tailored by the density matrix renormalization group (DMRG-TCC) restricted to single and double excitations, which was demonstrated on large and statically correlated systems [**Vei16**, **Vei18**]. Here, in section 3.3, we show a numerical and theoretical analysis of the DMRG-TCC method, and demonstrate it on the nitrogen dimer, providing also error analysis.

3.1. Tailored coupled cluster method

Several attempts have been made based on multireference coupled cluster theory [**Bar07**, **Lya12**] to make corrections for statically correlated systems, and outperform the single-reference CC method. These methods can be grouped [**Lya12**] into valence-universal, state-universal and state-specific approaches. One of the possible refinement of the CC method is partitioning of the cluster operator [**Pie93**, **Pie94**]. A notable advantage of the *tailored coupled cluster* (TCC) approach over the conventional multireference CC methods is that the cluster operator is the linear combination of commuting excitation operators [**Kin05**]. Clearly, it is worth partitioning the $L = \{1, \ldots, d\}$ orbitals and the cluster operator accordingly. So let us write the space of orbitals as $\mathcal{K} = \mathcal{K}_Y \oplus \mathcal{K}_{\bar{Y}}$, where $\mathcal{K}_Y$ is the *space of active orbitals* and $\mathcal{K}_{\bar{Y}}$ is the *space of external orbitals*, where $Y \subseteq L$ and $\bar{Y} = L \setminus Y$. The space of active orbitals is spanned by

$k = |Y|$ well-chosen orbitals, $\mathcal{K}_Y = \mathrm{Span}\{\varphi_i\}_{i\in Y}$, and the space of external orbitals is spanned by the remaining $d-k = |\bar{Y}|$ orbitals, $\mathcal{K}_{\bar{Y}} = \mathrm{Span}\{\varphi_i\}_{i\in \bar{Y}}$. This choice is of central importance, and discussed in the sequel (section 3.5). Once a reference (C.13) is fixed, we have the occupied and virtual orbitals for the active orbitals, $Y_\mathrm{o} := Y \cap L_\mathrm{o}$, $Y_\mathrm{v} := Y \cap L_\mathrm{v}$, respectively. Similarly we have the occupied and virtual orbitals for the external orbitals, $\bar{Y}_\mathrm{o} := \bar{Y} \cap L_\mathrm{o}$, $\bar{Y}_\mathrm{v} := \bar{Y} \cap L_\mathrm{v}$. This partition is made because we want to perform approximative calculations in which the electrons of the $\bar{Y}_\mathrm{o}$ orbitals are "frozen" and the $\bar{Y}_\mathrm{v}$ orbitals remain unoccupied. This can be formulated in the occupation number space by (2.73b), and this subspace is called *complete active space (CAS)*

$$\mathcal{N}_\mathrm{CAS} := \mathcal{N}^{|\bar{Y}_\mathrm{o}|,N-|\bar{Y}_\mathrm{o}|,0}_{\bar{Y}_\mathrm{o},Y,\bar{Y}_\mathrm{v}}. \tag{3.1a}$$

We can write the corresponding projection with the excitaiton operators,

$$P_\mathrm{CAS} := \sum_{\mu\in J(Y_\mathrm{o},Y_\mathrm{v})} |\mathrm{X}_\mu\Phi^\mathrm{HF}\rangle\langle \mathrm{X}_\mu\Phi^\mathrm{HF}| + |\Phi^\mathrm{HF}\rangle\langle\Phi^\mathrm{HF}|. \tag{3.1b}$$

The naming suggests that this subspace is of high importance and accurate numerical treatment is demanded. The orthogonal complement of CAS is the *external space*, $\mathcal{N}_\mathrm{ext}$ such that $\mathcal{N}^N_L = \mathcal{N}_\mathrm{CAS} \oplus \mathcal{N}_\mathrm{ext}$.

The TCC parametrization [**Kin05**] of the (intermediately normalized) state vector is

$$\begin{aligned} |\Phi^\mathrm{TCC}\rangle &= \mathrm{e}^{T+S}|\Phi^\mathrm{HF}\rangle = \mathrm{e}^{(T_1+T_2+\ldots)+(S_1+S_2+\ldots)}|\Phi^\mathrm{HF}\rangle, \\ S_M &= \sum_{\mu\in J_M(Y_\mathrm{o},Y_\mathrm{v})} s_\mu \mathrm{X}_\mu, \\ T_M &= \sum_{\mu\in \bar{J}_M(Y_\mathrm{o},Y_\mathrm{v})} t_\mu \mathrm{X}_\mu, \end{aligned} \tag{3.2}$$

where the full cluster operator (C.17) is partitioned into the sum $S+T$. In the cluster operator S of the CAS, such terms from the full cluster operator are included in which the excitation indices (both the M occupied and M virtual) are in Y, that is, $\mu \in J_M(Y_\mathrm{o}, Y_\mathrm{v})$. The cluster operator T of the rest, contains the remaining terms, that is, $\mu \in \bar{J}_M(Y_\mathrm{o}, Y_\mathrm{v}) := J_M(L_\mathrm{o}, L_\mathrm{v}) \setminus J_M(Y_\mathrm{o}, Y_\mathrm{v})$. This is merely a partition of the sum in the definition of the full cluster operator (C.17), therefore S and T commute, so $\mathrm{e}^{T+S} = \mathrm{e}^T\mathrm{e}^S$. Consequently, the TCC is an externally corrected approach, but fundamentally a single-reference method. The motivation of this partition is that the CAS amplitudes are to describe the so called *static correlations*, and the rest of the amplitudes are to describe the *dynamic correlations* in the system, hence calculated by different methods.

First, calculation in the $\mathcal{N}_\mathrm{CAS}$ subspace is performed. The approximate solution of (C.16) for the *CAS Hamiltonian* $H_\mathrm{CAS} := P_\mathrm{CAS} H P_\mathrm{CAS}$ is calculated, in our case with DMRG. Note that the H_CAS is not the restriction of the Hamiltonian to active orbital terms but also contains terms from the *frozen-core orbitals* $\bar{Y}_\mathrm{o}$. Then, the $\mu \in J(Y_\mathrm{o}, Y_\mathrm{v})$ excitation terms of the confiuration

interaction (CI) (C.15) and the CC (C.17) parametrization are matched, that is,

$$\begin{aligned} \mathrm{e}^{S_1+S_2+\ldots}|\Phi^{\mathrm{HF}}\rangle &= (\mathrm{I}+C_1+C_2+\ldots)|\Phi^{\mathrm{HF}}\rangle, \\ s_i^j &= c_i^j, && (i,j)\in J_1(Y_{\mathrm{o}},Y_{\mathrm{v}}), \\ s_{(i_1,i_2)}^{(j_1,j_2)} &= c_{(i_1,i_2)}^{(j_1,j_2)} - c_{i_1}^{j_1}c_{i_2}^{j_2} + c_{i_1}^{j_2}c_{i_2}^{j_1}, && ((i_1,i_2),(j_1,j_2))\in J_2(Y_{\mathrm{o}},Y_{\mathrm{v}}), \\ &\vdots && . \end{aligned} \tag{3.3}$$

Next, calculation in the $\mathcal{N}_{\mathrm{ext}}$ subspace is performed with a fixed solution in the CAS. That is, the amplitudes s in the CAS from (3.3) serve as input and kept fixed while solving the CC equations (C.18). To be more precise, in the linked CC formalism the tailored CC equations are solved,

$$\begin{cases} \mathcal{E}(t;s) = E = \langle\Phi^{\mathrm{HF}}|\mathrm{e}^{-S}\mathrm{e}^{-T}H\mathrm{e}^{T}\mathrm{e}^{S}|\Phi^{\mathrm{HF}}\rangle, \\ 0 = \langle\mathrm{X}_\mu\Phi^{\mathrm{HF}}|\mathrm{e}^{-S}\mathrm{e}^{-T}H\mathrm{e}^{T}\mathrm{e}^{S}|\Phi^{\mathrm{HF}}\rangle, \quad \mu\in\bar{J}(Y_{\mathrm{o}},Y_{\mathrm{v}}), \end{cases} \tag{3.4}$$

where $\bar{J}(Y_{\mathrm{o}},Y_{\mathrm{v}}) := J(L_{\mathrm{o}},L_{\mathrm{v}})\setminus J(Y_{\mathrm{o}},Y_{\mathrm{v}}) = \bar{J}_1(Y_{\mathrm{o}},Y_{\mathrm{v}})\cup\bar{J}_2(Y_{\mathrm{o}},Y_{\mathrm{v}})\cup\ldots$, that is, only the not-CAS equations are considered. It is also important to note that in this scheme the CAS cluster amplitudes $J(Y_{\mathrm{o}},Y_{\mathrm{v}})$ are independent of the rest of the amplitudes $\bar{J}(Y_{\mathrm{o}},Y_{\mathrm{v}})$.

3.2. Properties of the tailored coupled cluster approach

Here we consider the formal properties of the TCC aproach. First, the lack of equivalence of linked and unlinked TCC equations, then, the size-consistency of the TCC. These are the direct consequences of the parametrization (3.2) and the tailoring (3.3) and (3.4).

It is important to highlight that, unlike in the conventional CC case (C.18), the linked and unlinked TCC equations are in general not equivalent [**Fau19b**]. To show this, we follow the argument of textbooks [**Hel00**] adapted to the TCC case. We say that J is *excitation complete* (or *complete under deexcitations*) if for all $\mu,\nu\in J$ we have $(\mathrm{X}_\mu)^\dagger\mathrm{X}_\nu|\Phi^{\mathrm{HF}}\rangle\in\mathrm{Span}\{\mathrm{X}_\eta|\Phi^{\mathrm{HF}}\rangle \mid \eta\in J\}\oplus\mathrm{Span}\{|\Phi^{\mathrm{HF}}\rangle\}$. For example, CCSD, CCSDT,..., or CCD are of this kind. We assume that $J(Y_{\mathrm{o}},Y_{\mathrm{v}})$ is excitation complete, consequently,

$$\left(\sum_{\mu\in J(Y_{\mathrm{o}},Y_{\mathrm{v}})}|\mathrm{X}_\mu\Phi^{\mathrm{HF}}\rangle\langle\mathrm{X}_\mu\Phi^{\mathrm{HF}}| + \sum_{\mu\in\bar{J}(Y_{\mathrm{o}},Y_{\mathrm{v}})}|\mathrm{X}_\mu\Phi^{\mathrm{HF}}\rangle\langle\mathrm{X}_\mu\Phi^{\mathrm{HF}}| + |\Phi^{\mathrm{HF}}\rangle\langle\Phi^{\mathrm{HF}}|\right)\mathrm{e}^{-S}\mathrm{e}^{-T} = \mathrm{e}^{-S}\mathrm{e}^{-T}, \tag{3.5}$$

that is, the expression in the parenthesis acts identically on the exponential of cluster operators containing excitation complete excitations. Now, we consider the matrix $\langle\mathrm{X}_\nu\Phi^{\mathrm{HF}}|\mathrm{e}^{S}\mathrm{e}^{T}|\mathrm{X}_\mu\Phi^{\mathrm{HF}}\rangle$ for $\mu,\nu\in J(L_{\mathrm{o}},L_{\mathrm{v}})$, which is block-lower triangular with respect to the excitation rank, and all the diagonal elements are one, therefore being not singular. So with this matrix the system of equations for the linked TCC (3.4) can be transformed, that is, we have an equivalent system of

equations

$$\begin{aligned}0 =& \sum_{\mu\in\bar{J}(Y_\mathrm{o},Y_\mathrm{v})} \langle \mathrm{X}_\nu\Phi^\mathrm{HF}|\mathrm{e}^S\mathrm{e}^T|\mathrm{X}_\mu\Phi^\mathrm{HF}\rangle\langle \mathrm{X}_\mu\Phi^\mathrm{HF}|\mathrm{e}^{-S}\mathrm{e}^{-T}H\mathrm{e}^T\mathrm{e}^S|\Phi^\mathrm{HF}\rangle \\ =&\langle \mathrm{X}_\nu\Phi^\mathrm{HF}|H\mathrm{e}^T\mathrm{e}^S|\Phi^\mathrm{HF}\rangle - E\langle \mathrm{X}_\nu\Phi^\mathrm{HF}|\mathrm{e}^T\mathrm{e}^S|\Phi^\mathrm{HF}\rangle \\ &- \sum_{\mu\in J(Y_\mathrm{o},Y_\mathrm{v})} \langle \mathrm{X}_\nu\Phi^\mathrm{HF}|\mathrm{e}^S\mathrm{e}^T|\mathrm{X}_\mu\Phi^\mathrm{HF}\rangle\langle \mathrm{X}_\mu\Phi^\mathrm{HF}|\mathrm{e}^{-S}\mathrm{e}^{-T}H\mathrm{e}^T\mathrm{e}^S|\Phi^\mathrm{HF}\rangle\end{aligned} \tag{3.6}$$

for all $\nu \in \bar{J}(Y_\mathrm{o}, Y_\mathrm{v})$. In the second equation (3.5) and the energy expression of the linked TCC equations (3.4) are used. The first two terms in the right-hand-side of (3.6) cancel each other because they describe the unlinked CC equations (see section C.6), however, the last term is non-zero. This is because of the fact that the product of a CAS- and an external-type excitation results external-type excitation(s), that is, there are some non-zero vectors $\mathrm{X}_\eta\mathrm{X}_\mu|\Phi^\mathrm{HF}\rangle \in \mathrm{Span}\big\{\mathrm{X}_\nu|\Phi^\mathrm{HF}\rangle \;\big|\; \nu \in \bar{J}(Y_\mathrm{o}, Y_\mathrm{v})\big\}$, for some $\mu \in J(Y_\mathrm{o}, Y_\mathrm{v})$ and $\nu \in \bar{J}(Y_\mathrm{o}, Y_\mathrm{v})$. Obviously, if Y is the empty set, the TCC (3.4) simplifies to the conventional CC (C.18) approach, in which the sum over $\mu \in J(Y_\mathrm{o}, Y_\mathrm{v})$ is empty, proving the equivalence of the linked and unlinked formulations in that case.

To prove the size-extensivity of the DMRG-TCC, as in section C.5, consider the bipartition of the orbitals $L_A \subset L$ and $L_B = L \setminus L_A$, and the corresponding occupied and virtual orbitals, $L_{A,\mathrm{o}} := L_A \cap L_\mathrm{o}$ and $L_{A,\mathrm{v}} := L_A \cap L_\mathrm{v}$, respectively; and similarly for subsystem B. Let the projected Schrödinger equation in the linked TCC from (3.4) for subsystem A with the Hamiltonian of H_A be fulfilled by $|\Phi^{A,\mathrm{TCC}}\rangle = \mathrm{e}^{(T_1^A+T_2^A+\ldots)+(S_1^A+S_2^A+\ldots)}|\Phi^\mathrm{HF}\rangle$, where the CAS solution of A is described by $S_M^A = \sum_{\mu\in J_M(Y_{A,\mathrm{o}},Y_{A,\mathrm{v}})} s_\mu \mathrm{X}_\mu$, and TCC solution of A is described by $T_M^A = \sum_{\mu\in \bar{J}_M(Y_{A,\mathrm{o}},Y_{A,\mathrm{v}})} t_\mu \mathrm{X}_\mu$, that is, excitaion indices are only in subsystem A; and similarly for subsystem B. If the subsystems are independent, the Hamiltonian can be written as $H = H_A + H_B$, then the projected Schrödinger equation in the linked TCC from (3.4) for $H = H_A + H_B$ is fulfilled by $|\Phi^\mathrm{TCC}\rangle = \mathrm{e}^{S^A+T^A}\mathrm{e}^{S^B+T^B}|\Phi^\mathrm{HF}\rangle$, that is,

$$\begin{aligned}0 =&\langle \mathrm{X}_\mu\Phi^\mathrm{HF}|\mathrm{e}^{-S^A-T^A}\mathrm{e}^{-S^B-T^B}(H_A+H_B)\mathrm{e}^{S^A+T^A}\mathrm{e}^{S^B+T^B}|\Phi^\mathrm{HF}\rangle \\ =&\langle \mathrm{X}_\mu\Phi^\mathrm{HF}|\mathrm{e}^{-S^A-T^A}H_A\mathrm{e}^{S^A+T^A}|\Phi^\mathrm{HF}\rangle + \\ &\langle \mathrm{X}_\mu\Phi^\mathrm{HF}|\mathrm{e}^{-S^B-T^B}H_B\mathrm{e}^{S^B+T^B}|\Phi^\mathrm{HF}\rangle, \qquad \mu \in \bar{J}(Y_\mathrm{o}, Y_\mathrm{v}).\end{aligned} \tag{3.7}$$

In the second equation we used that the cluster operators of subsystem A (B) commutes with the Hamiltonian of the independent subsystem B (A). For indices $\mu \in \bar{J}(Y_{A,\mathrm{o}}, Y_{A,\mathrm{v}})$, the first term is zero by assumption, the second is zero because X_μ commutes with operators acting on the B subsystem. Similar argument applies for indices $\mu \in \bar{J}(Y_{B,\mathrm{o}}, Y_{B,\mathrm{v}})$. It remains to see that for indices in $\bar{J}(Y_\mathrm{o}, Y_\mathrm{v})\setminus\big(\bar{J}(Y_{A,\mathrm{o}}, Y_{A,\mathrm{v}})\cup\bar{J}(Y_{B,\mathrm{o}}, Y_{B,\mathrm{v}})\big)$ the expression (3.7) vanishes. This is because, X_μ acts non-trivially on both subsystems, but the similarity-transformed Hamiltonian is the sum of that of the subsystems. To be more precise, if the HF reference is $|\Phi^\mathrm{HF}\rangle = a_{i_1}^\dagger \ldots a_{i_{N_1}}^\dagger a_{j_1}^\dagger \ldots a_{j_{N_2}}^\dagger|\Phi^\mathrm{vac}\rangle$, with $\{\boldsymbol{i}\} = I_{N_1}^\wedge(L_{A,\mathrm{o}})$ and $\{\boldsymbol{j}\} = I_{N_2}^\wedge(L_{B,\mathrm{o}})$, then $\mathrm{X}_\mu|\Phi^\mathrm{HF}\rangle = a_{i'_1}^\dagger \ldots a_{i'_{N_1}}^\dagger a_{j'_1}^\dagger \ldots a_{j'_{N_2}}^\dagger|\Phi^\mathrm{vac}\rangle$, with different indices in both subsystems, with $\boldsymbol{i} \neq \boldsymbol{i'} \in I_{N_1}^\wedge(L_A)$ and $\boldsymbol{j} \neq \boldsymbol{j'} \in I_{N_2}^\wedge(L_B)$, resulting

orthogonality in both terms, which establish (3.7). Because of the exponential ansatz, the truncation of the excitation rank does not lead to the violation of size-consistency. The size-consistency of the conventional CC (C.18) follows from the special case if Y is the empty set.

3.3. Local analysis of the DMRG-TCC

As it was highlighted in section C.6, a major difference between the CI and CC method is that the CC is not variational, and since the TCC method is merely the partition of the cluster operator (3.2), it is also not variational. The analysis of the CC and TCC can be formulated as a nonlinear Galerkin scheme, which is a well-established framework in numerical analysis. Note that, however, the analysis of the TCC [**Fau19a**] is more involved than that of the CC [**Sch09**, **Roh13**, **Lae19**]. In spite of being nonvariational, thus not obeying (C.3), the *local uniqueness* and *quasioptimality* of the DMRG-TCC solution can be proved under two assumptions [**Fau19a**]. The quasioptimality means that taking a fixed DMRG solution in $\mathcal{N}_{\mathrm{CAS}}$, the CC solution in $\mathcal{N}_{\mathrm{ext}}$ converges in the truncation hierarchy (with respect to the excitation rank), and gives the best possible solution up to a multiplicative constant. Based on Zarantonello's theorem [**Zei90**, **Lae19**], this property can be formulated with an inequality, which replaces (C.3a) [**Fau19a**]. The local uniqueness means that taking a fixed DMRG solution in $\mathcal{N}_{\mathrm{CAS}}$, the CC solution in $\mathcal{N}_{\mathrm{ext}}$ is unique around the exact solution [**Fau19a**].

The two assumptions are the following. First, the Fock operator $F_1 \in \mathrm{Lin}(\mathcal{K})$, defined in (C.10), is assumed to be bounded and have a *CAS-external (CAS-ext) gap*

$$0 < \Delta(Y, \bar{Y} \cap L_{\mathrm{v}}) = (\min_{j \in \bar{Y}_{\mathrm{v}}} \epsilon_j) - (\max_{i \in Y} \epsilon_i) \tag{3.8}$$

in its spectrum, which is the gap between the energy of the lowest unoccupied external orbital and that of the highest active orbital (unoccupied or occupied). As it is noted in section C.6, the numerical convergence of the quasi-Newton method depends on the HOMO-LUMO gap (C.22), and this assumption is standard in the analysis of dynamically correlated systems. In our TCC approach we circumvent and replace this condition by the CAS-external gap (3.8) assumption. Moreover, it turns out that due to the fixed CAS amplitudes s, the crucial stability condition in the solution of the TCC equations (3.4) becomes larger than the CAS-external gap (3.8) and can be estimated by $\Delta(Y_{\mathrm{o}}, \bar{Y}_{\mathrm{v}})$, which is the gap between the energy of the LUMO in the external space and that of the HOMO in the CAS [**Fau19b**, **Fau19a**].

Second, let us have fixed CAS amplitudes s and the corresponding CAS cluster operator S, then the map

$$t \longmapsto \mathrm{e}^{-T}\mathrm{e}^{-S} W \mathrm{e}^{S}\mathrm{e}^{T}|\Phi^{\mathrm{HF}}\rangle \tag{3.9}$$

is assumed to have a *small enough* Lipschitz-continuity constant, where $W := \iota_{1,N}(H_1) + \iota_{2,N}(H_2) - \iota_{1,N}(F_1)$ is the *fluctuation operator*. Since W is the difference of the Hamiltonian and the Fock operator, it describes the difference between the effective electron-electron repulsion and the true two-electron (Coulomb) potential. The physical interpretation of the Lipschitz condition of the map (3.9), containing the similarity transformed W with fixed CAS amplitudes s, is at the moment unclear.

We note again that in this chapter the mathematical and numerical analysis was performed for a fixed orbital set. However, in the DMRG framework, both the extrapolation to the complete basis limit ($d \to \infty$) [**Fri22b**], and optimization of the underlying basis (see chapter 4) can be analysed.

3.4. Error estimates for the DMRG-TCC method

The energy error of the DMRG-TCC method, being nonvariational, does not obey the bound (C.3b). However, derivations shows that the absolute value of the energy error measured from the FCI energy obeys a quadratic bound in terms of the CC amplitudes [**Fau19a**]. Here we summarise the most important points of the analysis, for the precise construction and more details see [**Fau19a, Fau19b**].

In the FCI space $\mathcal{N}_L^N$, defined by $|L|$ orbitals used in the Ritz–Galerkin scheme, the numerically exact ground state $|\Phi^{\mathrm{FCI}}\rangle$ of H in the second quantized form (2.89) is still not accessible, and the task is to be approximated by the DMRG-TCCSD solution. The error estimation is given for a given CAS-ext partition $Y|\bar{Y}$, hence we write the unknown exact solution vector $|\Phi^{\mathrm{FCI}}\rangle$ and ground-state energy $E^{\mathrm{FCI}} = \mathcal{E}(t^{\mathrm{FCI}}; s^{\mathrm{FCI}})$ in the FCI space in the TCC parametrization (3.2),

$$H|\Phi^{\mathrm{FCI}}\rangle = \mathcal{E}(t^{\mathrm{FCI}}; s^{\mathrm{FCI}})|\Phi^{\mathrm{FCI}}\rangle, \qquad |\Phi^{\mathrm{FCI}}\rangle = \mathrm{e}^{T^{\mathrm{FCI}}}\mathrm{e}^{S^{\mathrm{FCI}}}|\Phi^{\mathrm{HF}}\rangle. \tag{3.10}$$

First we consider the eigenvalue problem of the CAS Hamiltonian,

$$H_{\mathrm{CAS}}|\Phi^{\mathrm{CAS}}\rangle = E^{\mathrm{CAS}}|\Phi^{\mathrm{CAS}}\rangle, \qquad |\Phi^{\mathrm{CAS}}\rangle = \mathrm{e}^{S^{\mathrm{CAS}}}|\Phi^{\mathrm{HF}}\rangle, \tag{3.11}$$

where the $H_{\mathrm{CAS}} = P_{\mathrm{CAS}} H P_{\mathrm{CAS}}$, with the projection (3.1b). So there is no coupling between the active and external orbitals, only the frozen-core contribution apperas. Therefore, the CAS solution (3.11) is not equal to the CAS part of the FCI solution (3.10), $s^{\mathrm{CAS}} \neq s^{\mathrm{FCI}}$. Moreover, in general we cannot access to the exact solution of H_{CAS}, only approximated, in our case by the DMRG solution $\mathrm{e}^{S^{\mathrm{DMRG}}}|\Phi^{\mathrm{HF}}\rangle$. To sum up, we have

$$\mathrm{e}^{S^{\mathrm{DMRG}}}|\Phi^{\mathrm{HF}}\rangle \approx \mathrm{e}^{S^{\mathrm{CAS}}}|\Phi^{\mathrm{HF}}\rangle \approx \mathrm{e}^{S^{\mathrm{FCI}}}|\Phi^{\mathrm{HF}}\rangle = P_{\mathrm{CAS}}|\Phi^{\mathrm{FCI}}\rangle. \tag{3.12}$$

The solution of the problem in the DMRG-TCCSD approach is

$$\mathcal{E}(\tilde{t}^{\mathrm{CCSD}}; \tilde{s}^{\mathrm{DMRG}}), \qquad |\Phi^{\text{DMRG-TCCSD}}\rangle = \mathrm{e}^{\tilde{T}^{\mathrm{CCSD}}}\mathrm{e}^{\tilde{S}^{\mathrm{DMRG}}}|\Phi^{\mathrm{HF}}\rangle, \tag{3.13}$$

that is, the amplitudes $(\tilde{s}^{\mathrm{DMRG}})_\mu := (s^{\mathrm{DMRG}})_\mu$ for singles and doubles $\mu \in J_1 \cup J_2$ have been extracted and passed as inputs for the system of equations (3.4). By the solution of the TCCSD part of the system of equations (3.4), we obtain $(\tilde{t}^{\mathrm{CCSD}})_\mu$ for singles and doubles $\mu \in \bar{J}_1 \cup \bar{J}_2$. For clarity, tilde is used for indicating the truncation in the excitation rank, that is, keeping only singles and doubles. (The solution up to higher excitation ranks are out of the scope of this work.) Then the total DMRG-TCCSD error measured from the exact FCI solution is estimated as

$$\Delta E := |\mathcal{E}(\tilde{t}^{\mathrm{CCSD}}; \tilde{s}^{\mathrm{DMRG}}) - \mathcal{E}(t^{\mathrm{FCI}}; s^{\mathrm{FCI}})| \leq \Delta\varepsilon + \Delta\varepsilon_{\mathrm{CAS}} + \Delta\varepsilon^*_{\mathrm{CAS}}, \tag{3.14}$$

where the terms on the right-hand side are the following. The first term,

$$\Delta\varepsilon = |\mathcal{E}(\tilde{t}^{\mathrm{CCSD}}; \tilde{s}^{\mathrm{DMRG}}) - \mathcal{E}(t^{\mathrm{CC}}; s^{\mathrm{DMRG}})|, \tag{3.15a}$$

describes the truncation error of the CCSD method from the untruncated CC for a fixed tailoring DMRG solution, that is, CAS amplitudes are truncated accordingly $\tilde{s}^{\mathrm{DMRG}}$, s^{DMRG}. Hence, the analysis of this error is similar to that of the conventional single-reference CC method [**Sch09**, **Roh13**]. The second term,

$$\Delta\varepsilon_{\mathrm{CAS}} = |\mathcal{E}(t^{\mathrm{CC}}; s^{\mathrm{DMRG}}) - \mathcal{E}(t^{\mathrm{CC}}; s^{\mathrm{CAS}})|, \tag{3.15b}$$

descibes the effect of different CAS solutions for a fixed external untruncated CC solution. This includes the error of the DMRG solution on the CAS compared to the FCI solution on the CAS, which can be controlled by the DMRG truncation error threshold (2.42). The third term,

$$\Delta\varepsilon^{*}_{\mathrm{CAS}} = |\mathcal{E}(t^{\mathrm{CC}}; s^{\mathrm{CAS}}) - \mathcal{E}(t^{\mathrm{FCI}}; s^{\mathrm{FCI}})|, \tag{3.15c}$$

is caused by the splitting $Y|\bar{Y}$, so the correlation "from" the external part "into" the CAS is ignored in the sense of fixing the CAS cluster amplitudes. Therefore, the best possible solution for a given splitting differs in general from the exact solution on $\mathcal{N}_L^N$. For the detailed analysis of the quadratic bounds of each error term, we refer to [**Fau19b**, **Fau19a**].

The TCC solution depends strongly on the choice of the active orbitals Y, and the derived error bounds has a highly complicated Y-dependence. Therefore the analysis [**Fau19a**] summarized above is not directly applicable, so it is motivated to further investigate the Y-dependence of the overall error ΔE (3.14). Let $(t^{\mathrm{CC}}; s^{\mathrm{DMRG}})$ be the solution of (3.4). If $s^{\mathrm{DMRG}} \to s^{\mathrm{CAS}}$ then we obtain that $(t^{\mathrm{CC}}; s^{\mathrm{CAS}})$ is also close to a solution of (3.4) since the TCC method is numerically stable (section 3.3), that is, a small perturbation in the input s corresponds to a small perturbation in the solution t. This $s^{\mathrm{DMRG}} \to s^{\mathrm{CAS}}$ limit can again be controlled and analysed by tuning the DMRG truncation error threshold (2.42). Furthermore, if we assume that $t^{\mathrm{CCSD}} \approx t^{\mathrm{CC}}$, which is reasonable for the equilibrium bond length of N_2, the error can be bound as

$$\Delta E \leq C_Y \Big(\sum_{\mu \in \bar{J}_1} (\tilde{t}^{\mathrm{CCSD}})^2_\mu + \|\tilde{t}^{\mathrm{CCSD}} - \tilde{t}^{\mathrm{FCI}}\|_2^2 + \|\tilde{s}^{\mathrm{DMRG}} - \tilde{s}^{\mathrm{FCI}}\|_2^2 \Big). \tag{3.16}$$

Here the subscript Y in C_Y highlights the CAS dependence, however, the amplitudes $\tilde{s}^{\mathrm{DMRG}}$ and $\tilde{t}^{\mathrm{CCSD}}$ are also depend on Y. In the sequel, we refer to the error arising from the choice of the active orbitals Y and the fact that the CAS amplitudes are kept fixed during the CC calculation as *methodological error* of the DMRG-TCC. These are discussed and investigated numerically in section 3.7.3.

3.5. The choice of the active space

As it was formulated in (3.2), the TCC method relies on the selection of the complete active space (CAS), that is, on the choice of the active orbitals $Y \subseteq L$. For this we have $\sum_{k=0}^{d} \binom{d}{k} = 2^d$ choices, assuming $|L| = d$. Including this dependence in the above shown error analysis explicitly is a highly non-trivial task, involving many mathematical obstacles and is a part of our ongoing work. Therefore, here we extend the mathematical results of the previous sections with a numerical study on this Y-dependence.

The DMRG-TCC method becomes the bare DMRG method in the special case when all orbitals are active, $Y = L$, on the other hand, if there are no active orbitals, $Y = \emptyset$, the problem reduces to the bare CC method. We note again that the CCSD method can not resolve static correlation and the DMRG method needs high bond dimension or small truncation error threshold for dynamically correlated systems. This suggests, qualitatively, a large enough CAS with well-chosen orbitals that covers the static correlation of the system. Consequently, we require a quantitative measurement for the quality of the CAS, which presents the first obstacle for creating a non-empirical model, since the chemical concept of correlation is not well-defined [**Lya12**]. In the DMRG-TCC method, we use a quantum information theory approach to classify the orbital correlation. This classification is based on the one-orbital entropy (2.20), $S(\varrho_{\{i\}})$, and the two-orital mutual information (2.23a), $I_{i|j} = S(\varrho_{\{i\}}) + S(\varrho_{\{j\}}) - S(\varrho_{\{i,j\}})$, where $i, j \in L$. We emphasize that in practice these are basis dependent quantities, which is in agreement with the chemical definition of correlation concepts [**Lya12**]. Note that the two-orbital mutual information describes two-orbital correlations, for a more general connection between multipartite correlations and chemical bonding, see [**Szal17**].

As we will see in the sequel for the entropy and mutual information profile of N_2, one can identify pairs of orbitals with to a high mutual information value as *strongly correlated*, the pairs contributing to the plateau region as *non-dynamically correlated* and the pairs contributing to the mutual information tail as *dynamically correlated*. Also one can draw the conclusion that the orbitals with large entropies (which at the same time correspond to orbitals contributing to the largest elements of the mutual information $I_{i|j}$) can be identified already from the low bond dimension calculations. This provides us a routine procedure to form the CAS with the strongly correlated orbitals. Thus, the decreasingly ordered values of the one-orbital entropy provide guide in what order to extend the CAS by including additional orbitals. In our study, the size of the active space $k = |Y(k)|$ is systematically increased by including orbitals with the largest one-orbital entropy values,

$$Y(k) := L_{\mathrm{o}} \cup \big\{ \{i_1, \ldots, i_{k-N}\} \subseteq L_{\mathrm{v}} \;\big|\; S_{i_1} \geq \ldots \geq S_{i_{k-N}} \big\}. \tag{3.17}$$

This results that there are no occupied external orbitals, $\bar{Y}_{\mathrm{o}}$, and the smallest active space consists of all the occupied spin-orbitals, $Y(N) = L_{\mathrm{o}}$, for which the dimension of the FCI space is $\dim(\mathcal{K}_{L_{\mathrm{o}}}^{\wedge N}) = 1$, so this also reduces to the CC method. By assumption (3.8), and to avoid numerical instabilities, the degenerate orbitals in orbital energy are not separated, hence $Y(k)$ for these k values are not considered. The preceding arguments suggest that the energy error ΔE in (3.14) takes its minimum for some $Y(k) \subset L$, so there exists an optimal choice of k determining the basis splitting. Note that this feature becomes important for large systems, since calculations with high bond dimensions become unfeasible.

3.6. Computational details of the DMRG-TCCSD method

Here we give a short description how to perform DMRG-TCCSD calculations in practice, that is, finding a good set of active orbitals and the corresponding TCCSD energy $\mathcal{E}(\tilde{t}^{\mathrm{CCSD}}; \tilde{s}^{\mathrm{DMRG}})$ that approximates the FCI energy E^{FCI} of the problem with high accuracy.

After choosing the molecule and setting its geometry (which may be optimized also), HF calculation is performed with a chosen atomic orbital set $\{|\varphi_j^{\mathrm{AO}}\rangle\}_{j\in[d]}$ by solving the Roothan–Hall equation (C.12). From the resulting HF canonical molecular orbitals (C.11), the integrals (C.7), that is, the coefficients in the Hamiltonian (2.89) are computed. Then, the following steps are carried out:

(i) determine the active orbitals $Y(k)$ in terms of k,
(ii) calculate the ground state of the CAS Hamiltonian H_{CAS} by DMRG (for each $Y(k)$),
(iii) extract amplitudes $\tilde{s}^{\mathrm{DMRG}}$ from the DMRG solution (for each $Y(k)$),
(iv) calculate the tailored CCSD energy $\mathcal{E}(\tilde{t}^{\mathrm{CCSD}};\tilde{s}^{\mathrm{DMRG}})$ (for each $Y(k)$),
(v) large-scale calculation for the best $Y(k)$.

Now let us detail each step.

In step (i), a preliminary DMRG calculation is carried out for the full orbital set, that is, by setting $Y = L$. First, the order of orbitals is optimized, which is routinely used in quantum chemistry DMRG calculations (see appendix A). Then, a DMRG with a fixed low bond dimension (or with a large truncation error threshold) is carried out, and the corresponding one-orbital entropies and two-orbital mutual informations are calculated. This rough calculation already provide a qualitatively good description of the entropy profile with respect to the exact solution, so the strongly correlated orbitals can be identified. With this, the series of active spaces $Y(k)$ is determined, as described above in (3.17). Our main concern is studying the k-dependence of the quantities.

In step (ii), for each active space $Y(k)$ the projected Hamiltoian $H_{\mathrm{CAS}} = P_{\mathrm{CAS}}HP_{\mathrm{CAS}}$ is formed. First, the order of the k orbitals is optimized again. Then, large-scale DMRG calculation is carried out (that is, low truncation error threshold is used) for the ground state to get an accurate approximation of the CAS ground state, $\mathrm{e}^{S^{\mathrm{DMRG}}}|\Phi^{\mathrm{HF}}\rangle \approx \mathrm{e}^{S^{\mathrm{CAS}}}|\Phi^{\mathrm{HF}}\rangle$.

In step (iii), the CC algorithm is *tailored* by the DMRG. The entries of the full coefficient tensor $\boldsymbol{\psi}$ of the state vector (2.28) are not appearing explicitly in the DMRG algorithm but they can be accessed by the contraction of the tensor network. The number of MPS matrix multiplication in (2.55) scales exponentially, however, only the coefficient of the reference, singly and doubly excited configuration are needed. Also, the contrations of the network are performed in an optimized way, that is, common matrix product strings are *pre-contracted* [**Fau19b**]. Note that the DMRG method yields the normalized MPS form (2.55), but in the CI parametrization (C.15) the state vector is intermediately normalized. By the connection between the CI and CC parametrization (3.3), the $\tilde{s}_{\mathrm{DMRG}}$ amplitudes are calculated, which form the input of the CCSD calculation.

In step (iv), the TCC equations (3.4) are solved for single and double excitations. That is, the cluster amplitudes $\tilde{t}^{\mathrm{CCSD}}$ for the external part and the corresponding energy $\mathcal{E}(\tilde{t}^{\mathrm{CCSD}};\tilde{s}^{\mathrm{DMRG}})$ are calculated with quasi-Newton iteration techniques, implemented by standard quantum chemistry program packages [**Nee22, Val10**].

In step (v), large-scale DMRG-TCCSD calculation is performed for the best k value. As we discussed above, finding the optimal Y is a highly non-trivial problem, and this presented protocol is considered as a heuristic approach in terms of rigorous mathematics. In practice,

we carry out steps (ii)-(iv) using a relatively cheap DMRG-TCCSD scheme, that is, for some high DMRG truncation error thresholds ω_{Tr}, to find local energy minima as a function of k, $N < k < d$ (see figure 3.5 later). This can be done parallel since runs for different values of k and ω_{Tr} are independent. Around such a local minimum we perform more accurate DMRG-TCCSD calculations by lowering the ω_{Tr} in order to refine the best k. We also monitor the maximal MPS bond dimension required to reach the a priori defined ω_{Tr} as a function of k. It can happen that several k values lead to low DMRG-TCCSD energy error ΔE, while the computational effort increases significantly with increasing k. Hence we select the best k that leads to low DMRG-TCCSD energy error and also have the lowest MPS bond dimension. Using this best k value we perform large-scale (that is, up to the available computational resource) DMRG-TCCSD calculation using a relatively tight ω_{Tr}.

Our numerical study was restricted to the DMRG-TCCSD method, but the results presented here should also hold for other TNS approaches [**Mur10**, **Nak13**, **Mur15**, **Sza15**, **Gun18**].

3.7. Analysis of the splitting error for the nitrogen dimer

In practice, a routine application of the TCC method to strongly correlated molecular systems, that is, to multireference problems, became possible only recently since it requires a very accurate solution in a large CAS including all static correlations. Tensor network state methods fulfil such a high accuracy criterion, but the efficiency of the DMRG-TCCSD method strongly depends on various parameters of the involved algorithms. Some of these are defined rigorously, while others are more heuristic from the mathematical point of view. In this section we present the optimization steps for the most important parameters of the DMRG-TCCSD method and outline how the numerical error study is performed.

In our numerical study we have the nitrogen dimer N_2 with the cc-pVDZ orbital set, which is a common basis for benchmark computations [**Dun89**]. The HF calculation yields $d = 28$ canonical spatial orbitals with $N = 14$ electrons, so the FCI space is $\mathcal{N}_L^N$, where the $L = \{(1,\uparrow), (1,\downarrow), \ldots, (d,\uparrow), (d,\downarrow)\}$, with the notations of section C.3. We exploit the total spin projection (Abelian) symmetry, that is, the ground state is searched in the subspace where the total spin projection of the electron system is zero, $\mathcal{N}_{L_\uparrow, L_\downarrow}^{N/2, N/2} \subseteq \mathcal{N}_L^N$ (where $L_\uparrow = \{(1,\uparrow), \ldots, (d,\uparrow)\}$). We remark here that in our calculations the FCI space $\mathcal{N}_L^N$ is used indeed, opposed to the typical frozen-core calculations, where the two 1s spatial orbitals are omitted from $\mathcal{H}_L$, leading to a smaller space $\mathcal{N}_{L'}^{N'}$, with $L' = L \setminus \{(1,\uparrow), (1,\downarrow), (2,\uparrow), (2,\downarrow)\}$ and $N' = N - 4$. The N_2 molecule is linear, so the geometry can be defined by one parameter, the distance r of the nuclei. We investigate three different geometries by stretching the molecule, thus the performance of DMRG-TCCSD method is assessed against pure DMRG and single-reference CC methods for bond lengths $r = 2.118\,a_0, 2.700\,a_0$ and $3.600\,a_0$, where a_0 is the Bohr radius. At $r = 2.118\,a_0$ the system is close to the equilibrium geometry, so the system is not strongly correlated, implying that single-reference CC methods yield reliable results. For increasing bond length r, the system shows multireference character, that is, static correlations become more dominant. For $r > 3.500\,a_0$ this results in the variational breakdown of single-reference CC methods [**Kow00**], which means that the CC energy goes well below the FCI energy. This breakdown can be overcome with

the DMRG-TCCSD method when a large and well-chosen CAS is used. Therefore we refer to the DMRG-TCCSD method as numerically stable with respect to the bond length along the potential energy surface.

As mentioned before, the DMRG method is in general less efficient for dynamic correlations since it requires large computational resources. However, due to our specific CAS choice, the computational resource for the DMRG part of the TCC scheme is expected to be significantly lower than a pure DMRG calculation for the same level of accuracy in terms of the overall error ΔE (3.14). We investigate the overall error dependence of DMRG-TCCSD as a function of the active orbitals $Y(k)$ via k (3.17) and as a function of the DMRG truncation error threshold ω_{Tr}. That is, for our numerical error study, we perform steps (i)-(iv) for different DMRG accuracies. Also, these steps are carried out for each geometry $r = 2.118\,a_0, 2.700\,a_0$ and $3.600\,a_0$ of the N_2 molecule. We obtain reference energies for the FCI solution by very high accuracy DMRG calculations on the full orbital set ($Y = L$) with setting a prior truncation error to $\omega_{\mathrm{Tr}} = 10^{-8}$.

3.7.1. Entropic quantities of the full orbital set Before we turn to the selection of the active orbitals $Y \subseteq L$ based on entropic quantities, we show DMRG results for the full orbital set, that is, the CAS is formed by the $Y = L$ orbitals, for various fixed bond dimension $\tilde{D}$ values and for various a priori defined truncation error thresholds up to $\omega_{\mathrm{Tr}} = 10^{-8}$. In the latter case the maximal bond dimension was set to $\tilde{D}_{\mathrm{max}} = 10000$. In figure 3.1 (a) we show the relative error ΔE_{rel} of the ground-state energy as a function of the DMRG truncation error threshold on a logarithmic scale. The reference energies for the relative errors are obtained by DMRG calculations with truncation error threshold $\omega_{\mathrm{Tr}} = 10^{-8}$. We note that for equilibrium geometry $r = 2.118\,a_0$ we could have choosen deeper referece energy available in the literature, obtained by CCSDTQPH-fc calculation [**Cha04**], however, for stretched geometries our DMRG energy with $\omega_{\mathrm{Tr}} = 10^{-8}$ are below that of CCSDTQPH-fc. It can be seen that the relative error is a linear function of the truncation error on a logarithmic scale, thus extrapolation to the truncation free solution of the energy can be carried out according to references [**Leg96, Leg03a**].

To establish step (i) in section 3.6, in figures 3.2 and 3.3, we present the sorted values of the one-orbital entropy and of the two-orbital mutual information, respectively, obtained for fixed $\tilde{D} = 64, 256, 512$ bond dimensions and with $\omega_{\mathrm{Tr}} = 10^{-8}$ truncation error threshold for the three geometries. Because of the spatial orbital formulation we have $\dim(\mathcal{N}_i) = 4$, so the entropy varies between 0 and $\ln(4)$, while the mutual information of two spatial orbitals varies between 0 and $2\ln(4)$. As it can be seen in the figures, the profiles of the entropic quantities are robust, that is, low-accuracy profiles already resemble the main characteristics of the high-accuracy profiles ($\tilde{D} \approx 10000$). This allows one to approximate the entropy and mutual information profile of the full system L from a prior DMRG computation with low bond dimension, so low computational cost. Therefore, orbitals with large one-orbital entropies, also contributing to large values of $I_{i|j}$, can easily be identified from a low-accuracy computation. According to (3.17), the active space can be extended systematically for our DMRG-TCCSD study, that is, performing steps (ii)-(v) in section 3.6.

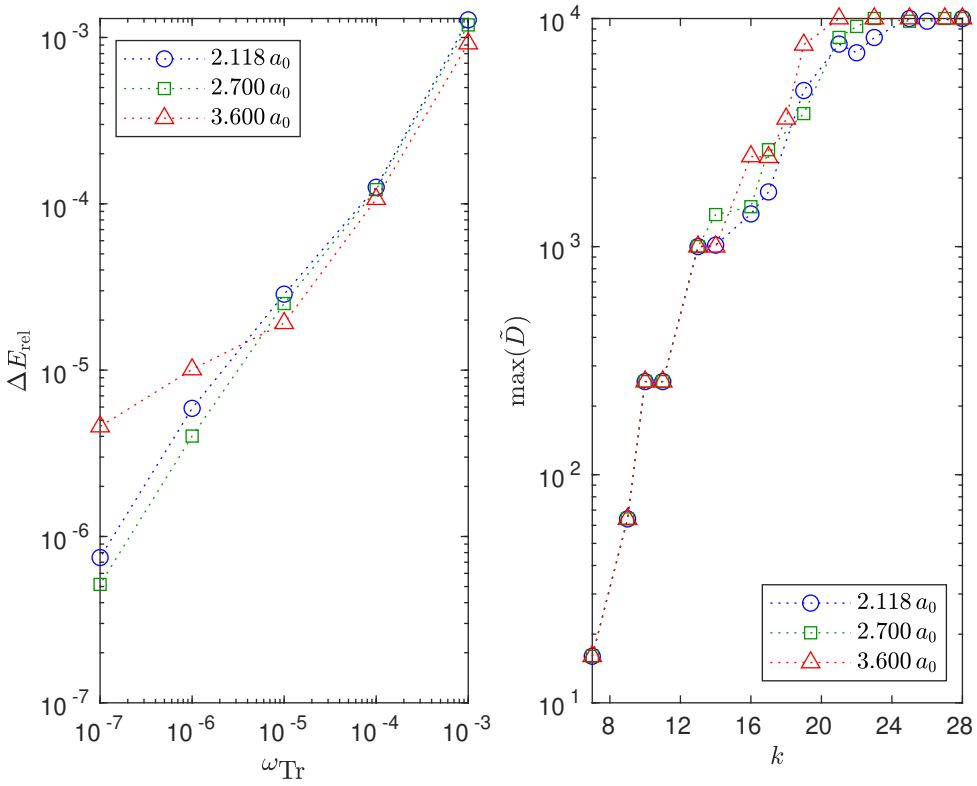

FIGURE 3.1. (a) Relative error of the ground-state energy as a function of the DMRG truncation error threshold on a logarithmic scale obtained for the full orbital set ($k = 28$) for $r = 2.118\,a_0$ (blue), $2.700\,a_0$ (green) and $3.600\,a_0$ (red). The reference energies are DMRG calculations with truncation error threshold $\omega_{\mathrm{Tr}} = 10^{-8}$. (b) Maximum bond dimension as a function of the number of the active orbitals for the a priori defined truncation error threshold $\omega_{\mathrm{Tr}} = 10^{-8}$.

Taking a look at figure 3.2, it becomes apparent that S_i shifts upwards for increasing r, indicating the higher contribution of static correlations for the stretched geometries. Similarly, the first 50-100 highest values of $I_{i|j}$ take larger values for larger r, while the exponential tail, corresponding to dynamic correlations, is less effected. The gap between large and small values of the orbital entropies gets larger, and its position shifts rightward for larger r. Thus, for the stretched geometries, more orbitals must be included in the CAS during the TCC scheme in order to determine the static correlations accurately. We remark here that the orbitals contributing to the high values of the one-orbital entropy and two-orbital mutual information values may change for the different geometries according to chemical bond forming and breaking processes [**Bog13**]. In figure 3.4, the one-orbital entropies are shown for more stretched geometries, and also the index label of the first six orbitals with highest entropy are inscribed. We note again that the orbitals are obtained from HF calculation, and the spactial orbital index labels $\{1, 2, \ldots, 28\}$ are such that bigger indices correspond to higher Hartree–Fock orbital energies. By this, we can

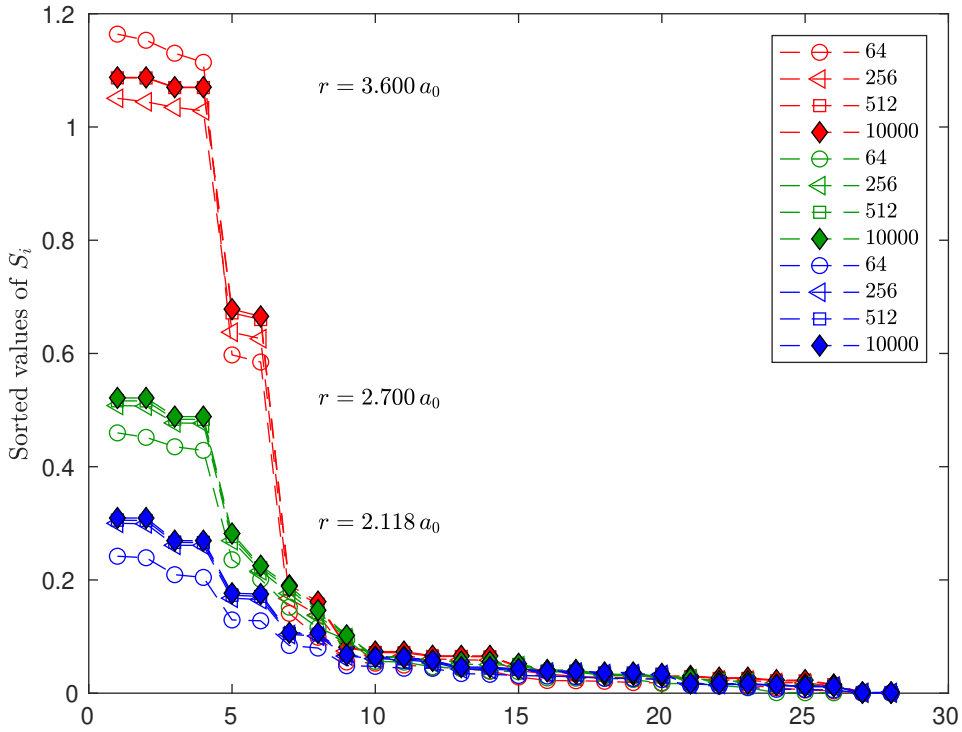

FIGURE 3.2. One-orbital entropies for $r = 2.118\,a_0$ (blue), $2.700\,a_0$ (green) and $3.600\,a_0$ (red) obtained for the full orbital set ($k = 28$) with DMRG for fixed $\tilde{D} = 64, 256, 512$ and for $\omega_{\mathrm{Tr}} = 10^{-8}$ with $\tilde{D}_{\max} = 10000$.

identify the four π and two σ molecular orbitals, coming from the 2p atomic orbitals, which take part in the bond breaking process indeed. The effect of stretching the geometry on the multireference character will be further discussed in chapter 4.

3.7.2. Numerical investigation of the CAS-dependence of the error Here we present the numerical results of the ground-state energy errors in terms of k for the DMRG-TCCSD for different accuracies and geometries. Single-reference coupled cluster calculations were also performed in NWChem program package [**Val10**], where we employed the cc-pVDZ basis set in the spherical representation. For the errors ΔE, shown in figures 3.5, 3.6 and 3.7, the reference energies are the DMRG energy with truncation error threshold $\omega_{\mathrm{Tr}} = 10^{-8}$ for the full orbitals set $k = d = 28$. In the figures, there are some missing data points in terms of k because, as before, some orbitals are added together to the active space due to symmetry considerations and also taking (3.8) into account, see the discussion after (3.17). This also manifests itself in the degenerate one-orbital entropies, so can be routinely checked in the workflow within step (i) in section 3.6.

We make the following findings from the ground-state errors.

1. The DMRG energy starts from the Hartree–Fock energy for $k = 7$ and decreases monotonically with increasing k, which is because of the variational property of the DMRG method,

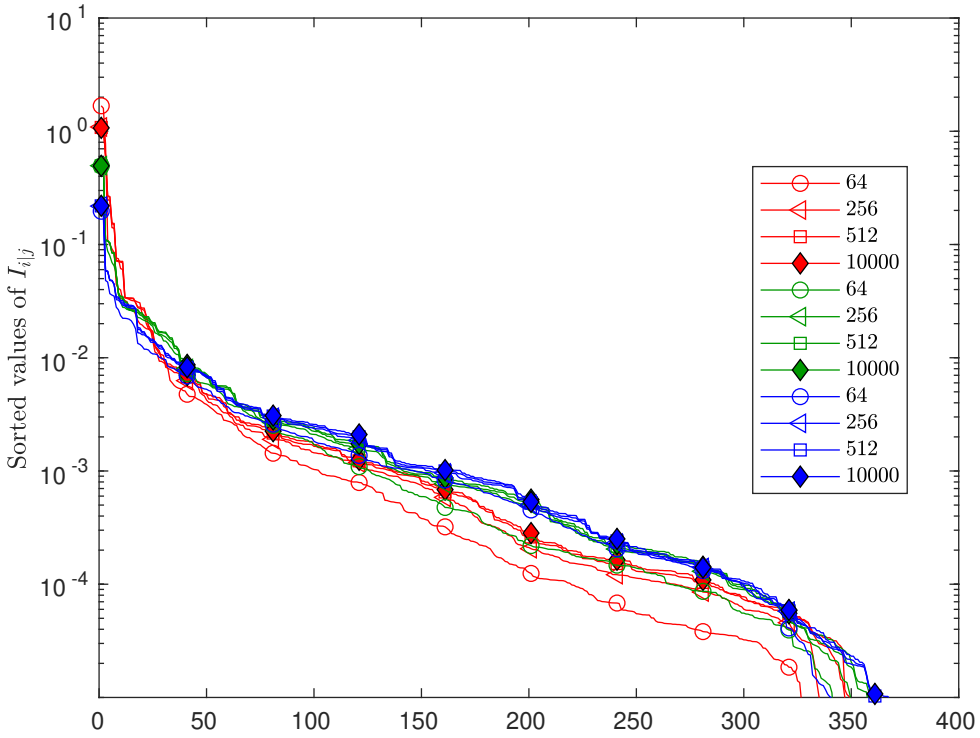

FIGURE 3.3. Two-orbital mutual informations for $r = 2.118\,a_0$ (blue), $2.700\,a_0$ (green) and $3.600\,a_0$ (red) obtained for the full orbital set ($k = 28$) with DMRG for fixed $\tilde{D} = 64, 256, 512$ and for $\omega_{\mathrm{Tr}} = 10^{-8}$ with $\tilde{D}_{\mathrm{max}} = 10000$.

until the full orbital solution with $k = 28$ is reached. It is remarkable that the DMRG-TCCSD energy is significantly below the CCSD energy for all CAS choices, even for a very small $k = 9$. The error, however, shows an irregular behaviour. This is clearly seen as the energy error increases between $k = 10$ and $k = 15$, even for different DMRG accuracies ω_{Tr}, although the CAS covers more of the static correlation of the system with increasing k. This is due to the fact that the DMRG-TCCSD approach suffers from a methodological error, discussed in section 3.4, since the CAS solution is frozen in the during the CCSD calculation. Therefore, whether orbital k is part of the CAS or external part provides a different methodological error. This supports the hypothesis of a k-dependent constant in (3.16) and is investigated in more detail in section 3.7.3.

2. Since several choices of CAS orbitals $Y(k)$ lead to small DMRG-TCCSD errors, the value of k, best from the computational point of view, is determined not only by the error minimum but also by the minimal computational time, that is, we need to take the computational requirements of the DMRG into account. Note that the bond dimension in the MPS contributes significantly to the computational cost of the DMRG calculation (2.59). The connection of the bond dimension to the CAS choice is shown in figure 3.1 (b), where the maximal bond dimension appearing in the DMRG algorithm is depicted as a function of k for the a priori defined truncation error threshold $\omega_{\mathrm{Tr}} = 10^{-8}$. In the DMRG calculations the total spin projection (Abelian) symmetry

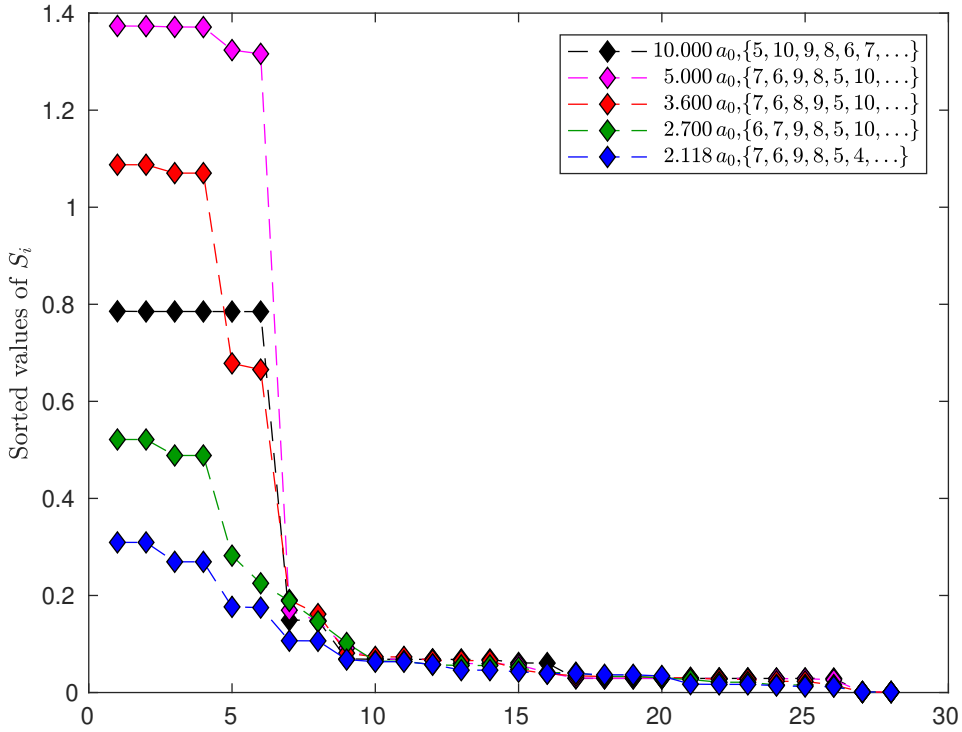

FIGURE 3.4. One-orbital entropies for equilibrium and stretched geometries obtained for the full orbital set ($k = 28$) with DMRG for $\omega_{\mathrm{Tr}} = 10^{-8}$ with $\tilde{D}_{\max} = 10000$. For each geometry we indicate the labels of the first six spatial orbitals with highest entropy. The labels of the orbitals $\{1, 2, \ldots, 28\}$ are assigned according to increasing Hartree–Fock energy.

is exploited, that is, the ground state is searched where the total spin projection of the electron system is zero. In our CAS construction all the 7 occupied spatial orbitals are included for all k, therefore the number of electrons are $N = 14$. These two facts yield that the dimension of the CAS with $Y(k)$ is $\dim\left(\mathcal{N}_{Y_\uparrow, Y_\downarrow}^{N/2,N/2}\right) = \binom{k}{7}^2$. The optimal CAS is therefore chosen such that the bond dimensions are not too large and the DMRG-TCCSD provides a low error, that is, a local minimum in the energy error with respect to k.

3. It is important to note that, based on figure 3.5, the DMRG-TCCSD energy got very close to, or even dropped below, the CCSDT energy for several k values. Since close to the equilibrium geometry the exact wave function is dominated by one determinant, it is expected that DMRG-TCCSD leads to even more robust improvements for the stretched geometries, that is, when the multireference character of the wave function is more pronounced. Our results for the stretched geometries, $r = 2.700\, a_0$ and $3.600\, a_0$, are shown in figures 3.2 and 3.3 for the entropic quantities, and in figures 3.6 and 3.7 for the ground-state energy errors. As mentioned in section 3.7.1, for larger r values static correlations gain importance, which is signaled by the increase in the one-orbital entropy in figure 3.2. Thus the multireference character of the wave

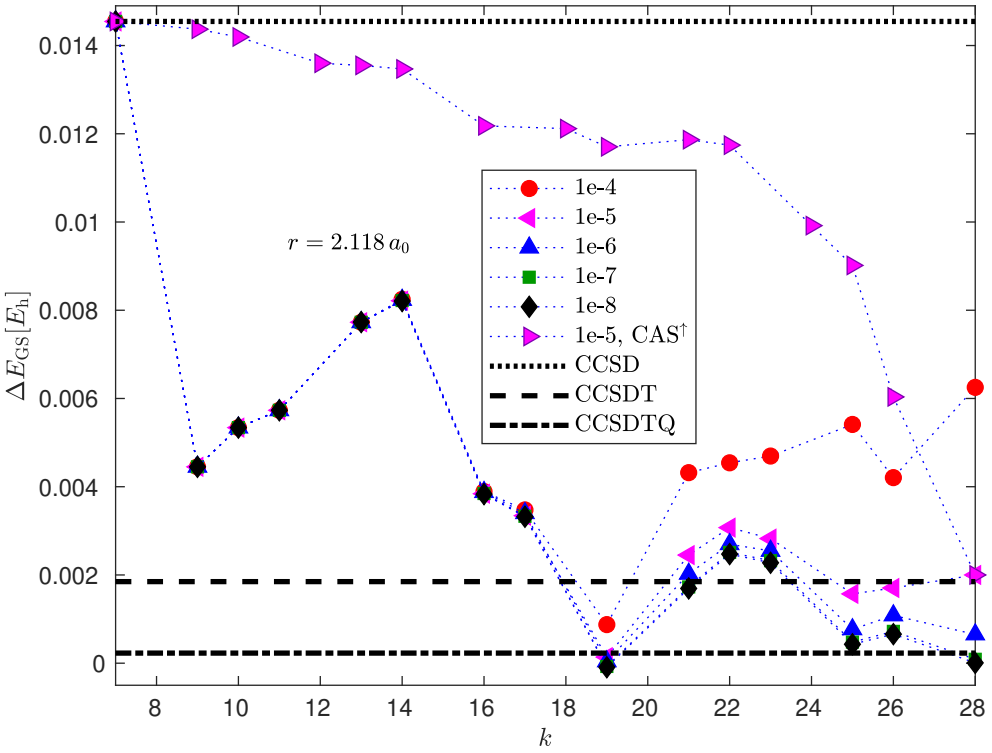

FIGURE 3.5. Ground-state energy of the N_2 molecule near the equilibrium geometry, $r = 2.118\,a_0$, obtained with DMRG-TCCSD for $7 \leq k \leq 28$ and for various DMRG truncation error thresholds ω_{Tr}. The CCSD, CCSDT and CCSDTQ reference energies are shown by dotted, dashed and dashed-dotted lines, respectively. The DMRG energy with $\omega_{\mathrm{Tr}} = 10^{-8}$ on the full space, that is, $k = 28$, is taken as a reference for the FCI energy. For $\omega_{\mathrm{Tr}} = 10^{-5}$ the reverse CAS extensions, labeled by CAS$^{\uparrow}$, was additionally formed by taking k orbitals according to increasing values of the one-orbital entropy.

function becomes apparent through the entropy profiles. For $r = 2.700\,a_0$, according to figure 3.6, the DMRG-TCCSD energy is again below the CCSD computation for all $k > 7$ values and it is even below the CCSDT reference energy for $k > 15$. For $r = 3.600\,a_0$, according to figure 3.7, the CC computation fluctuates with increasing excitation ranks, and CCSDT is even far below the reference energy, revealing the variational breakdown of the single-reference CC method for multireference problems [**Kow00**]. In contrast to this, for $r = 3.600\,a_0$ the DMRG-TCCSD energy is again below the CCSD energy for all $k > 7$, but above the CCSDT energy. The error furthermore shows a local minimum around $k = 19$. For the stretched geometries static correlations are more pronounced, there are more orbitals with large entropies, thus the maximal bond dimension in DMRG calculations increases more rapidly with k compared to the situation near the equilibrium geometry (see figure 3.1 (b)). Thus, obtaining an error margin within $1\,\mu E_{\mathrm{h}}$ for $k = 19 \ll 28$ leads to a significant save in computational time and resources. Here

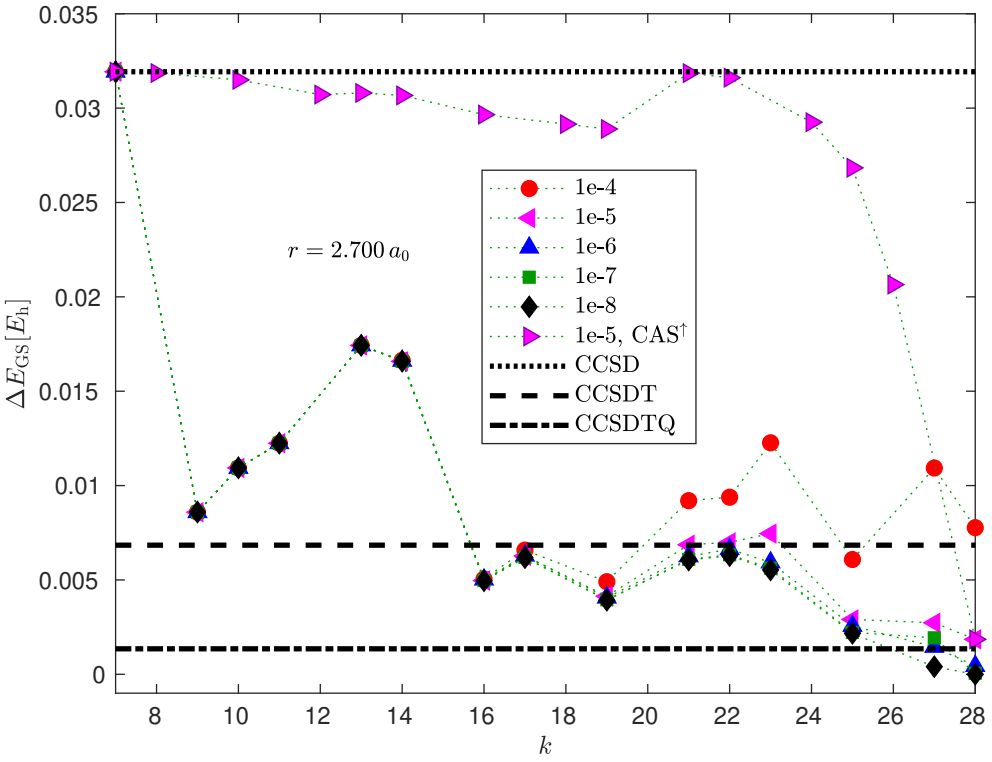

FIGURE 3.6. Ground-state energy of the N_2 molecule with bond length $r = 2.700\,a_0$, obtained with DMRG-TCCSD for $7 \leq k \leq 28$ and for various DMRG truncation error thresholds ω_{Tr}. The CCSD, CCSDT and CCSDTQ reference energies are shown by dotted, dashed and dashed-dotted lines, respectively. The DMRG energy with $\omega_{\mathrm{Tr}} = 10^{-8}$ on the full space, that is, $k = 28$, is taken as a reference for the FCI energy. For $\omega_{\mathrm{Tr}} = 10^{-5}$ the reverse CAS extensions, labeled by CAS$^{\uparrow}$, was additionally formed by taking k orbitals according to increasing values of the one-orbital entropy.

we emphasize again that DMRG-TCCSD is fundamentally a single-reference method, as it was formulated in (3.4), therefore, the choice of the reference determinant can effect its performance. However, we have verified that for $r \lesssim 4.000\,a_0$ and for all k values the weight of the Hartree–Fock determinant was significantly larger than all other determinants. In chapter 4, based on reference [**Mát23**], however, this multireference character is studied in terms of the weight of determinants in wide range of nuclei distances.

4. In practice, we do not intend to carry out untruncated DMRG calculations, that is, exact treatment of $\mathcal{N}_{Y_\uparrow,Y_\downarrow}^{N/2,N/2}$ space, thus usually a larger truncation error threshold is used. Therefore, we have made calculations for larger truncation errors thresholds in the range of 10^{-4} and 10^{-8} to study its influence. Our results are shown also in figures 3.5, 3.6 and 3.7. For small k the DMRG solution basically provides the exact limit since the a priori set minimum bond dimension $\tilde{D}_{\mathrm{min}} \approx 64$ already leads to a very small truncation by (2.42). (It is a common technique in

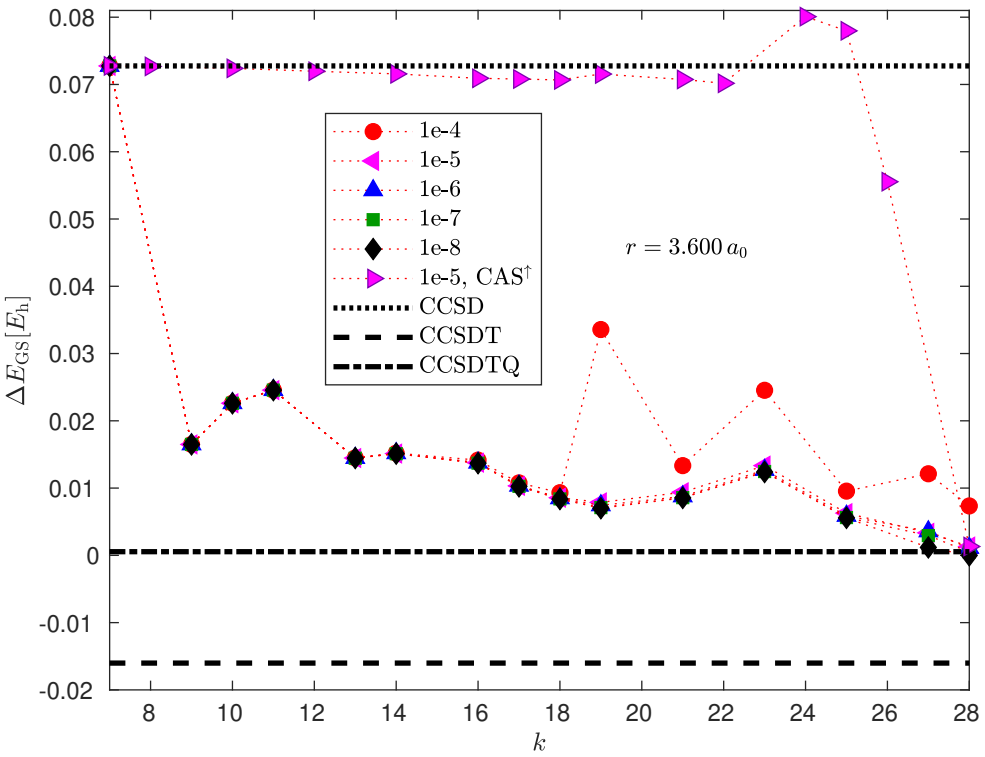

FIGURE 3.7. Ground-state energy of the N_2 molecule with bond length $r = 3.600\,a_0$, obtained with DMRG-TCCSD for $7 \leq k \leq 28$ and for various DMRG truncation error thresholds ω_{Tr}. The CCSD, CCSDT and CCSDTQ reference energies are shown by dotted, dashed and dashed-dotted lines, respectively. The DMRG energy with $\omega_{\mathrm{Tr}} = 10^{-8}$ on the full space, that is, $k = 28$, is taken as a reference for the FCI energy. For $\omega_{\mathrm{Tr}} = 10^{-5}$ the reverse CAS extensions, labeled by CAS$^{\uparrow}$, was additionally formed by taking k orbitals according to increasing values of the one-orbital entropy.

numerical practice to set such a minimum $\tilde{D}_{\mathrm{min}}$ to improve convergence.) Therefore, the error of the DMRG-TCCSD is dominated by the methodological error discussed in section 3.4, and the markers in the figures are on the top of each other for different truncation error thresholds ω_{Tr}. For $k > 15$ the effect of the DMRG truncation error becomes visible, and for large k the overall error ΔE is basically determined by the DMRG solution. For larger ω_{Tr} between 10^{-4} and 10^{-5}, the DMRG-TCCSD error shows a prominent, clearly visible minimum with respect to k. This is exactly the expected trend, since the CCSD method fails to capture static correlations while DMRG requires large bond dimension, that is, a low truncation error threshold, to capture dynamic correlations. In addition, the error minima for different truncation error thresholds ω_{Tr} happen to be around the same k values. This has an important practical consequence: not just the entropy profiles but also the best $Y(k)|\bar{Y}(k)$ split can be determined by performing cheap DMRG-TCCSD calculations using large DMRG truncation error threshold as a function of k.

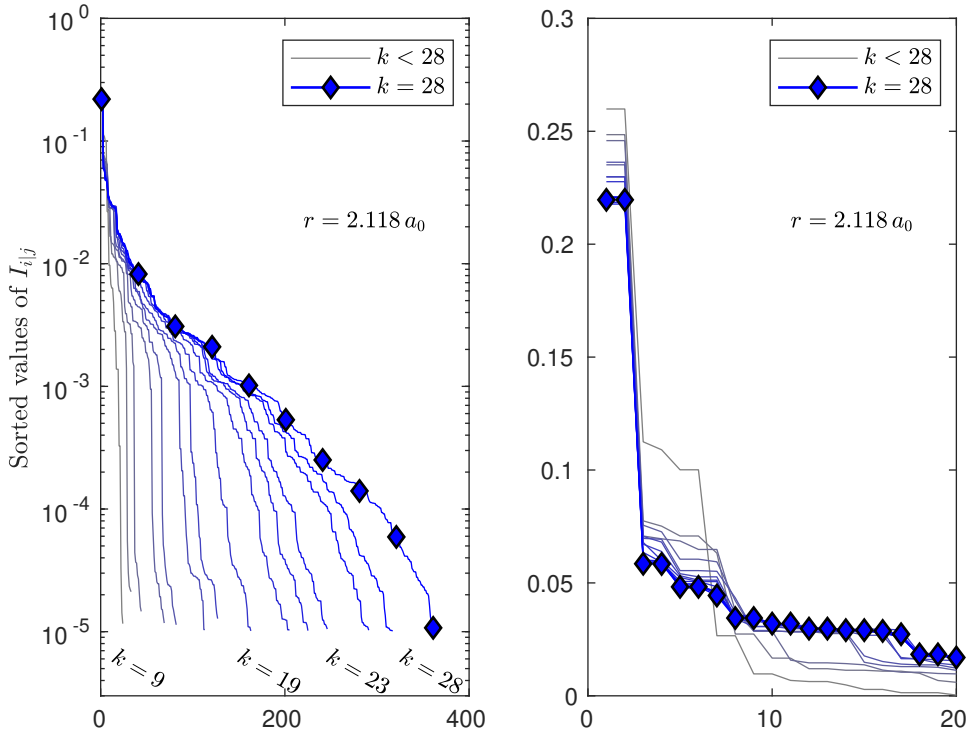

FIGURE 3.8. (a) Sorted values of the two-orbital mutual informations obtained by DMRG for $9 \leq k \leq 28$ on a semi-logarithmic scale for N_2 at $r = 2.118\,a_0$. (b) Sorted 20 largest matrix elements of two-orbital mutual informations obtained by DMRG for $9 \leq k \leq 28$ on a lin-lin scale for N_2 at $r = 2.118\,a_0$.

3.7.3. Numerical investigation on CAS-external correlations As we have seen, the figures 3.5, 3.6 and 3.7 show that ΔE has a high peak for $9 < k < 16$, where the DMRG is close to the numerical exact solution. This indicates the methodological error of the method (see section 3.1), that is, the Y-dependence of the energy. In order to demonstrate the importance of the choice of the CAS orbitals, we also performed calculations with *reverse CAS extension* for $\omega_{\mathrm{Tr}} = 10^{-5}$. That is, we form $Y(k)$ by taking k orbitals according to increasing values of the one-orbital entropy values. The corresponding error profiles as a function of k are labelled by $\mathrm{CAS}^{\uparrow}$ in figures 3.5, 3.6 and 3.7. As expected, the improvement of DMRG-TCCSD is marginal compared to CCSD up to a very large $k \approx 23$ split.

Taking another look at figure 3.2 we can confirm that already for small k values the most important orbitals, that is, those with the largest entropies, are included in the active ones. In figure 3.8 the sorted values of the two-orbital mutual informations of system $P_{\mathrm{CAS}} H P_{\mathrm{CAS}}$ are shown obtained by DMRG for $9 \leq k \leq 28$. It is apparent from the figure 3.8 (b) that the largest values of $I_{i|j}$ change only slightly with increasing k, thus static correlations are basically included for all restricted CAS. This verifies our claims about the CAS choice in section 3.5. The exponential tail of $I_{i|j}$ corresponding to dynamic correlations, however, becomes more visible

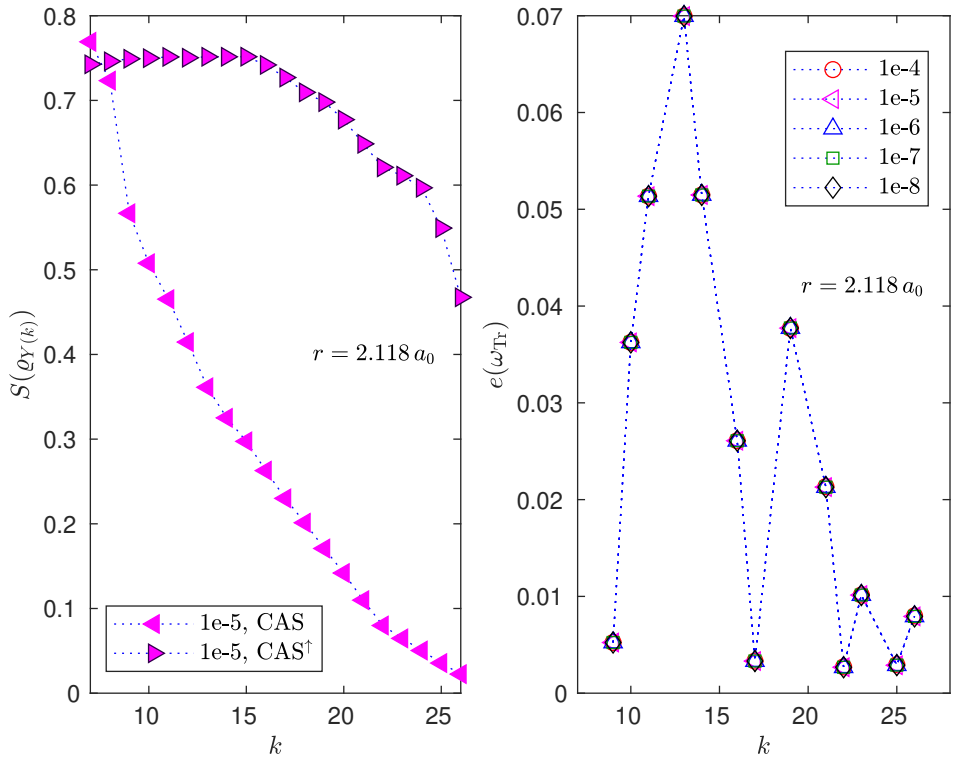

FIGURE 3.9. (a) The active-orbital entropy $S(\varrho_{Y(k)})$ as a function of k for $r = 2.118\,a_0$ obtained by DMRG with orbital ordering according to CAS extension (3.17) and the reversed CAS extension, labelled by CAS and CAS$^{\uparrow}$, respectively. (b) The amplitude expression $e(\omega_{\mathrm{Tr}})$ as a function of k for $r = 2.118\,a_0$ for DMRG truncation error thresholds ω_{Tr} between 10^{-4} and 10^{-8}.

only for larger k values, as figure 3.8 (a) shows. We conclude that for a given k split the DMRG method computes the static correlations efficiently, and the missing tail of the mutual information with respect to the full orbital set ($k = 28$) calculation is captured by the TCC scheme.

Correlations between the active and external orbitals can also be simulated by a DMRG calculation on the full orbital set using an orbital ordering defined by our CAS extension method according to (3.17). That is, the first k site in the DMRG chain represents orbitals $Y(k)$ (for $k \leq 7$, that is, for the occupied HF orbitals L_{o}, the order is arbitrary). The correlation in the pure ground state with respect to the bipartition $Y(k)|\overline{Y(k)}$ is twice the entropy of the reduced state $2S(\varrho_{Y(k)})$ (see (2.27a)). The construction of the reduced state $\varrho_{Y(k)}$ is inherent in the DMRG algorithm (2.51). The *active-orbital entropy* $S(\varrho_{Y(k)})$, shown in figure 3.9 (a), decays monotonically for $k > 7$, that is, the correlations between the active and external orbitals vanish with increasing k. In contrast to this, when an ordering according to CAS$^{\uparrow}$ is used, the correlation between CAS and external part remains always strong for $k < 28$, that is, some of the highly correlated orbitals are distributed among the active and external ones. Nevertheless, both curves are smooth and they cannot explain the error profile shown in figure 3.5.

Since correlation analysis based on the entropic quantities cannot reveal the error profile shown in figure 3.5, here we reinvestigate the error behaviour as a function of k but in terms of the CC amplitudes. Let us write out more explicitly the amplitude expression in (3.16),

$$e(\omega_{\mathrm{Tr}}) = \sum_{\mu\in\bar{J}_1} (\tilde{t}^{\mathrm{CCSD}}(\omega_{\mathrm{Tr}}))^2_\mu + \sum_{\mu\in\bar{J}_1\cup\bar{J}_2} (\tilde{t}^{\mathrm{CCSD}}(\omega_{\mathrm{Tr}}) - \tilde{t}^{\mathrm{FCI}})_\mu + \sum_{\mu\in J_1\cup J_2} (\tilde{s}^{\mathrm{DMRG}}(\omega_{\mathrm{Tr}}) - \tilde{s}^{\mathrm{FCI}})_\mu, \tag{3.18}$$

so $e(\omega_{\mathrm{Tr}})$ denotes the expression in the bracket in (3.16). Here we indicate the truncation error threshold ω_{Tr} used in the DMRG calculation in the DMRG-TCCSD method. Since the FCI solution is unknown, it is approximated by high-accuracy DMRG calculation for the full orbital set $k = 28$, and the amplitudes $\tilde{t}^{\mathrm{FCI}}$ and $\tilde{s}^{\mathrm{FCI}}$ were obtained according to (3.10) and (3.3). In figure 3.9 (b), the amplitude expression $e(\omega_{\mathrm{Tr}})$ is shown as a function of k for several DMRG truncation error thresholds ω_{Tr} for the near-equilibrium geometry. Note that the quantitative behaviour is quite robust with respect to the DMRG accuracy. We emphasize that the error contribution in figure 3.9 is dominated by the second term in (3.18), which this is an order of magnitude larger than the contribution from the first and third terms.D in (3.18), respectively. The first term in (3.18) is furthermore related to the usual T_1 diagnostic in CC [**Lee89b**], so it is not a surprise that a small value, in order of 10^{-3}, was found. Comparing this error profile to the one shown in figure 3.5, we can understand the irregular behaviour and the peak in the error in ΔE between $k = 9$ and 17, and the other peaks for $k > 17$, but the error minimum found for $k = 19$ remains unexplained. Furthermore, we can conclude from figure 3.9 (b) that the quotient $\Delta E/e(\omega_{\mathrm{Tr}})$ is not constant with respect to k. This indicates that the constant involved in (3.16) is indeed $Y(k)$-dependent.

3.8. Summary

In this chapter, we presented a fundamental study of the DMRG-TCCSD method. We showed formal properties, such as the energy size extensivity, and that, unlike the traditional single-reference CC method, the linked and unlinked TCC equations are in general not equivalent. We presented the mathematical error analysis of the DMRG-TCC method, performed in the original work [**Fau19a**], with emphasizing the quantum chemistry perspective. We recalled the local uniqueness and quasioptimality of the DMRG-TCC solution, and highlighted the importance of the CAS-ext gap, that is, a spectral gap assumption allowing to perform the analysis presented. Furthermore, the analysis resulted in a quadratic a priori error estimate for the DMRG-TCC method, which aligns the error behaviour of the DMRG-TCC method with variational methods except for the upper bound condition. The key point we emphasized is the strong CAS dependence of the DMRG-TCC solution, which was neglected in the former analysis [**Fau19a**] since the explicit consideration of this dependence carries many mathematical challenges. Therefore we extended our work with a numerical study of the CAS dependence of the DMRG-TCCSD error. We perform a systematic study on the nitrogen dimer with different geometries by increasing the size of the CAS according to entropic quantities. Our computations showed that these properties, for example, the one-orbital entropy and the two-orbital mutual

information are qualitatively very robust. This means that their qualitative behaviour is well-represented by means of an approximation with low bond dimension, which is a computational benefit. Also, we could clearly observe that the error indeed first decays (for $7 \leq k \leq 9$) and then increases again (for $25 \leq k \leq 28$) for low-rank approximations, that is, for truncation errors 10^{-4}, 10^{-5}. This oscillatory behaviour was not able to be answered so far using entropy based measures but a similar irregular behaviour can be detected by a cluster amplitude error analysis.

An important feature that we would like to highlight here is that a small CAS ($k = 9$) yields a significant improvement of the energy, and that the energies for all three geometries and all CAS choices outrun the single-reference CC method. Although the computational costs of the DMRG-TCCSD method exceed the costs of the CCSD method, this leads to a computational drawback of the method only if the treatment of large CAS becomes necessary. In addition, the DMRG-TCCSD method avoids the numerical breakdown of the CC approach even for multi-reference (strongly correlated) systems and, using concepts of quantum information theory, allows an efficient routine implementation. The practical result of our study is that we proposed a protocol to find the best active orbitals for carrying out large-scale DMRG-TCCSD calculations.

4. CHAPTER

Compressing multireference character via fermionic mode transformation

In this chapter, in section 4.1, we start with pointing out that the choice of orbital set for the discretisation (and truncation) is crucial in quantum chemistry. Also there are situations, for example, strongly open-shell systems, where the choice of a reference determinant becomes ambiguous, therefore, methods based on single-reference formulation (CC, DMRG-TCC) could potentially run into problems, and the choice of the reference is a bias in the method. Qualitatively we say that a many-body system is of multireference character if the single-reference methods fail. In this chapter we investigate the multireference character *quantitatively* via the tomography of the state. We demonstrate that orbital optimization based on entanglement localization has the potential to compress the multireference character of the state vector. In sections 4.2-4.4, we discuss orbital optimization within mode transformation in TNS methods and the numerical details of the joint optimization in the two-site DMRG framework. In sections 4.5-4.6, numerical simulations are performed for the nitrogen dimer for the equilibrium and for stretched geometries in the cc-pVDZ orbital set.

4.1. Orbital optimisation and multireference character

We recall concepts detailed in appendix C in the context of orbital optimisation. As we can see in the formulation (C.9), the HF method can be viewed as an orbital optimisation, where the cost function is the expectation value of the Hamiltonian with one Slater determinant. The optimal orbitals can be written as the unitary transformation of some arbitrary orthonormal orbital set, and the optimal energy is the HF energy. This optimization problem (C.9) leads to the eigenvalue problem of the Fock operator (C.10), or in the LCAO scheme (C.11) to the Roothan–Hall equation (C.12). In general, the optimization of the orbitals is not a new concept. For example, the *localized molecular orbitals* (LMO) has a long history in quantum chemistry. The aim of the localization of orbitals there is two-fold. On the one hand, localization leads to chemically intuitive orbitals for rationalizing electronic structure of molecular systems. On the other hand, LMOs has proven to be useful in making the high-level correlated quantum chemical methods more tractable computationally [**Pip89**, **Sto80**, **Sze03**, **Sir00**, **Smi85**]. Among many others, we can recall Foster–Boys localization [**Fos60**, **Boy60**], which minimizes the radial extent of the localized orbitals, or Pipek–Mezey localization [**Pip89**], which is based on maximizing the charge of each orbital. Optimal modes can lead to localization of the correlation and entanglement in the system [**Fer14**], so here we present an orbital optimization that is based

on the entanglement localization. Although only the quantum chemistry application is studied here, this optimisation scheme is more general [**Kru16**, **Kru21**] and can be applicable also in solid-state and nuclear physics.

In computational quantum chemistry it is of central importance how good a single-Slater-determinant approximation is, and to how much extent does the accurate wave function (in the FCI space) differs from it. In numerical methods the idea of the excitation operator is emerged from the assumption that the correlation energy can be resolved by dealing with low excitation ranks and using the HF Slater determinant as a reference (see the singe-reference CI and CC methods in sections C.5 and C.6). In section 3.7 we demonstrated with the nitrogen dimer how one can transfer the system from single- to multireference by stretching the geometry. In the CC approach the T_1 diagnostic (norm of the amplitude vector t_μ with single excitation, $\mu \in J_1$) was proposed to characterise the reliability of a single-reference calculation [**Lee89a**, **Lee89b**]. A TNS method provides an approximate solution of the Hamiltonian in the FCI space, and the coefficients of the eigenstate can be obtained by the contraction of the tensor network. The full tomography, that is, the calculation of all the coefficients are of exponential cost. Therefore, one might interested in the profile of the coefficients with the highest weight, which can reveal the multireference character of the system. So among other quantities this is used to monitor the performance of the orbital optimization.

4.2. Basis transformation on matrix product states

The entanglement in a state vector $|\psi\rangle$ for a given bipartition can be kept track easily in the MPS language by taking advantage of the gauge invariance [**Vid03**]. If $|\psi\rangle$ is in the mixed-canonical MPS form and the in-between tensor is decomposed into left- and right-canonical ones (see in (2.57)), the remaining tensor is diagonal and contains the Schmidt coefficients. From this, the von Neumann entropy (2.20) can be calculated, which is the entanglement (2.27b) for this bipartition. The Schmidt rank, which is the number of non-zero Schmidt coefficients in (2.18), gives the size of the matrices in the truncation-free MPS form. In case of truncation, the sum of the discarded squared Schmidt coefficients (2.41) provides a heuristic error measure. In (2.46), in the computational point of view, we might take advantage of optimising over the underlying basis too, resulting lower bond dimensions, therefore computational cost, for the description of the system with the same accuracy.

Let us have a unitary basis transformation $U_L \in \mathrm{U}(\mathcal{H}_L)$, which maps from the original tensor product structure $\bigotimes_{i=1}^{n} \mathcal{H}_i \equiv \mathcal{H}_L$ to a new tensor product structure $\bigotimes'^{n}_{i=1} \mathcal{H}'_i \cong \mathcal{H}_L$. We can consider this unitary map as the transformations of the basis vectors, $|\chi'_{\boldsymbol{\alpha}}\rangle := U_L|\chi_{\boldsymbol{\alpha}}\rangle$, given for each multiindex $\boldsymbol{\alpha} = (\alpha_1, \ldots, \alpha_n)$, where $\alpha_i = 1, \ldots, D_i$ for $i \in [n]$. For simplicity, if the unitary transformation does not change the dimensions of the factor spaces, $\dim(\mathcal{H}_i) = \dim(\mathcal{H}'_i) = D_i$ for all $i \in [n]$, we can write

$$|\chi'_{1,\alpha_1}\rangle \otimes' \ldots \otimes' |\chi'_{n,\alpha_n}\rangle := U_L(|\chi_{1,\alpha_1}\rangle \otimes \ldots \otimes |\chi_{n,\alpha_n}\rangle). \tag{4.1}$$

Then, obviously, the transformed MPS in the new basis can be expressed with the same matrices,

$$U_L|\psi\rangle = \sum_{\alpha_1,\alpha_2,\ldots,\alpha_n} \boldsymbol{A}^{(1)}_{\alpha_1}\boldsymbol{A}^{(2)}_{\alpha_2}\ldots\boldsymbol{A}^{(n)}_{\alpha_n}|\chi'_{1,\alpha_1}\rangle \otimes' \ldots \otimes' |\chi'_{n,\alpha_n}\rangle \in \mathcal{M}_{\tilde{\boldsymbol{D}}}(U_L), \tag{4.2a}$$

however, we cannot say anything about the bond dimensions when writing it in the original basis,

$$U_L|\psi\rangle = \sum_{\alpha_1,\ldots,\alpha_n} \Big(\sum_{\beta_1,\ldots,\beta_n} (U_L)_{\boldsymbol{\beta},\boldsymbol{\alpha}} \boldsymbol{A}^{(1)}_{\alpha_1}\boldsymbol{A}^{(2)}_{\alpha_2}\ldots\boldsymbol{A}^{(n)}_{\alpha_n}\Big)|\chi_{1,\beta_1}\rangle \otimes \ldots \otimes |\chi_{n,\beta_n}\rangle \notin \mathcal{M}_{\tilde{\boldsymbol{D}}}(\mathrm{I}), \tag{4.2b}$$

where the matrix entries of the unitary are $(U_L)_{\boldsymbol{\beta},\boldsymbol{\alpha}} = \langle\chi_{\boldsymbol{\beta}}|\chi'_{\boldsymbol{\alpha}}\rangle$ (in both bases). For graphical illustration see figure 4.1. Note that in terms of passive transformation, that is, expressing the original vector in the new basis, we say $|\psi\rangle \notin \mathcal{M}_{\tilde{\boldsymbol{D}}}(U_L)$. One can get the new MPS form, and find out the bond dimensions needed, again by the subsequent Schmidt decompositions (2.34).

We consider now basis transformations for identical particles, especially for fermions. Let us have a mode transformations by unitary U on the one-orbital basis $\mathcal{K}$. According to (2.79), the N-particle occupation number space $\mathcal{N}^N_{[d]} \subset \mathcal{N}_{[d]}$ is an invariant subspace of subspace of the unitary $g(U)$, and the tensor product structure of the MPSs is given by the whole occupation number space, $\mathcal{H}_L \cong \mathcal{N}_{[d]}$. The ground-state energy of the system within the MPS approximation in an optimal basis is

$$E_0^{\tilde{\boldsymbol{D}},\mathrm{opt}} = \min\Big\{ \langle\psi|H|\psi\rangle \;\Big|\; |\psi\rangle \in \mathcal{M}_{\tilde{\boldsymbol{D}}}\big(g(U)\big), U \in \mathrm{U}(\mathcal{K}) \Big\} \tag{4.3a}$$

$$= \min\Big\{ \langle\psi|g(U)Hg(U)^\dagger|\psi\rangle \;\Big|\; |\psi\rangle \in \mathcal{M}_{\tilde{\boldsymbol{D}}}(\mathrm{I}), U \in \mathrm{U}(\mathcal{K}) \Big\}. \tag{4.3b}$$

The optimization task (4.3a) can be seen as an optimization of $|\psi(U)\rangle = g(U)^\dagger|\psi\rangle$, that is, finding the minimal expectation value of the Hamiltonian H in the fixed bond dimension MPS manifold over the arbitrary transformed basis. Or (4.3b) can be seen as an optimization of both the transformed Hamiltonian $H(U) = g(U)Hg(U)^\dagger$ and the state vector in the fixed bond dimension MPS manifold. Obviously, by the optimization we have the inequality $E_0 \le E_0^{\tilde{\boldsymbol{D}},\mathrm{opt}} \le E_0^{\tilde{\boldsymbol{D}}}$. In the special case, for bond dimensions $\tilde{\boldsymbol{D}} = (1,1,\ldots,1)$ the optimization problem (4.3) reduces to the Hartree–Fock approximation (C.9c). Or as we have seen in section 2.13, if we have independent-particle model (2.90a), then the optimal unitary is the one that diagonalizes the one-particle operator, and with this the solution (2.90b) is a product, that is, $\tilde{\boldsymbol{D}} = (1,1,\ldots,1)$. On the other hand, there are lattice models which have product-state solutions in the momentum basis, which means that the optimal unitary transformation is the Fourier transformation. We note that an interesting result has been derived for $N = 2$ electron systems, namely, in the $D_{\max} = 3$ manifold one can find an optimizer U_{opt} in (4.3) such that the exact (FCI) energy is recovered, $E_0 = E_0^{3,\mathrm{opt}}$ [**Fri22a**]. Determining the minimizers or approximate solutions of (4.3) could provide information about the entanglement structure of quantum many-body systems. Since (4.3) is a non-convex problem, approximate approach is needed.

4.3. Joint optimization of the matrix product state and the underlying basis

The optimal unitary U and MPS $|\psi\rangle$ in (4.3) is approximated iteratively within the two-site DMRG framework. First note that acting with an (arbitrary) operator on a MPS-based

algorithm requires the MPO decomposition of the operator and the contraction of each physical indices. (For example, a global unitary is acting on the MPS in figure 4.1 (a).) Or equivalently in the s-site DMRG language (see figure 2.6), acting on the contracted MPS (2.50) requires the effective operator of form (2.48), which can be a costly calculation on-the-fly. However, the action of operators of type $\mathrm{I}_X \otimes O_Y \otimes \mathrm{I}_Z$ can be easily performed, as it is illustrated in figure 4.1. (The notations of section 2.6 is used, that is, at the ℓ-th cut we have the blocks $X = \{1, \dots, \ell\}$ and $Z = \{\ell+s+1, \dots, n\}$, and $Y = \{\ell+1, \dots, \ell+s\}$.) The subsequent action of *two-site operators* on sites $Y = \{\ell+1, \ell+2\}$ can be straightforwardly implemented in the two-site DMRG framework because the algorithm is based on sweeping through the tensor network. Also note that every unitary $U \in \mathrm{U}(\mathcal{K})$ in the one-particle space $\mathcal{K}$ can be written (non-uniquely) as the product of *two-mode unitaries* with maximal number of factors $d(d-1)/2$, where $d = \dim(\mathcal{K})$ [**Li13**]. Although there are unitaries in this decomposition acting on non-neighbouring orbitals, but orbital permutations can also be decomposed into unitaries acting on neighbouring orbitals. The two-mode unitaries are of the form $u \oplus \mathrm{I}_{\overline{\{i,j\}}}$, with $u \in \mathrm{U}(\mathcal{K}_{\{i,j\}})$, where $i, j \in [d]$, and they yield *bilocal unitaries* $g(u \oplus \mathrm{I}_{\overline{\{i,j\}}})$ in the occupation number space $\mathcal{N}_{[d]}^N$, which can be seen from the explicit formula (2.79). So, in principal every $U \in \mathrm{U}(\mathcal{K})$ can be achieved in the two-site DMRG algorithm.

Therefore, we use the following *joint optimization* strategy. First, as it is in a two-site DMRG step (2.49), we considered the minimization of the energy expectation value

$$E_0 = \min\Big\{ \langle \psi^{\mathrm{MPS}}(\boldsymbol{x}) | H | \psi^{\mathrm{MPS}}(\boldsymbol{x}) \rangle \;\Big|\; \boldsymbol{x} \in \mathbb{C}^{\tilde{D}_X \times D_{\ell+1} \times D_{\ell+2} \times \tilde{D}_Z}, \|\boldsymbol{x}\| = 1 \Big\}, \tag{4.4a}$$

and the state vector in terms of the minimizer coefficient tensor is $|\psi_*\rangle = |\psi^{\mathrm{MPS}}(\boldsymbol{x}_*)\rangle$. As we have seen in section 2.7, the two-site DMRG step leaves the fixed rank MPS manifold because $|\psi_*\rangle$ can have at most $\min\{\tilde{D}_X D_{\ell+1}, D_{\ell+2}\tilde{D}_Z\}$ non-zero Schmidt coefficients for the bipartition $X'|\overline{X'}$, where $X' = X \cup \{\ell+1\}$. When $|\psi_*\rangle$ is truncated back into the $\mathcal{M}_{\tilde{D}_{\max}}$ manifold, we have a truncation error $\epsilon(\tilde{D}_{\max})$ given by (2.41). To reduce this error, the optimal *two-mode* unitary

$$U_* = \arg\min\Big\{ f_{X'}(|\psi_*(U)\rangle) \;\Big|\; U = u \oplus \mathrm{I}, u \in \mathrm{U}(\mathcal{K}_{\{\ell+1,\ell+2\}}) \Big\}, \tag{4.4b}$$

is determined, where $f_{X'}$ is the cost function, and $|\psi_*(U)\rangle = g(U)^\dagger |\psi_*\rangle$ is the transformed state vector. The two-mode unitary in (4.4b) transforms "over the DMRG cut", that is, transforms the neighbouring modes $\ell+1$ and $\ell+2$, hence the Schmidt spectrum $\{\sqrt{\omega_\alpha}\}_\alpha$ with respect to bipartition $X'|\overline{X'}$ is modified. The cost function $f_{X'}$ is chosen such that it takes its minimum value when the truncation error $\epsilon(\tilde{D}_{\max})$ is minimal, or in other words, when the sum of the discarded squared Schmidt coefficients is minimal. For example, the one-norm of the Schmidt spectrum

$$f_{X'}(|\psi\rangle) = \sum_\alpha (\omega_\alpha)^{\frac{1}{2}} \tag{4.5}$$

is suitable. We note that this is a monotone function of the half-Rényi entropy (2.21) of the reduced state $\varrho_{X'}$, so by its minimization, the entanglement or correlation between $X'|\overline{X'}$ is minimized. With this mode transformation the energy expectation value (4.4a) is unchanged, $E_0 = \langle \psi_*(U_*) | H(U_*^\dagger) | \psi_*(U_*) \rangle$. The optimization continues with this transformation on the Hamiltonian, truncation on the MPS and step to the next bipartition, $\ell \mapsto \ell+1$. The product of

overlapping two-mode unitaries U_* build up a global unitary. To avoid sticking in local minima, we apply (global) reorderings during the optimization procedure. In this way we may converge to the solution of (4.4), that is to an optimal U_{opt} and an opimal MPS in the $\mathcal{M}_{\tilde{D}}\big(g(U_{\mathrm{opt}})\big)$ manifold.

4.4. Computational details of the orbital optimization

In the context of non-relativistic quantum chemistry, we have again the Schrödinger equation (C.1), and the concepts in appendix C apply. In case of time-reversal symmetry, which our presented system has, the problem can be solved over the field of real numbers. Therefore, a single real parameter θ can parametrize the two-mode unitary (orthogonal operator) in the one-particle space $\mathcal{K}$, and the corresponding bilocal unitary follows from (2.79) in the occupation number space $\mathcal{N}_{[d]}$,

$$u(\theta) = \begin{bmatrix} \cos\theta & \sin\theta \\ -\sin\theta & \cos\theta \end{bmatrix} \qquad g\big(u(\theta)\oplus \mathrm{I}\big) = \begin{bmatrix} 1 & 0 & 0 & 0 \\ 0 & \cos\theta & -\sin\theta & 0 \\ 0 & \sin\theta & \cos\theta & 0 \\ 0 & 0 & 0 & 1 \end{bmatrix} \otimes \mathrm{I}_{\overline{\{\ell+1,\ell+2\}}}, \tag{4.6}$$

respectively. The analysis, again, begins with choosing the molecule and setting its geometry, then HF calculation is performed with a chosen orbital set, resulting the HF canonical molecular orbitals, and the integrals (C.7) of them are computed. Next, with the aid of the entropy analysis (see section 3.5) and according to considerations from chemistry, the active space (3.1) is formed, that is, the orbitals to be optimized are selected, while keeping the rest of the orbitals unchanged. Here we give an overview of the computational details of the joint optimization procedure described in the foregoing, namely, the simultaneous optimization of MPS matrices and the underlying orbital basis.

In the *DMRG iteration step* we have a (leftward or rightward) step, as discussed in section 2.7, for the two-site case. That is, at cut ℓ the tensors at $Y = \{\ell+1, \ell+2\}$ are optimized, so we carry out the minimization of the energy expectation value (4.4a), then we decompose the minimizer tensor and truncate the MPS matrices (2.58).

The *micro-iteration step* is a two-site DMRG iteration step with an extra two-site unitary mode transformation on tensor spaces at $Y = \{\ell+1, \ell+2\}$. With this the DMRG step further optimizes the eigenvector, and the mode transformation reduces the entanglement in the eigenvector with respect to the split $X'|\overline{X'}$. That is, after optimizing the eigenvector in (4.4a), the optimal two-mode unitary is determined in (4.4b). The new state vector $g(U_*)^\dagger|\psi^{\mathrm{MPS}}(\boldsymbol{x}_*)\rangle$ is obtained by the transformation in terms of the coefficient tensor $\boldsymbol{x}_*$. For graphical illustration see figure 4.1. Then the decomposition and truncation of MPS matrices are carried out (2.58). Accordingly, the new Hamiltonian $g(U_*)^\dagger H g(U_*)$ is obtained by the transformation in terms of the integrals (2.91).

A *macro-iteration step* consists of two parts. First, for a small number of sweeps, bare DMRG iterations are performed to attain a sufficiently good tensor network approximation of the system. Then, micro-iteration steps are performed to optimize the orbitals. In order to

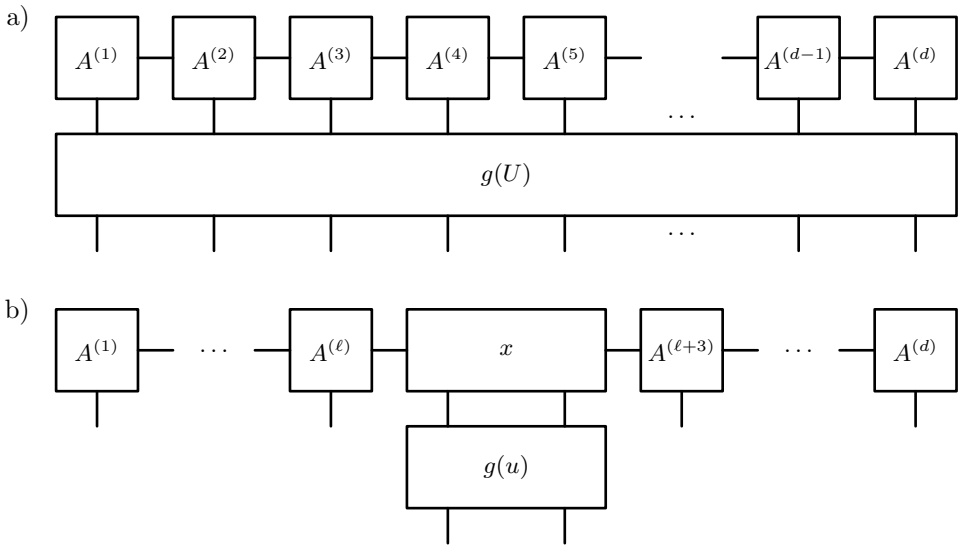

FIGURE 4.1. Mode transformation in terms of transformation on the tensor network. The global unitary $g(U)$ is acting on the MPS (a), and the bilocal (or two-site) unitary $g(u)$ is acting on the DMRG state vector of form (2.55).

monitor the optimization and to avoid sticking local minima, several quantities are calculated after the last micro-iteration, such as the one-orbital entropy (2.20), the two-orbital mutual information (2.23a), the total correlation (2.25), the correlation distance $I_{\text{dist}} = \sum_{i,j} I_{i,j}|i-j|^2$, the occupation number distribution $\langle n_i \rangle$, and the one-particle reduced density matrix (2.84) and its eigenvalues (natural occupation numbers) and eigenvectors (natural orbitals), where $i, j \in \{1, \dots, d\}$. Also the CI coefficients (C.15) are calculated, depending on the dimension of the FCI space $\mathcal{N}_{[d]}^N$, at least for singles and doubles. As it was discussed in section 2.6 and appendix B, to improve the convergence of the DMRG calculation, the DEAS procedure is utilized, which takes the values of the one-orbital entropy S_i and the new Hartree–Fock reference configuration (calculated from the occupations $\langle n_i \rangle$) as inputs. Also a new orbital order, that is, the permutation $U = P_\sigma$ is determined similarly as it is discussed in appendix A. These, together with the transformed integrals of the Hamiltonian, are all used as inputs to the subsequent macro-iteration.

4.5. Orbital optimization of the nitrogen dimer: small active space

In our numerical study we have the nitrogen dimer N_2 for various bond lengths with the cc-pVDZ orbital set [**Dun89**]. As it was discussed in 3.7, the HF calculation yields $d = 28$ canonical spatial orbitals with $N = 14$ electrons, so the FCI space is $\mathcal{N}_L^N$, where the $L = \{(1,\uparrow), (1,\downarrow), \dots, (d,\uparrow), (d,\downarrow)\}$, with the notations of section C.3. We exploit the total spin projection (Abelian) symmetry, that is, the ground state is searched in the subspace where the total spin projection of the electron system is zero, $\mathcal{N}_{L_\uparrow, L_\downarrow}^{N/2, N/2} \subseteq \mathcal{N}_L^N$ (where $L_\uparrow = \{(1,\uparrow), \dots, (d,\uparrow)\}$). To respect the total spin projection symmetry, the superpositions of modes with

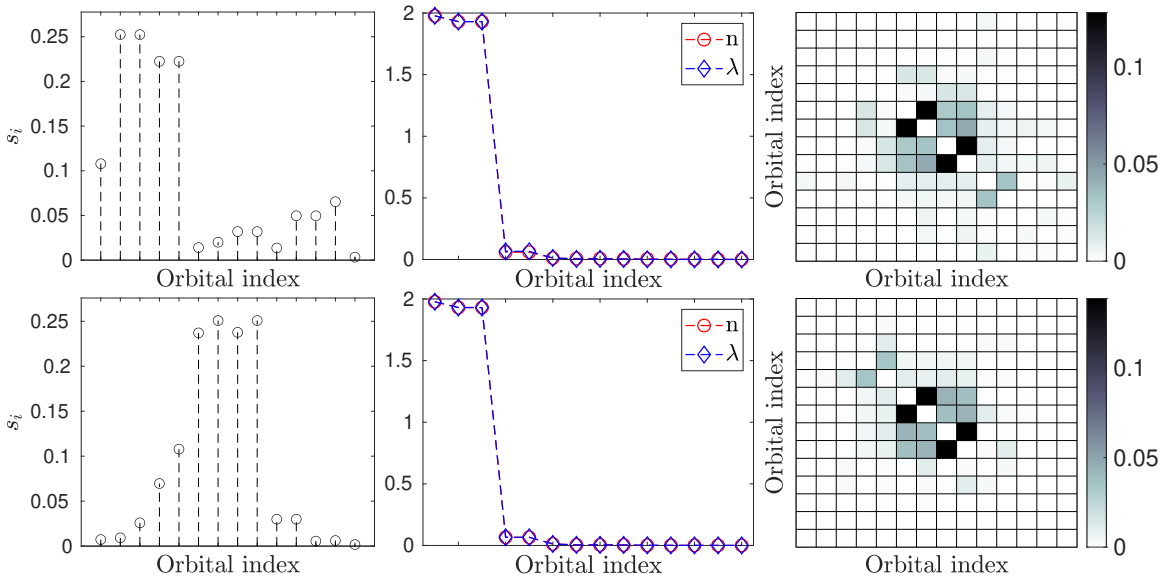

FIGURE 4.2. One-orbital entropy profiles $\{S_i\}$, sorted values of the natural orbital occupation numbers $\{\lambda_i\}$ and occupation numbers $\{\langle n_i \rangle\}$, and two-orbital mutual informations $\{I_{i,j}\}$ for the initial orbitals in CAS(6,14) (first row), and after the 20^{th} orbital optimization macro-iterations (second row) for the nitrogen dimer for bond length $r = 2.118\, a_0$ using bond dimension $\tilde{D} = 4096$.

different spins are omitted, so we have $\tilde{a}^\dagger_{i,\sigma} = \sum_{j\in[d]} U_{j,i,\sigma} a^\dagger_{j,\sigma}$, for $\sigma \in \{\uparrow, \downarrow\}$. We note that, due to the structure of the Hamiltonian for this system, it is not necessary to use different unitaries for spin up and down, $U_{i,j,\uparrow} = U_{i,j,\downarrow}$, although the implementation is applicable for the unrestricted case too. In the orbital optimization the bond dimension was systematically increased, $\tilde{D}_{\max} = 16, 64, 256, 512, 1024, 2048, 4096$, for each we have used 9 DMRG sweeps and 20 orbital optimization macro-iterations. When $\tilde{D}_{\max} \leq 512$ is used, after converging to U_{opt}, large scale DMRG calculations are performed in $\mathcal{M}_{\tilde{D}}\big(g(U_{\text{opt}})\big)$ and also in the original basis $\mathcal{M}_{\tilde{D}}(\text{I})$ with bond dimension $\tilde{D} = 4096$. We note that, for large $\tilde{D}_{\max}$ bond dimension, orbital optimization converges already after 4-5 macro-iterations.

In earlier works, it has been demonstrated that DMRG calculations after orbital optimization can lead to significantly more accurate results for the same computational complexity (for example, for the same truncated bond dimension $\tilde{D}$), due to the tremendous reduction of the entanglement in the system [**Kru16**, **Kru18**, **Kru21**]. Or one can say that the bond dimension $\tilde{D}$ can be pushed to a much lower value while keeping the same accuracy. Here we focus on the emerging orbitals and on the structure of the wave function. Therefore, first we choose a small active space, namely, 6 electrons on 14 spatial orbitals, which we denote by CAS(6,14). Here, we set the bond dimension to $\tilde{D}_{\max} = 4096$ to obtain numerically exact result (since $\boldsymbol{x}$ in (2.56) is of dimension $4^6 \times 4 \times 4 \times 4^6$). The dimension of the subspace of zero total spin projection is $\binom{14}{3}^2 \approx 10^5$, hence it is feasible to calculate all the entries of the coefficient tensor.

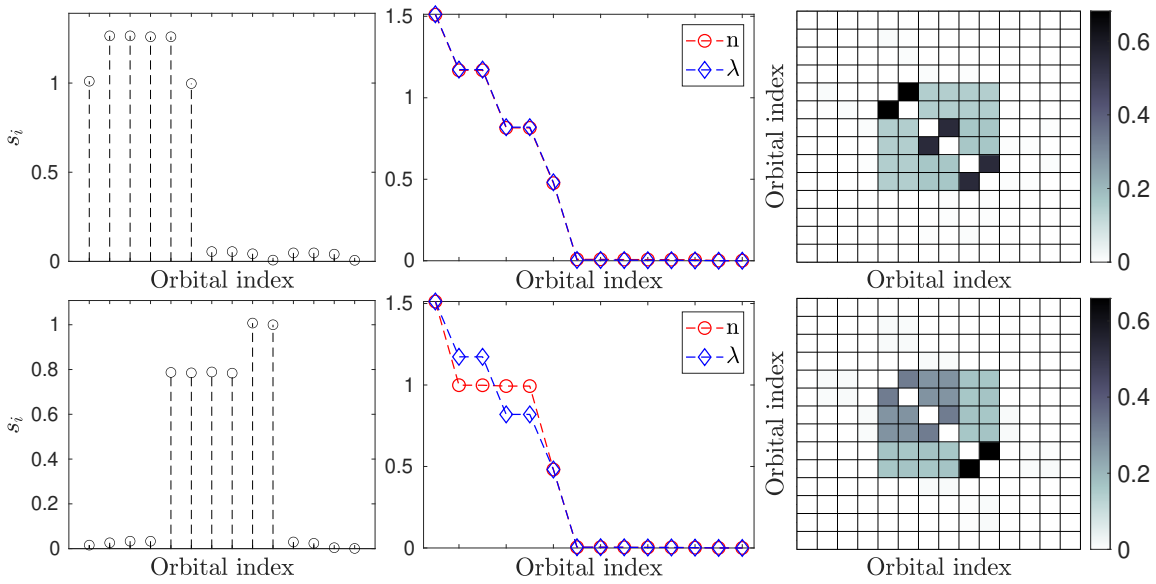

FIGURE 4.3. Similar to figure 4.2, but for a stretched geometry at $r = 4.200\,a_0$.

To monitor numerically the performance of the fermionic orbital optimization, a selected set of quantities are shown in figure 4.2 for the equilibrium geometry with bond length $r = 2.118\,a_0$, obtained in the initial orbitals (first row) and for the optimized orbitals (second row), that is, in the $\mathcal{M}_{\tilde{D}}(\mathrm{I})$ and $\mathcal{M}_{\tilde{D}}\big(g(U_{\mathrm{opt}})\big)$ manifolds, respectively, with $\tilde{D} = 4096$. Here it can clearly be seen that the orbital optimization has no effect, except that the orbitals have been reordered along the DMRG chain in order to reduce the correlation distance in the system (calculated from the two-orbital mutual informations plotted also in figure 4.2), $I_{\mathrm{dist}} = 18.8575$ changes to 12.6095. The ground-state energy $E = -109.0931\,E_{\mathrm{h}}$ is unchanged, the single-orbital entropy profiles changed only marginally (plotted also in figure 4.2), so I_{tot}, (calculated from the single-orbital entropies) changes slightly from 1.3373 to 1.2696. Three orbitals are almost doubly occupied, and the $\langle n_i \rangle$ and λ_i fall on the top of each other for the initial and optimized orbitals, resembling the characteristics of NO-like orbitals. The sharp Fermi edge indicates that the system is weakly correlated, that is, of single-reference problem.

In contrast to this, for a stretched geometry $r = 4.200\,a_0$, the sharp drop off in $\langle n_i \rangle$ and λ_i at the Fermi edge disappears, see in figure 4.3. The corresponding six partially occupied orbitals possess very large orbital entropies, indicating that these orbitals are in mixed states and are highly entangled with the rest of the system. The two orbitals with occupation number close to 1.5 and 0.5 are the σ bonding and antibonding orbitals, while the four orbitals with $0.5 \leq \langle n_i \rangle \leq 1.5$ are orbitals with π symmetry. The underlying bond breaking effect has already been analyzed in terms of entropies in reference [**Bog13**], however, such analysis depends on the choice of the orbital set and on the orbital optimization, as will be addressed below. Carrying out optimization, new orbitals are found, which are no longer natural-orbital-like (see the difference between the profiles of $\langle n_i \rangle$ and λ_i). Here, $\langle n_i \rangle = 1$ and $S_i \approx 0.8$ for four orbitals, that is,

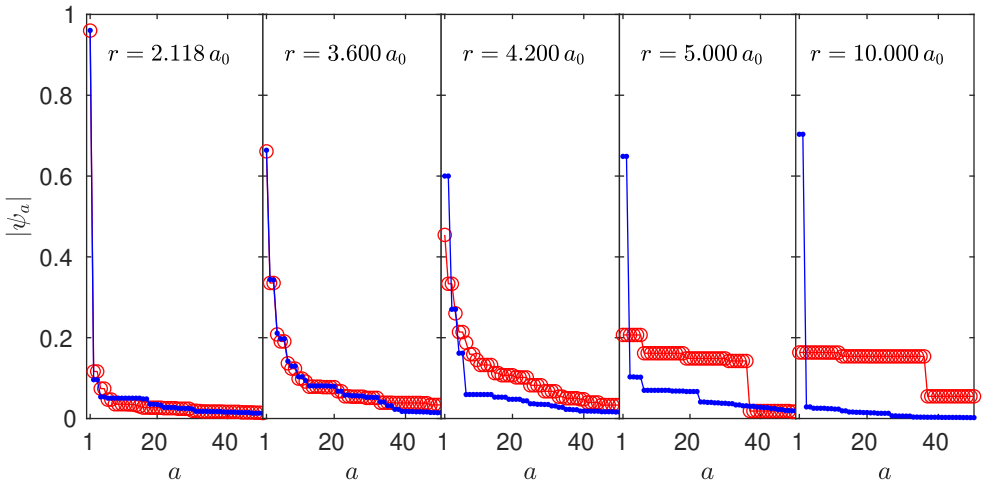

FIGURE 4.4. Absolute value of the 50 largest elements of the coefficient tensor $\boldsymbol{\psi}$ in decreasing order for various bond lengths for the initial orbitals (red) and for the optimized orbitals (blue), obtained by numerically exact calculations in CAS(6,14). Here the relabelling ψ_a for $a = 1, 2, \ldots, 4^d$ is used for the $\psi_{\alpha_1,\ldots,\alpha_d}$ elements of the coefficient tensor, such that $|\psi_a| \geq |\psi_b|$ if $a < b$.

the electrons are uniformly distributed on the corresponding π orbitals. The orbital entropy for the two σ orbitals remains close to one, which also signals that the π bonds break first. Note that the results of this quantitative analysis in terms of orbital entropies are the opposite as those in reference [**Bog13**], which demonstrates again that the entropic analysis depends on the orbital set and the orbital transformation. Although the ground-state energy does not change during the macro-iterations, $E = -108.7935\,E_\mathrm{h}$, the orbital entropies are reduced. Therefore, the overall quantum correlation encoded in the wave function, I_tot, reduces from 7.3585 to 5.3188, and I_dist from 36.6702 to 28.3941. Further stretching the nitrogen dimer, the orbital entropies of the partially occupied orbitals scale towards $\ln(4) \approx 1.38$ in the initial orbitals, while they are reduced to $\ln(2) \approx 0.69$ in the optimized orbitals. For the optimized orbitals, $\langle n_i \rangle$ takes values very close to one or zero, that is, the six electrons are distributed uniformly on the six partially occupied orbitals. Note that these six orbitals are almost uncorrelated with the rest of the orbitals, that is, the problem reduces to CAS(6,6), as expected. In this almost half-filled configuration, the empty and doubly occupied configurations provides no contribution for the orbitals of CAS(6,6), giving $S_i \approx \{\ln(2), 0\}$. For $r = 20.000\,a_0$, even the initial orbitals lead to the latter configuration.

Besides the entropic quantities and occupation numbers, it is interesting to study the entries of the coefficient tensor $\boldsymbol{\psi}$ in (2.28), extracted from the MPS wave function (2.35a) obtained by the DMRG algorithm (2.55). Figure 4.4 shows the absolute value of the 50 largest elements of the coefficient tensor $\psi_{\alpha_1,\ldots,\alpha_d}$ in decreasing order, for various bond lengths. It is clearly visible that at the equilibrium geometry ($r = 2.118\,a_0$) for the initial orbitals (red), there is one determinant of weight almost one, and the remaining coefficients are smaller by at least an

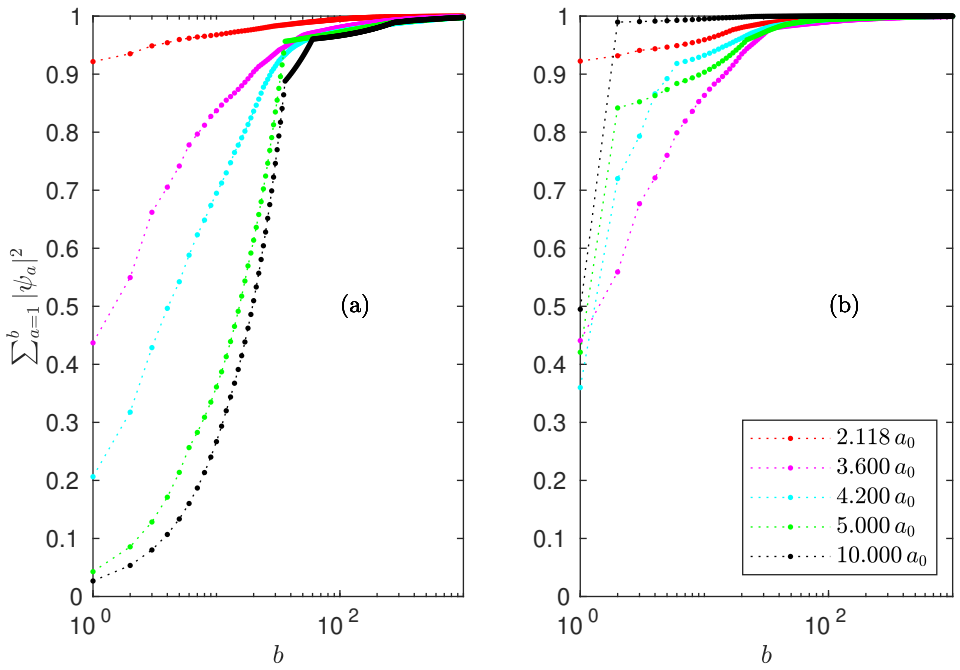

FIGURE 4.5. (a) Sum of the square of the absolute values of the 1000 largest CI coefficients for the nitrogen dimer in CAS(6,14) for various bond lengths, extracted from the MPS wave function, obtained by the DMRG algorithm, with a bond dimension $\tilde{D} = 4096$. (b) Similar to (a), but for the optimized orbitals.

order of magnitude. This single-reference property, however, changes as the nitrogen dimer is stretched, and the leading coefficient gets smaller and smaller, until degenerate plateaus appear. This multireference behaviour is in accordance with the entropic analysis discussed above. When orbital optimization is also utilized, the resulting profile of the entries of the coefficient tensor changes significantly with increasing bond length, compared to the initial orbitals, as is shown in figure 4.4 by blue colour. For the equilibrium geometry at $r = 2.118\,a_0$, the difference between the initial and optimized orbitals is negligible, as the initial orbitals already provides a single-reference approach for the problem. In contrast to this, for $r \geq 3.600\,a_0$, the effect of orbital optimization becomes more drastic. For $r \geq 4.200\,a_0$, the leading coefficients become two-fold degenerate, corresponding to a determinant and its spin flipped component, and their weight increase rapidly to the saturation value of $1/\sqrt{2}$ with increasing bond length. The plateau observed in the initial orbitals for $r \geq 10.000\,a_0$ completely disappears. Along these lines, the sum of the square of the absolute values of the largest coefficients also shows a more rapid convergence to one in the optimized modes for the stretched geometries, as shown in figure 4.5. The fast decay of the ψ tensor coefficients in the optimized orbitals leads to a more suitable basis for DMRG, thus lower computational demands are needed to reach the same level of accuracy, as mentioned before.

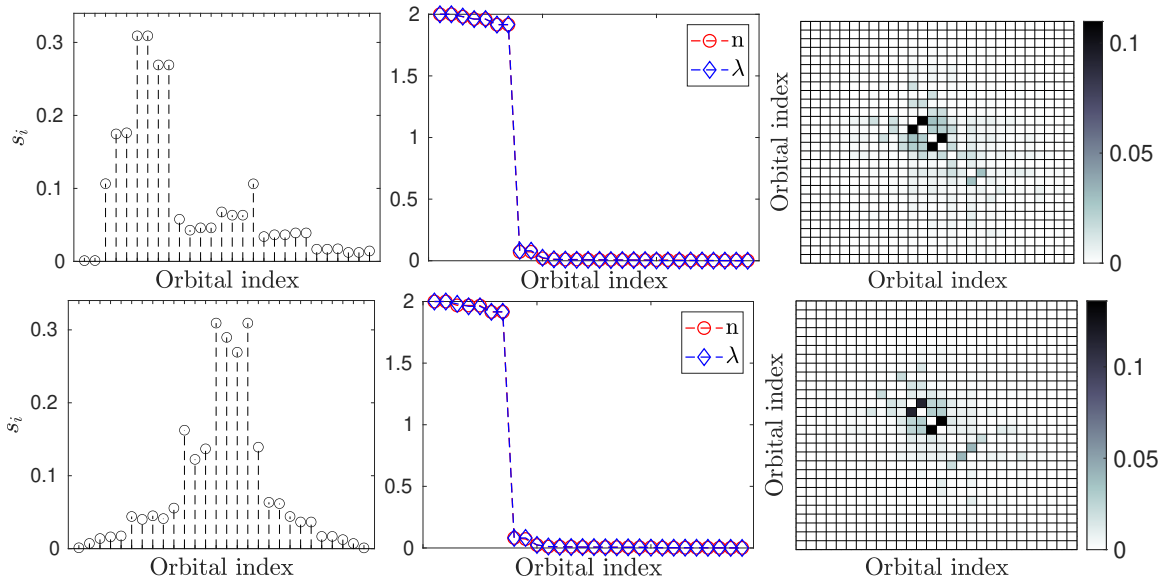

FIGURE 4.6. One-orbital entropy profiles $\{S_i\}$, sorted values of the natural orbital occupation numbers $\{\lambda_i\}$ and occupation numbers $\{\langle n_i \rangle\}$, and two-orbital mutual informations $\{I_{i,j}\}$ for the initial orbitals in CAS(14,28) (first row), and after the 20^{th} orbital optimization macro-iterations (second row) for the nitrogen dimer for bond length $r = 2.118\, a_0$ using bond dimension $\tilde{D} = 4096$.

4.6. Orbital optimization of the nitrogen dimer: full orbital set

Repeating the same analysis but for the full cc-pVDZ orbital set, namely, 14 electrons on 28 spatial orbitals, CAS(14,28), similar conclusions have been reached. Here, however, numerically exact calculations could not be performed, thus the effects of bond dimension truncation also influence the results. Also, since the number of the entries of the coefficient in the singlet sector is $\binom{28}{7}^2 \approx 10^{12}$, only single and double CI coefficients are calculated. Similarly to the analysis of the smaller active space, various selected quantities are shown in figures 4.6 and 4.7 for the full orbital set, to monitor the performance of the fermionic orbital optimization procedure. While figure 4.8 (a) shows the absolute value of the first 25 largest elements of the coefficient tensor $\boldsymbol{\psi}$ up to double excitation levels in decreasing order for various bond lengths. The reference determinant was obtained by the occupation number profile $\langle n_i \rangle$.

Here, for the equilibrium bond length $r = 2.118\, a_0$, a sharp Fermi edge separates again the almost doubly occupied seven orbitals from the remaining almost unoccupied orbitals for both the initial and the optimized orbitals. For the stretched geometries, six electrons get again shared among the six spatial orbitals that take part in the bond breaking, which get superposed under the action of orbital optimization. Since these orbitals are only marginally correlated with the rest of the orbitals, the previous analysis holds, the problem reduces to CAS(6,6).

For the initial orbitals, according to figure 4.8 (a), the absolute values of the leading $\psi_{\alpha_1,\ldots,\alpha_d}$ coefficients of the tensor, together with the norm squares of the wave function components

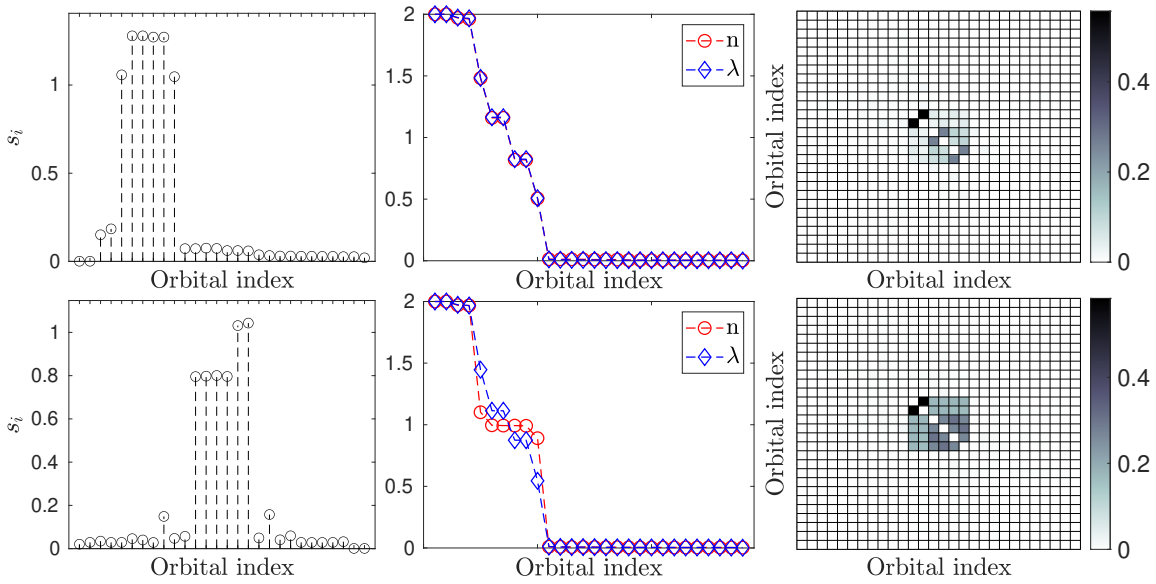

FIGURE 4.7. Similar to figure 4.6, but for a stretched geometry at $r = 4.200\,a_0$.

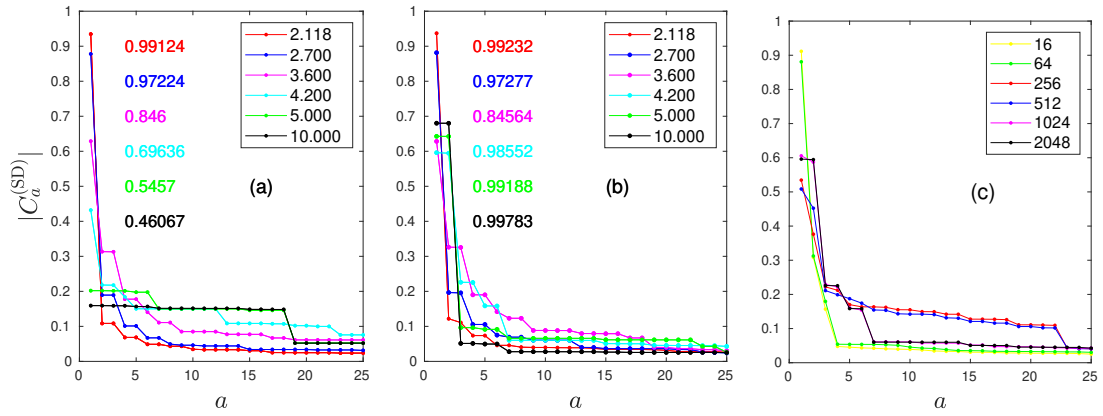

FIGURE 4.8. (a) Absolute values of the first 25 largest CI coefficients including single and double excitation levels for the initial orbitals in CAS(14,28) for various bond lengths of the nitrogen dimer, extracted from the MPS wave function, obtained by the DMRG algorithm, with a bond dimension $\tilde{D} = 4096$. The inscribed numbers are the norm squares of the wave function component corresponding to single and double excitations for the various bond lengths. (b) Similar to (a), but for the optimized orbitals with $\tilde{D}_{\max} = 512$. (c) Convergence of the absolute values of the first 25 largest CI coefficients including single and double excitation levels for $r = 4.200\,a_0$ for the optimized orbitals, as a function of the bond dimension $\tilde{D}$.

corresponding to single and double excitation levels systematically decrease with r increasing from $2.118\,a_0$ to $10.000\,a_0$, as expected. Thus, in the large r limit, higher level excitations besides singles and doubles get more and more weight. Here, since the initial orbitals are HF orbitals, we have used the original HF determinant as reference determinant, in which configuration the first seven orbitals are doubly occupied. For the optimized orbitals, however, the leading coefficient increases drastically, and, again, the fast decay of the values is observed, see in figure 4.8 (b). The two-fold degeneracy of the leading coefficient, on the other hand, is sensitive to the bond dimension. This is illustrated in figure 4.8 (c) for $r = 4.200$, where the optimized orbitals have been obtained with $\tilde{D}_{\max} = 512$, and the CI coefficients were extracted from DMRG calculations in the $\mathcal{M}_{\tilde{D}}\big((g(U_{\text{opt}})\big)$ manifold for different $\tilde{D}$ values. Here, two reference determinants, given by the occupation number profile, connected by spin-flip transformation, have been used. It is clear that for small bond dimensions, $16 \leq \tilde{D} \leq 256$, the problem looks like a single-reference one in the optimized orbitals, while for larger $\tilde{D}$ values, the correct degeneracy of the leading coefficient is recovered. In addition, for $\tilde{D} = 4096$, the norm square of the wave function component corresponding to single and double excitation levels gets close to one, see in figure 4.8(b), indicating that orbital optimization has the potential to convert higher level excitations to lower ones, that is, compressing multireference character of wave functions. This provides a significantly more optimal orbitals for DMRG computation, which is also validated by the resulting lower energies in the $\mathcal{M}_{\tilde{D}}\big(g(U_{\text{opt}})\big)$ manifold.

4.7. Summary

An optimization task was considered on a fixed rank MPS manifold and on the Stiefel manifold over the space spanned by the initial sites. To obtain approximate solution, a joint optimization procedure was utilized that fits to the TNS sturucture of the two-site DMRG, that is, subsequent two-site tensor optimizations are carried out. The algorithm consists of bare DMRG optimization steps, two-site unitary transformations and global reorderings. The method was demonstrated for the nitrogen dimer in the cc-pVDZ basis for the equilibrium and for stretched geometries. We analyzed the properties of the wave function, based on various entropic quantities, and on the profile of the coefficient tensor, highlighting the basis and orbital transformation dependent nature of such quantities. This orbital optimization has the potential to reduce significantly the correlation and entanglement encoded in the quantum many-body wave function, and to convert coefficients of higher level excitations to those of lower level ones, resulting in a rapidly decaying entries of the coefficient tensor of the wave function. These all together provide compression of the multirefernce character of wave functions, and significantly more optimal MOs for TNS methods (such as DMRG and DMRG-RAS) and conventional multireference methods.

5. CHAPTER

The Hubbard wheel - a crossover between one- and infinite dimensional models

In this chapter, we recall the challenges in the study of ultracold gases in section 5.1, especially the realization of the Bose–Einstein condensate. Then in section 5.2, we propose the *Hubbard wheel* lattice model of *hard-core bosons*, which exhibits a crossover between quasi-condensation and complete Bose–Einstein condensation. The model is studied both analytically and numerically in sections 5.3 and 5.4, then a potential experimental realization is proposed in section 5.4.

5.1. Quasi-condensation and Bose–Einstein condensation

After experimental realization of the Bose–Einstein condensation (BEC), the respective field of ultracold gases has become one of the most exciting fields of research with a fruitful interplay between theory and experiment. It allowed for the experimental verification of numerous other theoretical predictions as well, stimulated further theoretical investigations of trapped particles [**Dal99**] and even revealed phenomena not observed before such as the crossover from BEC-superfluidity to Bardeen–Cooper–Schrieffer (BCS) superconductivity [**Gre03**, **Bar04**, **Zwi04**, **Bou04**]. One of the most promising recent field has been the study of effectively one-dimensional quantum systems [**Gre01**, **Det01**, **GÖ1**, **Orz01**, **Par04b**, **Kin04**, **Stö04**]. Their most striking difference to three-dimensional systems is probably the absence of BEC. That is, already an infinitesimally weak interaction between the N bosons leads to a sublinear behaviour of the number of condensed bosons, $N_0(N) \propto N^\alpha$, where $0 < \alpha < 1$ [**Len64**, **Pop72**], which holds even at zero temperature, for homogeneous gases as well for gases in a harmonic trap and regardless of the form of the interaction [**Pop72**, **Wid73**, **Sch77**, **Gir01**, **For03**, **Gan04**, **Rig04b**, **Rig04a**]. A prominent system giving rise to this phase called *quasi-condensation* [**Pop72**] is the Lieb–Liniger model [**Lie63c**, **Lie63a**], a ring system with N spinless bosons interacting via a δ-potential. Tuning the coupling constant to infinity leads to impenetrable bosons, called *Tonks–Girardeau gas* [**Gir60**] with the proven scaling $N_0(N) \propto \sqrt{N}$ [**Len64**].

Thermodynamic phase transitions (at finite temperatures) in three dimensions have been studied for more than a century. However, the study of quantum phase transitions (at zero temperature) [**Sac11**], and particularly of the entanglement close to that transition [**Ost02**, **Osb02**] have attracted much attention only in recent years. The latter studies were performed mostly for low-dimensional lattice models. They have revealed a striking similarity between the behaviour of the order parameter and of quantum informational quantities, like entanglement entropy. As

discussed above, at zero-temperature an interacting Bose gas exhibits two qualitatively different phases, a quasi-condensate in one dimension and a true Bose–Einstein condensate in three or higher dimensions. Therefore, it is of interest to search for a model which exhibits a transition (or a crossover) between these two phases, and in particular allows to check whether this special transition has common properties with general quantum phase transitions.

The BEC was explored in cylindrical or torroidal trap geometries, both experimentally [**Gre01**, **Det01**, **GÖ1**, **Orz01**, **Par04b**, **Kin04**, **Stö04**] and theoretically [**Das02**, **Sal04**, **Sal05**]. But, changing the radial dimension of the confinement, neither the transition from the sublinear N-dependence of $N_0(N)$ of the quasi-condensate to the linear dependence of the true condensate, nor its entanglement properties have been investigated. The only systematic study of such a transition was performed for a one-dimensional Bose gas in a harmonic trap [**Pet00**]. However, that transition occurs only at temperatures $T > 0$.

Here we investigate strongly interacting bosons in the hard-core limit and a lattice model, consisting of a ring and a central site, which allows one to drive such a transition by changing just a single parameter, s/t, which is the ratio of the hopping rate s between the ring and the center site and hopping rate t between ring sites in the model, as explained below in section 5.2. One of our major results is to establish by this model a mechanism which can generate "infinite"-range hopping by increasing s/t. This is important since enhancing the mobility of bosons allows to overcompensate the destructive effects of the repulsive interactions, leading finally to maximal possible condensation, despite infinitely strong repulsion. A further important feature of the model is the generation of an excitation gap in the N-particle spectrum for $s/t > 0$. This makes BEC even robust to thermal noise and quantum fluctuations and thus may allow experimentalists to overcome the typical obstacles faced while realizing BEC. The other important result concerns the application of tools from quantum information theory. We show that the mutual information possesses the qualitatively similar dependence on s/t as the number $N_0(N)$ of condensed bosons. This supports the connection between the behaviour of an order parameter and of entanglement at a quantum phase transition even for the transition (or crossover) from a quasi-condensate to a true one.

All these key findings can be derived by analytical or exact numerical means despite the nonperturbative character of the system [**Mát21**]. It is also worth noticing that various other studies of BEC for inhomogeneous lattices differ significantly from the one presented below. They either consider the rather trivial case of ideal bosons [**Bur00**, **Bur01**, **Buo02**, **Bru04**, **Vid11**, **Oli13**, **Lyr14**] or restrict to the mean field regime [**Buo04**, **Hal12**]. At the same time, our proposed model could be particularly appealing to experimentalists since the underlying graph emerges from a Mexican hat potential (see in section 5.5) and hard-core bosons can be realized experimentally [**DeP99**, **Par04b**] by tuning the interactions at the Feshbach resonance [**Blo08**, **Chi10**, **Wei11**, **ZÏ2**].

5.2. The model: hard-core bosons on the Hubbard wheel

The lattice systems have the great advantage that the ratio between the kinetic energy and the interaction energy can be manipulated by varying the hopping (range) between the lattice

sites. The most prominent lattice model for (spinless) bosons is the widely studied Bose–Hubbard model of interacting spinless bosons [**Fis89**]

$$H_{\mathrm{BH}} = -\sum_{i,j=1}^{d} t_{i,j} a_i^\dagger a_j + U_{\mathrm{BH}} \sum_{i=1}^{d} a_i^\dagger a_i (a_i^\dagger a_i - \mathrm{I}), \tag{5.1}$$

where $a_i^\dagger$ and a_i are the bosonic creation and annihilation operators of site i in the Jordan–Wigner representation (2.75), and $t_{i,j}$ is the hopping rate between sites i and j, and U_{BH} is the on-site interaction between bosons. It was shown that the Bose–Hubbard model can be experimentally realized by ultracold bosonic atoms in an optical lattice [**Jak98**]. In general, the occurrence of the BEC also depends on the temperature and on the possible inhomogeneities or disorder, for example, due to the presence of an external field, but here we restrict our discussion to the *interaction strength* and the *spatial dimensionality* affecting the presence of the BEC.

Concerning the spatial dimensionality, that is, $t_{i,j}$ in (5.1), the effect of the interaction on BEC is distinctively destructive in one-dimensional systems. At zero temperature even an infinitesimally weak interaction already leads to a departure from BEC to the phase of quasi-condensation. This raises a fundamental question which shall be answered in an affirmative and constructive way: After having confined a three-dimensional Bose gas to one dimension, whether it is possible to tweak in an experimentally feasibly way this one-dimensional system with the effect of enhancing the mobility of the interacting bosons to reintroduce BEC. From a general point of view, one is immediately tempted to negate this question. The hopping amplitudes $t_{i,j}$ namely resemble the overlap of Wannier orbitals at sites i, j which in turn decays exponentially as function of the spatial separation $|i-j|$. Screening effects reduce the hopping even further and eventually motivate the common restriction of $t_{i,j}$ in the Bose–Hubbard model to just nearest neighbours. The potential physical significance of long-range hopping has motivated experimentalists in recent years to realize, at least, effective hopping terms beyond nearest neighbours. Despite a remarkable effort, the regime of infinite-range hopping has been out of reach but only the typical decay of $t_{i,j}$ could be slowed down to algebraic dipolar- and van der Walls-type ones [**Gü13, Sch15**]. It will be one of our key achievements to propose a model which eventually would allow one to enhance the mobility even to infinite-range. In contrast to the rather involved experimental realisation of algebraically decaying hopping rates our proposal to realize "infinite"-range hopping will be surprisingly simple, namely introducing a central site to the ring system.

Concerning the interaction strength, that is, U_{BH} in (5.1), the conflict between interaction and mobility is maximized in the limit of strong interactions $U_{\mathrm{BH}} \to \infty$, in which the bosons become *hard-core* [**Mat56, Mat57**]. Hard-core bosons were originally introduced as a model for liquid Helium-II in order to investigate superfluidity [**Mat56, Mat57**]. The hard-core constraint can be given by *hard-core boson creation* and *annihilation* operators, $h_i^\dagger$ and h_i, which obey to the *mixed commutation relations*,

$$[h_i, h_i^\dagger]_- = \mathrm{I}, \qquad [h_i, h_i]_- = 0, \qquad i \in [d], \tag{5.2a}$$

$$[h_i, h_j^\dagger]_+ = 0, \qquad [h_i, h_j]_+ = 0, \qquad i, j \in [d], i \neq j. \tag{5.2b}$$

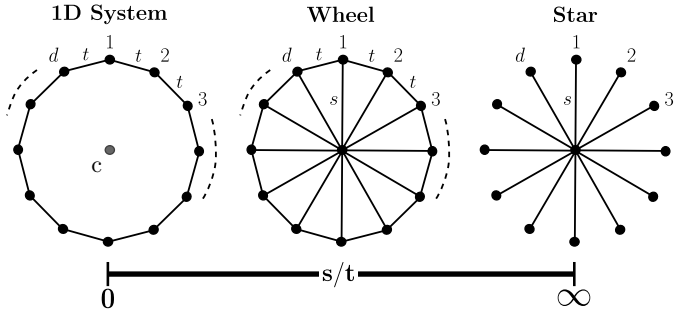

FIGURE 5.1. Topology of the Hubbard wheel lattice model. An interpolation between the one-dimensional regime and the star through the wheel with parameter s/t.

The first row shows a fermionic property, namely the maximal occupartion number of a site is one, while the second row expresses a bosonic property on different modes, namely hard-core bosons are symmetric under exchange. The defining mixed commutation relations (5.2) can be fullfiled by the tensor product of two-by-two matrices similar to the Jordan–Wigner representation (2.75) for fermions, but without the phases operator,

$$h_j^\dagger = \Big(\bigotimes_{k<j} \mathrm{I}_k\Big) \otimes \big(|\phi_{j,1}\rangle\langle\phi_{j,0}|\big) \otimes \Big(\bigotimes_{j<k} \mathrm{I}_k\Big). \tag{5.3}$$

In other words, the hard-core boson operators are obtained by the *standard extension* of the local operators [**Sza21**]. This is, however, not a true second quantized formulation since there is no first quantized picture behind, particularly an (2.72)-like isomorphism. Although, an interesting connection was shown in one dimension, where the fermions and hard-core bosons have similar phase-independent quantities, for example, similar energy spectra [**Gir60**]. So, in the hard-core limit, the (5.1) takes the compact form

$$H_{\mathrm{hc}} = -\sum_{i,j=1}^{d} t_{i,j} h_i^\dagger h_j. \tag{5.4}$$

Particularly the case of hard-core bosons makes clear the important role of the hopping range since hard-core bosons exhibit BEC even at finite temperatures for infinite-range hopping (a kind of mean field limit [**Fis89**]), despite their infinitely strong repulsion [**Tót90**, **Pen91**, **Kir00**]. The hard-core constraint itself results that there is a universal upper bound on the BEC,

$$N_0^{\max}(N,d) = N(d-N+1)/d, \tag{5.5}$$

which is independent of the topology, encoded in $t_{i,j}$ [**Ten17**].

The Hamiltonian of the Hubbard wheel of hard-core bosons reads

$$H = -t\sum_{i=1}^{d}(h_i^\dagger h_{i+1} + h_{i+1}^\dagger h_i) - s\sum_{i=1}^{d}(h_i^\dagger h_{\mathrm{c}} + h_{\mathrm{c}}^\dagger h_i), \tag{5.6}$$

where $h_{\mathrm{c}}^\dagger, h_{\mathrm{c}}$ denote the operators corresponding to the central site, and the periodicity in the peripheral sites can be expressed as $h_{d+1} \equiv h_1$, as it is illustrated in figure 5.1. We consider N

hard-core bosons on a lattice consisting of a ring with d sites, lattice constant a and one additional site at its center. We assume that the *particle number density* or *filling factor* $n = N/d < 1/2$, which is not a restriction due to the particle-hole duality. The ring gives rise to a hopping between nearest neighbors at a rate $t > 0$. The crucial point is now that the topology of the ring allows hopping between the central site and any ring site at a rate $s \geq 0$. Accordingly, the central site has an effect similar to an impurity, making the one-dimensional lattice inhomogeneous. We also refer to the ring model, that is, (5.6) with $s = 0$, as the *unperturbed* system.

5.3. Analytical results

Our model (5.6) reduces to the pure *ring model* in casae of $s/t \to 0$ (left of figure 5.1), and to the *star model* in the limit $s/t \to \infty$ (right of figure 5.1). The solutions of the eigenvalue problems for these two limiting cases are known. In the ring limit, we have the one-dimensional system of impenetrable bosons with periodic boundary condition, which exhibits only quasi-condensation [**Gir60**, **Lie63c**, **Lie63a**]. The population of this quasi-condensation has scaling $N_0 \propto \sqrt{N}$. In the continuous ring limit, $d \to \infty$ (with fixed ad, where a is the lattice constant), we have the Tonks–Girardeau gas [**Gir60**] of impenetrable (spinless) bosons, which was experimentally reallized with utracold gases [**Par04a**]. In the star limit, which is a model related to the infinite-range hopping, the existence of the true BEC was proved [**Ten17**]. Moreover the theoretical maximal possible number of condensed hard-core bosons (5.5) is attained. For intermediate values of s/t, the Hamiltonian (5.6) interpolates between the ring lattice and the star lattice (see figure 5.1). Hence, changing the single parameter s/t allows us to investigate in a systematic way the crossover from the regime of quasi-condensation to maximally possible condensation, eventually leading to a number of remarkable insights.

In the following only the crucial steps are mentioned. The technical details can be found in reference [**Mát21**] and particularly in its "Supplementary Information". The Hubbard wheel consists of sites $L = \{1, \ldots, d, \mathrm{c}\}$, where the sites on the ring are $[d] = \{1, \ldots, d\}$ and a central one is c. The central site couples the N- and $(N-1)$-particle ring-states, that is, the state space of N hard-core bosons on sites L can be partitioned into $(N-1)$- and N-particle state space on the ring, with the notation of (2.73b), $\mathcal{N}_L^N = \mathcal{N}_{[d],\mathrm{c}}^{N,0} \oplus \mathcal{N}_{[d],\mathrm{c}}^{N-1,1}$. Hence we can express the normalized state vector of the wheel by the superposition

$$|\Psi\rangle = \alpha|\Phi^{(N)}\rangle \otimes |\phi_{\mathrm{c},0}\rangle + \beta|\Phi^{(N-1)}\rangle \otimes |\phi_{\mathrm{c},1}\rangle, \tag{5.7}$$

where the normalized ring-states are $|\Phi^{(N)}\rangle$ and $|\Phi^{(N-1)}\rangle$, and the orthonormal basis of the central site is $\{|\phi_{\mathrm{c},\nu}\rangle\}_{\nu=0}^{1}$. The solution of the pure ring problem can be obtained by the Bethe ansatz, yielding the eigenvectors $|\phi_k^{(N)}\rangle$ and $|\phi_l^{(N-1)}\rangle$. With these eigenbases we write the N- and $(N-1)$-particle ring-states in (5.7) as

$$|\Phi^{(N)}\rangle = \sum_k A_k^{(N)} |\phi_k^{(N)}\rangle, \qquad |\Phi^{(N-1)}\rangle = \sum_l A_l^{(N-1)} |\phi_l^{(N-1)}\rangle, \tag{5.8}$$

where the summations run until $\binom{d}{N}$ and $\binom{d}{N-1}$, respectively. This expansion allows one to decouple the original eigenvalue problem. After implementing a number of steps, the eigenvalue

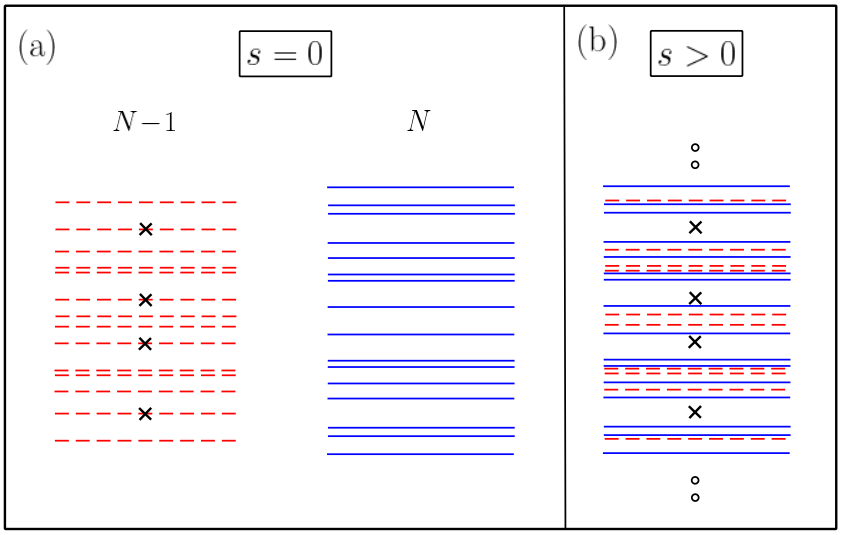

FIGURE 5.2. Schematic representation of the unperturbed and perturbed spectrum for $n \leq 1/2$ from [**Mát21**]. (a) The unperturbed band spectrum of $(N-1)$ hard-core bosons (red dashed lines) and N hard-core bosons (blue solid lines). The crosses mark those levels which disappear under the perturbation. (b) The perturbed spectrum consisting of the shifted unperturbed levels (dashed red and solid blue lines) and the crosses mark those levels of the unperturbed $(N-1)$-particle spectrum which have disappeared. The open circles are the new levels generated by the perturbation.

problem for Hamiltonian (5.6) can be rewritten in the general from

$$1 = s^2 F_d^{(N)}(E; \{A_k^{(N)}\}), \tag{5.9}$$

where a simple and fully analytic solution for the eigenvalue E does not exist.

Although (5.9) cannot be solved analytically for the entire regime of s, it allows us to derive important qualitatively correct features of the spectrum in a nontrivial way. The unperturbed $(N-1)$- and N-particle spectrum forms a band of discrete levels, illustrated in figure 5.2 (a), which becomes continuous for $d \to \infty$. The hopping between the central site and the ring introduces a "hybridization" of these two spectra. This leads, on the one hand, to a shift of order $1/d$ of the unperturbed band-levels, on the other hand, some energy levels (marked by crosses) of the smaller $(N-1)$-particle band are found to disappear. These levels, however, reappear as new discrete eigenvalues symmetrically below and above the perturbed N-particle band (see open circles in figure 5.2 (b)). The larger s and N are, the more of those new discrete energy levels occur. As a matter of fact, they follow from the eigenvalues of an effective Hamiltonian for N hard-core bosons with "infinite"-range,

$$H^{\text{eff}} = \tilde{s}^2 \frac{1}{d} \sum_{i,j=1}^{d} h_i^\dagger h_j, \tag{5.10}$$

where the parameter $\tilde{s} = \sqrt{d}s/t$ is the scaled dimensionless hopping rate. This mapping of the original model (5.6) to the effective one (5.10) holds for two asymptotic regimes, the *diluted* and the *strong coupling* regime. The system is diluted if $n \ll 1$ with $\tilde{s} \gg 2\sqrt{2}\,\pi/\sqrt{d}$, and it is in the strong coupling regime if $\tilde{s} \gg (4/\pi)\sqrt{d}\sin(\pi n)/\sqrt{n(1-n)}$ with $0 < n < 1$. Energy gap opens between the ground-state energy $E_0(N, d, \tilde{s})$ of (5.6) and the unperturbed ground-state energy $E_0(N, d, 0)$, that is, the lower edge of the N-particle band of the ring. The gap, in both the diluted and strong coupling cases, can be approximated by

$$\begin{aligned}\Delta E :=& E_0(N, d, 0) - E_0(N, d, \tilde{s}) \\ \approx& |E_\mathrm{F}/2|\big[\sqrt{1 + \tilde{s}^2 dn(1-n)/(E_\mathrm{F}/2t)^2} - 1\big],\end{aligned} \tag{5.11}$$

where $E_\mathrm{F} := E_0(N, d, 0) - E_0(N-1, d, 0)$ is the Fermi energy. Also the number N_0 of the condensed hard-core bosons can be approximated since it is related to the largest eigenvalue of H^eff. We obtain

$$\begin{aligned}N_0 =& \frac{1}{d}\langle\psi| \sum_{i,j\in[d]} h_i^\dagger h_j |\psi\rangle \\ \approx& N\big[(1-n) - |\beta|^2(1-2n)N^{-1}\big],\end{aligned} \tag{5.12}$$

where the prefactor $|\beta|^2$ of the $1/N$-correction depends on $(N, d, \tilde{s})$ and is given in the "Supplementary Information" of [**Mát21**].

5.4. Numerical results

In order to support and check the range of validity of the analytic results in the previous section and to extend those for to undiluted densities n and for intermediate coupling strengths $\tilde{s}$, large-scale DMRG computations have been performed. The DMRG calculations were performed for $d \leq 199$ and $N \leq 98$ such that various densities $n = N/d < 1/2$ and couplings $10^{-3} \leq \tilde{s} \leq 10^{+3}$ were simulated for each system size. We have set a tight error bound on the diagonalization procedure, that is, we set the residual error of the Davidson method to 10^{-9} and used 10 DMRG sweeps. We have checked that the various quantities of interest are practically insensitive on the bond dimension being larger than $\tilde{D} = 1024$. Besides the energy eigenvalues, we have calculated the one-site entropies (2.20), the two-site mutual informations (2.23a), the occupation number distribution $\langle n_i\rangle$ and the number of the condensed hard-core bosons (5.12), where $i, j \in \{1, \ldots, d, \mathrm{c}\}$. The corresponding results together with the analytical ones are presented in figures 5.3, 5.4 and 5.5.

In figure 5.3, the log-log plot of the gap ΔE in terms of $\tilde{s}$ reveals a distinctive crossover from a $\tilde{s}^2$-dependence for $\tilde{s} \ll 1$ to the linear dependence on $\tilde{s}$ for $\tilde{s} \gg 1$. For the diluted gas, that is, $n \ll 1$, the analytical and DMRG results in the $\tilde{s}^2$- and $\tilde{s}$-regime are in good agreement. When the density is increased, this agreement remains excellent in the linear (strong coupling) regime, while it gets worse in the complementary range.

Concerning figure 5.4, three main observations can be made. First, the DMRG-results for fixed (N, d) values exhibit the crossover from quasi-condensate to BEC in all cases. Of course, the transition from $N_0 \propto \sqrt{N}$ to $N_0 \propto N$ becomes more pronounced with the increase of N.

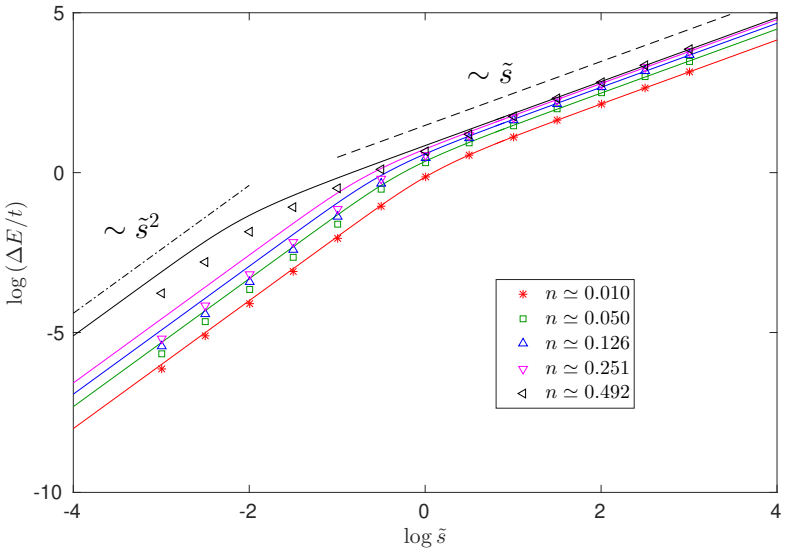

FIGURE 5.3. The log-log plot for the excitation gap as a function of $\tilde{s}$ for $d = 199$ and various densities n. Results from DMRG calculations (symbols) and the analytical result (5.11) (solid lines). The dashed-dotted and dashed lines represent slopes two and one, respectively.

Second, in case of the quasi-condensation ($\log(\tilde{s}) < 0$), the agreement between the DMRG-results and the result for impenetrable bosons [**For03**] is very good in the diluted regime. This holds because in the limit $d \to \infty$ with fixed N the ground state of hard-core bosons becomes identical to that of the impenetrable bosons. In this case, $N_0(N)$ for small N follows from the numerical exact computation of the Toeplitz determinant [**For03**], which is indicated by dotted lines. Yet, in the limit $N \to \infty$, $d \to \infty$ with fixed n not in the diluted regime, the hard-core bosons on the ring lattice differ from impenetrable bosons in one dimension. Third, in case of BEC ($\log(\tilde{s}) > 0$), that is, in the strong coupling regime, the DMRG results also fit well with the analytical one (5.12) for all densities. Even the non-monotone $\tilde{s}$-dependence stemming from the $1/N$-correction in (5.12) is reproduced for small N (see, for example, the result in figure 5.4 (a) for $d = 39$, corresponding to $N = 2$). With increasing N the DMRG-result approaches the maximally possible condensation (5.5), which is $N_0(N, n) \approx N(1 - n)$ for large d system sizes, which is indicated with full circles in figure 5.4 (b).

To explore a possible relation between BEC and the entanglement structure of the ground state, we have used DMRG for calculating the mutual information between the central site c and any ring site $i \in [d]$, $I_{i|c}$, and between two ℓ-th nearest neighbour ring sites, $I_{i|i+\ell}$. The corresponding results for $d = 199$ and $n \approx 0.05$ are shown in figure 5.5. The change in the respective pattern related to the crossover from quasi-condensation to genuine BEC is clearly visible through the mutual information, as well. The correlation between the central and any ring site, $I_{i|c}$, vanishes for small $\tilde{s}$ while it saturates to a finite value in the limit of large $\tilde{s}$ when the model exhibits "infinite"-range hopping. The correlation among ring-sites, $I_{i|i+\ell}$, saturates

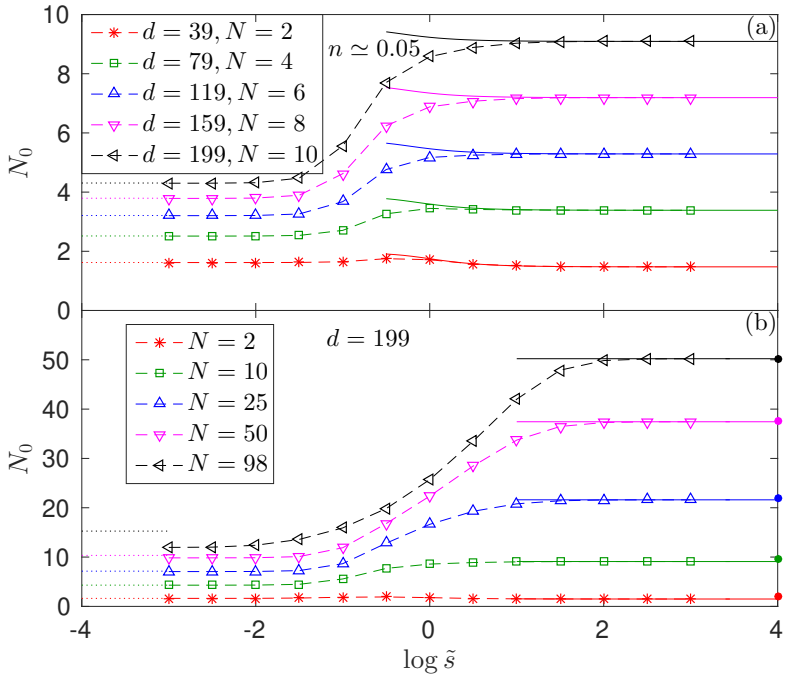

FIGURE 5.4. The number of condensed bosons. (a) N_0 as a function of $\log(\tilde{s})$ for fixed low density $n \approx 0.05$ and various site numbers d. (b) N_0 as a function of $\log(\tilde{s})$, various numbers of particles N, and fixed number of sites $d = 199$. The dots on the vertical axis represent $N(1-n)$. Symbols: Results from DMRG calculations, dashed lines: guide for the eye, solid lines: analytical result. The dotted lines mark the asymptotic values for finite N, $s = 0, d \to \infty$ obtained by the exact numerical calculation of a Toeplitz determinant [**For03**].

also with increasing $\tilde{s}$ to a constant value for all ℓ, demonstrating the growth of long range correlations. This relates to the generation of BEC. For $\tilde{s} = 0$ the correlation $I_{i|i+\ell}$ decays algebraically with increasing ℓ, which reflects the algebraic dependence of the quasi-condensate on N. Whereas for non-zero values of $\tilde{s}$ its decay becomes exponential as the gap opens, and saturates to a non-zero value for large $\ell \to d/2$ values.

5.5. Potential experimental realization

As a possible experimental realization of our model (5.6) we propose in a first step to confine N ultracold bosonic atoms into two dimensions subject to a Mexican-hat-type potential with d local wells. For illustration, see figure 5.6 (a). This is in complete analogy to several experiments from recent years [**Ami05**, **FA07**, **Ram11**, **Ami14**, **Bel16**]. Then, one may tune the interaction at the Feshbach resonance to realize hard-core bosons in the same way as reported in reference [**Par04b**] for a cigar-shaped confinement to realize quasi-condensation of hard-core bosons with $N_0(N) \propto \sqrt{N}$. Next, one may create a local well at the center of the hat, illustrated in figure 5.6 (b). Increasing its depth more and more would strongly enhance the mobility of the hard-core

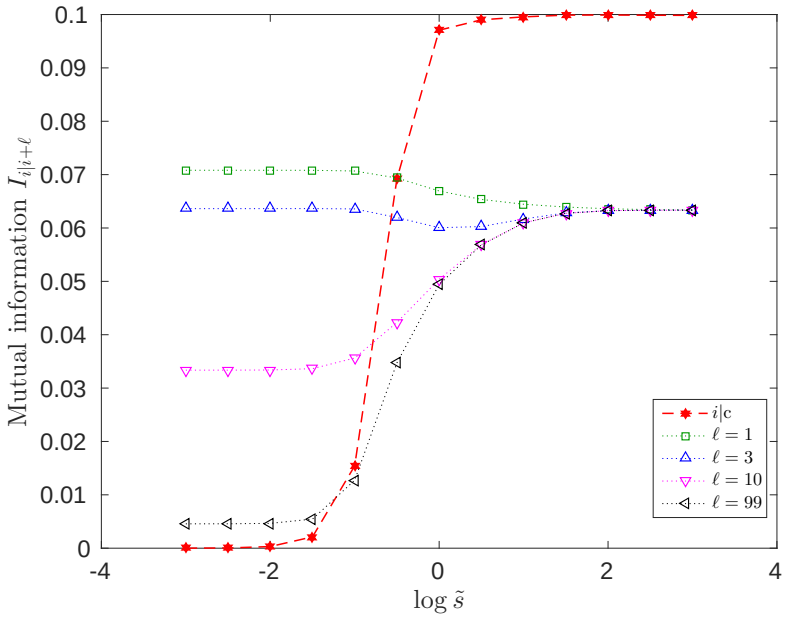

FIGURE 5.5. Two-site mutual information $I_{i|c}$ between the central site and a ring site (red stars), and $I_{i|i+\ell}$ for two sites on the ring separated by distance $\ell = 1, 3, 10, 99$ for $d = 199$ and $n \approx 0.05$. The dashed and dotted lines are a guide for the eye.

bosons due to their possible transitions back and forth between any ring-well and the central one. This would significantly change the physical behavior, and BEC would occur with $N_0(N) \propto N$. In order for this to happen already for *finite* and experimentally feasible d, it must be $s/t \gg 2\sqrt{2}\pi/d$ in case of a diluted gas (see previous section), which is the regime relevant for ultracold gases. The hopping occurs due to the tunneling between the corresponding wells. Let $(V_r, l_r = a)$ and $(V_c, l_c = ad/(2\pi))$ denote the potential barrier and tunneling distance, respectively, between two adjacent ring-wells and between a ring-well and the central one. Use of the WKB tunneling rate yields the estimate $s/t \approx (\gamma_c/\gamma_r)\exp[-\sqrt{ma^2/\hbar^2}(\sqrt{V_c}d/(2\pi) - \sqrt{V_r})]$ with m the particle's mass, and γ_r and γ_c the so-called attempt frequency related to the zero-point oscillation frequency in the corresponding ring and central well. For instance, if $d = 79$ and $N = 4$ (one data set in figure 5.4 (a)), then BEC-like behavior should occur for $s/t > 1$. This can be satisfied if $V_c/V_r \approx (2\pi/d)^2$ or if a compared to $\hbar/\sqrt{m \max\{V_c, V_r\}}$ is small enough, provided $\gamma_c/\gamma_r \approx 1$.

5.6. Summary

We proposed and comprehensively studied a physical model of strongly interacting bosons which allows one to drive a non-trivial transition from quasi-condensation to maximal BEC. It is particularly appealing that this necessitates the tuning of just a single control parameter, s/t, which changes the underlying topology in such a distinctive way that the infinite-range hopping model is simulated. Without solving the eigenvalue equation of the model exactly, we considered

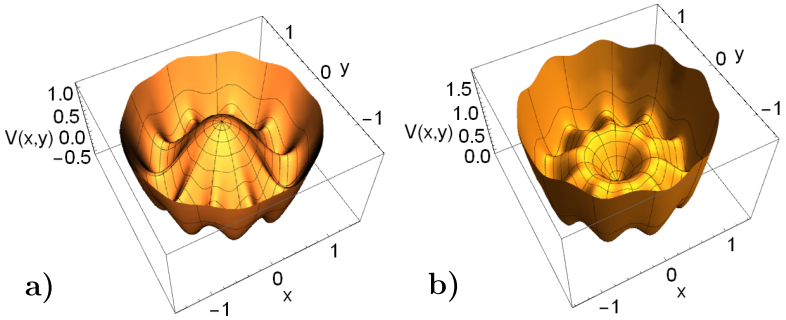

FIGURE 5.6. Illustration of the Mexican-hat-type trap potential from [Mát21]. (a) Realization of the ring lattice for $d = 10$ by a Mexican-hat-potential. (b) Realization of the wheel lattice for $d = 10$ by a Mexican-hat-like potential with a local well at its center. Loading hard-core bosons into the potential landscape in (a) and creating a local well as shown in (b) generates a crossover from quasi- to complete Bose–Einstein condensation.

effective model that is valid in the diluted and the strong coupling regime. This allowed us to show on a qualitative level why an excitation gap occurs in the N-particle spectrum. The transition is particularly pronounced for macroscopic N, however, the crossover already becomes visible for small N, as clearly demonstrated by the large scale DMRG computations. As argued above ultracold bosonic atoms in a Mexican-hat-like potential should allow the experimental observation of this dimensional crossover for BEC.

It is worth highlighting the striking potential of our mechanism for generating BEC. As a matter of fact, it is conceptually quite different to the well-known generation of BEC at finite temperatures for non-interacting bosons. The latter is either merely due to the opening of a gap in the "one-particle" spectrum or a deformation of the density of states (in analogy to the transition from $D \leq 2$ to $D = 3$) [**Bur00**, **Bur01**, **Buo02**, **Bru04**, **Vid11**, **Oli13**, **Lyr14**]. The same effectively applies to the experimental [**Gre01**, **Det01**, **GÖ1**, **Orz01**, **Par04b**, **Kin04**, **Stö04**] and theoretical studies [**Das02**, **Sal04**, **Sal05**] in which the cylindrical or torroidal confinement is relaxed to reach the mean-field regime. In our system, however, it is the interplay between mobility and interaction within the "non-perturbative" regime which generates genuine BEC. The enhanced mobility of the bosons then compensates for the destructive effects of the strong interaction to generate BEC.

6. CHAPTER

Conclusion and outlook

In this work strongly correlated systems were studied in the field of quantum chemistry and ultracold physics, and also the supporting algorithmic developments were carried out. The respective summaries of each study can be found at the end of chapters 3, 4 and 5. Here we give an outlook and possible research topics originating from our studies.

Concerning the *tailored coupled cluster method*, since the numerical error study showed a significant improvement for small CAS, we suspect the DMRG-TCCSD method to be of great use for larger systems with many strongly correlated orbitals as well as many dynamically correlated orbitals [**Vei16**, **Vei18**]. The oscillatory behavior of the error, however, remains unexplained at this point. Nevertheless, we note that the error minima are fairly robust with respect to the bond dimension. Hence, the DMRG-TCCSD method can be extended with a screening process using low bond-dimension approximations to detect possible error minima. Our analysis is basis dependent, thus there is a need for further investigations based on orbital optimizations. Also the investigations of the influence of higher-rank excitations, such as CI triples and quadruples, on the computed energies remain for future work. We note that the relativistic version of the TCC approach was developed and presented on a standard benchmark system, TlH, and also on more multireference systems such as AsH and SbH [**Bra20**]. The implementation, which was carried out with interfacing the Dirac program [**Sau20**] and the DMRG, is capable of treating systems which are of quaternion symmetry, that is, integrals for all spinors are present and are complex-valued.

Concerning the *mode optimization*, we presented that the compression of the multireference character yields significantly more optimal orbitals for the DMRG. Therefore, this orbital optimization can be regarded as a natural extension of the order optimizations, briefly summarized in appendix A. This numerical benefit can be understood, for example, by the initialization of the DMRG, where the space of the approximated block is spanned by configurations obtained from the CI expansion (see appendix B). Moreover, it can supply more optimal orbitals for algorithms such as coupled cluster, tailored coupled cluster, DMRG with restricted active space [**Bar22**, **Fri23**]. As it was noted in the TCC approach, its analysis and numerical study is basis dependent, so the numerical study of the DMRG-TCCSD, presented in chapter 3, should be extended with the orbital optimization. Since in the CI single and double excitations are considered, the compression of the multireference character is of central importance. We note that similar conclusion has also been drawn for the two-dimensional spinless fermionic lattice models

commonly studied in solid-state physics, where a single determinant is suitable for the description of the quantum many-body wave function for the non-interacting case, and for infinitely large interaction [**Kru21**].

Concerning the *Hubbard wheel of hard-core bosons*, we showed the existence of an excitation gap, which usually is highly demanding. Similarly to, for example, superconductivity, the quantum Hall effect and the Haldane phase the existence of such a gap has an enormous influence on the physical behavior, that is, making the BEC robust to thermal noise and perturbations in general. The non-trivial influence of the interaction is also well-illustrated by the analytical result for the ground-state gap (5.11), which in the regime of maximal BEC differs from the one of non-interacting bosons by the crucial factor $\sqrt{1-n}$. Remarkably, $1-n$ is nothing else than the universal reduction of the maximal possible degree of condensation due to the hard-core constraint [**Ten17**], which is the quantum depletion. In case of *finite* on-site interactions, this depletion factor $\nu(n)$ is expected to interpolate between both extremal cases of hard-core and ideal bosons, $1-n \leq \nu(n) \leq 1$. This would provide a remarkable exact relation between the ground-state gap, quantum depletion and the interaction strength of the ultracold atoms. Since the latter can systematically be tuned at the Feshbach resonance [**Blo08**, **Chi10**, **Wei11**, **ZÏ12**], this would open an avenue for steering ground-state gaps and controlling the number of bosons in BEC. Finally, inspired by the fruitful interplay of theory and experiments in the field of ultracold gases, our work based on analytical and exact large scale DMRG calculations shall be understood as a proposal to the experimentalists as well. Our model could be particularly appealing since the underlying graph can emerge from a Mexican-hat-type potential, and the entire transition can be driven by tuning just a single control parameter. It is then exactly the respective central site which can be probed to confirm that transition. At the same time, this would also exploit the link [**Ost02**, **Osb02**] between quantum phase transitions and entanglement or related promising quantum informational theoretical concepts.

Concerning *algorithmic developments*, the DMRG-TCCSD protocol was implemented, in which the selection of the active space orbitals and the detection of the error minima are fairly robust with respect to the bond dimension. For the efficient calculation of the CI coefficients, both for the tailoring in the DMRG-TCCSD and the monitoring of the performance of the mode optimization, MPS routines were implemented and optimised. Although one can get insights into the entanglement structure of the system, the orbital optimization is also proposed to be a routinely used preliminary process, therefore low numerical cost is required. Also, it remains to investigate the influence on convergence of different admissible cost functions of the mode optimization.

A. APPENDIX

Order optimization

The DMRG was developed for the simulation of one-dimensional systems, where the order of sites is obvious. Namely, neighbourhooding physical objects, for example, spins in a lattice, should be also neighbourhooding in the tensor network, here in the MPS. On the other hand, the numerical renormalization group (NRG) method was developed for impurity models in which the logarithmic discretization of the spectrum results in a semi-infinite chain with exponentially decaying couplings [**Wil75**, **Bul08**]. However, in two- or higher dimensional models one should take care of the mapping because nearest neighbour couplings (for example, hopping or repulsion) in the physical space inevitably yields some long-range couplings in the one-dimensional MPS chain.

In quantum chemistry the simulated systems do not indicate a natural order of orbitals, moreover, the Hamiltonian of a general interacting many-body system is of the form (2.89), that is, all sites are coupled. Finding the optimal order among the $d!$ permutations is a hard task, and it is based on numerical experience [**OA15**, **Sza15**]. In case of Hartree–Fock orbitals, the simplest guess is the ordering according to the HF energy [**Whi99**]. A genetic algorithm was proposed for the finding the optimal order with respect to the energy, which, however, requires low-cost but many subsequent DMRG runs [**Mor05**]. Another strategy is determining the optimal order from the minimising the bandwidth of an adjacency matrix with the reverse Cuthill–McKee algorithm. The adjacency between orbitals might be defined as having one-electron integral above a threshold [**Cha02**], or one can use the one-electron integrals and also the exchange terms from the two-electron integrals [**Mor05**]. The more subtle algorithms utilize correlation measures, which, however, require the knowledge of the approximate state vector. (See figures 3.2, 3.3 and 3.4 that demonstrate the roboustness of the entropy profile with respect to the bond dimension.) Ordering highly entangled sites (that is, with high one-site entropy S_i) to the middle of the MPS chain leads to faster convergence [**Leg03b**]. A heuristic cost function is considered [**Ris06**] to minimize the correlation in the tensor network,

$$\min_{\sigma\in S_d} \sum_{ij} I(\varrho_{ij})|\sigma_i - \sigma_j|^2, \tag{A.1}$$

that is, the distance of the sites are weighted with the mutual information. To find the optimal (or at least a good) σ ordering permutation in (A.1), first, we apply the Fiedler vector approach as an initial guess, then, a genetic algorithm is utilized [**Bar11**]. A better ordering can result in a better approximation to the state vector, by which more accurate correlation measures can be obtained. Therefore, in practice, sequence of low-cost DMRG calculations are performed, each followed by ordering algorithms.

B. APPENDIX

Initialization of the MPS tensors

In section 2.6, a generic DMRG iteration step was described, which was assumed to be well after the initial steps of the run. Here we consider the initialization of the MPS tensors. Note that poorly initialized tensors can result DMRG converging to a local minimum [**Leg03a**, **Leg03b**, **Mor06**]. (See section 3.2.2 in [**Kru18**] for a toy example and mode details.)

The traditional strategy is the *infinite lattice DMRG algorithm* [**Sch11**], and the rigorous method for many-body systems is the *dynamically extended active space (DEAS)* algorithm [**Cha02**, **Leg03b**, **Mor06**, **Bar11**, **Sza15**]. In the infinite lattice DMRG algorithm, the tensor network is built up by the systematic increase of the system size. For example, to initialize a system with 8 sites, the subsystem labels (X, Y, Z) evolve as $(\{1\}, \{2, 7\}, \{8\})$, $(\{1, 2\}, \{3, 6\}, \{7, 8\})$, $(\{1, 2, 3\}, \{4, 5\}, \{6, 7, 8\})$. At each iteration step, the corresponding renormalized operators of the extended subsystems, $\tilde{H}_{X',k}$ and $\tilde{H}_{Z',k}$, are generated according to (2.52).

In the DEAS algorithm, the tensor network is built up by a "warm-up" sweep, in which operators of the right bolck $\tilde{H}_{Z,k}$ are approximated. For example, to initialize a system with 8 sites, the subsystem labels (X, Y, Z) evolve as $(\{1\}, \{2, 3\}, \{4, \dots 8\})$, $(\{1, 2\}, \{3, 4\}, \{5, \dots 8\})$, $(\{1, 2, 3\}, \{4, 5\}, \{6, \dots 8\})$. The first rows of figure 2.5 illustrates also this case. To be more precise, let us write out the relevant subspaces in the quantum chemistry context. In case of particle number conservation, the DMRG subspace is $\tilde{\mathcal{H}}_X \otimes \mathcal{H}_Y \otimes \tilde{\mathcal{H}}_Z \subseteq \mathcal{N}_{[d]}^N$. In the warm-up sweep, which is a rightward sweep, the left subspace $\tilde{\mathcal{H}}_X$ is obtained via the renormalization (2.52a), the $\mathcal{H}_Y$ is written without approximation. Using the notations of section 2.9 as well as (2.73), we can write the decomposition of the N particle subspace of d modes with respect to the bipartition $\bar{Z}|Z$ as

$$\mathcal{N}_{[d]}^N = \bigoplus_{M=M_{\min}}^{M_{\max}} \mathcal{N}_{\bar{Z}|Z}^{N-M,M}, \tag{B.1a}$$

where the minimum and maximum occupation numbers in subsystem Z are $M_{\min} = \max\{0, N - |\bar{Z}|\}$ and $M_{\max} = \min\{N, |Z|\}$, respectively. The subspaces are spanned by the basis vectors with the given occupation number restrictions,

$$\mathcal{N}_{\bar{Z}|Z}^{N-M,M} = \mathrm{Span}\Big\{ |\phi_{\boldsymbol{\nu}}\rangle \;\Big|\; \sum_{i\in\bar{Z}} \nu_i = N - M, \sum_{i\in Z} \nu_i = M \Big\}. \tag{B.1b}$$

The basis vectors can be written as the tensor product of the component basis vectors [**Sza21**], $|\phi_{\boldsymbol{\nu}}\rangle \equiv |\phi_{\boldsymbol{\nu}_{\bar{Z}}\boldsymbol{\nu}_Z}\rangle = |\phi_{\boldsymbol{\nu}_{\bar{Z}}}\rangle \otimes |\phi_{\boldsymbol{\nu}_Z}\rangle$, where we separate the occupation numbers $\boldsymbol{\nu}_{\bar{Z}} \in \nu\big(I_{N-M}^{\wedge}(\bar{Z})\big)$ and $\boldsymbol{\nu}_Z \in \nu\big(I_M^{\wedge}(Z)\big)$. Having no prior knowledge of the MPS tensors of the right block, the right block $\tilde{\mathcal{H}}_Z$ is defined as the span of some occupation number basis vectors $|\phi_{\boldsymbol{\nu}_Z}\rangle$. That is, some

$\boldsymbol{\nu_Z}$ indices are considered, taking into account the occupation number restrictions (B.1b), until the dimension of the right block reaches the predefined maximum bond dimension. A possible approach is to prioritize such $\boldsymbol{\nu_Z}$ indices in which the low-energy HF orbitals are occupied, and because of the discarded configurations it was advantageous to add a small noise to the density matrix [**Cha02**]. It is better in terms of convergence to add first Slater determinants consisting of highly entangled orbitals [**Leg03b**, **Mor06**]. A more sophisticated approach is the *configuration interaction based DEAS (CI-DEAS)* [**Bar11**, **Sza15**]. As it was noted in section 2.6, the CI-DEAS is closely connected with the restricted active space (RAS) method [**Bar22**]. The DMRG-RAS algorithm iterates in a similar way as the DMRG (see figure 2.5 for the illustration of sweeping). The difference is that the sweeping is carried out along the sites $\{1, \ldots, d_{\mathrm{CAS}}\}$ only, and the sites $\{d_{\mathrm{CAS}} + 1, \ldots, d\}$ are treated by the CI-DEAS procedure [**Bar22**].

C. APPENDIX

Single-reference methods in quantum chemistry

In this chapter, we start with the problem of the Schrödinger equation in non-relativistic quantum chemistry. Since, in this work, we do not intend to analyse such kind of elliptic differential equation [**Bre10**, **Ree78**, **Ree80**, **Kat51**], we turn in sections C.1-C.2 to the Galerkin discretisation by choosing a finite orbital set, which defines the *full configuration interaction* (FCI) space. We deal with methods that approximate the solution of the Schrödinger equation in the FCI space (without semiempirical considerations), in quantum chemistry named as *ab initio* and *wave-function-based* methods. Other broad fields, not considered here, are the density functional theory based methods [**DSS09**], which circumvent the curse of dimensionality, and quantum Monte Carlo [**Boo09**, **Poz13**, **Vei18**]. Our aim here, and also in the next chapter, is to approach the energy in the FCI space. Another direction is the extrapolation to the complete basis limit [**Fri22b**]. To provide context for the present work, in sections C.4-C.6, we recall the *Hartree–Fock*, *configuration interaction* and *coupled cluster* (CC) methods.

C.1. Schrödinger equation and Galerkin–Ritz approximation

In chapter 2, the general form of the Hamiltonian of interacting identical particles (2.89) was recalled, based on the one-particle Hilbert space $\mathcal{K}$ of finite modes. To formulate the Hamiltonian for physical models, especially interacting electrons in external potential, one usually work on the *configuration space* $\mathcal{X} = \mathbb{R}^3 \times \{\pm\frac{1}{2}\}$, that is, the $x = (\boldsymbol{r}, s) \in \mathcal{X}$ is the composite variable of the spatial- and spin variables of an electron, $\boldsymbol{r}$ and s, respectively. Alternatively, with Fourier transformation, the momentum-space representation is more useful in many cases, which is given by the same continuous configuration space.

Here we consider the non-relativistic system of electrons in the Born–Oppenheimer approximation for modelling molecules. So the problem of N interacting electrons in the external potential of the nuclei is described by the Schrödinger equation

$$\begin{aligned}(H_{(N)}\Psi)(x_1,\dots,x_N) &= \left[\sum_{r=1}^{N}\left(\frac{-\hbar^2}{2m_{\mathrm{el}}}\boldsymbol{\nabla}_r^2 + U(x_r)\right) + \sum_{\substack{r,r'=1\\ r<r'}}^{N} V(x_r,x_{r'})\right]\Psi(x_1,\dots,x_N) \\ &= E\Psi(x_1,\dots,x_N).\end{aligned} \tag{C.1}$$

Partial differential equations of this type are elliptic, and the solutions are in the $\mathcal{W}^{1,2}(\mathcal{X}^N)$ Sobolev space [**Eva10**, **Ree78**, **Ree80**, **Bre10**], moreover, to respect the antisymmetrization postulate, the solution is searched in the space $\mathcal{L}^{\wedge N} := \mathcal{W}^{1,2}(\mathcal{X}^N) \cap L^2(\mathcal{X})^{\wedge N}$. The Schrödinger operator $H_{(N)}$ is self adjoint [**Neu30**, **Kat51**], and its spectrum can be characterised by the

Hunziker–van Winter–Zhislin theorem [**Hun66**, **VW64**, **VW65**, **Zhi60**]. This tells us that below the *ionization energy* the spectrum is discrete, the solutions correspond to the bound states of the system, and above the ionization energy there is the essential spectrum of the Schrödinger operator.

In quantum chemistry, the bound states, especially the ground state are of interest. The *min-max theorem* provides a variational characterization of the essential and discrete spectrum of a compact self-adjoint operator [**Ree78**]. Accordingly, the *Rayleigh–Ritz variational principle* states that the lowest eigenvalue E_0 of self-adjoint operator $H_{(N)}$ bounded below can be given by the minimum of the Rayleigh quotient $\frac{\langle\Psi,H_{(N)}\Psi\rangle}{\langle\Psi,\Psi\rangle}$, or with normalized vectors,

$$E_0 = \min\Big\{\langle\Psi, H_{(N)}\Psi\rangle \;\Big|\; \Psi\in\mathcal{L}^{\wedge N}, \|\Psi\|=1\Big\}. \tag{C.2a}$$

The *Ritz–Galerkin method* is a general framework in numerical analysis that discretizes the problem of a continuous (differential) operator by examining the problem in a subspace spanned by finite number of orthonormal vectors. That is, let $\{\varphi_i\}_{i\in[d]}$ be an orthonormal system in $\mathcal{W}^{1,2}(\mathcal{X})$ and the spanned subspace $\mathcal{L}_d := \mathrm{Span}\{\varphi_i\}_{i\in[d]}$, then the approximate solution of the Schrödinger equation in this subspace is

$$E_0^{\mathrm{FCI}} = \min\Big\{\langle\Psi, H_{(N)}\Psi\rangle \;\Big|\; \Psi\in\mathcal{L}_d^{\wedge N}, \|\Psi\|=1\Big\} \tag{C.2b}$$

The following fundamental result of the Galerkin scheme formulates the approximation of (C.2a) by (C.2b). Let $\{\mathcal{L}_d\}_{d\in\mathbb{N}}$ be a dense family of subspaces in $\mathcal{W}^{1,2}(\mathcal{X})$, therefore $\{\mathcal{L}_d^{\wedge N}\}_d$ is dense in $\mathcal{L}^{\wedge N}$, furthermore Ψ_0 and Ψ_0^{FCI} be the normalized minimizers of (C.2a) and (C.2b), respectively, with the corresponding non-degenerate energies E_0 and E_0^{FCI}, then

$$\|\Psi_0 - \Psi_0^{\mathrm{FCI}}\| \le C \inf_{\Phi\in\mathcal{L}_d^{\wedge N}} \|\Psi_0 - \Phi\|, \tag{C.3a}$$

$$0 \le E_0^{\mathrm{FCI}} - E_0 \le C\|\Psi_0 - \Psi_0^{\mathrm{FCI}}\|^2, \tag{C.3b}$$

with some constant C. This result is often cited as the *quasioptimal* convergence of the eigenfunction and the *quadratic convergence* of the eigenvalue compared to the eigenfunction [**Yse03**].

C.2. Full configuration interaction space

To be able to use formalism of section 2.8, we make correspondence between vectors of two d dimensional Hilbert spaces $|\psi\rangle\in\mathcal{K}$ and $\psi\in\mathcal{L}_d$. To this end, for an arbitrary $|\psi\rangle\in\mathcal{K}$ let us have the formal definition

$$\langle e_x|\psi\rangle =: \psi(x). \tag{C.4}$$

Here the left-hand-side is not an inner product just a pairing because $\{|e_x\rangle\}_{x\in\mathcal{X}}$ is not in the Hilbert space $\mathcal{K}$, but rather in the space of distributions. The right-hand-side is the pointwise definition of the function $\psi\in\mathcal{W}^{1,2}(\mathcal{X})$, also called *orbital* or *one-particle wave function*. The inner product in $\mathcal{L}_d$ is

$$\langle\psi|\kappa\rangle = \langle\psi,\kappa\rangle = \int_{\mathcal{X}} \mathrm{d}x\, \psi(x)^*\kappa(x) = \sum_{s=\pm\frac{1}{2}} \int_{\mathbb{R}^3} \mathrm{d}\boldsymbol{r}\, \psi(\boldsymbol{r},s)^*\kappa(\boldsymbol{r},s). \tag{C.5}$$

For N particles, for an arbitrary elementary symmetric and antisymmetric vector $|\psi_1\rangle \overset{\vee}{\wedge} \ldots \overset{\vee}{\wedge} |\psi_N\rangle \in \mathcal{K}^{\overset{\vee}{\wedge} N}$ let us have the formal definition

$$\begin{aligned} \langle e_{\boldsymbol{x}}|(|\psi_1\rangle \overset{\vee}{\wedge} \ldots \overset{\vee}{\wedge} |\psi_N\rangle) =: \\ (\psi_1 \overset{\vee}{\wedge} \ldots \overset{\vee}{\wedge} \psi_N)(x_1, \ldots x_N) &= \frac{1}{\sqrt{N!}} \sum_{\sigma \in \mathrm{S}_{[N]}} (\pm 1)^{\mathrm{Par}(\sigma)} R_\sigma(\psi_1 \otimes \ldots \otimes \psi_N)(x_1, \ldots x_N) \\ &= \frac{1}{\sqrt{N!}} \sum_{\sigma \in \mathrm{S}_{[N]}} (\pm 1)^{\mathrm{Par}(\sigma)} \psi_{\sigma(1)}(x_1) \ldots \psi_{\sigma(N)}(x_N). \end{aligned} \tag{C.6}$$

Here, again, the left-hand-side is not an inner product just a pairing because $\{|e_{\boldsymbol{x}}\rangle := |e_{x_1}\rangle \otimes \ldots \otimes |e_{x_N}\rangle\}_{\boldsymbol{x} \in \mathcal{X}^{\times N}}$ is not in the Hilbert space $\mathcal{K}^{\overset{\vee}{\wedge} N}$, but rather in the space of distributions, The right-hand-side is the pointwise definition of the N-variable function $\psi_1 \overset{\vee}{\wedge} \ldots \overset{\vee}{\wedge} \psi_N \in \mathcal{L}_d^{\overset{\vee}{\wedge} N}$ also called *N-particle fermionic/bosonic wave function*. If the one-particle wave functions φ_i are orthonormal, then the N-particle fermionic wave function $\varphi_{\boldsymbol{i}} = \varphi_{i_1} \wedge \ldots \wedge \varphi_{i_N}$ it is called *Slater determinant*. We note that $\psi_{\sigma(1)}(x_1) \ldots \psi_{\sigma(N)}(x_N) = \psi_1(x_{\sigma^{-1}(1)}) \ldots \psi_N(x_{\sigma^{-1}(N)})$, that is $R_\sigma^\dagger = R_{\sigma^{-1}}$.

With this identification between $\mathcal{L}_d$ and $\mathcal{K}$, the N-particle Schrödinger operator in (C.1) is $H_{(N)} = \iota_{1,N}(H_1) + \iota_{2,N}(H_2)$. The one-particle operator $H_1 = \frac{-\hbar^2}{2m_{\mathrm{el}}} \boldsymbol{\nabla}^2 + \mathrm{M}_U$ contains the kinetic and the external potential term, and the two-particle operator $H_2 = \mathrm{M}_V$ describes the permutational invariant interaction, where M is the multiplication operator. For clarity, we use the term "wave function" for the elements in $\mathcal{L}_d$ and "state vector" for the kets in the general $\mathcal{K}$. In the sequel, the space of operators are not indicated, because it will be clear from the vector it acts on. That is, the bare form is used for the wave function space, $\psi \in \mathcal{L}_d$, and the bracket formalism for the abstract space, $|\psi\rangle \in \mathcal{K}$. The second quantized vectors and operators are obtained in the same way as in section 2.9, particularly with the isomorphism (2.72) we have the second quantized Hamiltonian (2.89) $H = F(\iota_1(H_1) + \iota_2(H_2))F^{-1}$. In this chapter only fermions are considered.

In conventional quantum chemistry calculations the number of electrons N is fixed, therefore we only deal with the subspace of N electrons on $d = \dim(\mathcal{K})$ orbitals, $\mathcal{N}_{[d]}^N = F\mathcal{K}^{\wedge N} \subset \mathcal{N}_{[d]}$, which is commonly named as *full configuration interaction* (FCI) space in quantum chemistry community. Note that "configuration" does not refer to the configuration space $\mathcal{X}$, but rather to an index $\boldsymbol{i} = (i_1, \ldots, i_N)$ and the corresponding Slater determinant $|\varphi_{\boldsymbol{i}}\rangle = |\varphi_{i_1}\rangle \wedge \ldots \wedge |\varphi_{i_N}\rangle$; and the "interaction" refers to that all the Slater determinants are included in the method, in this sense it is "full", that is, $\mathrm{Span}\{|\varphi_{\boldsymbol{i}}\rangle\}_{\boldsymbol{i} \in I_N^\wedge} = \mathcal{K}^{\wedge N}$ indeed. The solution of the minimization problem (C.2b) can be obtained by the diagonalization of the matrix $\langle \varphi_{\boldsymbol{i}}, H_{(N)} \varphi_{\boldsymbol{j}} \rangle$ for $\boldsymbol{i}, \boldsymbol{j} \in I_N^\wedge$, or in the second quantized framework (2.89), where the one-electron integrals are

$$\langle \varphi_i, H_1 \varphi_j \rangle = \int_{\mathcal{X}} \mathrm{d}x \, \varphi_i(x)^* \Big(\frac{-\hbar^2}{2m_{\mathrm{el}}} \boldsymbol{\nabla}^2 + U(x) \Big) \varphi_j(x), \tag{C.7a}$$

and two-electron integrals are

$$\langle \varphi_{i_1} \otimes \varphi_{i_2}, H_2 \varphi_{j_1} \otimes \varphi_{j_2} \rangle = \int_{\mathcal{X}} \int_{\mathcal{X}} \mathrm{d}x \mathrm{d}x' \, \varphi_{i_1}(x)^* \varphi_{i_2}(x')^* V(x, x') \varphi_{j_1}(x) \varphi_{j_2}(x'), \tag{C.7b}$$

where $i, j, i_1, i_2, j_1, j_2 \in [d]$. The calculations in this space, having dimension $\binom{d}{N}$, is feasible for only small molecules. One can further reduce the dimension, therefore computational cost, for example, by freezing the low lying core orbitals or exploiting symmetries, such as searching the solution in a total spin projection subspace of the electrons. The selection and the restriction of the orbital set $\{\varphi_i\}_{i\in[d]}$ is a crucial task and of central importance in computational chemistry [**Hel00**, **Leh19**]. Within the chosen d orbitals the exact FCI calculations for small molecules can serve as a reference for benchmarking other numerical methods.

C.3. Spatial orbitals

We emphasize here, the methods in this work are discussed with *spin-orbitals* for clarity, however, in the non-relativistic theory, *spatial orbitals* are more useful in applications (see, for example, sections 3.7, 4.5 and 4.6). In the spin-orbital formulation we have modes, which can be empty or occupied. We have the ordered set $L = \{1, \dots, d\}$, and the corresponding one-mode Hilbert spaces $\mathcal{N}_i$ for $i \in L$. So when turning to applications, for example, with DMRG algorithm, the elementary factor spaces in (2.28) are simply $\mathcal{H}_i \cong \mathcal{N}_i$. We say that a spin-orbital can be empty or occupied. In the spatial orbital formulation, the spin part is separated from the configuration space. On the one hand, since the spin part of the configuration space $\mathcal{X} = \mathbb{R}^3 \times \{\pm\frac{1}{2}\}$ is two dimensional, one can choose an orthonormal basis $\{\varphi_\uparrow^{\mathrm{spin}}, \varphi_\downarrow^{\mathrm{spin}}\}$. Then every orbital $\varphi \in \mathcal{L}_{2d}$ can be written as $\varphi(\boldsymbol{r}, s) = \varphi_\uparrow^{\mathrm{spat}}(\boldsymbol{r})\varphi_\uparrow^{\mathrm{spin}}(s) + \varphi_\downarrow^{\mathrm{spat}}(\boldsymbol{r})\varphi_\downarrow^{\mathrm{spin}}(s)$, where we indicate the arguments of the functions for clarity. On the other hand, in the non-relativistic Schrödinger equation (C.1) the spin part and the spatial part is not coupled, hence they can be factorized [**Hel00**]. So the *spin-orbital* corresponding to the (j, σ) composite index is the product of the j-th *spatial orbital* and the σ-th *spin function*, $\varphi_{(j,\sigma)}(\boldsymbol{r}, s) = \varphi_j^{\mathrm{spat}}(\boldsymbol{r})\varphi_\sigma^{\mathrm{spin}}(s)$, where the spatial part has no spin dependence any more. By this, in the spatial orbital formulation, we have composite indices of spatial orbitals and spin projections, that is, the ordered set $L = \{(1,\uparrow), (1,\downarrow), \dots, (d,\uparrow), (d,\downarrow)\}$, and the corresponding one-mode Hilbert spaces $\mathcal{N}_i$ for $i \in L$. So in the spatial orbital implementation, the elementary factor spaces in (2.28) are the product that of the spin-up and spin-down pairs, $\mathcal{H}_j \cong \mathcal{N}_{(j,\uparrow)} \otimes \mathcal{N}_{(j,\downarrow)}$, We say that a spatial orbital can be empty, singly occupied with either a spin-up or spin-down electron, or doubly occupied with opposite-spin electrons. By this, the Jordan–Wigner representation of the creation operators (2.75) become

$$\begin{aligned} a_{j,\uparrow}^\dagger &= \Big(\bigotimes_{k<j} \mathrm{P}_{(k,\uparrow)} \otimes \mathrm{P}_{(k,\downarrow)}\Big) \otimes \big(|\phi_{(j,\uparrow),1}\rangle\langle\phi_{(j,\uparrow),0}| \otimes \mathrm{I}_{(j,\downarrow)}\big) \otimes \Big(\bigotimes_{j<k} \mathrm{I}_{(k,\uparrow)} \otimes \mathrm{I}_{(k,\downarrow)}\Big), \\ a_{j,\downarrow}^\dagger &= \Big(\bigotimes_{k<j} \mathrm{P}_{(k,\uparrow)} \otimes \mathrm{P}_{(k,\downarrow)}\Big) \otimes \big(\mathrm{P}_{(j,\uparrow)} \otimes |\phi_{(j,\downarrow),1}\rangle\langle\phi_{(j,\downarrow),0}|\big) \otimes \Big(\bigotimes_{j<k} \mathrm{I}_{(k,\uparrow)} \otimes \mathrm{I}_{(k,\downarrow)}\Big). \end{aligned} \tag{C.8}$$

C.4. Hartree–Fock method

On the contrary to the exact diagonalization of the Hamiltonian in the FCI space, one of the simplest approximate solution of the interacting Schrödinger equation (C.1) is given by the *Hartree–Fock method*, in which the best Slater determinant is searched for [**Sza96**]. The

ground-state energy in the Hartree–Fock approximation is

$$E_0^{\mathrm{HF}} = \min\Big\{ \langle \varphi_{\boldsymbol{i}} | H_{(N)} | \varphi_{\boldsymbol{i}} \rangle \;\Big|\; |\varphi_{\boldsymbol{i}}\rangle = |\varphi_1\rangle \wedge \ldots \wedge |\varphi_N\rangle, \{|\varphi_1\rangle, \ldots, |\varphi_N\rangle\} \text{ orthonormal} \Big\} \tag{C.9a}$$

or we can express as the minimization among orbital transformations for a fixed Slater determinant, $|\varphi'_{\boldsymbol{i}}\rangle \in \mathcal{K}^{\wedge N}$, as

$$E_0^{\mathrm{HF}} = \min\Big\{ \langle \varphi'_{\boldsymbol{i}} | U^{\otimes N} H_{(N)} (U^{\otimes N})^\dagger | \varphi'_{\boldsymbol{i}} \rangle \;\Big|\; U \in \mathrm{U}(\mathcal{K}) \Big\} \tag{C.9b}$$

$$= \min\Big\{ \langle F\varphi'_{\boldsymbol{i}} | g(U) H g(U)^\dagger | F\varphi'_{\boldsymbol{i}} \rangle \;\Big|\; U \in \mathrm{U}(\mathcal{K}) \Big\}, \tag{C.9c}$$

see section 2.9. The minimization (C.9a) leads to an effective one-electron non-linear Schrödinger equation, namely the eigenvalue problem of the one-particle *Fock operator* F_1,

$$\begin{aligned} F_1|\varphi_{i_r}\rangle &= H_1|\varphi_{i_r}\rangle + \sum_{r'=1}^{N} \Big(\mathrm{Tr}_2\Big(\big(\mathrm{I} \otimes |\varphi_{i_{r'}}\rangle\langle\varphi_{i_{r'}}|\big) H_2 \Big) |\varphi_{i_r}\rangle - \mathrm{Tr}_2\Big(\big(\mathrm{I} \otimes |\varphi_{i_r}\rangle\langle\varphi_{i_{r'}}|\big) H_2 \Big) |\varphi_{i_{r'}}\rangle \Big) \\ &= \epsilon_{i_r} |\varphi_{i_r}\rangle, \end{aligned} \tag{C.10}$$

showing that the electron-electron interaction is treated by a mean-field approach. The first part of the sum in (C.10) is the *Coulomb operator* and the second is the *exchange operator*.

For numerical reasons, mainly for the evaluation of the integrals (C.7), the orbitals are expressed as the *linear combination of atomic orbitals*,

$$|\varphi_i\rangle = \sum_{j=1}^{d} c_{j,i} |\varphi_j^{\mathrm{AO}}\rangle \tag{C.11}$$

where the *atomic orbitals* $\{|\varphi_j^{\mathrm{AO}}\rangle\}_{j\in[d]}$ are usually Slater-type orbitals, Gaussian-type orbitals or numerical atomic orbitals [**Leh19**]. When the (C.11) is determined or optimized according to some considerations in a molecule, the $|\varphi_i\rangle$ orbitals are called *molecular orbitals*. With this, equation (C.10) can be formulated in terms of the coefficients $c_{i,j}$, yielding the *Roothan–Hall equation*,

$$\sum_{j=1}^{d} \langle \varphi_{i_r}^{\mathrm{AO}} | F_1(\{c\}) | \varphi_j^{\mathrm{AO}} \rangle c_{j,i_r} = \epsilon_{i_r} \sum_{j=1}^{d} \langle \varphi_{i_r}^{\mathrm{AO}} | \varphi_j^{\mathrm{AO}} \rangle c_{j,i_r} \qquad r = 1, \ldots, N, \quad j = 1, \ldots, d \tag{C.12}$$

Since the Fock operator depends on the coefficients $c_{i,j}$, this non-linear generalized eigenvalue problem is solved numerically in an iterative self-consistent manner. The N solution of (C.12) are the coefficients of the N *HF occupied orbitals* $\{|\varphi_{j_r}\rangle\}_{r\in[N]}$. This can be completed with $d-N$ *HF virtual orbitals* to form the *HF canonical molecular orbitals* $\{|\varphi_i\rangle\}_{i\in[d]}$ with the corresponding *HF orbital energies* ϵ_{i_r}. It is important to say that the natural orbitals (2.84) of the HF state $|\varphi_{\boldsymbol{i}}\rangle\langle\varphi_{\boldsymbol{i}}|$ are the canonical HF molecular orbitals $\{|\varphi_i\rangle\}_{i\in[d]}$ themselves with natural occupations $\lambda_i = 1$ for $i \in \boldsymbol{i}$, and $\lambda_i = 0$ for the rest. That is, the HF canonical orbitals are obtained by such a mode transformation (2.77) where the unitary is the one which diagonalizes the one-electron reduced state. From this point of view, the Hartree–Fock method is an orbital optimization yielding the HF canonical molecular orbitals, therefore it is a common starting point for many other quantum chemistry methods. The interpretation of the HF orbital energies ϵ_j is given

by the *Koopmans theorem*. Let $|\varphi_{\boldsymbol{i}}\rangle$ be the minimizer of (C.9a) with energy E_0^{HF}, then we get $\epsilon_j = E_0^{\mathrm{HF}} - \langle\varphi_{\boldsymbol{i}\setminus\{j\}}|H_{(N-1)}|\varphi_{\boldsymbol{i}\setminus\{j\}}\rangle$, which is the ionization energy (in the HF approximation) of orbital $j \in \boldsymbol{i}$, that is, the energy needed to remove an electron from the system form the j-th orbital. If $j \notin \boldsymbol{i}$, then $\epsilon_j = E_0^{\mathrm{HF}} - \langle\varphi_{\boldsymbol{i}\cup\{j\}}|H_{(N+1)}|\varphi_{\boldsymbol{i}\cup\{j\}}\rangle$ is the electron affinity [**Sza96**]. As a result, the total HF energy $\langle\varphi_{\boldsymbol{i}}|H_{(N)}|\varphi_{\boldsymbol{i}}\rangle \neq \sum_r \epsilon_{i_r}$ since in the sum of the orbital energies the electron-electron interaction is counted twice. In the context of solid-state physics, this fact is known as that the total ground-state energy of an interacting system is the sum of the energies of the quasiparticles corrected by subtracting half of the self-energies [**Sól11**].

Another important property of the HF solution is the *Brillouin theorem*. This says that the matrix elements of the Hamiltonian between the HF solution $|F\varphi_{\boldsymbol{i}}\rangle$ and a "singly excited" Slater determinant is zero, $\langle F\varphi_{\boldsymbol{i}}|Ha_i^\dagger a_j|F\varphi_{\boldsymbol{i}}\rangle = 0$, where $j \in \boldsymbol{i}$ and $i \notin \boldsymbol{i}$. This follows from taking the derivative of $g(U)$ (2.79) in terms of the matrix entries of the anti-Hermitian matrix $(\ln U)_{i,j}$. So the condition of the minimum of (C.9c) is $\langle F\varphi_{\boldsymbol{i}}|[H, a_i^\dagger a_j]_+|F\varphi_{\boldsymbol{i}}\rangle = 0$. The Brillouin theorem is often interpreted as that the HF solution is stable with respect to "single excitations". This serves the motivation of the configuration interaction (CI) and coupled cluster (CC) parametrizations.

C.5. Configuration interaction method

In section 2.8 by fixing single mode basis vectors $|\varphi_i\rangle \in \mathcal{K}$, where $i \in L = \{1, \dots, d\}$, the (2.64) basis vectors $|\varphi_{\boldsymbol{i}}\rangle \in \mathcal{F}$ in the Fock space and the (2.65b) labelling $\boldsymbol{i} \in I_N^\wedge(L)$ in the first quantized scheme arises in the standard way, and, in section 2.9, the occupation number space accordingly. The parametrization of the configuration interaction (CI) and the coupled cluster (CC) scheme is based on the fact, that the creation and annihilation operators (corresponding to the fixed one mode basis) transforms basis vectors $|\varphi_{\boldsymbol{i}}\rangle$ into each other up to a -1 phase factor. The HF calculation is a common starting point of many other quantum chemistry methods, and the resulting Slater determinant $|\varphi_{\boldsymbol{i}}\rangle = |\varphi_{i_1}\rangle \wedge \ldots \wedge |\varphi_{i_N}\rangle$ is the best independent-particle approximation of the system, so it can serve as a *reference* state vector,

$$|\Phi^{\mathrm{HF}}\rangle = F(|\varphi_{i_1}\rangle \wedge \ldots \wedge |\varphi_{i_N}\rangle) \in \mathcal{N}_L^N, \qquad i_1, \dots, i_N \in L_{\mathrm{o}}, \tag{C.13}$$

where $L_{\mathrm{o}} \subseteq L$ is the index set of the $|L_{\mathrm{o}}| = N$ *occupied orbitals*, the rest $L_{\mathrm{v}} = L \setminus L_{\mathrm{o}}$ is that of the $d - N$ *virtual orbitals* (which, of course, should not to be confused with the virtual indices of tensor networks in section 2.4). To obtain all the other N-electron Slater determinants the one-electron *excitation operator* $\mathrm{X}_i^j := a_j^\dagger a_i$ is considered, where $\mathrm{X}_i^j|\Phi^{\mathrm{HF}}\rangle$ is non-zero if $i \in L_{\mathrm{o}}$ and $j \in L_{\mathrm{v}}$, therefore, only this type of index pairs are considered. For M electrons the excitation operator is $\mathrm{X}_\mu \equiv \mathrm{X}_{i_1,\dots,i_M}^{j_1,\dots,j_M} := \mathrm{X}_{i_M}^{j_M} \dots \mathrm{X}_{i_1}^{j_1}$, where $\mathrm{X}_\mu|\Phi^{\mathrm{HF}}\rangle$ is non-zero, if the *excitation index*

$$\mu = (\boldsymbol{i}, \boldsymbol{j}) \in J_M(L_{\mathrm{o}}, L_{\mathrm{v}}) := I_M^\wedge(L_{\mathrm{o}}) \times I_M^\wedge(L_{\mathrm{v}}), \tag{C.14}$$

that is, we excite from occupied to virtual orbitals, and both index tuples are ordered increasingly. The $|\mu| = M$ is the *excitation rank* (not to be confused with other ranks, for example, that of the linear operators, Schmidt rank), where $M = 1$ stands for singles, $M = 2$ for doubles, and so on. For $M = 0$, there is only one element of J_0, which is the pair of empty indices, and we define the corresponding excitation operator as the identity operator. The maximal

excitation rank $M_{\max} := \min\{N, d-N\}$ is reached when we excite from all occupied or we excite to all virtual orbitals. In general, let a set of excitation indices be the subset of all possible excitation indices, $J(L_{\rm o}, L_{\rm v}) \subseteq J_1(L_{\rm o}, L_{\rm v}) \cup \ldots \cup J_{M_{\max}}(L_{\rm o}, L_{\rm v})$. It follows from the canonical anticommutation relations (2.76) that the excitation operators with respect to the same reference (C.13) commute, $[\mathrm{X}_\mu, \mathrm{X}_\nu]_+ = 0$ for all $\mu, \nu \in J(L_{\rm o}, L_{\rm v})$. In the sequel the argument of the index sets may be omitted if it does not lead to confusion. For more details on the algebra of the excitation operators, see [**Sch09**].

The CI parametrization of the state vector in $\mathcal{N}_L^N$ is

$$|\Phi^{\rm CI}\rangle = (\mathrm{I} + C_1 + C_2 + \ldots)|\Phi^{\rm HF}\rangle, \qquad C_M = \sum_{\mu \in J_M} c_\mu \mathrm{X}_\mu, \tag{C.15}$$

where C_M is the *configuration interaction operator* of rank M, and $c_\mu \in \mathbb{C}$ numbers are the *configuration interaction coefficients*. Note, that this parametrization results the convenient *intermediate normalization*, $\langle \Phi^{\rm HF}|\Phi^{\rm CI}\rangle = 1$. Substituting this ansatz (C.15) to the Rayleigh quotient in (C.2b) and taking derivative in the variational parameters c_μ^* gives

$$\begin{cases} E^{\rm CI} = \langle \Phi^{\rm HF}|H|\Phi^{\rm CI}\rangle, \\ \quad 0 = \langle \mathrm{X}_\mu \Phi^{\rm HF}|(H - E^{\rm CI}\mathrm{I})|\Phi^{\rm CI}\rangle, \quad \mu \in J, \end{cases} \tag{C.16}$$

which is nothing else than the eigenvalue problem $\sum_{\mu \in J_0 \cup J} H_{\nu,\mu} c_\mu = E^{\rm CI} c_\nu$ of the Hamiltonian matrix $H_{\nu,\mu} = \langle \mathrm{X}_\nu \Phi^{\rm HF}|H|\mathrm{X}_\mu \Phi^{\rm HF}\rangle$. Note that same system of equations can be obtained by projecting the Schrödinger equation $H|\Phi^{\rm CI}\rangle = E_0^{\rm CI}|\Phi^{\rm CI}\rangle$ with vectors $\langle \mathrm{X}_\mu \Phi^{\rm HF}|$. That is, the CI approach is a variational method in which the problem is restricted to the subspace $\mathrm{Span}\{|\mathrm{X}_\mu \Phi^{\rm HF}\rangle \mid \mu \in J_0 \cup J\} \subseteq \mathcal{N}_L^N$. For example, in the *CI single and double* (CISD) approximation the excitation index is restricted to $\mu \in J = J_1 \cup J_2$. If all the possible excitaions are taken into account, $\mu \in J = J_1 \cup \ldots \cup J_{M_{\max}}$, then the system of equations (C.16) is the *full CI* (FCI) problem of the system. This approximation, being a dimensional reduction, yields a computationally more feasible method, which is, however, no longer size-extensive [**Hel00**]. This means the following. Consider the bipartition of the orbitals $L_A \subset L$ and $L_B = L \setminus L_A$, and the corresponding occupied and virtual orbitals, $L_{A,\rm o} := L_A \cap L_{\rm o}$ and $L_{A,\rm v} := L_A \cap L_{\rm v}$, respectively; and similarly for subsystem B. Let the Schrödinger equation (C.16) for subsystem A with the Hamiltonian H_A be fulfilled by $|\Phi^{A,\rm CI}\rangle = (\mathrm{I} + C_1^A + C_2^A + \ldots)|\Phi^{\rm HF}\rangle$, where $C_M^A = \sum_{\mu \in J_M(L_{A,\rm o}, L_{A,\rm v})} c_\mu \mathrm{X}_\mu$, that is, excitaion indices are only in subsystem A; and similarly for subsystem B. If the subsystems are independent, the Hamiltonian can be written as $H = H_A + H_B$, then the Schrödinger equation (C.16) for $H = H_A + H_B$ is fulfilled by $|\Phi^{\rm CI}\rangle = (\mathrm{I} + C_1^A + C_2^A + \ldots)(\mathrm{I} + C_1^B + C_2^B + \ldots)|\Phi_{\rm HF}\rangle$. However, if $|\Phi^{A,\rm CI}\rangle$ is obtained with maximized excitations rank, for example, CISD, that is, $\mu_A \in J_1(L_{A,\rm o}, L_{A,\rm v}) \cup J_2(L_{A,\rm o}, L_{A,\rm v})$, and similarly for B, then $|\Phi^{\rm CI}\rangle$ is not of the form CISD, that is, $\mu \in J_1(L_{\rm o}, L_{\rm v}) \cup J_2(L_{\rm o}, L_{\rm v})$, because higher extitaions, triples and quadruples, appear. In the CI approach the size-extensivity can be restored only if all the possible excitaions are taken into account, which is again the FCI problem of the system. This impractical property, being the consequence of the linear parametrization (C.15), can be resolved by the coupled cluster parametrization, which is of an exponential form.

C.6. Coupled cluster method

The CC parametrization [**Hub57**, **Hug57**, **Bar07**] of the (intermediately normalized) state vector in $\mathcal{N}_L^N$ is

$$|\Phi^{\mathrm{CC}}\rangle = \mathrm{e}^{T}|\Phi^{\mathrm{HF}}\rangle = \mathrm{e}^{T_1+T_2+\cdots}|\Phi^{\mathrm{HF}}\rangle, \qquad T_M = \sum_{\mu\in J_M} t_\mu \mathrm{X}_\mu, \tag{C.17}$$

where T_M is the *cluster operator* of rank M, which is of the same form as that of the CI operator C_M in (C.15), and $t_\mu \in \mathbb{C}$ numbers are the *coupled cluster amplitudes*. We note that there is a one-to-one correspondence between state vectors in $\mathcal{N}_L$ and cluster operators T [**Živ78**, **Sch09**], which also holds in the infinite dimensional case $\mathcal{L}^{\wedge N}$ [**Roh13**]. System of equations are obtained by projecting the Schrödinger equation $H|\Phi^{\mathrm{CC}}\rangle = E^{\mathrm{CC}}|\Phi^{\mathrm{CC}}\rangle$ with vectors $\langle \mathrm{X}_\mu\Phi^{\mathrm{HF}}|$ or $\langle \mathrm{X}_\mu\Phi^{\mathrm{HF}}|\mathrm{e}^{-T}$ yielding the *unlinked* or *linked CC equations*, respectively. They are equivalent in the CC approach [**Hel00**], however, not in the tailored CC formalism [**Fau19b**], which is discussed in the next section. The linked CC equations are

$$\begin{cases} E^{\mathrm{CC}} = \langle\Phi^{\mathrm{HF}}|\mathrm{e}^{-T}H\mathrm{e}^{T}|\Phi^{\mathrm{HF}}\rangle, \\ 0 = \langle \mathrm{X}_\mu\Phi^{\mathrm{HF}}|\mathrm{e}^{-T}H\mathrm{e}^{T}|\Phi^{\mathrm{HF}}\rangle, \quad \mu \in J(L_{\mathrm{o}}, L_{\mathrm{v}}), \end{cases} \tag{C.18}$$

Because of the exponential parametrization, the treatment of the CC ansatz in the variational formalism (by the derivatives of the Rayleigh quotient) is untractable, since all Slater determinants in the FCI space are present in the system of equations [**Hel00**, **Lae19**]. The approximation in the CC approach is the restriction of the excitation indices in (C.18). For example, in the *CC single and double* (CCSD) approximation the excitation index is restricted to $\mu \in J = J_1 \cup J_2$. But contrary to the CI method, this does not restrict the problem to a subspace. Therefore, the CC method is not variational, that is, the CC energy is in general not equal to the expectation value of the Hamiltonian, so it is neither an upper bound to the FCI energy (C.2b) nor to the exact ground-state energy (C.2a). If all the possible excitaions are taken into account, $\mu \in J = J_1 \cup \ldots \cup J_{M_{\max}}$, then the system of equations (C.18) is the FCI problem of the system [**Živ78**, **Sch09**]. The CC method is size-extensive, which follows from the exponential parametisation (C.17) of the state vector [**Číž66**, **Číž69**, **Pal72**]. In computational sense, this is a favourable property, which can and will be shown in the tailored CC formalism in the section 3.2.:wq

The CC energy in (C.18) can be expressed [**Hel00**] as

$$E^{\mathrm{CC}} = \langle\Phi^{\mathrm{HF}}|H\Big(\mathrm{I} + T_2 + \frac{1}{2}T_1^2\Big)|\Phi^{\mathrm{HF}}\rangle. \tag{C.19}$$

It follows from the Slater–Condon rules (which are the consequences that the Hamiltonian (2.89) is a linear combination of monomials of form $a^\dagger a$ and $a^\dagger a^\dagger aa$) that amplitudes with rank higher that two not contribute. The fact that the pure rank-one excitations with respect to the HF reference do not contribute is the consequence of the Brillouin theorem [**Lev68**]. This obviously does not mean that the CCSD suffices for the energy calculation because the amplitudes in (C.18) are optimized simultaneously. In the Baker–Campbell–Hausdorff (BCH) expansion of the similarity-transformed Hamiltonian $\mathrm{e}^{-T}H\mathrm{e}^{T}$, the series of inner products with the nested

commutators $[\cdot,\cdot]_{(k)}$ terminates after the quartic term [**Hel00**],

$$\langle \mathrm{X}_\mu \Phi^{\mathrm{HF}} | \mathrm{e}^{-T} H \mathrm{e}^{T} | \Phi^{\mathrm{HF}} \rangle = \langle \mathrm{X}_\mu \Phi^{\mathrm{HF}} | \sum_{k=0}^{4} \frac{1}{k!} [H,T]_{(k)} | \Phi^{\mathrm{HF}} \rangle, \tag{C.20}$$

independently of the truncation of the excitation rank of the cluster operator. This makes the projected equations tractable. One can derive equations by the BCH expansion, and matching the terms according to the excitation rank, yielding a non-linear system of equations $f(\boldsymbol{t})_\mu = \langle \mathrm{X}_\mu \Phi^{\mathrm{HF}} | \mathrm{e}^{-T} H \mathrm{e}^{T} | \Phi^{\mathrm{HF}} \rangle = 0$ in terms of the amplitude vector $(\boldsymbol{t})_\mu := t_\mu$ for all $\mu \in J$. In applications it is usually solved by quasi-Newton method, which uses an approximate Jacobian with the HF energies (C.10),

$$t_\mu \longmapsto t_\mu - \varepsilon_\mu^{-1} f(\boldsymbol{t})_\mu, \qquad \varepsilon_\mu \equiv \varepsilon_{(\boldsymbol{i},\boldsymbol{j})} := \sum_{m=1}^{M} (\epsilon_{j_m} - \epsilon_{i_m}). \tag{C.21}$$

This requires a sufficiently large energy gap between the highest occupied molecular orbital and the lowest unoccupied molecular orbital (*HOMO-LUMO gap*),

$$\Delta(L_\mathrm{o}, L_\mathrm{v}) := (\min_{j \in L_\mathrm{v}} \epsilon_j) - (\max_{i \in L_\mathrm{o}} \epsilon_i) = \min_\mu \varepsilon_\mu \tag{C.22}$$

in the spectrum of the Fock operator for convergence stability [**Sch09**, **Hel00**, **Roh13**]. This requirement can fail in case of multireference systems, and this is one of the motivations for our tailored coupled cluster approach. Assuming that we have less occupied than virtual orbitals, $N < d - N$, which is the common case in practice, the computational cost of the CCSD, CCSDT and CCSD(T) methods scale as $\mathcal{O}(N^2(d-N)^4)$, $\mathcal{O}(N^3(d-N)^5)$ and $\mathcal{O}(N^3(d-N)^4)$, respectively [**Pur82**, **Rag89**, **Hel00**].

Bibliography

[Ací00] A. Acín, A. Andrianov, L. Costa, E. Jané, J. I. Latorre, R. Tarrach. Generalized Schmidt decomposition and classification of three-quantum-bit states. *Phys. Rev. Lett.*, **85**, 1560, 2000. doi:10.1103/PhysRevLett.85.1560

[Ali01] R. Alicki, M. Fannes. *Quantum Dynamical Systems*. Oxford University Press, 2001. ISBN 9780198504009. doi:10.1093/acprof:oso/9780198504009.001.0001

[Ami05] L. Amico, A. Osterloh, F. Cataliotti. Quantum many particle systems in ring-shaped optical lattices. *Phys. Rev. Lett.*, **95**, 063201, 2005. doi:10.1103/PhysRevLett.95.063201

[Ami14] L. Amico, D. Aghamalyan, F. Auksztol, H. Crepaz, R. Dumke, L. C. Kwek. Superfluid qubit systems with ring shaped optical lattices. *Scientific Reports*, **4 (1)**, 4298, 2014. ISSN 2045-2322. doi:10.1038/srep04298

[And95] M. H. Anderson, J. R. Ensher, M. R. Matthews, C. E. Wieman, E. A. Cornell. Observation of Bose–Einstein condensation in a dilute atomic vapor. *Science*, **269 (5221)**, 198, 1995. doi:10.1126/science.269.5221.198

[And04] J. O. Andersen. Theory of the weakly interacting Bose gas. *Rev. Mod. Phys.*, **76**, 599, 2004. doi:10.1103/RevModPhys.76.599

[Bai00] Z. Bai, J. Demmel, J. Dongarra, A. Ruhe, H. van der Vorst. *Templates for the Solution of Algebraic Eigenvalue Problems*. Society for Industrial and Applied Mathematics, 2000. doi:10.1137/1.9780898719581

[Bai20] A. Baiardi, M. Reiher. The density matrix renormalization group in chemistry and molecular physics: Recent developments and new challenges. *The Journal of Chemical Physics*, **152 (4)**, 040903, 2020. doi:10.1063/1.5129672

[Bar90] R. J. Bartlett, J. Watts, S. Kucharski, J. Noga. Non-iterative fifth-order triple and quadruple excitation energy corrections in correlated methods. *Chemical Physics Letters*, **165 (6)**, 513, 1990. ISSN 0009-2614. doi:10.1016/0009-2614(90)87031-L

[Bar04] M. Bartenstein, A. Altmeyer, S. Riedl, S. Jochim, C. Chin, J. H. Denschlag, R. Grimm. Crossover from a molecular Bose–Einstein condensate to a degenerate Fermi gas. *Phys. Rev. Lett.*, **92**, 120401, 2004. doi:10.1103/PhysRevLett.92.120401

[Bar07] R. J. Bartlett, M. Musiał. Coupled-cluster theory in quantum chemistry. *Rev. Mod. Phys.*, **79**, 291, 2007. doi:10.1103/RevModPhys.79.291

[Bar11] G. Barcza, Ö. Legeza, K. H. Marti, M. Reiher. Quantum-information analysis of electronic states of different molecular structures. *Phys. Rev. A*, **83**, 012508, 2011. doi:10.1103/PhysRevA.83.012508

[Bar22] G. Barcza, M. A. Werner, G. Zaránd, A. Pershin, Z. Benedek, Ö. Legeza, T. Szilvási. Toward large-scale restricted active space calculations inspired by the schmidt decomposition. *The Journal of Physical Chemistry A*, **126 (51)**, 9709, 2022. doi:10.1021/acs.jpca.2c05952

[Bau11] B. Bauer, P. Corboz, R. Orús, M. Troyer. Implementing global abelian symmetries in projected entangled-pair state algorithms. *Phys. Rev. B*, **83**, 125106, 2011. doi:10.1103/PhysRevB.83.125106

[Bel58] S. T. Beliaev. Energy-spectrum of a non-ideal Bose gas. *Sov. Phys. JETP*, **34 (7)**, 299, 1958

[Bel16] T. A. Bell, J. A. P. Glidden, L. Humbert, M. W. J. Bromley, S. A. Haine, M. J. Davis, T. W. Neely, M. A. Baker, H. Rubinsztein-Dunlop. Corrigendum: Bose–einstein condensation in large time-averaged optical ring potentials (2016new j. phys.18035003). *New Journal of Physics*, **18 (8)**, 089501, 2016. doi:10.1088/1367-2630/18/8/089501

[Ben96a] C. H. Bennett, H. J. Bernstein, S. Popescu, B. Schumacher. Concentrating partial entanglement by local operations. *Phys. Rev. A*, **53**, 2046, 1996. doi:10.1103/PhysRevA.53.2046

[Ben96b] C. H. Bennett, D. P. DiVincenzo, J. A. Smolin, W. K. Wootters. Mixed-state entanglement and quantum error correction. *Phys. Rev. A*, **54**, 3824, 1996. doi:10.1103/PhysRevA.54.3824

[Ben06] I. Bengtsson, K. Życzkowski. *Geometry of Quantum States: An Introduction to Quantum Entanglement*. Cambridge University Press, 2006. ISBN 0521814510. doi:10.1017/CBO9780511535048

[Bir73] G. Birkhoff. *Lattice Theory*. American Mathematical Society, New York, 3rd edition, 1973. ISBN 9780821810255

[Blo08] I. Bloch, J. Dalibard, W. Zwerger. Many-body physics with ultracold gases. *Rev. Mod. Phys.*, **80**, 885, 2008. doi:10.1103/RevModPhys.80.885

[Bog47] N. N. Bogoliubov. On the theory of superfluidity. *J. Phys. USSR*, **11**, 23, 1947. doi:10.1016/B978-0-08-015816-7.50020-1

[Bog13] K. Boguslawski, P. Tecmer, G. Barcza, Ö. Legeza, M. Reiher. Orbital entanglement in bond-formation processes. *Journal of Chemical Theory and Computation*, **9 (7)**, 2959, 2013. doi:10.1021/ct400247p

[Boo09] G. H. Booth, A. J. W. Thom, A. Alavi. Fermion Monte Carlo without fixed nodes: A game of life, death, and annihilation in Slater determinant space. *The Journal of Chemical Physics*, **131 (5)**, 054106, 2009. ISSN 0021-9606. doi:10.1063/1.3193710

[Bou04] T. Bourdel, L. Khaykovich, J. Cubizolles, J. Zhang, F. Chevy, M. Teichmann, L. Tarruell, S. J. J. M. F. Kokkelmans, C. Salomon. Experimental study of the BEC-BCS crossover region in lithium 6. *Phys. Rev. Lett.*, **93**, 050401, 2004. doi:10.1103/PhysRevLett.93.050401

[Boy60] S. F. Boys. Construction of some molecular orbitals to be approximately invariant for changes from one molecule to another. *Rev. Mod. Phys.*, **32**, 296, 1960. doi:10.1103/RevModPhys.32.296

[Bra95] C. C. Bradley, C. A. Sackett, J. J. Tollett, R. G. Hulet. Evidence of Bose–Einstein condensation in an atomic gas with attractive interactions. *Phys. Rev. Lett.*, **75**, 1687, 1995. doi:10.1103/PhysRevLett.75.1687

[Bra20] J. Brandejs, J. Višňák, L. Veis, M. Máté, Ö. Legeza, J. Pittner. Toward DMRG-tailored coupled cluster method in the 4c-relativistic domain. *The Journal of Chemical Physics*, **152 (17)**, 174107, 2020. doi:10.1063/1.5144974

[Bre10] H. Brezis. *Functional Analysis, Sobolev Spaces and Partial Differential Equations*. Universitext. Springer New York, 2010. ISBN 9780387709130

[Bru57a] K. A. Brueckner, K. Sawada. Bose–Einstein gas with repulsive interactions: General theory. *Phys. Rev.*, **106**, 1117, 1957. doi:10.1103/PhysRev.106.1117

[Bru57b] K. A. Brueckner, K. Sawada. Bose–Einstein gas with repulsive interactions: Hard spheres at high density. *Phys. Rev.*, **106**, 1128, 1957. doi:10.1103/PhysRev.106.1128

[Bru04] I. Brunelli, G. Giusiano, F. Mancini, P. Sodano, A. Trombettoni. Topology-induced spatial Bose–Einstein condensation for bosons on star-shaped optical networks. *Journal of Physics B: Atomic, Molecular and Optical Physics*, **37 (7)**, S275, 2004. doi:10.1088/0953-4075/37/7/072

[Bul08] R. Bulla, T. A. Costi, T. Pruschke. Numerical renormalization group method for quantum impurity systems. *Rev. Mod. Phys.*, **80**, 395, 2008. doi:10.1103/RevModPhys.80.395

[Buo02] P. Buonsante, R. Burioni, D. Cassi, A. Vezzani. Bose-Einstein condensation on inhomogeneous networks: Mesoscopic aspects versus thermodynamic limit. *Phys. Rev. B*, **66**, 094207, 2002. doi:10.1103/PhysRevB.66.094207

[Buo04] P. Buonsante, R. Burioni, D. Cassi, V. Penna, A. Vezzani. Topology-induced confined superfluidity in inhomogeneous arrays. *Phys. Rev. B*, **70**, 224510, 2004. doi:10.1103/PhysRevB.70.224510

[Bur27] Ø. Burrau. Berechnung des energiewertes des wasserstoffmolekel-ions (h2+) im normalzustand. *Naturwissenschaften*, **15 (1)**, 16, 1927. ISSN 1432-1904. doi:10.1007/BF01504875

[Bur00] R. Burioni, D. Cassi, I. Meccoli, M. Rasetti, S. Regina, P. Sodano, A. Vezzani. Bose-Einstein condensation in inhomogeneous Josephson arrays. *Europhysics Letters*, **52 (3)**, 251, 2000. doi:10.1209/epl/i2000-00431-5

[Bur01] R. Burioni, D. Cassi, M. Rasetti, P. Sodano, A. Vezzani. Bose-Einstein condensation on inhomogeneous complex networks. *Journal of Physics B: Atomic, Molecular and Optical Physics*, **34 (23)**, 4697, 2001. doi:10.1088/0953-4075/34/23/314

[Caz11] M. A. Cazalilla, R. Citro, T. Giamarchi, E. Orignac, M. Rigol. One dimensional bosons: From condensed matter systems to ultracold gases. *Rev. Mod. Phys.*, **83**, 1405, 2011. doi:10.1103/RevModPhys.83.1405

[Cha02] G. K.-L. Chan, M. Head-Gordon. Highly correlated calculations with a polynomial cost algorithm: A study of the density matrix renormalization group. *The Journal of Chemical Physics*, **116 (11)**, 4462, 2002. doi:10.1063/1.1449459

[Cha04] G. K.-L. Chan, M. Kállay, J. Gauss. State-of-the-art density matrix renormalization group and coupled cluster theory studies of the nitrogen binding curve. *The Journal of Chemical Physics*, **121 (13)**, 6110, 2004. doi:10.1063/1.1783212

[Cha08] G. K.-L. Chan, J. J. Dorando, D. Ghosh, J. Hachmann, E. Neuscamman, H. Wang, T. Yanai. An introduction to the density matrix renormalization group ansatz in quantum chemistry. In S. Wilson, P. J. Grout, J. Maruani, G. Delgado-Barrio, P. Piecuch, editors, *Frontiers in Quantum Systems in Chemistry and Physics*, volume 18 of *Progress in Theoretical Chemistry and Physics*. Springer, Netherlands, 2008. doi:10.1007/978-1-4020-8707-3

[Cha16] G. K.-L. Chan, A. Keselman, N. Nakatani, Z. Li, S. R. White. Matrix product operators, matrix product states, and ab initio density matrix renormalization group algorithms. *The Journal of Chemical Physics*, **145 (1)**, 014102, 2016. doi:10.1063/1.4955108

[Che22] Y. Cheng, Z. Xie, H. Ma. Post-density matrix renormalization group methods for describing dynamic electron correlation with large active spaces. *The Journal of Physical Chemistry Letters*, **13 (3)**, 904, 2022. doi:10.1021/acs.jpclett.1c04078

[Chi10] C. Chin, R. Grimm, P. Julienne, E. Tiesinga. Feshbach resonances in ultracold gases. *Rev. Mod. Phys.*, **82**, 1225, 2010. doi:10.1103/RevModPhys.82.1225

[Cir21] J. I. Cirac, D. Pérez-García, N. Schuch, F. Verstraete. Matrix product states and projected entangled pair states: Concepts, symmetries, theorems. *Rev. Mod. Phys.*, **93**, 045003, 2021. doi:10.1103/RevModPhys.93.045003

[Číž66] J. Čížek. On the correlation problem in atomic and molecular systems. calculation of wavefunction components in Ursell-type expansion using quantum-field theoretical methods. *The Journal of Chemical Physics*, **45 (11)**, 4256, 1966. ISSN 0021-9606. doi:10.1063/1.1727484

[Číž69] J. Čížek. *On the Use of the Cluster Expansion and the Technique of Diagrams in Calculations of Correlation Effects in Atoms and Molecules*, pages 35–89. John Wiley & Sons, Ltd, 1969. ISBN 9780470143599. doi:10.1002/9780470143599.ch2

[Cul02] J. K. Cullum, R. A. Willoughby. *Lanczos Algorithms for Large Symmetric Eigenvalue Computations*. Society for Industrial and Applied Mathematics, 2002. doi:10.1137/1.9780898719192

[Dal99] F. Dalfovo, S. Giorgini, L. P. Pitaevskii, S. Stringari. Theory of Bose-Einstein condensation in trapped gases. *Rev. Mod. Phys.*, **71**, 463, 1999. doi:10.1103/RevModPhys.71.463

[Das02] K. K. Das, M. D. Girardeau, E. M. Wright. Crossover from one to three dimensions for a gas of hard-core bosons. *Phys. Rev. Lett.*, **89**, 110402, 2002. doi:10.1103/PhysRevLett.89.110402

[Dav75] E. R. Davidson. The iterative calculation of a few of the lowest eigenvalues and corresponding eigenvectors of large real-symmetric matrices. *Journal of Computational Physics*, **17 (1)**, 87, 1975. doi:10.1016/0021-9991(75)90065-0

[Dav95] K. B. Davis, M. O. Mewes, M. R. Andrews, N. J. van Druten, D. S. Durfee, D. M. Kurn, W. Ketterle. Bose–Einstein condensation in a gas of sodium atoms. *Phys. Rev. Lett.*, **75**, 3969, 1995. doi:10.1103/PhysRevLett.75.3969

[Dav02] B. A. Davey, H. A. Priestley. *Introduction to Lattices and Order*. Cambridge University Press, second edition, 2002. ISBN 9780521784511. doi:10.1017/CBO9780511809088

[DeP99] M. T. DePue, C. McCormick, S. L. Winoto, S. Oliver, W. D. S. Unity Occupation of Sites in a 3D Optical Lattice. *Phys. Rev. Lett.*, **82**, 2262, 1999

[Det01] S. Dettmer, D. Hellweg, P. Ryytty, J. J. Arlt, W. Ertmer, K. Sengstock, D. S. Petrov, G. V. Shlyapnikov, H. Kreutzmann, L. Santos, M. Lewenstein. Observation of phase fluctuations in elongated Bose–Einstein condensates. *Phys. Rev. Lett.*, **87**, 160406, 2001. doi:10.1103/PhysRevLett.87.160406

[DSS09] J. A. S. David S. Sholl. *Density Functional Theory: A Practical Introduction*. Wiley, 2009. ISBN 9780470373170. doi:10.1002/9780470447710

[Dun89] T. H. Dunning. Gaussian basis sets for use in correlated molecular calculations. i. the atoms boron through neon and hydrogen. *The Journal of Chemical Physics*, **90 (2)**, 1007, 1989. doi:10.1063/1.456153

[Dür99] W. Dür, J. I. Cirac, R. Tarrach. Separability and distillability of multiparticle quantum systems. *Phys. Rev. Lett.*, **83**, 3562, 1999. doi:10.1103/PhysRevLett.83.3562

[Dür00] W. Dür, J. I. Cirac. Classification of multiqubit mixed states: Separability and distillability properties. *Phys. Rev. A*, **61**, 042314, 2000. doi:10.1103/PhysRevA.61.042314

[Eva10] L. C. Evans. *Partial differential equations*, volume 19. American Mathematical Society, 2010. ISBN 978-0821849743

[Eve09] G. Evenbly, G. Vidal. Algorithms for entanglement renormalization. *Phys. Rev. B*, **79**, 144108, 2009. doi:10.1103/PhysRevB.79.144108

[FA07] S. Franke-Arnold, J. Leach, M. J. Padgett, V. E. Lembessis, D. Ellinas, A. J. Wright, J. M. Girkin, P. Öhberg, A. S. Arnold. Optical ferris wheel for ultracold atoms. *Opt. Express*, **15 (14)**, 8619, 2007. doi:10.1364/OE.15.008619

[Fau19a] F. M. Faulstich, A. Laestadius, O. Legeza, R. Schneider, S. Kvaal. Analysis of the tailored coupled-cluster method in quantum chemistry. *SIAM Journal on Numerical Analysis*, **57 (6)**, 2579, 2019. doi:10.1137/18M1171436

[Fau19b] F. M. Faulstich, M. Máté, A. Laestadius, M. A. Csirik, L. Veis, A. Antalík, J. Brabec, R. Schneider, J. Pittner, S. Kvaal, Ö. Legeza. Numerical and theoretical aspects of the DMRG-TCC method exemplified by the nitrogen dimer. *Journal of Chemical Theory and Computation*, **15 (4)**, 2206, 2019. doi:10.1021/acs.jctc.8b00960

[Fer14] E. Fertitta, B. Paulus, G. Barcza, O. Legeza. Investigation of metal–insulator-like transition through the ab initio density matrix renormalization group approach. *Phys. Rev. B*, **90**, 245129, 2014. doi:10.1103/PhysRevB.90.245129

[Fis89] M. P. A. Fisher, P. B. Weichman, G. Grinstein, D. S. Fisher. Boson localization and the superfluid-insulator transition. *Phys. Rev. B*, **40**, 546, 1989. doi:10.1103/PhysRevB.40.546

[For03] P. J. Forrester, N. E. Frankel, T. M. Garoni, N. S. Witte. Finite one-dimensional impenetrable bose systems: Occupation numbers. *Phys. Rev A*, **67**, 043607, 2003. doi:10.1103/PhysRevA.67.043607

[Fos60] J. M. Foster, S. F. Boys. Canonical configurational interaction procedure. *Rev. Mod. Phys.*, **32**, 300, 1960. doi:10.1103/RevModPhys.32.300

[Fri22a] G. Friesecke, B. R. Graswald. Two-electron wavefunctions are matrix product states with bond dimension three. *Journal of Mathematical Physics*, **63 (9)**, 2022. ISSN 0022-2488. doi:10.1063/5.0072261

[Fri22b] G. Friesecke, B. R. Graswald, O. Legeza. Exact matrix product state representation and convergence of a fully correlated electronic wavefunction in the infinite-basis limit. *Phys. Rev. B*, **105**, 165144, 2022. doi:10.1103/PhysRevB.105.165144

[Fri23] G. Friesecke, G. Barcza, Örs Legeza. Predicting the fci energy of large systems to chemical accuracy from restricted active space density matrix renormalization group calculations. *arXiv*, [**physics.chem-ph**], 2209.14190, 2023. doi:10.48550/arXiv.2209.14190

[GÖ1] A. Görlitz, J. M. Vogels, A. E. Leanhardt, C. Raman, T. L. Gustavson, J. R. Abo-Shaeer, A. P. Chikkatur, S. Gupta, S. Inouye, T. Rosenband, W. Ketterle. Realization of Bose–Einstein condensates in lower dimensions. *Phys. Rev. Lett.*, **87**, 130402, 2001. doi:10.1103/PhysRevLett.87.130402

[Gan04] D. M. Gangardt. Universal correlations of trapped one-dimensional impenetrable bosons. *Journal of Physics A: Mathematical and General*, **37 (40)**, 9335, 2004. doi:10.1088/0305-4470/37/40/002

[Gir60] M. Girardeau. Relationship between systems of impenetrable bosons and fermions in one dimension. *Journal of Mathematical Physics*, **1 (6)**, 516, 1960. doi:10.1063/1.1703687

[Gir01] M. D. Girardeau, E. M. Wright. Bose–Fermi variational theory of the Bose–Einstein condensate crossover to the Tonks gas. *Phys. Rev. Lett.*, **87**, 210401, 2001. doi:10.1103/PhysRevLett.87.210401

[Gis89] N. Gisin. Stochastic quantum dynamics and relativity. *Helvetica Physica Acta*, **62**, 363, 1989. doi:10.5169/seals-116034

[Gol13] G. H. Golub, C. F. Van Loan. *Matrix computations*. Johns Hopkins Studies in the Mathematical Sciences. Johns Hopkins University Press, Baltimore, MD, fourth edition, 2013. ISBN 978-1-4214-0794-4. doi:10.56021/9781421407944

[Gre01] M. Greiner, I. Bloch, O. Mandel, T. W. Hänsch, T. Esslinger. Exploring phase coherence in a 2d lattice of Bose–Einstein condensates. *Phys. Rev. Lett.*, **87**, 160405, 2001. doi:10.1103/PhysRevLett.87.160405

[Gre03] M. Greiner, C. A. Regal, D. S. Jin. Emergence of a molecular bose–einstein condensate from a fermi gas. *Nature*, **426 (6966)**, 537, 2003. doi:10.1038/nature02199

[Gri95] A. Griffin, D. W. Snoke, S. Stringari. *Bose–Einstein Condensation*. Cambridge University Press, Cambridge, 1995. doi:10.1017/CBO9780511524240

[Gro61] E. P. Gross. Structure of a quantized vortex in boson systems. *Il Nuovo Cimento (1955-1965)*, **20 (3)**, 454, 1961. ISSN 1827-6121. doi:10.1007/BF02731494

[Gro63] E. P. Gross. Hydrodynamics of a superfluid condensate. *Journal of Mathematical Physics*, **4 (2)**, 195, 1963. doi:10.1063/1.1703944

[Gun18] K. Gunst, F. Verstraete, S. Wouters, Ö. Legeza, D. Van Neck. T3NS: Three-legged tree tensor network states. *Journal of Chemical Theory and Computation*, **14 (4)**, 2026, 2018. ISSN 1549-9618. doi:10.1021/acs.jctc.8b00098

[Gü13] G. Günter, H. Schempp, M. R. de Saint-Vincent, V. Gavryusev, S. Helmrich, C. S. Hofmann, S. Whitlock, M. Weidemüller. Observing the dynamics of dipole-mediated energy transport by interaction-enhanced imaging. *Science*, **342 (6161)**, 954, 2013. doi:10.1126/science.1244843

[Hac12] W. Hackbusch. *Tensor Spaces and Numerical Tensor Calculus*. Springer Cham, 2 edition, 2012. ISBN 978-3-030-35553-1. doi:10.1007/978-3-030-35554-8

[Hae14] J. Haegeman, M. Mariën, T. J. Osborne, F. Verstraete. Geometry of matrix product states: Metric, parallel transport, and curvature. *Journal of Mathematical Physics*, **55 (2)**, 021902, 2014. doi:10.1063/1.4862851

[Hal12] A. Halu, L. Ferretti, A. Vezzani, G. Bianconi. Phase diagram of the Bose–Hubbard model on complex networks. *Europhysics Letters*, **99 (1)**, 18001, 2012. doi:10.1209/0295-5075/99/18001

[Hei27] W. Heitler, F. London. Wechselwirkung neutraler atome und homöopolare bindung nach der quantenmechanik. *Zeitschrift für Physik*, **44 (6)**, 455, 1927. ISSN 0044-3328. doi:10.1007/BF01397394

[Hel00] T. Helgaker, P. Jørgensen, J. Olsen. *Molecular Electronic-Structure Theory*. John Wiley & Sons, Ltd, 2000. ISBN 9781119019572. doi:10.1002/9781119019572

[Her04] F. Herbut. On mutual information in multipartite quantum states and equality in strong subadditivity of entropy. *Journal of Physics A: Mathematical and General*, **37 (10)**, 3535, 2004. doi:10.1088/0305-4470/37/10/016

[Hia91] F. Hiai, D. Petz. The proper formula for relative entropy and its asymptotics in quantum probability. *Commun. Math. Phys.*, **143 (1)**, 99, 1991. ISSN 0010-3616. doi:10.1007/BF02100287

[Hil13] C. J. Hillar, L.-H. Lim. Most tensor problems are NP-hard. *J. ACM*, **60 (6)**, 2013. ISSN 0004-5411. doi:10.1145/2512329

[Hol12a] S. Holtz, T. Rohwedder, R. Schneider. The alternating linear scheme for tensor optimization in the tensor train format. *SIAM Journal on Scientific Computing*, **34 (2)**, A683, 2012. doi:10.1137/100818893

[Hol12b] S. Holtz, T. Rohwedder, R. Schneider. On manifolds of tensors of fixed tt-rank. *Numerische Mathematik*, **120 (4)**, 701, 2012

[Hor01] M. Horodecki. Entanglement measures. *Quant. Inf. Comp.*, **1 (1)**, 3, 2001. doi:10.26421/QIC1.1-2

[Hor09] R. Horodecki, P. Horodecki, M. Horodecki, K. Horodecki. Quantum entanglement. *Rev. Mod. Phys.*, **81**, 865, 2009. doi:10.1103/RevModPhys.81.865

[Hub57] J. Hubbard. The description of collective motions in terms of many-body perturbation theory. *Proceedings of the Royal Society of London. Series A, Mathematical and Physical Sciences*, **240 (1223)**, 539, 1957. ISSN 00804630

[Hug57] N. Hugenholtz. Perturbation approach to the Fermi gas model of heavy nuclei. *Physica*, **23 (1)**, 533, 1957. ISSN 0031-8914. doi:10.1016/S0031-8914(57)93009-4

[Hug59] N. M. Hugenholtz, D. Pines. Ground-state energy and excitation spectrum of a system of interacting bosons. *Phys. Rev.*, **116**, 489, 1959. doi:10.1103/PhysRev.116.489

[Hug93] L. P. Hughston, R. Jozsa, W. K. Wootters. A complete classification of quantum ensembles having a given density matrix. *Physics Letters A*, **183 (1)**, 14, 1993. ISSN 0375-9601. doi:10.1016/0375-9601(93)90880-9

[Hun66] W. Hunziker. On the spectra of Schrödinger multiparticle Hamiltonians. *Helvetica Physica Acta*, **39**, 1966. doi:10.5169/seals-113698

[Jak98] D. Jaksch, C. Bruder, J. I. Cirac, C. W. Gardiner, P. Zoller. Cold bosonic atoms in optical lattices. *Phys. Rev. Lett.*, **81**, 3108, 1998. doi:10.1103/PhysRevLett.81.3108

[Jor28] P. Jordan, E. Wigner. Über das paulische Äquivalenzverbot. *Zeitschrift für Physik*, **47 (9)**, 631, 1928. ISSN 0044-3328. doi:10.1007/BF01331938

[Kat51] T. Kato. Fundamental properties of hamiltonian operators of schrodinger type. *Transactions of the American Mathematical Society*, **70 (2)**, 195, 1951. ISSN 00029947

[Kel16] S. Keller, M. Reiher. Spin-adapted matrix product states and operators. *The Journal of Chemical Physics*, **144 (13)**, 134101, 2016. ISSN 0021-9606. doi:10.1063/1.4944921

[Khi57] A. I. Khinchin. *Mathematical Foundations of Information Theory*. Dover Publications, 1957. ISBN 978-0486604343

[Kin04] T. Kinoshita, T. Wenger, D. S. Weiss. Observation of a one-dimensional Tonks-Girardeau gas. *Science*, **305 (5687)**, 1125, 2004. doi:10.1126/science.1100700

[Kin05] T. Kinoshita, O. Hino, R. J. Bartlett. Coupled-cluster method tailored by configuration interaction. *The Journal of Chemical Physics*, **123 (7)**, 074106, 2005. doi:10.1063/1.2000251

[Kir00] M. W. Kirson. Bose-Einstein condensation in an exactly solvable model for strongly interacting bosons. *J. Phys. A: Math. Gen.*, **33**, 731, 2000

[Kow00] K. Kowalski, P. Piecuch. Renormalized ccsd(t) and ccsd(tq) approaches: Dissociation of the n2 triple bond. *The Journal of Chemical Physics*, **113 (14)**, 5644, 2000. doi:10.1063/1.1290609

[Kru16] C. Krumnow, L. Veis, Ö. Legeza, J. Eisert. Fermionic orbital optimization in tensor network states. *Phys. Rev. Lett.*, **117**, 210402, 2016. doi:10.1103/PhysRevLett.117.210402

[Kru18] C. D. Krumnow. *Detecting and Understanding Efficient Structures in Finite Fermionic Systems*. Ph.D. thesis, Freie Universität Berlin, 2018

[Kru21] C. Krumnow, L. Veis, J. Eisert, Ö. Legeza. Effective dimension reduction with mode transformations: Simulating two-dimensional fermionic condensed matter systems with matrix-product states. *Phys. Rev. B*, **104**, 075137, 2021. doi:10.1103/PhysRevB.104.075137

[Kur09] Y. Kurashige, T. Yanai. High-performance ab initio density matrix renormalization group method: Applicability to large-scale multireference problems for metal compounds. *The Journal of Chemical Physics*, **130 (23)**, 234114, 2009. ISSN 0021-9606. doi:10.1063/1.3152576

[Lae19] A. Laestadius, F. M. Faulstich. The coupled-cluster formalism – a mathematical perspective. *Molecular Physics*, **117 (17)**, 2362, 2019. doi:10.1080/00268976.2018.1564848

[Lan50] C. Lanczos. An iteration method for the solution of the eigenvalue problem of linear differential and integral operators. **45 (4)**, 255, 1950

[Lee57a] T. D. Lee, K. Huang, C. N. Yang. Eigenvalues and eigenfunctions of a Bose system of hard spheres and its low-temperature properties. *Phys. Rev.*, **106**, 1135, 1957. doi:10.1103/PhysRev.106.1135

[Lee57b] T. D. Lee, C. N. Yang. Many-body problem in quantum mechanics and quantum statistical mechanics. *Phys. Rev.*, **105**, 1119, 1957. doi:10.1103/PhysRev.105.1119

[Lee89a] T. J. Lee, J. E. Rice, G. E. Scuseria, H. F. Schaefer. Theoretical investigations of molecules composed only of fluorine, oxygen and nitrogen: determination of the equilibrium structures of foof, (no)2 and fnnf and the transition state structure for fnnf cis-trans isomerization. *Theoretica chimica acta*, **75 (2)**, 81, 1989

[Lee89b] T. J. Lee, P. R. Taylor. A diagnostic for determining the quality of single-reference electron correlation methods. *International Journal of Quantum Chemistry*, **36 (S23)**, 199, 1989. doi:10.1002/qua.560360824

[Leg96] O. Legeza, G. Fáth. Accuracy of the density-matrix renormalization-group method. *Phys. Rev. B*, **53**, 14349, 1996. doi:10.1103/PhysRevB.53.14349

[Leg97] O. Legeza, J. Sólyom. Stability of the haldane phase in anisotropic magnetic ladders. *Phys. Rev. B*, **56**, 14449, 1997. doi:10.1103/PhysRevB.56.14449

[Leg03a] Ö. Legeza, J. Röder, B. A. Hess. Controlling the accuracy of the density-matrix renormalization-group method: The dynamical block state selection approach. *Phys. Rev. B*, **67**, 125114, 2003. doi:10.1103/PhysRevB.67.125114

[Leg03b] Ö. Legeza, J. Sólyom. Optimizing the density-matrix renormalization group method using quantum information entropy. *Phys. Rev. B*, **68**, 195116, 2003. doi:10.1103/PhysRevB.68.195116

[Leg06] A. J. Leggett. *Quantum Liquids: Bose condensation and Cooper pairing in condensed-matter systems*. Oxford University Press, 2006. ISBN 9780198526438. doi:10.1093/acprof:oso/9780198526438.001.0001

[Leg08] Ö. Legeza, R. Noack, J. Sólyom, L. Tincani. Applications of quantum information in the density-matrix renormalization group. In H. Fehske, R. Schneider, A. Weiße, editors, *Computational Many-Particle Physics*, volume 739 of *Lecture Notes in Physics*, pages 653–664. Springer, Berlin, Heidelberg, 2008. ISBN 978-3-540-74685-0. doi:10.1007/978-3-540-74686-7_24

[Leg14] Ö. Legeza, T. Rohwedder, R. Schneider, Sz. Szalay. *Tensor Product Approximation (DMRG) and Coupled Cluster Method in Quantum Chemistry*, pages 53–76. Springer International Publishing, Cham, 2014. ISBN 978-3-319-06379-9. doi:10.1007/978-3-319-06379-9_3

[Leh19] S. Lehtola. A review on non-relativistic, fully numerical electronic structure calculations on atoms and diatomic molecules. *International Journal of Quantum Chemistry*, **119 (19)**, e25968, 2019. doi:10.1002/qua.25968

[Len64] A. Lenard. Momentum distribution in the ground state of the one-dimensional systems of impenetrable bosons. *J. Math. Phys.*, **5**, 930, 1964

[Lev68] B. Levy, G. Berthier. Generalized Brillouin theorem for multiconfigurational SCF theories. *International Journal of Quantum Chemistry*, **2 (2)**, 307, 1968. doi:10.1002/qua.560020210

[Lew16] G. N. Lewis. The atom and the molecule. *Journal of the American Chemical Society*, **38 (4)**, 762, 1916. ISSN 0002-7863. doi:10.1021/ja02261a002

[Li13] C.-K. Li, R. Roberts, X. Yin. Decomposition of unitary matrices and quantum gates. *International Journal of Quantum Information*, **11 (01)**, 1350015, 2013. doi:10.1142/S0219749913500159

[Lie63a] E. H. Lieb. Exact analysis of an interacting Bose gas. ii. the excitation spectrum. *Phys. Rev.*, **130**, 1616, 1963. doi:10.1103/PhysRev.130.1616

[Lie63b] E. H. Lieb. Simplified approach to the ground-state energy of an imperfect Bose gas. *Phys. Rev.*, **130**, 2518, 1963. doi:10.1103/PhysRev.130.2518

[Lie63c] E. H. Lieb, W. Liniger. Exact analysis of an interacting Bose gas. i. the general solution and the ground state. *Phys. Rev.*, **130**, 1605, 1963. doi:10.1103/PhysRev.130.1605

[Lod20] A. U. J. Lode, C. Lévêque, L. B. Madsen, A. I. Streltsov, O. E. Alon. Colloquium: Multiconfigurational time-dependent hartree approaches for indistinguishable particles. *Rev. Mod. Phys.*, **92**, 011001, 2020. doi:10.1103/RevModPhys.92.011001

[Lya12] D. I. Lyakh, M. Musiał, V. F. Lotrich, R. J. Bartlett. Multireference nature of chemistry: The coupled-cluster view. *Chemical Reviews*, **112 (1)**, 182, 2012. ISSN 0009-2665. doi:10.1021/cr2001417

[Lyr14] M. L. Lyra, F. A. B. F. de Moura, I. N. de Oliveira, M. Serva. Bose-einstein condensation in diamond hierarchical lattices. *Phys. Rev. E*, **89**, 052133, 2014. doi:10.1103/PhysRevE.89.052133

[Mar10] K. H. Marti, M. Reiher. The density matrix renormalization group algorithm in quantum chemistry. *Zeitschrift für Physikalische Chemie*, **224**, 583, 2010. ISSN 0942-9352. doi:10.1524/zpch.2010.6125

[Mat56] T. Matsubara, H. Matsuda. A lattice model of liquid helium, I. *Progress of Theoretical Physics*, **16 (6)**, 569, 1956. ISSN 0033-068X. doi:10.1143/PTP.16.569

[Mat57] H. Matsuda, T. Matsubara. A lattice model of liquid helium, II. *Progress of Theoretical Physics*, **17 (1)**, 19, 1957. ISSN 0033-068X. doi:10.1143/PTP.17.19

[Mát21] M. Máté, Ö. Legeza, R. Schilling, M. Yousif, C. Schilling. How creating one additional well can generate Bose–Einstein condensation. *Communications Physics*, **4 (1)**, 29, 2021. doi:10.1038/s42005-021-00533-3

[Mát23] M. Máté, K. Petrov, Sz. Szalay, Ö. Legeza. Compressing multireference character of wave functions via fermionic mode optimization. *Journal of Mathematical Chemistry*, **61 (2)**, 362, 2023. ISSN 1572-8897. doi:10.1007/s10910-022-01379-y

[McC02] I. P. McCulloch, M. Gulácsi. The non-abelian density matrix renormalization group algorithm. *Europhysics Letters*, **57 (6)**, 852, 2002. doi:10.1209/epl/i2002-00393-0

[McC07] I. P. McCulloch. From density-matrix renormalization group to matrix product states. *Journal of Statistical Mechanics: Theory and Experiment*, **2007 (10)**, P10014, 2007. doi:10.1088/1742-5468/2007/10/P10014

[Men23] A. Menczer, Ö. Legeza. Massively parallel tensor network state algorithms on hybrid CPU-GPU based architectures. *arXiv [quant-ph]*, 2305.05581, 2023

[Mod10] K. Modi, T. Paterek, W. Son, V. Vedral, M. Williamson. Unified view of quantum and classical correlations. *Phys. Rev. Lett.*, **104**, 080501, 2010. doi:10.1103/PhysRevLett.104.080501

[Mor05] G. Moritz, B. A. Hess, M. Reiher. Convergence behavior of the density-matrix renormalization group algorithm for optimized orbital orderings. *The Journal of Chemical Physics*, **122 (2)**, 024107, 2005. doi:10.1063/1.1824891

[Mor06] G. Moritz, M. Reiher. Construction of environment states in quantum-chemical density-matrix renormalization group calculations. *The Journal of Chemical Physics*, **124 (3)**, 034103, 2006. doi:10.1063/1.2139998

[Mur07] V. Murg, F. Verstraete, J. I. Cirac. Variational study of hard-core bosons in a two-dimensional optical lattice using projected entangled pair states. *Phys. Rev. A*, **75**, 033605, 2007. doi:10.1103/PhysRevA.75.033605

[Mur10] V. Murg, F. Verstraete, Ö. Legeza, R. M. Noack. Simulating strongly correlated quantum systems with tree tensor networks. *Phys. Rev. B*, **82**, 205105, 2010. doi:10.1103/PhysRevB.82.205105

[Mur15] V. Murg, F. Verstraete, R. Schneider, P. R. Nagy, Ö. Legeza. Tree tensor network state with variable tensor order: An efficient multireference method for strongly correlated systems. *Journal of Chemical Theory and Computation*, **11 (3)**, 1027, 2015. ISSN 1549-9618. doi:10.1021/ct501187j

[Nak13] N. Nakatani, G. K.-L. Chan. Efficient tree tensor network states (TTNS) for quantum chemistry: Generalizations of the density matrix renormalization group algorithm. *The Journal of Chemical Physics*, **138 (13)**, 134113, 2013. ISSN 0021-9606. doi:10.1063/1.4798639

[Nee22] F. Neese. Software update: The orca program system—version 5.0. *WIREs Computational Molecular Science*, **12 (5)**, e1606, 2022. doi:10.1002/wcms.1606

[Neu27] J. von Neumann. Thermodynamik quantenmechanischer gesamtheiten. *Nachrichten von der Gesellschaft der Wissenschaften zu Göttingen, Mathematisch-Physikalische Klasse*, **1927**, 273, 1927

[Neu30] J. von Neumann. Allgemeine eigenwerttheorie hermitescher funktionaloperatoren. *Mathematische Annalen*, **102 (1)**, 49, 1930. ISSN 1432-1807. doi:10.1007/BF01782338

[Neu32] J. von Neumann. *Mathematische Grundlagen der Quantenmechanik*. Springer, 1932

[Nie00] M. A. Nielsen, I. L. Chuang. *Quantum Computation and Quantum Information*. Cambridge University Press, 1 edition, 2000. ISBN 0521635039. doi:10.1017/CBO9780511976667

[Nis01] T. Nishino, Y. Hieida, K. Okunishi, N. Maeshima, Y. Akutsu, A. Gendiar. Two-dimensional tensor product variational formulation. *Progress of Theoretical Physics*, **105 (3)**, 409, 2001. ISSN 0033-068X. doi:10.1143/PTP.105.409

[Noa05] R. M. Noack, S. R. Manmana. Diagonalization- and numerical renormalization-group-based methods for interacting quantum systems. *AIP Conference Proceedings*, **789 (1)**, 93, 2005. ISSN 0094-243X. doi:10.1063/1.2080349

[Ö95] S. Östlund, S. Rommer. Thermodynamic limit of density matrix renormalization. *Phys. Rev. Lett.*, **75**, 3537, 1995. doi:10.1103/PhysRevLett.75.3537

[OA15] R. Olivares-Amaya, W. Hu, N. Nakatani, S. Sharma, J. Yang, G. K.-L. Chan. The ab-initio density matrix renormalization group in practice. *The Journal of Chemical Physics*, **142 (3)**, 034102, 2015. doi:10.1063/1.4905329

[Ohy93] M. Ohya, D. Petz. *Quantum Entropy and Its Use*. Springer Verlag, 1 edition, 1993. ISBN 978-3-540-20806-8

[Oli13] I. N. de Oliveira, T. B. dos Santos, F. A. B. F. de Moura, M. L. Lyra, M. Serva. Critical behavior of the ideal-gas Bose–Einstein condensation in the Apollonian network. *Phys. Rev. E*, **88**, 022139, 2013. doi:10.1103/PhysRevE.88.022139

[Orz01] C. Orzel, A. K. Tuchman, M. L. Fenselau, M. Yasuda, M. A. Kasevich. Squeezed states in a Bose–Einstein condensate. *Science*, **291 (5512)**, 2386, 2001. doi:10.1126/science.1058149

[Osb02] T. J. Osborne, M. A. Nielsen. Entanglement in a simple quantum phase transition. *Phys. Rev. A*, **66**, 032110, 2002. doi:10.1103/PhysRevA.66.032110

[Ost02] A. Osterloh, L. Amico, G. Falci, R. Fazio. Scaling of entanglement close to a quantum phase transition. *Nature*, **416 (6881)**, 608, 2002. doi:10.1038/416608a

[Pal72] J. Paldus, J. Čížek, I. Shavitt. Correlation problems in atomic and molecular systems. iv. extended coupled-pair many-electron theory and its application to the bh_3 molecule. *Phys. Rev. A*, **5**, 50, 1972. doi:10.1103/PhysRevA.5.50

[Par04a] B. Paredes, A. Widera, V. Murg, O. Mandel, S. Fölling, I. Cirac, G. V. Shlyapnikov, T. W. Hänsch, I. Bloch. Tonks–girardeau gas of ultracold atoms in an optical lattice. *Nature*, **429 (6989)**, 277, 2004. ISSN 1476-4687. doi:10.1038/nature02530

[Par04b] B. Paredes, A. Widera, V. Murg, O. Mandel, S. Fölling, I. Cirac, G. V. Shlyapnikov, T. W. Hänsch, I. Bloch. Tonks-Girardeau gas of ultracold atoms in an optical lattice. *Nature*, **429**, 277, 2004. doi:10.1038/nature02530

[Pen91] O. Penrose. Bose-Einstein condensation in an exactly soluble system of interacting particles. *J. Stat. Phys.*, **63 (3)**, 761, 1991. ISSN 1572-9613. doi:10.1007/BF01029210

[Pet00] D. S. Petrov, G. V. Shlyapnikov, J. T. M. Walraven. Regimes of Quantum Degeneracy in Trapped 1D Gases. *Phys. Rev. Lett.*, **85**, 3745, 2000. doi:10.1103/PhysRevLett.85.3745

[Pet02] C. Pethick, H. Smith. *Bose-Einstein Condensation in Dilute Gases*. Cambridge University Press, 2 edition, 2002. doi:10.1017/CBO9780511802850

[Pet08] D. Petz. *Quantum Information Theory and Quantum Statistics*. Springer, 1 edition, 2008. ISBN 978-3-540-74634-8. doi:10.1007/978-3-540-74636-2

[Pie93] P. Piecuch, N. Oliphant, L. Adamowicz. A state-selective multireference coupled-cluster theory employing the single-reference formalism. *The Journal of Chemical Physics*, **99 (3)**, 1875, 1993. ISSN 0021-9606. doi:10.1063/1.466179

[Pie94] P. Piecuch, L. Adamowicz. State-selective multireference coupled-cluster theory employing the single-reference formalism: Implementation and appl ication to the H8 model system. *The Journal of Chemical Physics*, **100 (8)**, 5792, 1994. ISSN 0021-9606. doi:10.1063/1.467143

[Pip89] J. Pipek, P. G. Mezey. A fast intrinsic localization procedure applicable for ab initio and semiempirical linear combination of atomic orbital wave functions. *The Journal of Chemical Physics*, **90 (9)**, 4916, 1989. doi:10.1063/1.456588

[Pip10] P. Pippan, S. R. White, H. G. Evertz. Efficient matrix-product state method for periodic boundary conditions. *Phys. Rev. B*, **81**, 081103, 2010. doi:10.1103/PhysRevB.81.081103

[Pir11] B. Pirvu, F. Verstraete, G. Vidal. Exploiting translational invariance in matrix product state simulations of spin chains with periodic boundary conditions. *Phys. Rev. B*, **83**, 125104, 2011. doi:10.1103/PhysRevB.83.125104

[Pit61] L. P. Pitaevskiii. Vortex lines in an imperfect Bose gas. *Sov. Phys. JETP*, **13**, 451, 1961

[Pit06] S. Pittel, N. Sandulescu. Density matrix renormalization group and the nuclear shell model. *Phys. Rev. C*, **73**, 014301, 2006. doi:10.1103/PhysRevC.73.014301

[Pit16] L. Pitaevskii, S. Stringari. *Bose–Einstein Condensation and Superfluidity*. Oxford University Press, 2016. ISBN 9780198758884. doi:10.1093/acprof:oso/9780198758884.001.0001

[Pop72] V. N. Popov. On the theory of the superfluidity of two- and one-dimensional bose systems. *Theoretical and Mathematical Physics*, **11 (3)**, 565, 1972. ISSN 1573-9333. doi:10.1007/BF01028373

[Por06] D. Porras, F. Verstraete, J. I. Cirac. Renormalization algorithm for the calculation of spectra of interacting quantum systems. *Phys. Rev. B*, **73**, 014410, 2006. doi:10.1103/PhysRevB.73.014410

[Poz13] Z. D. Pozun, X. Su, K. D. Jordan. Establishing the ground state of the disjoint diradical tetramethyleneethane with quantum monte carlo. *Journal of the American Chemical Society*, **135 (37)**, 13862, 2013. ISSN 0002-7863. doi:10.1021/ja406002n

[Pur82] I. Purvis, George D., R. J. Bartlett. A full coupled-cluster singles and doubles model: The inclusion of disconnected triples. *The Journal of Chemical Physics*, **76 (4)**, 1910, 1982. ISSN 0021-9606. doi:10.1063/1.443164

[Rag89] K. Raghavachari, G. W. Trucks, J. A. Pople, M. Head-Gordon. A fifth-order perturbation comparison of electron correlation theories. *Chemical Physics Letters*, **157 (6)**, 479, 1989. ISSN 0009-2614. doi:10.1016/S0009-2614(89)87395-6

[Ram11] A. Ramanathan, K. C. Wright, S. R. Muniz, M. Zelan, W. T. Hill, C. J. Lobb, K. Helmerson, W. D. Phillips, G. K. Campbell. Superflow in a toroidal Bose-Einstein condensate: An atom circuit with a tunable weak link. *Phys. Rev. Lett.*, **106**, 130401, 2011. doi:10.1103/PhysRevLett.106.130401

[Ree78] M. Reed, B. Simon. *Methods of modern mathematical physics. IV: Analysis of operators*. Academic Press, 1978. ISBN 9780080570457

[Ree80] M. Reed, B. Simon. *Methods of modern mathematical physics. I: Functional Analysis*. Academic Press, 1980. ISBN 9780080570488

[Rén61] A. Rényi. On measures of entropy and information. In *Proceedings of the Fourth Berkeley Symposium on Mathematical Statistics and Probability, Volume 1: Contributions to the Theory of Statistics*, volume 4, pages 547–562. University of California Press, 1961

[Rig04a] M. Rigol, A. Muramatsu. Emergence of quasicondensates of hard-core bosons at finite momentum. *Phys. Rev. Lett.*, **93**, 230404, 2004. doi:10.1103/PhysRevLett.93.230404

[Rig04b] M. Rigol, A. Muramatsu. Universal properties of hard-core bosons confined on one-dimensional lattices. *Phys. Rev. A*, **70**, 031603R, 2004. doi:10.1103/PhysRevA.70.031603

[Ris06] J. Rissler, R. M. Noack, S. R. White. Measuring orbital interaction using quantum information theory. *Chemical Physics*, **323 (2)**, 519, 2006. ISSN 0301-0104. doi:10.1016/j.chemphys.2005.10.018

[Roh13] T. Rohwedder. The continuous coupled cluster formulation for the electronic schrödinger equation. *ESAIM: M2AN*, **47 (2)**, 421, 2013. doi:10.1051/m2an/2012035

[Rom97] S. Rommer, S. Östlund. Class of ansatz wave functions for one-dimensional spin systems and their relation to the density matrix renormalization group. *Phys. Rev. B*, **55**, 2164, 1997. doi:10.1103/PhysRevB.55.2164

[Sac11] S. Sachdev. *Quantum Phase Transitions*. Cambridge University Press, 2 edition, 2011. doi:10.1017/CBO9780511973765

[Sal04] L. Salasnich, A. Parola, L. Reatto. Transition from three dimensions to one dimension in Bose gases at zero temperature. *Phys. Rev. A*, **70**, 013606, 2004. doi:10.1103/PhysRevA.70.013606

[Sal05] L. Salasnich, A. Parola, L. Reatto. Quasi-one-dimensional bosons in three-dimensional traps: From strong-coupling to weak-coupling regime. *Phys. Rev. A*, **72**, 025602, 2005. doi:10.1103/PhysRevA.72.025602

[Sau20] T. Saue, R. Bast, A. S. P. Gomes, H. J. A. Jensen, L. Visscher, I. A. Aucar, R. Di Remigio, K. G. Dyall, E. Eliav, E. Fasshauer, T. Fleig, L. Halbert, E. D. Hedegård, B. Helmich-Paris, M. Iliaš, C. R. Jacob, S. Knecht, J. K. Laerdahl, M. L. Vidal, M. K. Nayak, M. Olejniczak, J. M. H. Olsen, M. Pernpointner, B. Senjean, A. Shee, A. Sunaga, J. N. P. van Stralen. The DIRAC code for relativistic molecular calculations. *The Journal of Chemical Physics*, **152 (20)**, 204104, 2020. ISSN 0021-9606. doi:10.1063/5.0004844

[Sch07] E. Schmidt. Zur theorie der linearen und nichtlinearen integralgleichungen. *Mathematische Annalen*, **63 (4)**, 433, 1907. ISSN 1432-1807. doi:10.1007/BF01449770

[Sch26] E. Schrödinger. Quantisierung als eigenwertproblem. *Annalen der Physik*, **385 (13)**, 437, 1926. doi:10.1002/andp.19263851302

[Sch36] E. Schrödinger. Probability relations between separated systems. *Mathematical Proceedings of the Cambridge Philosophical Society*, **32 (3)**, 446–452, 1936. doi:10.1017/S0305004100019137

[Sch77] M. Schwartz. Off-diagonal long-range behavior of interacting Bose systems. *Phys. Rev. B*, **15**, 1399, 1977. doi:10.1103/PhysRevB.15.1399

[Sch95] B. Schumacher. Quantum coding. *Phys. Rev. A*, **51**, 2738, 1995. doi:10.1103/PhysRevA.51.2738

[Sch05] U. Schollwöck. The density-matrix renormalization group. *Rev. Mod. Phys.*, **77**, 259, 2005. doi:10.1103/RevModPhys.77.259

[Sch07] N. Schuch, M. M. Wolf, F. Verstraete, J. I. Cirac. Computational complexity of projected entangled pair states. *Phys. Rev. Lett.*, **98**, 140506, 2007. doi:10.1103/PhysRevLett.98.140506

[Sch09] R. Schneider. Analysis of the projected coupled cluster method in electronic structure calculation. *Numerische Mathematik*, **113 (3)**, 433, 2009. ISSN 0945-3245. doi:10.1007/s00211-009-0237-3

[Sch11] U. Schollwöck. The density-matrix renormalization group in the age of matrix product states. *Annals of Physics*, **326 (1)**, 96 , 2011. ISSN 0003-4916. doi:10.1016/j.aop.2010.09.012

[Sch15] H. Schempp, G. Günter, S. Wüster, M. Weidemüller, S. Whitlock. Correlated exciton transport in Rydberg-dressed-atom spin chains. *Phys. Rev. Lett.*, **115**, 093002, 2015. doi:10.1103/PhysRevLett.115.093002

[See08] M. Seevinck, J. Uffink. Partial separability and entanglement criteria for multiqubit quantum states. *Phys. Rev. A*, **78 (3)**, 032101, 2008. doi:10.1103/PhysRevA.78.032101

[Sha49] C. Shannon, W. Weaver. *The Mathematical Theory of Communication*. University of Illinois Press, 1949. ISBN 0-252-72548-4

[Sha12] S. Sharma, G. K.-L. Chan. Spin-adapted density matrix renormalization group algorithms for quantum chemistry. *The Journal of Chemical Physics*, **136 (12)**, 124121, 2012. ISSN 0021-9606. doi:10.1063/1.3695642

[Shi06] Y.-Y. Shi, L.-M. Duan, G. Vidal. Classical simulation of quantum many-body systems with a tree tensor network. *Phys. Rev. A*, **74**, 022320, 2006. doi:10.1103/PhysRevA.74.022320

[Sie97] G. Sierra, T. Nishino. The density matrix renormalization group method applied to interaction round a face hamiltonians. *Nuclear Physics B*, **495 (3)**, 505, 1997. ISSN 0550-3213. doi:10.1016/S0550-3213(97)00217-4

[Sin10] S. Singh, R. N. C. Pfeifer, G. Vidal. Tensor network decompositions in the presence of a global symmetry. *Phys. Rev. A*, **82**, 050301, 2010. doi:10.1103/PhysRevA.82.050301

[Sin12] S. Singh, G. Vidal. Tensor network states and algorithms in the presence of a global su(2) symmetry. *Phys. Rev. B*, **86**, 195114, 2012. doi:10.1103/PhysRevB.86.195114

[Sir00] M. Sironi, A. Famulari. An orthogonal approach to determine extremely localised molecular orbitals. *Theoretical Chemistry Accounts*, **103 (5)**, 417, 2000. ISSN 1432-2234. doi:10.1007/s002149900073

[Sle96] G. L. G. Sleijpen, H. A. Van der Vorst. A Jacobi–Davidson iteration method for linear eigenvalue problems. *SIAM J. Matrix Anal. Appl.*, **17 (2)**, 401, 1996. ISSN 0895-4798. doi:10.1137/S0895479894270427

[Smi85] G. F. Smits, C. Altona. Calculation and properties of non-orthogonal, strictly local molecular orbitals. *Theoretica chimica acta*, **67 (6)**, 461, 1985. ISSN 1432-2234. doi:10.1007/BF00528141

[Sól11] J. Sólyom. *Fundamentals of the Physics of Solids, Vol. 3, Normal, Broken-Symmetry, and Correlated Systems*. Springer, 2011. ISBN 978-3-642-04517-2

[Sto80] H. Stoll, G. Wagenblast, H. Preuβ. On the use of local basis sets for localized molecular orbitals. *Theoretica chimica acta*, **57 (2)**, 169, 1980. ISSN 1432-2234. doi:10.1007/BF00574903

[Stö04] T. Stöferle, H. Moritz, C. Schori, M. Köhl, T. Esslinger. Transition from a strongly interacting 1d superfluid to a Mott insulator. *Phys. Rev. Lett.*, **92**, 130403, 2004. doi:10.1103/PhysRevLett.92.130403

[Sza96] A. Szabo, N. S. Ostlund. *Modern Quantum Chemistry: Introduction to Advanced Electronic Structure Theory*. Dover Books on Chemistry. Dover Publications, 1996. ISBN 9780486691862

[Sza15] Sz. Szalay, M. Pfeffer, V. Murg, G. Barcza, F. Verstraete, R. Schneider, Ö. Legeza. Tensor product methods and entanglement optimization for ab initio quantum chemistry. *International Journal of Quantum Chemistry*, **115 (19)**, 1342, 2015. doi:10.1002/qua.24898

[Sza21] Sz. Szalay, Z. Zimborás, M. Máté, G. Barcza, C. Schilling, Ö. Legeza. Fermionic systems for quantum information people. *Journal of Physics A: Mathematical and Theoretical*, **54 (39)**, 393001, 2021. doi:10.1088/1751-8121/ac0646

[Szal12] Sz. Szalay, Z. Kökényesi. Partial separability revisited: Necessary and sufficient criteria. *Phys. Rev. A*, **86**, 032341, 2012. doi:10.1103/PhysRevA.86.032341

[Szal13] Sz. Szalay. Quantum entanglement in finite-dimensional Hilbert spaces. *arXiv [quant-ph]*, 1302.4654, 2013. doi:10.48550/arXiv.1302.4654

[Szal15] Sz. Szalay. Multipartite entanglement measures. *Phys. Rev. A*, **7**, 042329, 2015. doi:10.1103/PhysRevA.92.042329

[Szal17] Sz. Szalay, G. Barcza, T. Szilvási, L. Veis, Örs Legeza. The correlation theory of the chemical bond. *Scientific Reports*, **7 (1)**, 2237, 2017. doi:10.1038/s41598-017-02447-z

[Sze03] Z. Szekeres, P. R. Surján. Direct determination of fragment localized molecular orbitals and the orthogonality constraint. *Chemical Physics Letters*, **369 (1)**, 125, 2003. ISSN 0009-2614. doi:10.1016/S0009-2614(02)01988-7

[Tak99] H. Takasaki, T. Hikihara, T. Nishino. Fixed point of the finite system dmrg. *Journal of the Physical Society of Japan*, **68 (5)**, 1537, 1999. doi:10.1143/JPSJ.68.1537

[Ten17] F. Tennie, V. Vedral, C. Schilling. Universal upper bounds on the Bose–Einstein condensate and the Hubbard star. *Phys. Rev. B*, **96**, 064502, 2017. doi:10.1103/PhysRevB.96.064502

[Tót90] B. Tóth. Phase transition in an interacting Bose system. An application of the theory of Ventsel' and Freidlin. *Journal of Statistical Physics*, **61 (3)**, 749, 1990. ISSN 1572-9613. doi:10.1007/BF01027300

[Tót08] A. I. Tóth, C. P. Moca, Ö. Legeza, G. Zaránd. Density matrix numerical renormalization group for non-abelian symmetries. *Phys. Rev. B*, **78**, 245109, 2008. doi:10.1103/PhysRevB.78.245109

[Ume62] H. Umegaki. Conditional expectation in an operator algebra. IV. entropy and information. *Kodai Mathematical Seminar Reports*, **14 (2)**, 59, 1962. doi:10.2996/kmj/1138844604

[Val10] M. Valiev, E. Bylaska, N. Govind, K. Kowalski, T. Straatsma, H. Van Dam, D. Wang, J. Nieplocha, E. Apra, T. Windus, W. de Jong. NWChem: A comprehensive and scalable open-source solution for large scale molecular simulations. *Computer Physics Communications*, **181 (9)**, 1477, 2010. ISSN 0010-4655. doi:10.1016/j.cpc.2010.04.018

[Ved98] V. Vedral, M. B. Plenio. Entanglement measures and purification procedures. *Phys. Rev. A*, **57**, 1619, 1998. doi:10.1103/PhysRevA.57.1619

[Vei16] L. Veis, A. Antalík, J. Brabec, F. Neese, Ö. Legeza, J. Pittner. Coupled cluster method with single and double excitations tailored by matrix product state wave functions. *The Journal of Physical Chemistry Letters*, **7 (20)**, 4072, 2016. doi:10.1021/acs.jpclett.6b01908

[Vei18] L. Veis, A. Antalík, Ö. Legeza, A. Alavi, J. Pittner. The intricate case of tetramethyleneethane: A full configuration interaction quantum monte carlo benchmark and multireference coupled cluster studies. *Journal of Chemical Theory and Computation*, **14 (5)**, 2439, 2018. ISSN 1549-9618. doi:10.1021/acs.jctc.8b00022

[Ver04] F. Verstraete, D. Porras, J. I. Cirac. Density matrix renormalization group and periodic boundary conditions: A quantum information perspective. *Phys. Rev. Lett.*, **93**, 227205, 2004. doi:10.1103/PhysRevLett.93.227205

[Ver06a] F. Verstraete, J. I. Cirac. Matrix product states represent ground states faithfully. *Phys. Rev. B*, **73**, 094423, 2006. doi:10.1103/PhysRevB.73.094423

[Ver06b] F. Verstraete, M. M. Wolf, D. Perez-Garcia, J. I. Cirac. Criticality, the area law, and the computational power of projected entangled pair states. *Phys. Rev. Lett.*, **96**, 220601, 2006. doi:10.1103/PhysRevLett.96.220601

[Ver08] F. Verstraete, V. Murg, J. Cirac. Matrix product states, projected entangled pair states, and variational renormalization group methods for quantum spin systems. *Advances in Physics*, **57 (2)**, 143, 2008. doi:10.1080/14789940801912366

[Vid03] G. Vidal. Efficient classical simulation of slightly entangled quantum computations. *Phys. Rev. Lett.*, **91**, 147902, 2003. doi:10.1103/PhysRevLett.91.147902

[Vid07] G. Vidal. Entanglement renormalization. *Phys. Rev. Lett.*, **99**, 220405, 2007. doi:10.1103/PhysRevLett.99.220405

[Vid11] E. J. G. G. Vidal, R. P. A. Lima, M. L. Lyra. Bose-Einstein condensation in the infinitely ramified star and wheel graphs. *Phys. Rev. E*, **83**, 061137, 2011. doi:10.1103/PhysRevE.83.061137

[VW64] C. Van Winter. Theory of finite systems of particles. I. the Green function. *Kgl. Danske Videnskab. Selskab, Mat. Fys. Skrifer*, **2 (8)**, 1964

[VW65] C. Van Winter. Theory of finite systems of particles. II. scattering theory. *Kongel. Dan. Vidensk. Selsk., Mat.-Fys. Skr.*, **2 (10)**, 1965

[Wei11] M. Weidemüller, C. Zimmermann. *Interactions in ultracold gases: from atoms to molecules*. John Wiley & Sons, 2011

[Wei12] A. Weichselbaum. Non-abelian symmetries in tensor networks: A quantum symmetry space approach. *Annals of Physics*, **327 (12)**, 2972, 2012. ISSN 0003-4916. doi:10.1016/j.aop.2012.07.009

[Wer89] R. F. Werner. Quantum states with Einstein–Podolsky–Rosen correlations admitting a hidden-variable model. *Phys. Rev. A*, **40 (8)**, 4277, 1989. doi:10.1103/PhysRevA.40.4277

[Wer20] M. A. Werner, C. u. u. u. u. P. m. c. Moca, O. Legeza, G. Zaránd. Quantum quench and charge oscillations in the su(3) hubbard model: A test of time evolving block decimation with general non-abelian symmetries. *Phys. Rev. B*, **102**, 155108, 2020. doi:10.1103/PhysRevB.102.155108

[Whi92] S. R. White. Density matrix formulation for quantum renormalization groups. *Phys. Rev. Lett.*, **69**, 2863, 1992. doi:10.1103/PhysRevLett.69.2863

[Whi93] S. R. White. Density-matrix algorithms for quantum renormalization groups. *Phys. Rev. B*, **48**, 10345, 1993. doi:10.1103/PhysRevB.48.10345

[Whi96] S. R. White. Spin gaps in a frustrated heisenberg model for cav_4O_9. *Phys. Rev. Lett.*, **77**, 3633, 1996. doi:10.1103/PhysRevLett.77.3633

[Whi99] S. R. White, R. L. Martin. Ab initio quantum chemistry using the density matrix renormalization group. *The Journal of Chemical Physics*, **110 (9)**, 4127, 1999. ISSN 0021-9606. doi:10.1063/1.478295

[Whi05] S. R. White. Density matrix renormalization group algorithms with a single center site. *Phys. Rev. B*, **72**, 180403, 2005. doi:10.1103/PhysRevB.72.180403

[Wid73] H. Widom. Toeplitz determinants with singular generating functions. *American Journal of Mathematics*, **95 (2)**, 333, 1973. doi:10.2307/2373789

[Wil75] K. G. Wilson. The renormalization group: Critical phenomena and the kondo problem. *Rev. Mod. Phys.*, **47**, 773, 1975. doi:10.1103/RevModPhys.47.773

[Wil13] M. M. Wilde. *Quantum Information Theory*. Cambridge University Press, 2013. ISBN 9781139525343. doi:10.1017/CBO9781139525343

[Wou12] S. Wouters, P. A. Limacher, D. Van Neck, P. W. Ayers. Longitudinal static optical properties of hydrogen chains: Finite field extrapolations of matrix product state calculations. *The Journal of Chemical Physics*, **136 (13)**, 134110, 2012. ISSN 0021-9606. doi:10.1063/1.3700087

[Wou14] S. Wouters, W. Poelmans, P. W. Ayers, D. V. Neck. CheMPS2: A free open-source spin-adapted implementation of the density matrix renormalization group for ab initio quantum chemistry. *Computer Physics Communications*, **185 (6)**, 1501 , 2014. ISSN 0010-4655. doi:10.1016/j.cpc.2014.01.019

[Xia96] T. Xiang. Density-matrix renormalization-group method in momentum space. *Phys. Rev. B*, **53**, R10445, 1996. doi:10.1103/PhysRevB.53.R10445

[Yan09] T. Yanai, Y. Kurashige, D. Ghosh, G. K.-L. Chan. Accelerating convergence in iterative solution for large-scale complete active space self-consistent-field calculations. *International Journal of Quantum Chemistry*, **109 (10)**, 2178, 2009. ISSN 1097-461X. doi:10.1002/qua.22099

[Yse03] H. Yserentant. On the electronic schrödinger equation. Technical report, Universität Tübingen, 2003

[ZÏ12] G. Zürn, F. Serwane, T. Lompe, A. N. Wenz, M. G. Ries, J. E. Bohn, S. Jochim. Fermionization of two distinguishable fermions. *Phys. Rev. Lett.*, **108**, 075303, 2012. doi:10.1103/PhysRevLett.108.075303

[Zei90] E. Zeidler. *Nonlinear Functional Analysis and Its Applications: II/ B: Nonlinear Monotone Operators*. Springer New York, New York, NY, 1990. ISBN 978-1-4612-0981-2. doi:10.1007/978-1-4612-0981-2

[Zgi08] D. Zgid, M. Nooijen. On the spin and symmetry adaptation of the density matrix renormalization group method. *The Journal of Chemical Physics*, **128 (1)**, 014107, 2008. ISSN 0021-9606. doi:10.1063/1.2814150

[Zhi60] G. M. Zhislin. A study of the spectrum of the Schrödinger operator for a system of several particles. *Trudy Moskovskogo Matematicheskogo Obshchestva*, **9**, 81, 1960

[Živ78] T. P. Živković, H. J. Monkhorst. Analytic connection between configuration–interaction and coupled-cluster solutions. *Journal of Mathematical Physics*, **19 (5)**, 1007, 1978. doi:10.1063/1.523761

[Zwi04] M. W. Zwierlein, C. A. Stan, C. H. Schunck, S. M. F. Raupach, A. J. Kerman, W. Ketterle. Condensation of pairs of fermionic atoms near a Feshbach resonance. *Phys. Rev. Lett.*, **92**, 120403, 2004. doi:10.1103/PhysRevLett.92.120403

One-page summary

Although the density matrix renormalization group (DMRG) method was developed to simulate one-dimensional strongly correlated systems in solid-state physics, it also shows its potential in higher-dimensional as well as in many other strongly correlated many-body problems. In my thesis, I investigate the application of DMRG in quantum chemistry and in ultracold physics, and study numerical methods that are supported by DMRG.

First, the *coupled cluster method tailored by DMRG* (DMRG-TCC) was investigated theoretically and exemplified numerically by the nitrogen dimer for different geometries. We perform a systematic study on the error of the DMRG-TCC, in particular when the system become strongly correlated. We showed the strong dependence of the DMRG-TCC solution on the choice of the active orbitals. We show the robustness of the entropic quantities, which are the guides in determining the optimal basis splitting, with respect to the DMRG accuracy. In order to minimize the energy error and carry out large-scale DMRG-TCCSD calculations, we developed a rigorous routine procedure to determine the optimal basis splitting.

Second, the *orbital optimization based on entanglement minimization* within the framework of two-site DMRG was studied and exemplified numerically by the nitrogen dimer for different geometries. The analysis, based on the tomography of the state, occupation numbers and entropic quantities, shows that the developed joint optimization of the basis and the matrix product state (MPS) has the potential to compress the multireference character of the wave function. The optimized orbitals provide significantly more optimal orbitals for tensor network state methods and other conventional quantum chemistry methods.

Third, the *Hubbard wheel* lattice model of *hard-core bosons* was proposed and investigated theoretically and numerically. The tuning of just a single control parameter allows a crossover from one- to "infinite"-dimensionality, which also drives a transition from quasi-condensation to complete Bose–Einstein condensation. Our numerical simulations showed that the mutual information possesses the qualitatively similar dependence on the control parameter as the number of the condensed bosons. We showed the existence of an excitation gap, which is usually highly demanding, and a possible experimental realization was also proposed.

As outcomes of the projects, several algorithmic developments have been implemented, such as MPS-based routines and interfacing with standard quantum chemistry program packages.

Egyoldalas összefoglaló

Bár a sűrűségmátrixos renormálásicsoport (DMRG) módszert egydimenziós, erősen korrelált rendszerek szimulálására fejlesztették ki a szilárdtestfizikában, a megfelelő fejlesztésekkel lehetőség nyílt a magasabb dimenziós rendszerek, valamint sok más, erősen korrelált soktestrendszerek vizsgálatára is. Dolgozatomban a DMRG alkalmazását vizsgálom a kvantumkémiában és az ultrahideg fizikában, valamint DMRG által támogatott módszerek tanulmányoztam.

Először, a *DMRG által szabott csatolt klaszter* (DMRG-TCC) módszert elméletileg vizsgáltuk, és numerikusan demonstráltuk a nitrogén dimeren különböző geometriákra. Szisztematikus vizsgálatot végzünk a DMRG-TCC módszer hibájára vonatkozóan, különösen akkor, ha a rendszer erősen korrelált. Megmutattuk, hogy a DMRG-TCC által adott megoldás erősen függ az aktív pályák megválasztásától. Megmutattuk az entropikus mennyiségek robusztusságát a DMRG pontosságára nézve, ezért ez alapján az optimális pályafelosztás meghatározható. Az energiahiba minimalizálása és a nagyskálájú DMRG-TCCSD számítások elvégzése érdekében, egy rutin eljárást dolgoztunk ki az optimális pályafelosztás meghatározására.

Másodszor, az *összefonódás minimalizációján alapuló pályaoptimalizációt* tanulmányoztuk a két rácspontos DMRG-algoritmus keretében, valamint numerikusan demonstráltuk a nitrogén dimeren különböző geometriákra. A betöltési számok, az entropikus mennyiségek és az állapot tomográfiája alapján végzett elemzés azt mutatta, hogy a bázis és az mátrixszorzatos állapot (MPS) együttes optimalizációja során lehetőség nyílik a hullámfüggvény multireferenciás jellegének tömörítésére. Az így nyert optimalizált pályák lényegesen optimálisabb pályákat biztosítanak a tenzorhálózat-alapú és más hagyományos kvantumkémiai módszerek számára.

Harmadszor, a *keménymagú bozonok Hubbard-kerék* rácsmodelljét mutattuk be, valamint elméletileg és numerikusan is vizsgáltuk. Egyetlen paraméter hangolása lehetővé teszi az átmenetet az egydimenziósról a „végtelen” dimenziós rendszerre, ami egyben átmenetet is eredményez a kvázi-kondenzációról a teljes Bose–Einstein-kondenzációra. Numerikus szimulációink azt mutatták, hogy a kölcsönös információ a paraméter függvényében minőségileg hasonlóan viselkedik, mint a kondenzált bozonok száma. Megmutattuk, hogy létezik egy gerjesztési energiarés, amely kísérletekben általában kulcsfontosságú, valamint egy lehetséges kísérleti megvalósítást is javasoltunk.

A projektek folyományaképpen számos algoritmikus fejlesztés valósult meg, mint például az MPS-alapú rutinok és a standard kvantumkémiai programcsomagokkal való interfészelés.